

Aus dem Institut für Physiologische Chemie
Geschäftsführender Direktor: Prof. Dr. Gerhard Schrott
Des Fachbereichs Medizin der Philipps-Universität Marburg

**Activity-dependent regulation of miRNAs in different
subcellular compartments of neurons and its
implications for neuronal morphogenesis and plasticity**

Kumulative Dissertation

zur

Erlangung des Doktorgrades
der gesamten Naturwissenschaften
(Dr. rer. nat.)

dem

Fachbereich Medizin
der Philipps-Universität Marburg

vorgelegt von

Sharof Abdumalikovich Khudayberdiev

aus Samarkand, Usbekistan

Marburg, 2014

Angenommen vom Fachbereich Medizin der Philipps-Universität Marburg am: 27.02.2014

Gedruckt mit Genehmigung des Fachbereichs.

Dekan: Prof. Dr. H. Schäfer

Referent: Prof. Dr. G. Schratt

Korreferent: Prof. Dr. T. Stiewe

Table of Contents

List of abbreviations	4
List of publications	8
SUMMARY	9
ZUSAMMENFASSUNG	11
1 INTRODUCTION	14
1.1 microRNA biogenesis, silencing mechanism and degradation	14
1.1.1 miRNA biogenesis pathway	14
1.1.2 Mechanism of miRNA-mediated post-transcriptional silencing	15
1.1.3 miRNA degradation	17
1.2 miRNAs in the nervous system	18
1.2.1 miRNAs in neural differentiation	18
1.2.2 miRNAs in post-mitotic neurons.....	18
1.3 Activity-dependent regulation and miRNAs	19
1.3.1 Activity-dependent regulation of individual miRNAs.....	19
1.3.2 Modulation of the miRISC activity	20
1.4 Subcellular localization of miRNAs in neurons	21
1.4.1 miRNA localization to neuronal processes	21
1.4.2 miRNA localization in the nucleus.....	22
2 SUMMARIES OF PUBLICATIONS:	26
2.1 Publication 1	26
2.2 Publication 2	30
2.3 Publication 3	33
3 CONTRIBUTION	35
4 REFERENCES	36
5 REPRINTS OF ORIGINAL PUBLICATIONS	45
5.1 Mef2-mediated transcription of the mir379-410 cluster regulates activity-dependent dendritogenesis by fine-tuning Pumilio2 protein levels	46
5.2 The DEAH-box helicase DHX36 mediates dendritic localization of the neuronal precursor-microRNA-134	70

5.3 A comprehensive characterization of the nuclear microRNA repertoire of post-mitotic neurons	98
5.3.1 Abstract.....	99
5.3.2 Introduction	100
5.3.3 Materials and Methods.....	102
5.3.3.1 Primary neuronal culture	102
5.3.3.2 Nuclear fractionation protocol.....	102
5.3.3.3 Western blotting	102
5.3.3.4 RNA extraction, size selection of small RNAs and microarray procedure	103
5.3.3.5 Deep sequencing	103
5.3.3.6 Quantitative real-time PCR.....	104
5.3.3.7 Northern blot.....	105
5.3.3.8 Fluorescence <i>in-situ</i> hybridization (FISH).....	105
5.3.3.9 Immunocytochemistry.....	106
5.3.3.10 Developmental expression score	106
5.3.3.11 IsomiR analysis	106
5.3.3.12 Statistical analysis	107
5.3.4 Results	108
5.3.4.1 Microarray profiling of nuclear and cytoplasmic miRNAs.....	108
5.3.4.2 Deep sequencing of small RNAs from nuclear and cytoplasmic fractions	109
5.3.4.3 Comparison of microarray and deep sequencing	110
5.3.4.4 Validation of nuclear-enriched miRNA candidates identified by profiling approaches	111
5.3.4.5 Developmental expression levels of miRNAs and their nuclear enrichment.....	113
5.3.4.6 MiR-25 and miR-92a are specifically enriched in neuronal nuclei, but not in glia	113
5.3.4.7 Inspection of nuclear miRNAs for common sequence characteristics.....	115
5.3.4.8 IsomiRs with a 3'-terminal guanine preferentially localize to a nucleus	116
5.3.5 Discussion.....	118
5.3.6 Conflict of interest statement.....	122

5.3.7	Author contributions	122
5.3.8	Acknowledgements	122
5.3.9	References.....	122
5.3.10	Tables.....	128
5.3.11	Figures.....	130
5.3.12	Supplementary table legends	147
6.	APPENDIX	148
6.1	Publications.....	148
6.2	List of academic teachers.....	149
6.3	Acknowledgements	150

List of abbreviations

3' UTR	3' untranslated region
3'_NTA_X	3' non-templated addition of X (X=C,G,U,A) nucleotide
3'_TA_X	3' templated addition of X (X=C,G,U,A) nucleotide
3'_trim_X	3' trimming of X (X=C,G,U,A) nucleotide
AGO	argonaute protein
APT1	acyl protein thioesterase 1
BAF	BRG1-associated factor
BDNF	brain-derived neurotrophic factor
bp	base pairs
CamKII	Ca ²⁺ /calmodulin-dependent protein kinase II
cAMP	cyclic adenosine monophosphate
CCNB1	cyclin B1
CDC2	cell division cycle 2
CDCA8	cell division cycle associated 8
CDR1	cerebellar degeneration-related protein 1
CNS	central nervous system
CREB	cAMP response element-binding protein
CSDC2	cold-shock domain containing protein C2
CYT	cytoplasm
DCP	mRNA Decapping protein
DEAH-box	Asp-Glu-Ala-His box
DEPC	diethylpyrocarbonate
DES	developmental expression score
DGCR8	DiGeorge syndrome critical region gene 8
DHX36	DEAH box protein
DIG	digoxigenin
disc	discarded
DIV	days <i>in vitro</i>
DTT	dithiothreitol
E2F	E2 promoter binding factor
EDTA	ethylenediaminetetraacetic acid
EGTA	ethyleneglycotetraacetic acid

EMSA	electrophoretic mobility shift assay
ERI-1	exoribonuclease 1
EZH2	enhancer of zeste homolog 2
FBS	fetal bovine serum
FISH	fluorescent <i>in situ</i> hybridization
FMRP	Fragile X mental retardation protein
FUDR	fluorodeoxyuridine
GABA	γ -Aminobutyric acid
GAPDH	glyceraldehyde-3-phosphate dehydrogenase
GFAP	glial fibrillary acidic protein
GW182	glycine-triptophan protein of 182 kDa
H3K27me3	trimethylated histone H3 on lysine 27
H3K4me3	trimethylated histone H3 on lysine 4
H3K9me2	dimethylated histone H3 on lysine 9
HHB	hypotonic homogenation buffer
HIV	human immunodeficiency virus
HOX	homeobox
HP1	heterochromatin protein 1
hPNPase	human polynucleotide phosphorylase
HuD	Hu antigen D
IHB	isotonic homogenation buffer
KSRP	KH-type splicing regulatory protein
LIMK1	LIM domain kinase 1
LNA	locked nucleic acid
MAP2	microtubule-associated protein
MEF2	myocyte enhancer factor-2
MID	middle
miRISC	miRNA-containing RISC
miRLC	miRISC loading complex
miRNA	microRNA
MOV10	moloney leukemia virus 10
mRNA	messenger RNA
Mt	mitochondria
NB	neurobasal

NEnS	nuclear enrichment score
NES	nuclear export signal
NLS	nuclear localization signal
NOT	negative regulator of transcription
NSC	neural stem cell
nt	nucleotide
NTA	non-templated addition
NUC	nucleus
p250RhoGAP	Rho GTPase-activating protein of 250 kDa
PACT	protein activator of the interferon induced protein kinase
PAGE	polyacrylamide gel electrophoresis
PAN	PAB-dependent poly(A)-specific ribonuclease subunit
PAZ	Piwi-Argonaute-Zwille
P-body	processing body
PBS	phosphate-buffered saline
PcG	polycomb group
PFA	paraformaldehyde
piRNA	Piwi-interacting RNAs
PIWI	P-element induced wimpy testis
POLR3D	polymerase (RNA) III (DNA directed) polypeptide D
PR	progesterone receptor
pri-miRNA	primary miRNA
PTBP1	polypyrimidine tract-binding protein 1
PUM2	pumilio 2
qRT-PCR	quantitative real-time polymerase chain reaction
RB1	retinoblastoma 1
RBP	RNA binding protein
RhoG	Ras homology growth-related
RISC	RNA induced silencing complex
RNA	ribonucleic acid
RNAPII	RNA polymerase II
rNEnS	relative nuclear enrichment score
rRNA	ribosomal RNA
RRP41	ribosomal RNA-processing protein 41

SCP1	small C-terminal domain phosphatase 1
SD	standard deviation
SDS	sodium dodecyl sulfate
SERCA2	sarco(endo)plasmic reticulum Ca ²⁺ ATPase 2
siRNA	small interfering RNA
SIRT1	sirtuin 1
Slc1a1	solute carrier family 1, member 1
snoRNA	small nucleolar RNA
snRNA	small nuclear RNA
SOX9	SRY (sex determining region Y)-box 9
SRF	serum response factor
SSC	saline-sodium citrate
TA	templated addition
TBE	tris-borate-EDTA
TEA	tris-acetate-EDTA
TNRC6	trinucleotide repeat containing 6
TRBP	HIV-1 TAR RNA binding protein
tRNA	transfer RNA
TSS	transcription start site
XRN	5'-3' exoribonuclease

List of publications

This thesis summarizes the work carried out by me from August 2007 to November 2013 in the laboratory of Prof. Dr. Gerhard Schratt in the Universities of Heidelberg and Marburg, Germany.

The thesis is written as a cumulative dissertation based on two publications and one manuscript (accepted for publication).

Publication 1:

Mef2-mediated transcription of the mir379-410 cluster regulates activity-dependent dendritogenesis by fine-tuning Pumilio2 protein levels.

Fiore R*, **Khudayberdiev S***, Christensen M, Siegel G, Flavell SW, Kim TK, Greenberg ME, Schratt G (2009) EMBO J 28: 697-710

* with equal contribution

Publication 2:

The DEAH-box helicase DHX36 mediates dendritic localization of the neuronal precursor-microRNA-134.

Bicker S, **Khudayberdiev S**, Weiss K, Zocher K, Baumeister S, Schratt G (2013) Genes Dev 27: 991-996

Publication 3:

A comprehensive characterization of the nuclear microRNA repertoire of post-mitotic neurons.

Khudayberdiev SA, Zampa F, Rajman M, Schratt G (2013) Front. Mol. Neurosci. 6:43. doi: 10.3389/fnmol.2013.00043 (accepted for publication)

SUMMARY

The activity-dependent spatiotemporal regulation of gene expression in neurons is essential for the formation and function of neuronal circuits within the brain. Recently microRNAs (miRNAs), a new class of post-transcriptional regulators of gene expression were implicated in the regulation of neuronal differentiation and development. Furthermore, in mature fully developed neurons, miRNAs (e.g. miR-134) were shown to be involved in the control of local protein synthesis in the vicinity of dendritic spines (Schratt et al., 2006). Activity-dependent local protein synthesis is required for synaptic plasticity, which is believed to be one of the molecular substrates of learning and memory. Nonetheless, the molecular mechanisms underlying the function and regulation of miRNAs during synaptic plasticity are poorly understood.

In a previous publication from our lab, it was shown that the activity of the brain-enriched miRNA - miR-134 is regulated by brain-derived neurotrophic factor (BDNF), which is released upon synaptic stimulation in neurons (Schratt et al, 2006). Interestingly, in the mouse genome this miRNA is encoded in a large miRNA cluster (miR379-410 cluster) consisting of 39 miRNAs. The expression of the miR379-410 cluster is induced upon neuronal activity by virtue of myocyte-enhancing factor 2 (MEF2), a transcription factor that binds to a regulatory region upstream of this cluster (Fiore et al., 2009). The transcriptional upregulation of a subset of miRNAs from the miR379-410 cluster (miR-134, -381 and -329) is necessary for activity-dependent dendritic development of rat hippocampal neurons. Furthermore, we found that the post-transcriptional regulation of the RNA-binding protein Pumilio 2 (PUM2) by miR-134 is essential for activity-dependent dendritogenesis. Taken together, we defined a novel MEF2-miRNA-PUM2 pathway involved in the activity-dependent regulation of dendritogenesis in primary neurons.

MiR-134 localizes within dendrites of hippocampal neurons, where it can regulate the local translation of proteins important for spine structure and plasticity. However, at the beginning of this project, it was unknown how this miRNA is targeted to dendrites. I was involved in a project that aimed at identifying and characterizing the transport mechanism of miR-134 to dendrites. We found that the dendritic localization of miR-134 is mediated by the DEAH-box helicase DHX36 protein, which binds to a cis-acting element located within the loop region of the miR-134 precursor (pre-miR-134; Bicker et al., 2013). Furthermore, we showed that depletion of DHX36 increased protein levels of LIM kinase 1 (LIMK1), a dendritically localized target of miR-134 (Schratt et al, 2006). Moreover, the depletion of DHX36 led to an increase in dendritic spine size, a similar

phenotype as observed upon inhibition of miR-134 activity. In summary, we described a novel mechanism for dendritic targeting of pre-miR-134 relevant for the function of miR-134 in spine morphogenesis.

Activity-dependent regulation of gene expression in the nucleus is important for the development and function of the nervous system, including synaptic plasticity and memory formation. Interestingly, several recent reports suggested that miRNAs (and/or siRNAs) might be involved in the regulation of epigenetic modifications and alternative mRNA splicing events in the nucleus of non-neuronal cells. However, whether miRNAs employ this mechanism to regulate gene expression in the neuronal nucleus was not known. A prerequisite for the study of miRNA function in the nucleus of post-mitotic neurons is the *a priori* knowledge of the nuclear miRNA repertoire. Therefore, using microarray and deep sequencing technologies, I identified miRNAs which are enriched in the nuclei of rat primary cortical neurons (Khudayberdiev et al. 2013; *Frontiers in Mol. Neurosci*, accepted for publication). Subsequently, I validated differential expression of specific nuclear-enriched miRNAs by Northern blot, quantitative real-time PCR (qPCR) and fluorescence *in situ* hybridization (FISH). By cross-comparison to published reports, I found that nuclear accumulation of miRNAs might be linked to a down-regulation of their expression during *in vitro* development of cortical neurons. Importantly, I found a significant overrepresentation of guanine nucleotides at the 3' terminus of nuclear-enriched miRNA isoforms (isomiRs), suggesting the presence of neuron-specific mechanisms involved in miRNA nuclear localization. In conclusion, these results provide a starting point for future studies addressing the nuclear function of specific miRNAs and the detailed mechanisms underlying subcellular localization of miRNAs in neurons.

Taken together, the results presented in my cumulative PhD thesis demonstrate that activity-dependent regulation of specific miRNAs in different subcellular neuronal compartments (dendrites, nucleus, and soma) plays an important role in neuronal morphogenesis (dendrite and spine development) and plasticity.

ZUSAMMENFASSUNG

Die aktivitätsabhängige sowie räumlich-zeitlich koordinierte Regulation der Genexpression in Neuronen ist essentiell für die Bildung und Funktion neuronaler Schaltkreise im Gehirn. Vor kurzem wurden microRNAs (miRNAs), eine neue Klasse posttranskriptionaler Regulatoren der Genexpression, mit der Regulation neuronaler Differenzierung und Entwicklung in Verbindung gebracht. Des Weiteren konnte in reifen, voll entwickelten Neuronen gezeigt werden, dass miRNAs (z.B. miR-134) in der Kontrolle lokaler dendritischer Proteinsynthese in der Nähe von Dornfortsätzen involviert sind (Schratt et al., 2006). Diese aktivitätsabhängige lokale Proteinsynthese ist notwendig für synaptische Plastizität, welche als molekulare Grundlage von Lernen und Gedächtnis angesehen wird. Die molekularen Mechanismen, welche der Funktion und Regulation von miRNAs während synaptischer Plastizitätsvorgänge zugrunde liegen, sind jedoch noch weitestgehend unbekannt.

In einer früheren Publikation unseres Labors wurde gezeigt, dass die Aktivität der im Gehirn angereicherten miRNA miR-134 durch den Wachstumsfaktor BDNF (brain-derived neurotrophic factor) reguliert wird (Schratt et al., 2006), welcher im Rahmen synaptischer Stimulation in Neuronen freigesetzt wird. Interessanterweise ist diese miRNA im Mausgenom in einem großen miRNA Cluster (miR379-410 Cluster) kodiert, das aus insgesamt 39 miRNAs besteht. Die Expression des miR379-410 Clusters wird durch neuronale Aktivität mittels des Transkriptionsfaktors MEF2 (myocyte-enhancing factor 2) induziert, welcher an eine dem Cluster vorgeschaltete regulatorische Region bindet (Fiore et al., 2009). Die transkriptionelle Hochregulierung einer Reihe von miRNAs des miR379-410 Clusters (miR-134, -381 and -329) ist notwendig für die aktivitätsabhängige Dendritenentwicklung in hippocampalen Rattenneuronen. Des Weiteren zeigte sich, dass die posttranskriptionale Regulation des RNA-Bindeproteins Pumilio2 (PUM2) durch miR-134 essentiell für die aktivitätsabhängige Dendritogenese ist. Zusammenfassend haben wir einen neuen MEF2-miRNA-PUM2 Signalweg identifiziert, der an der aktivitätsabhängigen Regulation der Dendritogenese in Primärneuronen beteiligt ist.

MiR-134 ist in Dendriten hippocampaler Neuronen lokalisiert, wo sie die lokale Translation von Proteinen regulieren kann, die für die Struktur und Plastizität von Dornfortsätzen wichtig sind. Zu Beginn dieses Projekts war jedoch nicht bekannt, wie diese miRNA gezielt in Dendriten gelangt. Ich war an einem Projekt beteiligt, welches zum Ziel hatte, die Transportmechanismen von miR-134 in Dendriten zu

charakterisieren. Wir konnten zeigen, dass die dendritische miR-134 Lokalisierung von der DEAH-box Helikase DHX36 vermittelt wird, welche an ein Cis-Element in der Loopregion des miR-134 Vorläufers (pre-miR-134) bindet (Bicker et al., 2013). Darüber hinaus beobachteten wir, dass Verlust von DHX36 zu erhöhten Proteinmengen von LIMK1 (LIM domain kinase 1) führt, einem dendritisch lokalisierten Zielgen von miR-134 (Schratt et al, 2006). Zusammenfassend haben wir einen neuen Mechanismus der dendritischen Lokalisierung von pre-miR-134 beschrieben, der relevant ist für die Funktion von miR-134 in der Morphogenese dendritischer Dornfortsätze.

Die aktivitätsabhängige Regulation der Genexpression im Zellkern spielt eine wichtige Rolle für die Entwicklung und Funktion des Nervensystems, wie etwa für synaptische Plastizität und Gedächtnisbildung. Interessanterweise deuten mehrere kürzlich veröffentlichte Publikationen darauf hin, dass miRNAs (und/oder siRNAs) bei der Regulation epigenetischer Modifikationen und alternativen Spleißens im Zellkern nicht-neuronaler Zellen eine Rolle spielen. Es war jedoch bislang unklar, ob miRNAs auch in neuronalen Zellkernen die Genexpression durch diesen Mechanismus regulieren können. Voraussetzung für die Analyse der miRNA Funktion im Zellkern von post-mitotischen Neuronen ist die Kenntnis des gesamten im Zellkern vorliegenden miRNA Repertoires. Mittels Microarray und Deep Sequencing Technologien habe ich deshalb zunächst jene miRNAs identifiziert, die im Zellkern von kortikalen Primärneuronen aus der Ratte angereichert sind (Khudayberdiev et al., 2013; *Frontiers in Mol. Neurosci.*, zur Veröffentlichung angenommen). Danach habe ich die unterschiedliche Expression spezifischer im Zellkern angereicherter miRNAs mittels Northern blot, quantitativer real-time PCR (qPCR) und fluoreszenter *in situ* Hybridisierung (FISH) validiert. Durch Quervergleich mit publizierten Daten konnte ich herausfinden, dass die Anreicherung von miRNAs im Zellkern möglicherweise mit ihrer Herunterregulation während der *in vitro* Entwicklung kortikaler Neuronen einhergeht. Des Weiteren konnte ich eine Überrepräsentation von Guanin am 3' Ende von im Zellkern angereicherten miRNA Isoformen (isomiRs) nachweisen, die auf einen Neuronen-spezifischen Mechanismus der nukleären miRNA Lokalisierung hindeutet. Insgesamt stellen diese Resultate einen Ausgangspunkt für künftige Studien dar, die sich der Funktion spezifischer miRNAs im Zellkern und den detaillierten Mechanismen der subzellulären Lokalisierung von miRNAs in Neuronen widmen.

Zusammenfassend zeigen die in meiner kumulativen Dissertation beschriebenen Arbeiten, dass die aktivitätsabhängige Regulation spezifischer miRNAs in verschiedenen subzellulären neuronalen Kompartimenten (Dendriten, Zellkern, Zellkörper) eine wichtige

Rolle für die neuronale Morphogenese (Entwicklung von Dendriten und dendritischen Dornfortsätzen) und Plastizität spielt.

1 INTRODUCTION

1.1 microRNA biogenesis, silencing mechanism and degradation

MicroRNAs (miRNAs) represent an important class of small regulatory RNAs with a size of 18-25 nucleotides (nts). They are the largest group of small non-coding RNAs studied so far, consisting of 2024 genes in the human genome (miRBase version 19, <http://www.mirbase.org/>). MiRNAs regulate post-transcriptional gene expression by sequence-specific binding to the 3'-UTR of messenger RNAs (mRNAs), which leads to translational repression and/or degradation of the target mRNA (reviewed in Bartel, 2009). In mammals, computational predictions suggest that up to 50% of all cellular mRNAs could be regulated at the post-transcriptional level by miRNAs (Presutti et al., 2006). Increasing evidence implicates miRNAs in a variety of cellular and developmental processes, including, but not limited to, proliferation, differentiation and apoptosis (reviewed in Bartel, 2004). On the other hand, dysregulation of miRNA function might lead to different anatomical, physiological and developmental pathologies in humans.

1.1.1 miRNA biogenesis pathway

The biogenesis of miRNA is a multi-step process, which usually starts with the generation of primary microRNA (pri-miRNA) transcripts via RNA polymerase II mediated transcription (Figure 1). The stem-loop structures within pri-miRNA transcripts are recognized and cleaved by the microprocessor, a multiprotein complex containing the two core RNA binding proteins Drosha and Di George Syndrome critical region gene 8 (DGCR8). Microprocessor mediated cleavage of pri-miRNAs produces ~ 70 nt hairpin-like precursor miRNAs (pre-miRNA; reviewed in Bartel, 2004). Alternatively, some pre-miRNAs, which are located in the intronic region of protein-coding genes, are generated by co-transcriptional splicing events thereby bypassing microprocessor mediated processing. These miRNAs are referred to as "mirtrons" (reviewed in Curtis et al., 2012).

Pre-miRNA hairpins are exported to the cytoplasm by the nuclear export receptor Exportin-5 (Zeng and Cullen, 2004). In the cytoplasm, pre-miRNAs are associated with the miRISC (miRNA induced silencing complex) loading complex (miRLC), consisting of three main effector proteins, the RNase III enzyme Dicer, HIV-1 transactivation response RNA-binding protein (TRBP) and Argonaute (AGO) family proteins (Kim and Kim, 2012). Dicer-mediated cleavage of pre-miRNA at the proximity of terminal loop leads to the

generation of ~ 22 nt duplex RNA with two nucleotide overhangs at both 3' ends (reviewed in Krol et al., 2010b). Subsequently, miRNA duplexes are handed over to AGO, which in turn separates the two strands of the duplex by an active “wedging mechanism” (Kwak and Tomari, 2012). Usually only one strand, known as the mature miRNA (or guide strand) is retained in AGO (Khvorova et al., 2003), whereas the other strand, which is known as miRNA* (or passenger strand) is removed from miRISC and often degraded. Subsequently, the mature miRNA containing AGO protein constitutes a core component of the functional miRISC complex which exerts the gene regulatory function on target RNAs.

Interestingly, some miRNAs do not require the Dicer processing step to form functional miRISC complex. Specifically, an endonucleolytic active member of AGO protein family in mammals – AGO2 binds and cleaves the passenger strand of pre-mir-451 hairpin; thereby producing AGO2-cleaved (ac)-pre-mir-451 (Yang et al., 2010). This intermediate product is further trimmed to generate the mature miRNA which then becomes part of the functional miRISC.

1.1.2 Mechanism of miRNA-mediated post-transcriptional silencing

In animals, miRISC specifically recognizes its target mRNAs via base-pairing of the mature miRNA to partial complementary sequences in the 3' UTR region of mRNAs (reviewed in Bartel, 2009). The full complementarity of 2-8 nucleotides located at the miRNA 5' end (known as the seed region) with its targets is essential, since mismatches in that region typically abolish miRNA-mediated repression (Lewis et al., 2005). Mismatches and bulges at the miRNA 3' end instead are tolerated and seem to play a modest role in target recognition (Grimson et al., 2007). After sequence-specific recognition of mRNAs by miRISC, the protein components of this complex initiate post-transcriptional gene silencing.

The key components of miRISC are Argonaute (AGO) and glycine-tryptophan repeat containing protein 182 (GW182; the human paralogs are TNRC6A, B and C). AGO proteins are represented by four members (AGO1-4) in mammals. Unlike other AGO proteins, AGO2 possesses endonucleolytic activity and therefore is involved in both miRNA- and siRNA-mediated gene silencing (reviewed in Meister, 2013). GW182 is a downstream effector of AGO, and functions as scaffold protein to assemble silencing complexes on mRNAs during miRNA-mediated gene silencing (reviewed in Braun et al., 2012).

The molecular mechanism of miRISC mediated gene silencing is still subject to intensive research, often resulting in controversial results (reviewed in Fabian and Sonenberg, 2012). On one hand, there is evidence that mRNAs targeted by miRISC are primarily repressed at the level of mRNA translation, without major alterations in mRNA expression (Bhattacharyya et al., 2006). On the other hand, it was proposed that deadenylation (deadenylation complexes CCR4-NOT and PAN2-PAN3) and subsequent degradation (decapping complex DCP1-DCP2 and exonuclease XRN1) of mRNAs is the main cause of the observed decreases in protein expression induced by miRNAs (Baek et al., 2008; Guo et al., 2010). Interestingly, recent findings suggest that translational repression and degradation might in fact be coupled (Bazzini et al., 2012; Djuranovic et al., 2012; Bethune et al., 2012), whereby translational repression precedes mRNA degradation.

1.1.3 miRNA degradation

Mature miRNAs are generally rather stable molecules with a half-life of several hours to days (Bail et al., 2010; Gantier et al., 2011). However, several recent reports suggest that miRNA turnover can be regulated by physiological stimuli (Avraham et al., 2010). In contrast to other systems, rapid turn-over of miRNAs might be a general feature of neuronal cells. In particular, a fast decay of the members of the miR-183/96/182 cluster was observed in the mouse retina, when animals were shifted from light to dark conditions (Krol et al., 2010a), which is associated with increased neuronal activity. In agreement, the blocking of neuronal activity in dissociated hippocampal and cortical cultures with tetrodotoxin reduced turnover of miRNAs, while stimulation with glutamate accelerated it (Krol et al., 2010a). Interestingly, the treatment of *Aplysia* sensory neurons with the neurotransmitter serotonin led to a rapid decrease in miR-124 and miR-181 levels, which in turn contributed to learning-related synaptic plasticity (Rajaseethupathy et al., 2009).

Several exonucleases, such as XRN1 (Chatterjee and Großhans, 2009; Bail et al., 2010), XRN2 (Chatterjee et al., 2011), RRP41 (Bail et al., 2010; Yao et al., 2012), ERI-1 (Thomas et al., 2012) and hPNPase (Das et al., 2010) were implicated in the degradation of miRNAs, although the detailed molecular mechanism of miRNA turnover is still elusive.

1.2 miRNAs in the nervous system

1.2.1 miRNAs in neural differentiation

MiRNAs are abundantly expressed in the developing and mature nervous system, some of which with very specific spatio-temporal expression patterns (reviewed in Kosik, 2006). The importance of miRNA function in early nervous system development *in vivo* is exemplified by studies of brain-specific conditional knockout mice deficient for the miRNA biogenesis factor Dicer (De Pietri Tonelli et al., 2008; Kawase-Koga et al., 2010). Conditional Dicer ablation in the developing brain of these animals affected neural differentiation, resulting in dramatic defects in brain organization, such as cortical hypertrophy, defective layering, as well as smaller and massively disorganized hippocampi (De Pietri Tonelli et al., 2008; Kawase-Koga et al., 2010). Several brain-specific, highly abundant and well-studied miRNAs such as miR-9 (Shibata et al., 2008; Zhao et al., 2009) and miR-124 (Makeyev et al., 2007; Yoo et al., 2009; Cheng et al., 2009) have been shown to possess specific functions in neural progenitor cell proliferation, the promotion toward neurogenesis, and the acquisition and stabilization of neuronal properties *in vitro* and *in vivo* (Shibata et al., 2011; Sanuki et al., 2011) thereby demonstrating that individual miRNAs can fulfill important roles during neurogenesis and early neuronal differentiation.

1.2.2 miRNAs in post-mitotic neurons

Early observations that miRNAs are abundantly expressed in cultured rodent primary neurons (Kim et al., 2004) and in broad regions of the adult brain (Lagos-Quintana et al., 2002; Miska et al., 2004) suggested that miRNAs could play important roles in post-mitotic neurons (reviewed in Schratt, 2009; McNeill and Van Vactor, 2012). Indeed, mice with the conditional ablation of *Dicer* and *DGCR8* genes in the post-mitotic forebrain neurons displayed several phenotypes, including microcephaly, reduced dendritic complexity and increased dendritic spine length (Davis et al., 2008; Babiarz et al., 2011). Interestingly, even the deletion of one copy of *DGCR8* in mice was sufficient to affect dendritic complexity and spine size of CA1 hippocampal neurons (Stark et al., 2008), suggesting that a tight regulation of miRNA biogenesis is required for the proper neuronal morphogenesis.

Profiling of small RNAs from specific neuron subtypes using transgenic AGO2 animals in combination with a cell-type-specific Cre/Lox system resulted in very specific miRNA signatures (He et al., 2012), suggesting that miRNAs could be involved in the

regulation of neuron-type-specific functions. Furthermore, some miRNAs are enriched in neuronal processes, both dendrites (Schratt et al., 2006; Siegel et al., 2009; Lugli et al., 2008) and axons (Natera-Naranjo et al., 2010), suggesting that they could be involved in local protein synthesis which is essential in the regulation of synaptic plasticity and axon guidance (reviewed in Sutton and Schuman, 2006; Schratt, 2009; McNeill and Van Vactor, 2012). Until now, regulatory functions have been described for a number of specific miRNAs in axonogenesis, dendritogenesis, synapse maturation and function. (for a detailed review, see Fiore et al., 2011).

Arguably the best studied examples in the context of synapse development and plasticity are miR-132 and miR-134, and I will specifically summarize the role of these miRNAs in activity-dependent neuronal development in the following chapter.

1.3 Activity-dependent regulation and miRNAs

The proper development of neural circuits requires both spontaneous and experience-driven neuronal activity. Upon experience-dependent stimulation of synapses, the neurotransmitter (e.g. glutamate) or growth factor (e.g. BDNF) binding to receptors causes the induction of multiple cellular signaling pathways. This leads to the activation of activity-dependent gene transcription in the nucleus that is essential during all steps of neuronal development and function (reviewed in West and Greenberg, 2011). A central role in this process play activity-inducible transcription factors, such as cAMP response element binding protein (CREB), myocyte enhancer factor 2 (MEF2) and serum response factor (SRF). Their distinct activities probably ensure the integration of a variety of extracellular stimuli (reviewed in West et al., 2002).

1.3.1 Activity-dependent regulation of individual miRNAs

The neuronal activity-dependent effects of CREB-induced transcription, are at least in part, mediated by transcriptional upregulation of the miR-212/132 cluster. Specifically, a transcriptional induction of miR-132 upon elevation of neuronal activity in hippocampal neuron cultures, e.g. by treatment with BDNF or the GABA receptor blocker bicuculline, is necessary and sufficient to promote dendritogenesis (Vo et al., 2005; Wayman et al., 2008). In the later stages of development, miR-132 was further shown to increase dendritic spine size of hippocampal neurons in an activity-dependent manner (Impey et al., 2010; Edbauer et al., 2010). In line with experiments in neuronal cultures, deletion of the mir-212/132 locus in the murine hippocampus *in vivo* resulted in decreased spine density in pyramidal neurons (Magill et al., 2010). Importantly, two

recent reports demonstrated that miR-132 is involved in specific forms of activity-dependent synaptic plasticity *in vivo*. First, inhibition of miR-132 in mice prevented ocular dominance plasticity induced by monocular deprivation (Mellios et al., 2011). Second, in a doxycycline-regulated miR-132 transgenic mouse, low levels of miR-132 enhanced, while high levels of miR-132 impaired hippocampus-dependent learning in a spatial memory task (Hansen et al., 2012).

Similar to miR-132, transcription of miR-134, is also upregulated by increased neuronal activity in cultured neurons (e.g. upon treatment with BDNF or membrane depolarization; Schratt et al., 2006). Part of miR-134 was found to localize within the synapto-dendritic compartment of rat hippocampal neurons, where it inhibits the local synthesis of LIMK1, an important activator of actin polymerization (Schratt et al., 2006). Thereby, miR-134 reduces dendritic spine size, a correlate of synaptic strength. Interestingly, the application of BDNF relieved miR-134-mediated repression of LIMK1, suggesting that miR-134 function can be regulated during synaptic plasticity (Schratt et al., 2006). Importantly, a subsequent *in vivo* study confirmed the role of miR-134 in synaptic plasticity. Specifically, overexpression of miR-134 impaired both long-term potentiation (LTP; a form of synaptic plasticity) and memory formation during contextual-fear conditioning test in mice (Gao et al., 2010). In this context, miR-134-dependent regulation of CREB appeared to be important. Moreover, miR-134 expression was regulated by the histone deacetylase sirtuin 1 (SIRT1), which repressed miR-134 transcription by recruiting a repressor complex containing the transcription factor Ying Yang 1 to a region upstream of the miR-134 gene (Gao et al., 2010). Furthermore, the silencing of miR-134 produced neuroprotective and prolonged-seizure suppressive effects in status epilepticus models of mice (Jimenez-Mateos et al., 2012).

It should be noted that, in addition to miR-132 and miR-134, neuronal activity regulates the expression of many other miRNAs in cultured neurons (Remenyi et al., 2010; van Spronsen et al., 2013) and in the brain *in vivo* (Eacker et al., 2011). However, whether altered expression of these miRNAs is due to a regulation of transcription or due to the turnover is not known, and the function of most of these miRNAs remains to be determined.

1.3.2 Modulation of the miRISC activity

In addition to synthesis and turnover, activity-dependent regulation of miRNA function can occur at the level of miRISC. For example, activity-dependent degradation

of the miRISC associated RNA helicase Armitage/MOV10 by the proteasome pathway, both in *Drosophila* and rat neurons, resulted in an attenuation of miRNA mediated repression at synapses. The concomitant increase in the translation of synaptic proteins (CamKII, LimK1 and APT1) correlated with memory formation (Ashraf et al., 2006; Banerjee et al., 2009).

Furthermore, Fragile-X mental retardation protein (FMRP), another miRISC associated RNA-binding protein, was inactivated by glutamatergic stimulation of primary neurons (Muddashetty et al., 2007). The resulting relief of miRNA-mediated translational repression of synaptic mRNAs was associated with changes in dendritic spine morphology and function (Edbauer et al., 2010; Muddashetty et al., 2011).

1.4 Subcellular localization of miRNAs in neurons

MiRNA-mediated inhibition of gene expression occurs by an interaction of miRNAs with target mRNAs in the cytoplasm (reviewed in Krol et al., 2010b). The specific subcellular location within the cytoplasm where miRNAs exert their repressive function is currently under intense investigation. MiRNAs and their target mRNAs co-localize within processing (P-) bodies, distinct cytoplasmic foci known for their role in mRNA degradation (Liu et al., 2005). Intriguingly, two recent reports (in human Hela cells and plants) uncovered that miRNA-mediated gene silencing can also happen on the cytoplasmic surface of the endoplasmic reticulum (Stalder et al., 2013; Li et al., 2013). In addition, a subset of miRNAs is found to be associated with the outer membrane of mitochondria and the mitochondrial matrix (reviewed in Sripada et al., 2012). However, their functional relevance in the physiology of the cell awaits further studies.

1.4.1 miRNA localization to neuronal processes

A specific feature of neurons is their high degree of polarization, with the formation of extensive processes which usually consist of a single axon and multiple dendrites. Using deep sequencing, it was shown that hundreds of mRNAs are present in dendrites and axons (Cajigas et al., 2012) where they can be locally translated in response to appropriate stimuli (reviewed in Doyle and Kiebler, 2011). In this regard, the (reversible) inhibition of local mRNA translation by miRNAs represents an intriguing possibility to tightly regulate local translation. Indeed, specific mature miRNAs could be detected in axons (Natero-Naranjo et al., 2010), dendrites (Kye et al., 2007) and synaptosomes, a biochemical preparation enriched for pre- and postsynaptic membranes (Siegel et al., 2009).

More recently, specific pre-miRNAs were found to be enriched in synaptoneurosomes (Lugli et al., 2008). Moreover, the pre-miRNA processing enzyme Dicer localizes to the synapto-dendritic compartment (Lugli et al., 2005), suggesting that miRNA maturation could potentially occur in the vicinity of dendritic spines. Regulated local processing of pre-miRNAs could represent an additional layer of activity-dependent gene expression.

1.4.2 miRNA localization in the nucleus

Although initial studies in mammalian cells suggested that miRNA (siRNA)-mediated gene silencing occurs solely in the cytoplasm (Zeng and Cullen, 2002), subsequent research demonstrated miRNA localization and function in the nucleus. However, the molecular mechanism underlying miRNA function in the nucleus are likely distinct from the cytoplasmic ones and largely unknown (reviewed in Morris, 2011; Huang and Li, 2012).

The first indication of a possible miRNA function in the nucleus came from the observation that siRNA- and miRNA-programmed RISC was present in the nuclear compartment and led to a specific knockdown of a strictly nuclear RNA (snRNA 7SK) (Robb et al., 2005). In addition, another miRISC protein (TNRC6A) was shown to shuttle between the cytoplasm and the nucleus due to the presence of two distinct nuclear export (NES) and localization signals (NLS) (Nishi et al., 2013). Finally, Dicer and some its interacting proteins, such as TRBP and protein kinase RNA activator (PACT) were also detected in the nucleus (Ando et al., 2011; Redfern et al., 2013).

Several labs assessed the expression of specific endogenous miRNAs in the nucleus (and nucleolus) with high-throughput assays, such as microarray (Politz et al., 2009; rat L6 myoblasts), TaqMan low density array (Jeffries et al., 2011; human neural stem cells) and deep sequencing (Liao et al., 2010; nasopharyngeal carcinoma cell line 5-8F). Surprisingly, there is only little overlap between the nuclear-enriched miRNAs identified in these studies. This discrepancy might be explained by the use of different cell lines and expression analysis tools.

For one particular miRNA, miR-29b, a cis-acting element responsible for nuclear targeting could be identified. This miRNA is enriched in the nucleus of cycling HeLa and NIH 3T3 cells, and a hexanucleotide motif (AGUGUU) located at the 3'-end of miR-29b was necessary and sufficient for nuclear accumulation of miR-29b and heterologous small RNAs (Hwang et al., 2007). AGUGUU-mediated targeting to the nucleus might be specific for miR-29b, since no other miRNA present in the database contains this

sequence element. The physiological significance of miR-29b accumulation in the nucleus is currently not known.

The possible roles of nuclear miRNAs are only beginning to be elucidated. It appears that nuclear miRNAs are involved in both transcriptional and post-transcriptional gene regulation by binding to nascent RNA transcripts (reviewed in Morris, 2011; Huang and Li, 2012). MiRNAs that possess complementary sequences to the promoters of target genes can regulate gene expression by inducing or silencing transcription. The first observation implicating mammalian miRNAs in transcriptional activation of gene expression was obtained in human cells, where transfection of miR-373 mimics transcriptionally induced expression of *E-cadherin* and *cold-shock domain containing protein C2 (CSDC2)*; Place et al., 2008). Later, it was demonstrated that miR-744 and miR-205 can activate expression of mouse *cyclin B1 (CCNB1)* and interleukin tumor suppressor genes (*IL24* and *IL32*), possibly by base pairing to partially complementary sequences within the promoter region (Huang et al., 2011; Majid et al., 2010). In addition, transfection of miR-744 increased the association of AGO1 with RNA polymerase II (RNAPII) and tri-methylation of histone 3 lysine 4 (H3K4me3) at the *CCNB1* promoter region (Huang et al., 2011). The molecular mechanisms underlying transcriptional activation by miRNAs are unclear, but experiments based on promoter-targeted siRNAs suggested that it may require transcription running through the promoters of target genes. In addition, epigenetic changes, such as histone acetylation and methylation are observed (reviewed in Portnoy et al., 2011).

MiRNA-mediated transcriptional gene silencing in mammalian cells first was shown for miR-320. MiR-320 expression induced an enrichment of AGO1, Polycomb group (PcG) component EZH2 and tri-methyl H3 lysine 27 (H3K27me3) at the promoter region of the cell cycle gene *POLR3D* (Kim et al., 2008). MiR-320 is encoded in the antisense orientation of *POLR3D* gene promoter and therefore possesses perfect sequence complementarity to that region. Whether other miRNAs which are encoded in promoter regions of protein-coding genes employ similar mechanisms awaits future studies (Kim et al., 2008). Interestingly, Tan and colleagues demonstrated that although miR-10a is encoded upstream of the homeobox gene *HOXB4*, it did not silence the expression of *HOXB4*. However, this miRNA inhibited the transcription of the *HOXD4* gene (a paralog of *HOXB4*) in a Dicer- and AGO1/3-dependent manner. Furthermore, miR-10a-mediated inhibition of transcription was associated with DNA methylation of the *HOXD4* promoter (Tan et al., 2009).

In contrast to previous reports associating AGO1 with transcriptional inhibition, it was recently proposed that AGO2 could instead be the effector component in miRNA-mediated transcriptional silencing (Younger and Corey, 2011; Benhamed et al., 2012). It was shown that miR-423-5p mimics target a highly conserved region of the *progesterone receptor (PR)* promoter. MiRNA targeting decreased the RNAPII occupancy and increased H3 lysine 9 di-methylation (H3K9me₂), hallmarks of epigenetic silencing at the *PR* promoter. This effect was independent of DNA methylation, and associated with recruitment of AGO2 to a non-coding RNA transcript that overlaps the *PR* promoter region (Younger and Corey, 2011).

To date the most systematic study on the physiological impact of miRNA-directed transcriptional gene silencing in mammalian cells was provided by Benhamed and colleagues (Benhamed et al., 2012). First they identified that in senescence-induced human cells the number of E2F-target genes (proliferation-promoting genes regulated by the retinoblastoma (RB1)/E2F repressor complex), whose promoters are associated with AGO protein, were increased in comparison to wild type cells (Benhamed et al., 2012). Moreover, AGO2 was shown to accumulate in the nucleus and induce formation of epigenetic silencing marks (H3K9me₂ and H3K27) at the promoters of E2F-target genes. Interestingly, these authors also found a high correlation between miRNAs that could be immunoprecipitated either with AGO or H3K9me₃-specific antibodies, consistent with an involvement of miRNAs in epigenetic silencing. Indeed, *let-7f* was identified to target the promoters of *CDC2* (also known as *CDK1*) and *CDCA8* (also known as *BOREALIN*) in an AGO2-dependent manner and increased H3K27me₃ marks at these promoters. Finally, the inhibition of *let-7* perturbed the timely execution of senescence, implying that cells undergoing senescence employ miRNA-mediated transcription silencing of proliferation promoting genes (Benhamed et al., 2012).

In summary, a growing body of evidence supports the notion that miRNAs direct transcriptional silencing/activation by recruiting regulatory complexes to chromatin, which in turn are capable to perform epigenetic modifications of histones and/or DNA at the gene promoters.

Interestingly, miRNA-mediated post-transcriptional regulation of gene expression has been also observed in the nucleus. Two recent publications suggest that nuclear mature miRNAs can promote (*let-7*; Zisoulis et al., 2012) or prevent (miR-709; Tang et al., 2012) processing of target pri-miRNAs (*pri-let-7* and *pri-mir-15a/16-1*, respectively) by base-pairing to miRNA recognition elements located within the primary transcripts.

The molecular mechanism underlying the observed effect is unclear, but AGO proteins appear to be required (Zisoulis et al., 2012). Interestingly, Hansen and colleagues showed that nuclear miR-671 can downregulate the expression of the Cerebellar Degeneration-related protein 1(CDR1) mRNA by direct cleavage of its circular antisense transcript (CDR1as) in an AGO2-slicer-dependent manner in human HeLa cells (Hansen et al., 2011).

Additionally, it was shown that siRNA-dependent targeting of AGO1 to the intronic or exonic sequences close to an alternative exon can regulate the splicing of that exon (Allo et al., 2008). The regions that are targeted by the siRNA exhibit increased chromatin silencing marks such as H3K9m2 and H3K27m3. In addition, this mode of silencing required Dicer and the chromatin associated protein –HP1 α (Allo et al., 2008). Similar findings by another research group showed that AGO1 and AGO2 can facilitate spliceosome recruitment and modulate RNAPII elongation rate, thereby affecting alternative splicing (Ameyar-Zazoua et al., 2012). Since miRNAs use similar effector complex (RISC) components as siRNAs, it is conceivable that miRNAs might also be involved in the regulation of transcription-coupled splicing events.

Taken together, it is becoming apparent that miRNAs in various cell types are involved in the regulation of nuclear gene expression by employing a plethora of different mechanisms. However, the identity of nuclear miRNAs in mammalian neurons as well as their potential physiological significance is completely unknown.

2 SUMMARIES OF PUBLICATIONS

2.1 Publication 1

Mef2-mediated transcription of the mir379-410 cluster regulates activity-dependent dendritogenesis by fine-tuning Pumilio2 protein levels.

Fiore R*, **Khudayberdiev S***, Christensen M, Siegel G, Flavell SW, Kim TK, Greenberg ME, Schratt G (2009) EMBO J 28: 697-710

* with equal contribution

This publication is summarized by an article addendum "MicroRNA as modulators of neuronal responses" **Khudayberdiev S**, Fiore R, Schratt G (2009) Commun Integr Biol 2: 411-413.

Article Addendum

MicroRNA as modulators of neuronal responses

Sharof Khudayberdiev, Roberto Fiore and Gerhard Schratt*

Interdisziplinäres Zentrum für Neurowissenschaften; SFB488 Junior Group; Universität Heidelberg; and Institut für Neuroanatomie; Universitätsklinikum Heidelberg; Heidelberg, Germany

Key words: mef2, pumilio, miRNA, plasticity, dendrite, neuron

Neuronal activity controls the correct establishment and refinement of neuronal circuits by regulating key aspects such as dendritogenesis and spine development. Both transcriptional and post-transcriptional gene expression programs induced by neuronal activity have to be coordinated in a tight spatio-temporal manner in order for proper functioning of the neuron. In this context microRNAs (miRNAs), which are implicated in post-transcriptional gene regulation, are good candidates to control dendritic and spine development. In a recent study we have demonstrated that neuronal activity induces myocyte enhancing factor 2 (Mef2) dependent transcription of a large cluster of brain-specific miRNAs (miR379-410). Expression of at least three microRNAs (miR-329, -134 and -381) from this cluster is essential for activity-dependent dendritic outgrowth of hippocampal neurons. One of these three miRNAs, miR-134, promotes dendritic outgrowth by inhibiting translation of the mRNA encoding the translational regulator Pumilio2 (Pum2). In brief, our results suggest a novel role for Mef2 in promoting activity-dependent dendritogenesis by inducing the transcription of the miR379-410 cluster.

The proper development and functioning of neuronal circuits require elaborate gene expression programs that have to be coordinated in a tight spatio-temporal manner. While intrinsic gene expression programs are heavily involved in the early stages of neuronal development, activity-dependent gene expression is necessary for the correct establishment and refinement of neuronal circuits by regulating key aspects such as dendritogenesis and

spine development.¹ Increasing evidence suggests that non-coding RNAs, in particular miRNAs, cooperate with canonical activity regulated transcriptional and post-transcriptional factors (CREB and CPEB, respectively),^{2,3} to regulate gene expression in response to neuronal activity.^{4,5} MiRNAs are involved in the posttranscriptional regulation of gene expression by targeting the RNA-induced silencing complex (RISC) to the 3'-UTR of an mRNA, leading to its translational repression or degradation.

In our recent study we discovered that the transcriptional expression of miRNAs from the miR379-410 cluster, located within the *Gtl2/Dlk1* locus and composed of more than 50 miRNAs, is induced in response to neuronal activity (KCl and BDNF) in a Mef2—dependent manner.⁶ At least three miRNAs (miR-134, -381 and -329) from the cluster are necessary for an increase in dendritic complexity observed upon neuronal activity (Fig. 1A). Activity-dependent changes in dendritic complexity are well documented both in in vitro cell culture models and in in vivo animal models. For example, the dendritic tree of cortical neurons is extensively elaborated in response to the increased neuronal network activity in animals exposed to an enriched environment.⁷ Furthermore, abnormalities of the dendritic tree are a common hallmark of several cognitive diseases characterized by synaptic dysfunction such as mental retardation.⁸ Recently, defects in miRNA biogenesis were shown to contribute to dendritic abnormalities in a mouse model of schizophrenia⁹ and in Dicer-deficient mice.¹⁰ Therefore, it will be important to study the role of the activity-dependent expression of the miR379-410 cluster in dendrite development in vivo. Since only a few members of the cluster appear to be required for activity-dependent dendritogenesis, it is likely that multiple other aspects of neuronal development (neuronal survival, synapse development) may be coordinately controlled by the miR379-410 cluster. Combining gene targeting approaches with genome wide profiling will yield valuable insight into the signaling pathways regulated by the miR379-410 cluster.

We identified the transcription factor Mef2 as necessary for activity-dependent regulation of the miR379-410 cluster. Mef2 was recently shown to act as a negative regulator of synapse number.¹¹ We uncovered a novel role of Mef2, namely as a positive effector of dendritic outgrowth. Furthermore, it was recently shown that, during early postnatal development, dendritic arborization is accompanied by a concomitant reduction in unitary

*Correspondence to: Gerhard Schratt; Interdisziplinäres Zentrum für Neurowissenschaften; SFB488 Junior Group; Universität Heidelberg; and Institut für Neuroanatomie; Universitätsklinikum Heidelberg; Im Neuenheimer Feld 345; Heidelberg 69120 Germany; Tel.: +49.6221.566210; Fax: +49.6221.567897; Email: schratt@ana.uni-heidelberg.de

Submitted: 04/24/09; Accepted: 04/25/09

Previously published online as a *Communicative & Integrative Biology*

E-publication:

<http://www.landesbioscience.com/journals/cib/article/8834>

Addendum to: Fiore R, Khudayberdiev S, Christensen M, Siegel G, Flavell SW, Kim TK, et al. Mef2-mediated transcription of the miR379-410 cluster regulates activity-dependent dendritogenesis by fine-tuning Pumilio2 protein levels. *EMBO J* 2009; 28:697–710. PMID: 19197241; DOI: 10.1038/emboj.2009.10.

excitatory synaptic strength.¹² This latter finding might provide a rationale to reconcile the seemingly opposing functions of Mef2; upon neuronal activity Mef2 could in parallel induce excitatory synapse downscaling and dendritic outgrowth. A key role for Mef2 in reducing neuronal excitability is further suggested by the observation that under conditions of high neuronal activity, Mef2 induces expression of the neurotrophin BDNF and the transcription factor Npas4, two positive regulators of inhibitory synapse development.^{13,14}

MiR-134 is one of the miR379-410 cluster miRNAs necessary for activity-dependent dendritogenesis. Previously we have shown that miR-134 restricts dendritic spine growth by reversibly inhibiting the local synthesis of the actin cytoskeleton regulator Limk1.¹⁵ In the recent study, the effect of miR-134 on dendritic outgrowth appears to be mediated by a different target, the RNA-binding protein Pumilio 2 (Pum2). Pumilio proteins can act either as translational activators or inhibitors and control several aspects of neuronal function, including neuronal morphology and excitability.^{16,17} Both the Pum2 protein and mRNA are localized in dendrites. Thus miR-134 might couple global nuclear programs of gene expression with the spatially restricted control of protein synthesis in dendrites. To test this hypothesis it will be necessary to determine the localization of the Pum2-miR-134 interaction and the subset of mRNAs whose translation is regulated by Pum2. These studies could elucidate how a neuron coordinates transcriptional and post-transcriptional programs of gene expression in response to activity.

Surprisingly, our study also revealed a dual effect of neuronal activity on miR-134 function. In young neurons, activity increases miR-134 levels to facilitate the translational inhibition of Pum2 and dendritic outgrowth. In more mature neuronal cultures, BDNF release locally suppresses the miR-134 mediated Limk1 translational inhibition. It is tempting to speculate that these different effects might not only reflect different functions of miR-134 at different stages of development, but also represent a mechanism of neuronal homeostasis in response to increased or decreased network activity. Homeostatic plasticity is defined as the capability of individual neurons within a circuit to adjust to different levels of presynaptic input by changing the strength of the postsynaptic responses. One example is synaptic downscaling, a mechanism that decreases the average magnitude of postsynaptic responses to keep the overall neuronal excitability within the physiological range.¹⁸ One could speculate that the increased global levels of miR-134 in response to activity might contribute to synaptic downscaling by restricting spine growth. Moreover, synaptic activity leads to BDNF secretion that can locally block miR-134 activity. These two forms of activity-dependent miR-134 regulation would permit the potentiation of individual active synapses without compromising neuronal homeostasis in the very same neuron (Fig. 1B). The coordination of global and local control of miRNAs by neuronal activity and their function in homeostatic and Hebbian forms of synaptic plasticity is an exciting topic for future investigation.

It is becoming evident that many neurological diseases arise from a failure in homeostatic mechanisms within the neuronal network.¹⁹ Understanding how miRNAs modulate experience-

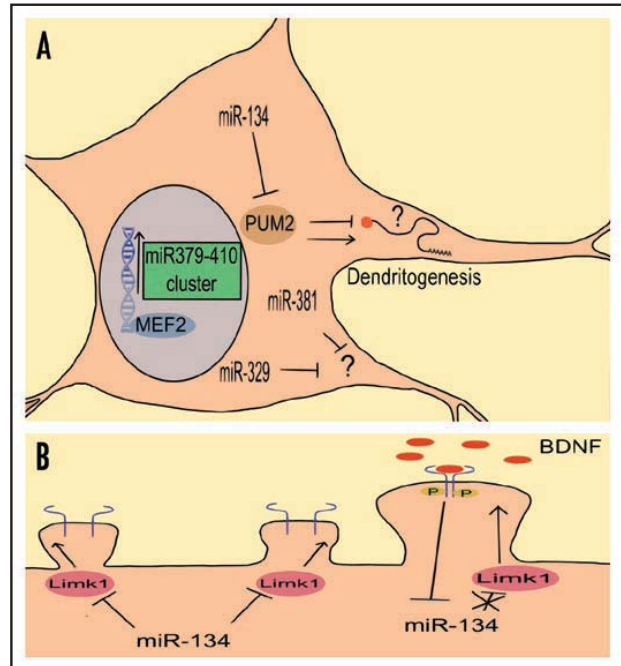


Figure 1. The effect of neuronal activity on the function of the miR379-410 cluster member miR-134. (A) Schematic representation of miR379-410 cluster dependent dendritogenesis pathway. Neuronal activity induces Mef2-dependent transcription of microRNAs from the miR379-410 cluster. At least three of them (miR-134, -329 and -381) are necessary for activity-dependent dendritogenesis. The targets of miR-329/381 are unknown. One of the miR-134 targets important for dendritogenesis is Pum2. Enhanced expression of miR-134 blocks Pum2 translation. Reduced Pum2 expression, in turn, allows the synthesis of dendrite growth promoting factors (and/or interferes with the synthesis of inhibiting factors). (B) miR-134 regulates dendritic spine size.¹⁵ Bdnf (neuronal activity) application inhibits the repressive effect of miR-134 on translation of Limk1 mRNA which leads to increased spine size.

dependent neuronal responses should shed some light on the etiology of complex brain disorders and potentially provide new means for therapeutic intervention.

Acknowledgements

We thank R. Saba for critically reading the manuscript. This work was supported by grants from the DFG (SFB488), HFSP (CDA) and NIDA (4R21DAO25102-01).

References

1. Flavell SW, Greenberg ME. Signaling mechanisms linking neuronal activity to gene expression and plasticity of the nervous system. *Annu Rev Neurosci* 2008; 31:563-90.
2. West AE, Griffith EC, Greenberg ME. Regulation of transcription factors by neuronal activity. *Nat Rev Neurosci* 2002; 3:921-31.
3. Richter JD. CPEB: a life in translation. *Trends Biochem Sci* 2007; 32:279-85.
4. Kosik KS. The neuronal microRNA system. *Nat Rev Neurosci* 2006; 7:911-20.
5. Fiore R, Siegel G, Schratt G. MicroRNA function in neuronal development, plasticity and disease. *Biochim Biophys Acta* 2008; 1779:471-8.
6. Fiore R, Khudayberdiev S, Christensen M, Siegel G, Flavell SW, Kim TK, et al. Mef2-mediated transcription of the miR379-410 cluster regulates activity-dependent dendritogenesis by fine-tuning Pumilio2 protein levels. *EMBO J* 2009; 28:697-710.
7. Konur S, Ghosh A. Calcium signaling and the control of dendritic development. *Neuron* 2005; 46:401-5.

Neuronal activity and miRNAs

8. Bagni C, Greenough WT. From mRNP trafficking to spine dysmorphogenesis: the roots of fragile X syndrome. *Nat Rev Neurosci* 2005; 6:376-87.
9. Stark KL, Xu B, Bagchi A, Lai WS, Liu H, Hsu R, et al. Altered brain microRNA biogenesis contributes to phenotypic deficits in a 22q11-deletion mouse model. *Nat Genet* 2008; 40:751-60.
10. Davis TH, Cuellar TL, Koch SM, Barker AJ, Harfe BD, McManus MT, et al. Conditional loss of Dicer disrupts cellular and tissue morphogenesis in the cortex and hippocampus. *J Neurosci* 2008; 28:4322-30.
11. Flavell SW, Cowan CW, Kim TK, Greer PL, Lin Y, Paradis S, et al. Activity-dependent regulation of MEF2 transcription factors suppresses excitatory synapse number. *Science* 2006; 311:1008-12.
12. Peng YR, He S, Marie H, Zeng SY, Ma J, Tan ZJ, et al. Coordinated changes in dendritic arborization and synaptic strength during neural circuit development. *Neuron* 2009; 61:71-84.
13. Flavell SW, Kim TK, Gray JM, Harmin DA, Hemberg M, Hong EJ, et al. Genome-wide analysis of MEF2 transcriptional program reveals synaptic target genes and neuronal activity-dependent polyadenylation site selection. *Neuron* 2008; 60:1022-38.
14. Lin Y, Bloodgood BL, Hauser JL, Lapan AD, Koon AC, Kim TK, et al. Activity-dependent regulation of inhibitory synapse development by Npas4. *Nature* 2008; 455:1198-204.
15. Schrott GM, Tuebing F, Nigh EA, Kane CG, Sabatini ME, Kiebler M, et al. A brain-specific microRNA regulates dendritic spine development. *Nature* 2006; 439:283-9.
16. Kaye JA, Rose NC, Goldsworthy B, Goga A, L'Etoile ND. A 3'UTR pumilio-binding element directs translational activation in olfactory sensory neurons. *Neuron* 2009; 61:57-70.
17. Baines RA. Neuronal homeostasis through translational control. *Mol Neurobiol* 2005; 32:113-21.
18. Turrigiano GG. The self-tuning neuron: synaptic scaling of excitatory synapses. *Cell* 2008; 135:422-35.
19. Ramocki MB, Zoghbi HY. Failure of neuronal homeostasis results in common neuropsychiatric phenotypes. *Nature* 2008; 455:912-8.

2.2 Publication 2

The DEAH-box helicase DHX36 mediates dendritic localization of the neuronal precursor-microRNA-134.

Bicker S, **Khudayberdiev S**, Weiss K, Zocher K, Baumeister S, Schratt G (2013) *Genes Dev* 27: 991-996

In previous work from our laboratory, a subset of dendritically localized mature microRNAs that are involved in the regulation of dendritic spine morphogenesis were identified (Schratt et al., 2006; Siegel et al., 2009). Some of these miRNAs inhibit the local translation of target mRNAs which encode regulatory proteins with important function in the regulation of dendritic spine structure and function. However, how these miRNAs reached their final destination in dendrites close to the synapses was not known. We hypothesized that at least part of the dendritic localization of specific miRNAs could occur at the pre-miRNA stage, since pre-miRNAs could possess cis-acting elements within their terminal loop that serve as binding sites for RNA binding proteins (RBPs).

QPCR analysis of 16 previously identified synaptically enriched miRNAs (Schratt et al., 2006; Siegel et al., 2009) revealed that two of the corresponding pre-miRNAs (pre-miR-7a-2 and pre-miR-134) were significantly enriched in synaptosomes prepared from postnatal day 15 (P15) rat forebrains. Locked nucleic acid (LNA)-based fluorescent *in situ* hybridization (FISH) assay with hippocampal neurons and qPCR analysis of RNA prepared from compartmentalized hippocampal neuron cultures confirmed our results obtained with synaptosomes. Together, these findings suggested a specific localization of endogenous pre-miR-134 in dendrites of primary hippocampal neurons and at synapses in the brain *in vivo*.

Mechanistically, dendritic localization of pre-miR-134 was achieved by a specific cis-acting element at the terminal loop sequence, as assessed by transfection of synthetic Cy3 labeled pre-miR-134 into hippocampal neurons followed by confocal fluorescence microscopy. In brief, replacement of the pre-miR-134 loop sequence with that of pre-miR-150 (non-dendritic miRNA) abolished dendritic localization. Conversely, putting the pre-miR-134 loop sequence within the context of the pre-miR-150 stem conferred dendritic localization to pre-miR-150. Furthermore, mutagenesis analysis

revealed that the five central loop nucleotides in the pre-miR-134 are crucial for dendritic targeting.

A biochemical *in vitro* pull-down approach followed by mass spectrometry analysis was used to identify proteins interacting with the pre-miR-134 loop. This approach led to the identification of DHX36, an RNA helicase of the DEAH-box family. Using RNA immunoprecipitation, we could confirm an association of DHX36 and pre-miR-134 in intact neurons. Both full-length DHX36 and the DHX36 N-terminal domain, which contains an RNA-binding motif, associated with radiolabeled pre-miR-134 in electrophoretic mobility shift assay (EMSA) *in vitro*, demonstrating a direct interaction between DHX36 and pre-miR-134. Using *in vitro* pre-miRNA cleavage assays, we found that DHX36 interfered with the cleavage of synthetic pre-miR-134 by recombinant Dicer. Together, our experiments demonstrate that DHX36 directly interacts with pre-miR-134 *in vitro* and *in vivo*, and reduces Dicer-mediated pre-miR-134 cleavage *in vitro*.

We further characterized DHX36 function in dendritic transport in neurons. Using compartmentalized cultures, we detected DHX36 expression in both the cell body and, to a lesser extent, the process compartment. shRNA-mediated depletion of DHX36 in neurons led to a significant reduction in dendritic localization of Cy3-labeled pre-miR-134. Taken together these results suggest that DHX36 is specifically required for the accumulation of pre-miR-134 in neuronal dendrites.

To determine the role of DHX36-mediated dendritic transport in miR-134 dependent target gene regulation we performed luciferase reporter gene assays. Knockdown of DHX36 increased the expression of a luciferase reporter gene that contains a miR-134 perfect binding site in the context of the LIMK1 3'UTR, which was shown to localize to dendrites (Schratt et al., 2006). In addition, both a PUM2 luciferase reporter gene containing single miR-134-binding site (Fiore et al., 2009) and endogenous LIMK1 protein expression were similarly induced in DHX36 depleted cells. These results demonstrate that DHX36 knockdown results in an increased expression of known dendritic miR-134 target genes, possibly due to reduced dendritic pre-miR-134 accumulation and miR-134 production. We further studied the impact of DHX36 depletion on neuronal function. Previously it was shown that inhibition of miR-134 activity with antisense oligonucleotides leads to increased spine size (Schratt et al., 2006). Consistent with reduced dendritic miR-134 activity upon DHX36 knockdown, we found that the average dendritic spine volume in DHX36 depleted neurons was significantly increased. Together, these results suggest that DHX36 negatively regulates spine

morphogenesis in hippocampal neurons possibly by promoting miR-134 activity in dendrites.

2.3 Publication 3

A comprehensive characterization of the nuclear microRNA repertoire of post-mitotic neurons.

Khudayberdiev SA, Zampa F, Rajman M, Schrott G (2013) *Front. Mol. Neurosci.* 6:43. doi: 10.3389/fnmol.2013.00043 (accepted for publication)

In addition to a well-described role of miRNAs in post-transcriptional regulation of gene expression in the cytoplasm, several recent studies suggest that miRNAs may also be involved in the regulation of gene expression in the nucleus of mammalian cells. Specifically, miRNAs that possess sequence complementarity to genomic sequences, such as promoters, induce epigenetic modifications, thereby affecting gene expression directly in the nucleus. However, whether miRNAs can regulate gene expression by a similar mechanism in the neuronal nucleus is not known. I hypothesized that miRNAs that are enriched in the neuronal nucleus might represent promising candidates involved in this process. Hence, I decided to identify and characterize the nuclear miRNA profile of rat primary cortical neurons.

Using two different high-throughput technologies, microarray and deep sequencing, I analyzed and compared the miRNA expression profiles from nuclear and cytoplasmic fractions of neurons. In general, miRNAs were detectable in both cellular compartments. However, in agreement with a cytoplasmic function of miRNA, the expression of the majority of miRNAs was higher in the cytoplasm than in the nucleus. Nevertheless, I found that a small subset of miRNAs was enriched in the nuclei of neurons. Next, I validated differential expression of specific nuclear-enriched miRNAs by Northern blot, qPCR and FISH. The cross-comparison of miRNA subcellular distribution to published reports revealed that miRNAs that are most highly enriched in the neuronal nucleus tend to be down-regulated during neuronal development. This result suggests that some miRNAs, depending on the developmental stage, could function in different neuronal compartments. Moreover, I found that miRNAs that are highly enriched in the neuronal nucleus (for example, miR-25 and miR-92a) do not show the same subcellular distribution in other cell types (e.g. glia), implying that the molecular mechanisms that regulate subcellular localization of miRNAs are cell-type specific.

By performing a comprehensive analysis of miRNA isoforms (isomiRs) from the nuclear and cytoplasmic fractions, I found that a guanine nucleotide located at the 3' terminus is overrepresented in isomiRs that are highly enriched in the nucleus.

Interestingly, isomiRs with a non-templated addition of a guanine nucleotide to the 3' terminus represented the most highly enriched nuclear isomiR population. This suggests that molecular mechanisms involving 3' guanylyltransferases might be important for the direction of miRNAs to the neuronal nucleus.

In summary, these results present a roadmap for future studies addressing the detailed mechanisms underlying nuclear localization and function of miRNAs in neurons.

3 CONTRIBUTION

Publication 1: Mef2-mediated transcription of the mir379-410 cluster regulates activity-dependent dendritogenesis by fine-tuning Pumilio2 protein levels.

Fiore R*, **Khudayberdiev S***, Christensen M, Siegel G, Flavell SW, Kim TK, Greenberg ME, Schrott G (2009) EMBO J 28: 697-710

* with equal contribution

In this publication, I carried out the experiments related to the transcriptional induction of miRNA expression (Fig. 1A, B, C). I also identified and characterized the MEF2-responsive element localized upstream of mir379-410 cluster (Fig. 2A, B, C; Fig. 3A, B, C).

Publication 2: The DEAH-box helicase DHX36 mediates dendritic localization of the neuronal precursor-microRNA-134.

Bicker S, **Khudayberdiev S**, Weiss K, Zocher K, Baumeister S, Schrott G (2013) Genes Dev 27: 991-996

I performed electrophoretic mobility shift (Fig. S8A and S8B) and dicer cleavage assays (Fig. 3F) for this publication.

Publication 3: A comprehensive characterization of the nuclear microRNA repertoire of post-mitotic neurons.

Khudayberdiev SA, Zampa F, Rajman M, Schrott G (2013) Front. Mol. Neurosci. 6:43. doi: 10.3389/fnmol.2013.00043 (accepted for publication)

I performed all experiments (except Fig. 1C and Fig. S2A), data analysis (except the preliminary analysis of the microarray data) and wrote the first draft of the manuscript.

4 REFERENCES

Allo M, Buggiano V, Fededa JP, Petrillo E, Schor I, de la Mata M, Agirre E, Plass M, Eyras E, Elela SA, Klinck R, Chabot B, Kornblihtt AR (2009) Control of alternative splicing through siRNA-mediated transcriptional gene silencing. *Nat Struct Mol Biol* 16: 717-724

Ameyar-Zazoua M, Rachez C, Souidi M, Robin P, Fritsch L, Young R, Morozova N, Fenouil R, Descostes N, Andrau JC, Mathieu J, Hamiche A, Ait-Si-Ali S, Muchardt C, Batsche E, Harel-Bellan A (2012) Argonaute proteins couple chromatin silencing to alternative splicing. *Nat Struct Mol Biol* 19: 998-1004

Ando Y, Tomaru Y, Morinaga A, Burroughs AM, Kawaji H, Kubosaki A, Kimura R, Tagata M, Ino Y, Hirano H, Chiba J, Suzuki H, Carninci P, Hayashizaki Y (2011) Nuclear pore complex protein mediated nuclear localization of dicer protein in human cells. *PLoS One* 6: e23385

Ashraf SI, McLoon AL, Sclarsic SM, Kunes S (2006) Synaptic protein synthesis associated with memory is regulated by the RISC pathway in *Drosophila*. *Cell* 124: 191-205

Avraham R, Sas-Chen A, Manor O, Steinfeld I, Shalgi R, Tarcic G, Bossel N, Zeisel A, Amit I, Zwang Y, Enerly E, Russnes HG, Biagioni F, Mottolese M, Strano S, Blandino G, Borresen-Dale AL, Pilpel Y, Yakhini Z, Segal E, Yarden Y (2010) EGF decreases the abundance of microRNAs that restrain oncogenic transcription factors. *Sci Signal* 3: ra43

Babiarz, J.E., Hsu, R., Melton, C., Thomas, M., Ullian, E.M., and Blalock, R. (2011). A role for noncanonical microRNAs in the mammalian brain revealed by phenotypic differences in *Dgcr8* versus *Dicer1* knockouts and small RNA sequencing. *RNA* 17, 1489-1501.

Baek D, Villen J, Shin C, Camargo FD, Gygi SP, Bartel DP (2008) The impact of microRNAs on protein output. *Nature* 455: 64-71

Bail S, Swerdel M, Liu H, Jiao X, Goff LA, Hart RP, Kiledjian M (2010) Differential regulation of microRNA stability. *RNA* 16: 1032-1039

Banerjee S, Neveu P, Kosik KS (2009) A coordinated local translational control point at the synapse involving relief from silencing and MOV10 degradation. *Neuron* 64: 871-884

Bartel DP (2004) MicroRNAs: genomics, biogenesis, mechanism, and function. *Cell* 116: 281-297

Bartel DP (2009) MicroRNAs: target recognition and regulatory functions. *Cell* 136: 215-233

Bazzini AA, Lee MT, Giraldez AJ (2012) Ribosome profiling shows that miR-430 reduces translation before causing mRNA decay in zebrafish. *Science* 336: 233-237

Benhamed M, Herbig U, Ye T, Dejean A, Bischof O (2012) Senescence is an endogenous trigger for microRNA-directed transcriptional gene silencing in human cells. *Nat Cell Biol* 14: 266-+

Bethune J, Artus-Revel CG, Filipowicz W (2012) Kinetic analysis reveals successive steps leading to miRNA-mediated silencing in mammalian cells. *EMBO Rep*

Bhattacharyya SN, Habermacher R, Martine U, Closs EI, Filipowicz W (2006) Relief of microRNA-mediated translational repression in human cells subjected to stress. *Cell* 125: 1111-1124

Bicker, S., Khudayberdiev, S., Weiss, K., Zocher, K., Baumeister, S., and Schrott, G. (2013). The DEAH-box helicase DHX36 mediates dendritic localization of the neuronal precursor-microRNA-134. *Genes Dev* 27, 991-996.

Braun JE, Huntzinger E, Izaurralde E (2012) A molecular link between miRISCs and deadenylases provides new insight into the mechanism of gene silencing by microRNAs. *Cold Spring Harb Perspect Biol* 4

Cajigas IJ, Tushev G, Will TJ, tom Dieck S, Fuerst N, Schuman EM (2012) The local transcriptome in the synaptic neuropil revealed by deep sequencing and high-resolution imaging. *Neuron* 74: 453-466

Chatterjee S, Fasler M, Bussing I, Grosshans H (2011) Target-mediated protection of endogenous microRNAs in *C. elegans*. *Dev Cell* 20: 388-396

Chatterjee S, Grosshans H (2009) Active turnover modulates mature microRNA activity in *Caenorhabditis elegans*. *Nature* 461: 546-549

Cheng LC, Pastrana E, Tavazoie M, Doetsch F (2009) miR-124 regulates adult neurogenesis in the subventricular zone stem cell niche. *Nat Neurosci* 12: 399-408

Curtis HJ, Sibley CR, Wood MJ (2012) Mirtrons, an emerging class of atypical miRNA. *Wiley Interdiscip Rev RNA* 3: 617-632

Das SK, Sokhi UK, Bhutia SK, Azab B, Su ZZ, Sarkar D, Fisher PB (2010) Human polynucleotide phosphorylase selectively and preferentially degrades microRNA-221 in human melanoma cells. *Proc Natl Acad Sci U S A* 107: 11948-11953

Davis, T.H., Cuellar, T.L., Koch, S.M., Barker, A.J., Harfe, B.D., McManus, M.T., and Ullian, E.M. (2008). Conditional loss of Dicer disrupts cellular and tissue morphogenesis in the cortex and hippocampus. *J Neurosci* 28, 4322-4330.

- De Pietri Tonelli D, Pulvers JN, Haffner C, Murchison EP, Hannon GJ, Huttner WB (2008) miRNAs are essential for survival and differentiation of newborn neurons but not for expansion of neural progenitors during early neurogenesis in the mouse embryonic neocortex. *Development* 135: 3911-3921
- Djuranovic S, Nahvi A, Green R (2012) miRNA-mediated gene silencing by translational repression followed by mRNA deadenylation and decay. *Science* 336: 237-240
- Doyle M, Kiebler MA (2011) Mechanisms of dendritic mRNA transport and its role in synaptic tagging. *EMBO J* 30: 3540-3552
- Eacker SM, Keuss MJ, Berezikov E, Dawson VL, Dawson TM (2011) Neuronal activity regulates hippocampal miRNA expression. *PLoS One* 6: e25068
- Edbauer D, Neilson JR, Foster KA, Wang CF, Seeburg DP, Battersby MN, Tada T, Dolan BM, Sharp PA, Sheng M (2010) Regulation of synaptic structure and function by FMRP-associated microRNAs miR-125b and miR-132. *Neuron* 65: 373-384
- Fabian MR, Sonenberg N (2012) The mechanics of miRNA-mediated gene silencing: a look under the hood of miRISC. *Nat Struct Mol Biol* 19: 586-593
- Fiore, R., Khudayberdiev, S., Christensen, M., Siegel, G., Flavell, S.W., Kim, T.K., Greenberg, M.E., and Schratt, G. (2009). Mef2-mediated transcription of the miR379-410 cluster regulates activity-dependent dendritogenesis by fine-tuning Pumilio2 protein levels. *EMBO J* 28, 697-710.
- Fiore, R., Khudayberdiev, S., Saba, R., and Schratt, G. (2011). MicroRNA function in the nervous system. *Prog Mol Biol Transl Sci* 102, 47-100.
- Gantier MP, McCoy CE, Rusinova I, Saulep D, Wang D, Xu D, Irving AT, Behlke MA, Hertzog PJ, Mackay F, Williams BR (2011) Analysis of microRNA turnover in mammalian cells following Dicer1 ablation. *Nucleic Acids Res* 39: 5692-5703
- Gao J, Wang WY, Mao YW, Graff J, Guan JS, Pan L, Mak G, Kim D, Su SC, Tsai LH (2010) A novel pathway regulates memory and plasticity via SIRT1 and miR-134. *Nature* 466: 1105-1109
- Grimson A, Farh KK, Johnston WK, Garrett-Engle P, Lim LP, Bartel DP (2007) MicroRNA targeting specificity in mammals: determinants beyond seed pairing. *Mol Cell* 27: 91-105
- Guo H, Ingolia NT, Weissman JS, Bartel DP (2010) Mammalian microRNAs predominantly act to decrease target mRNA levels. *Nature* 466: 835-840
- Hansen KF, Karelina K, Sakamoto K, Wayman GA, Impey S, Obrietan K (2012) miRNA-132: a dynamic regulator of cognitive capacity. *Brain Struct Funct*

- Hansen TB, Wiklund ED, Bramsen JB, Villadsen SB, Statham AL, Clark SJ, Kjems J (2011) miRNA-dependent gene silencing involving Ago2-mediated cleavage of a circular antisense RNA. *EMBO J* 30: 4414-4422
- He M, Liu Y, Wang X, Zhang MQ, Hannon GJ, Huang ZJ (2012) Cell-type-based analysis of microRNA profiles in the mouse brain. *Neuron* 73: 35-48
- Huang V, Li LC (2012) miRNA goes nuclear. *RNA Biol* 9: 269-273
- Huang V, Place RF, Portnoy V, Wang J, Qi Z, Jia Z, Yu A, Shuman M, Yu J, Li LC (2012) Upregulation of Cyclin B1 by miRNA and its implications in cancer. *Nucleic Acids Res* 40: 1695-1707
- Hwang HW, Wentzel EA, Mendell JT (2007) A hexanucleotide element directs microRNA nuclear import. *Science* 315: 97-100
- Impey S, Davare M, Lesiak A, Fortin D, Ando H, Varlamova O, Obrietan K, Soderling TR, Goodman RH, Wayman GA (2010) An activity-induced microRNA controls dendritic spine formation by regulating Rac1-PAK signaling. *Mol Cell Neurosci* 43: 146-156
- Jeffries CD, Fried HM, Perkins DO (2011) Nuclear and cytoplasmic localization of neural stem cell microRNAs. *RNA* 17: 675-686
- Jimenez-Mateos EM, Engel T, Merino-Serrais P, McKiernan RC, Tanaka K, Mouri G, Sano T, O'Tuathaigh C, Waddington JL, Prenter S, Delanty N, Farrell MA, O'Brien DF, Conroy RM, Stallings RL, Defelipe J, Henshall DC (2012) Silencing microRNA-134 produces neuroprotective and prolonged seizure-suppressive effects. *Nat Med*
- Kawase-Koga Y, Low R, Otaegi G, Pollock A, Deng H, Eisenhaber F, Maurer-Stroh S, Sun T (2010) RNAase-III enzyme Dicer maintains signaling pathways for differentiation and survival in mouse cortical neural stem cells. *J Cell Sci* 123: 586-594
- Khudayberdiev SA, Zampa F, Rajman M, Schratt G (2013) A comprehensive characterization of the nuclear microRNA repertoire of post-mitotic neurons. *Front. Mol. Neurosci.* 6:43. doi: 10.3389/fnmol.2013.00043
- Khvorova A, Reynolds A, Jayasena SD (2003) Functional siRNAs and miRNAs exhibit strand bias. *Cell* 115: 209-216
- Kim DH, Saetrom P, Snove O, Jr., Rossi JJ (2008) MicroRNA-directed transcriptional gene silencing in mammalian cells. *Proc Natl Acad Sci U S A* 105: 16230-16235
- Kim J, Krichevsky A, Grad Y, Hayes GD, Kosik KS, Church GM, Ruvkun G (2004) Identification of many microRNAs that copurify with polyribosomes in mammalian neurons. *Proc Natl Acad Sci U S A* 101: 360-365
- Kim Y, Kim VN (2012) MicroRNA factory: RISC assembly from precursor microRNAs. *Mol Cell* 46: 384-386

- Kosik KS (2006) The neuronal microRNA system. *Nat Rev Neurosci* 7: 911-920
- Krol J, Buskamp V, Markiewicz I, Stadler MB, Ribi S, Richter J, Duebel J, Bicker S, Fehling HJ, Schubeler D, Oertner TG, Schratt G, Bibel M, Roska B, Filipowicz W (2010a) Characterizing light-regulated retinal microRNAs reveals rapid turnover as a common property of neuronal microRNAs. *Cell* 141: 618-631
- Krol J, Loedige I, Filipowicz W (2010b) The widespread regulation of microRNA biogenesis, function and decay. *Nat Rev Genet* 11: 597-610
- Kwak PB, Tomari Y (2012) The N domain of Argonaute drives duplex unwinding during RISC assembly. *Nat Struct Mol Biol* 19: 145-151
- Kye, M.J., Liu, T., Levy, S.F., Xu, N.L., Groves, B.B., Bonneau, R., Lao, K., and Kosik, K.S. (2007). Somatodendritic microRNAs identified by laser capture and multiplex RT-PCR. *RNA* 13, 1224-1234.
- Lagos-Quintana M, Rauhut R, Yalcin A, Meyer J, Lendeckel W, Tuschl T (2002) Identification of tissue-specific microRNAs from mouse. *Curr Biol* 12: 735-739
- Lewis BP, Burge CB, Bartel DP (2005) Conserved seed pairing, often flanked by adenosines, indicates that thousands of human genes are microRNA targets. *Cell* 120: 15-20
- Li S, Liu L, Zhuang X, Yu Y, Liu X, Cui X, Ji L, Pan Z, Cao X, Mo B, Zhang F, Raikhel N, Jiang L, Chen X (2013) MicroRNAs inhibit the translation of target mRNAs on the endoplasmic reticulum in Arabidopsis. *Cell* 153: 562-574
- Liao JY, Ma LM, Guo YH, Zhang YC, Zhou H, Shao P, Chen YQ, Qu LH (2010) Deep sequencing of human nuclear and cytoplasmic small RNAs reveals an unexpectedly complex subcellular distribution of miRNAs and tRNA 3' trailers. *PLoS One* 5: e10563
- Liu J, Valencia-Sanchez MA, Hannon GJ, Parker R (2005) MicroRNA-dependent localization of targeted mRNAs to mammalian P-bodies. *Nat Cell Biol* 7: 719-723
- Lugli, G., Larson, J., Martone, M.E., Jones, Y., and Smalheiser, N.R. (2005). Dicer and eIF2c are enriched at postsynaptic densities in adult mouse brain and are modified by neuronal activity in a calpain-dependent manner. *J Neurochem* 94, 896-905.
- Lugli G, Torvik VI, Larson J, Smalheiser NR (2008) Expression of microRNAs and their precursors in synaptic fractions of adult mouse forebrain. *J Neurochem* 106: 650-661
- Magill ST, Cambronne XA, Luikart BW, Liroy DT, Leighton BH, Westbrook GL, Mandel G, Goodman RH (2010) microRNA-132 regulates dendritic growth and arborization of newborn neurons in the adult hippocampus. *Proc Natl Acad Sci U S A* 107: 20382-20387

- Majid S, Dar AA, Saini S, Yamamura S, Hirata H, Tanaka Y, Deng G, Dahiya R (2010) MicroRNA-205-directed transcriptional activation of tumor suppressor genes in prostate cancer. *Cancer* 116: 5637-5649
- Makeyev EV, Zhang J, Carrasco MA, Maniatis T (2007) The MicroRNA miR-124 promotes neuronal differentiation by triggering brain-specific alternative pre-mRNA splicing. *Mol Cell* 27: 435-448
- McNeill E, Van Vactor D (2012) MicroRNAs shape the neuronal landscape. *Neuron* 75: 363-379
- Meister G (2013) Argonaute proteins: functional insights and emerging roles. *Nat Rev Genet* 14: 447-459
- Mellios N, Sugihara H, Castro J, Banerjee A, Le C, Kumar A, Crawford B, Strathmann J, Tropea D, Levine SS, Edbauer D, Sur M (2011) miR-132, an experience-dependent microRNA, is essential for visual cortex plasticity. *Nat Neurosci* 14: 1240-1242
- Miska EA, Alvarez-Saavedra E, Townsend M, Yoshii A, Sestan N, Rakic P, Constantine-Paton M, Horvitz HR (2004) Microarray analysis of microRNA expression in the developing mammalian brain. *Genome Biol* 5: R68
- Morris KV (2011) The emerging role of RNA in the regulation of gene transcription in human cells. *Semin Cell Dev Biol* 22: 351-358
- Muddashetty RS, Kelic S, Gross C, Xu M, Bassell GJ (2007) Dysregulated metabotropic glutamate receptor-dependent translation of AMPA receptor and postsynaptic density-95 mRNAs at synapses in a mouse model of fragile X syndrome. *J Neurosci* 27: 5338-5348
- Muddashetty RS, Nalavadi VC, Gross C, Yao X, Xing L, Laur O, Warren ST, Bassell GJ (2011) Reversible inhibition of PSD-95 mRNA translation by miR-125a, FMRP phosphorylation, and mGluR signaling. *Mol Cell* 42: 673-688
- Natera-Naranjo O, Aschrafi A, Gioio AE, Kaplan BB (2010) Identification and quantitative analyses of microRNAs located in the distal axons of sympathetic neurons. *RNA* 16: 1516-1529
- Nishi K, Nishi A, Nagasawa T, Ui-Tei K (2013) Human TNRC6A is an Argonaute-navigator protein for microRNA-mediated gene silencing in the nucleus. *RNA* 19: 17-35
- Place RF, Li LC, Pookot D, Noonan EJ, Dahiya R (2008) MicroRNA-373 induces expression of genes with complementary promoter sequences. *Proc Natl Acad Sci U S A* 105: 1608-1613
- Politz JC, Hogan EM, Pederson T (2009) MicroRNAs with a nucleolar location. *RNA* 15: 1705-1715

- Portnoy V, Huang V, Place RF, Li LC (2011) Small RNA and transcriptional upregulation. *Wiley Interdiscip Rev RNA* 2: 748-760
- Presutti C, Rosati J, Vincenti S, Nasi S (2006) Non coding RNA and brain. *BMC Neurosci* 7 Suppl 1: S5
- Rajasethupathy P, Fiumara F, Sheridan R, Betel D, Puthanveettil SV, Russo JJ, Sander C, Tuschl T, Kandel E (2009) Characterization of small RNAs in *Aplysia* reveals a role for miR-124 in constraining synaptic plasticity through CREB. *Neuron* 63: 803-817
- Redfern AD, Colley SM, Beveridge DJ, Ikeda N, Epis MR, Li X, Foulds CE, Stuart LM, Barker A, Russell VJ, Ramsay K, Kobelke SJ, Hatchell EC, Payne C, Giles KM, Messineo A, Gatignol A, Lanz RB, O'Malley BW, Leedman PJ (2013) RNA-induced silencing complex (RISC) Proteins PACT, TRBP, and Dicer are SRA binding nuclear receptor coregulators. *Proc Natl Acad Sci U S A* 110: 6536-6541
- Remenyi J, Hunter CJ, Cole C, Ando H, Impey S, Monk CE, Martin KJ, Barton GJ, Hutvagner G, Arthur JS (2010) Regulation of the miR-212/132 locus by MSK1 and CREB in response to neurotrophins. *Biochem J* 428: 281-291
- Robb GB, Brown KM, Khurana J, Rana TM (2005) Specific and potent RNAi in the nucleus of human cells. *Nat Struct Mol Biol* 12: 133-137
- Sanuki, R., Onishi, A., Koike, C., Muramatsu, R., Watanabe, S., Muranishi, Y., Irie, S., Uneo, S., Koyasu, T., Matsui, R., Cherasse, Y., Urade, Y., Watanabe, D., Kondo, M., Yamashita, T., and Furukawa, T. (2011). miR-124a is required for hippocampal axogenesis and retinal cone survival through Lhx2 suppression. *Nat Neurosci* 14, 1125-1134.
- Schratt G (2009) microRNAs at the synapse. *Nat Rev Neurosci* 10: 842-849
- Schratt GM, Tuebing F, Nigh EA, Kane CG, Sabatini ME, Kiebler M, Greenberg ME (2006) A brain-specific microRNA regulates dendritic spine development. *Nature* 439: 283-289
- Shibata, M., Kurokawa, D., Nakao, H., Ohmura, T., and Aizawa, S. (2008). MicroRNA-9 modulates Cajal-Retzius cell differentiation by suppressing Foxg1 expression in mouse medial pallium. *J Neurosci* 28, 10415-10421.
- Shibata, M., Nakao, H., Kiyonari, H., Abe, T., and Aizawa, S. (2011). MicroRNA-9 regulates neurogenesis in mouse telencephalon by targeting multiple transcription factors. *J Neurosci* 31, 3407-3422.
- Siegel G, Obernosterer G, Fiore R, Oehmen M, Bicker S, Christensen M, Khudayberdiev S, Leuschner PF, Busch CJ, Kane C, Hubel K, Dekker F, Hedberg C, Rengarajan B, Drepper C, Waldmann H, Kauppinen S, Greenberg ME, Draguhn A, Rehmsmeier M, Martinez J, Schratt GM (2009) A functional screen implicates microRNA-138-dependent

regulation of the depalmitoylation enzyme APT1 in dendritic spine morphogenesis. *Nat Cell Biol* 11: 705-716

Sripada L, Tomar D, Singh R (2012) Mitochondria: one of the destinations of miRNAs. *Mitochondrion* 12: 593-599

Stalder L, Heusermann W, Sokol L, Trojer D, Wirz J, Hean J, Fritzsche A, Aeschmann F, Pfanzagl V, Basselet P, Weiler J, Hintersteiner M, Morrissey DV, Meisner-Kober NC (2013) The rough endoplasmic reticulum is a central nucleation site of siRNA-mediated RNA silencing. *EMBO J* 32: 1115-1127

Stark, K.L., Xu, B., Bagchi, A., Lai, W.S., Liu, H., Hsu, R., Wan, X., Pavlidis, P., Mills, A.A., Karayiorgou, M., and Gogos, J.A. (2008). Altered brain microRNA biogenesis contributes to phenotypic deficits in a 22q11-deletion mouse model. *Nat Genet* 40, 751-760.

Sutton MA, Schuman EM (2006) Dendritic protein synthesis, synaptic plasticity, and memory. *Cell* 127: 49-58

Tan Y, Zhang B, Wu T, Skogerbo G, Zhu X, Guo X, He S, Chen R (2009) Transcriptional inhibition of *Hoxd4* expression by miRNA-10a in human breast cancer cells. *BMC Mol Biol* 10: 12

Tang R, Li L, Zhu D, Hou D, Cao T, Gu H, Zhang J, Chen J, Zhang CY, Zen K (2012) Mouse miRNA-709 directly regulates miRNA-15a/16-1 biogenesis at the posttranscriptional level in the nucleus: evidence for a microRNA hierarchy system. *Cell Res* 22: 504-515

Thomas MF, Abdul-Wajid S, Panduro M, Babiarz JE, Rajaram M, Woodruff P, Lanier LL, Heissmeyer V, Ansel KM (2012) Eri1 regulates microRNA homeostasis and mouse lymphocyte development and antiviral function. *Blood* 120: 130-142

Van Spronsen, M., Van Battum, E.Y., Kuijpers, M., Vangoor, V.R., Rietman, M.L., Pothof, J., Gummy, L.F., Van Ijcken, W.F., Akhmanova, A., Pasterkamp, R.J., and Hoogenraad, C.C. (2013). Developmental and Activity-Dependent miRNA Expression Profiling in Primary Hippocampal Neuron Cultures. *PLoS One* 8, e74907.

Vo N, Klein ME, Varlamova O, Keller DM, Yamamoto T, Goodman RH, Impey S (2005) A cAMP-response element binding protein-induced microRNA regulates neuronal morphogenesis. *Proc Natl Acad Sci U S A* 102: 16426-16431

Wayman GA, Davare M, Ando H, Fortin D, Varlamova O, Cheng HY, Marks D, Obrietan K, Soderling TR, Goodman RH, Impey S (2008) An activity-regulated microRNA controls dendritic plasticity by down-regulating p250GAP. *Proc Natl Acad Sci U S A* 105: 9093-9098

West AE, Greenberg ME (2011) Neuronal activity-regulated gene transcription in synapse development and cognitive function. *Cold Spring Harb Perspect Biol* 3

West AE, Griffith EC, Greenberg ME (2002) Regulation of transcription factors by neuronal activity. *Nat Rev Neurosci* 3: 921-931

Yang JS, Maurin T, Robine N, Rasmussen KD, Jeffrey KL, Chandwani R, Papapetrou EP, Sadelain M, O'Carroll D, Lai EC (2010) Conserved vertebrate mir-451 provides a platform for Dicer-independent, Ago2-mediated microRNA biogenesis. *Proc Natl Acad Sci U S A* 107: 15163-15168

Yao B, La LB, Chen YC, Chang LJ, Chan EK (2012) Defining a new role of GW182 in maintaining miRNA stability. *EMBO Rep* 13: 1102-1108

Yoo AS, Staahl BT, Chen L, Crabtree GR (2009) MicroRNA-mediated switching of chromatin-remodelling complexes in neural development. *Nature* 460: 642-646

Younger ST, Corey DR (2011) Transcriptional gene silencing in mammalian cells by miRNA mimics that target gene promoters. *Nucleic Acids Res* 39: 5682-5691

Zeng Y, Cullen BR (2002) RNA interference in human cells is restricted to the cytoplasm. *RNA* 8: 855-860

Zeng Y, Cullen BR (2004) Structural requirements for pre-microRNA binding and nuclear export by Exportin 5. *Nucleic Acids Res* 32: 4776-4785

Zhao, C., Sun, G., Li, S., and Shi, Y. (2009). A feedback regulatory loop involving microRNA-9 and nuclear receptor TLX in neural stem cell fate determination. *Nat Struct Mol Biol* 16, 365-371.

Zisoulis DG, Kai ZS, Chang RK, Pasquinelli AE (2012) Autoregulation of microRNA biogenesis by let-7 and Argonaute. *Nature* 486: 541-544

5 REPRINTS OF ORIGINAL PUBLICATIONS

5.1 Mef2-mediated transcription of the mir379-410 cluster regulates activity-dependent dendritogenesis by fine-tuning Pumilio2 protein levels.

Fiore R*, **Khudayberdiev S***, Christensen M, Siegel G, Flavell SW, Kim TK, Greenberg ME, Schratt G (2009) EMBO J 28: 697-710

* with equal contribution

Mef2-mediated transcription of the miR379–410 cluster regulates activity-dependent dendritogenesis by fine-tuning Pumilio2 protein levels

This is an open-access article distributed under the terms of the Creative Commons Attribution License, which permits distribution, and reproduction in any medium, provided the original author and source are credited. This license does not permit commercial exploitation without specific permission.

Roberto Fiore^{1,4}, Sharof Khudayberdiev^{1,4},
Mette Christensen^{1,2}, Gabriele Siegel¹,
Steven W Flavell³, Tae-Kyung Kim³,
Michael E Greenberg³ and
Gerhard Schratt^{1,*}

¹Interdisziplinäres Zentrum für Neurowissenschaften, SFB488 Junior Group, Universität Heidelberg, and Institut für Neuroanatomie, Universitätsklinikum Heidelberg, Heidelberg, Germany, ²Wilhelm Johannsen Center for Functional Genome Research, Department of Cellular and Molecular Medicine, University of Copenhagen, Blegdamsvej, Denmark and ³Department of Neurobiology, Harvard Medical School, Boston, MA, USA

Neuronal activity orchestrates the proper development of the neuronal circuitry by regulating both transcriptional and post-transcriptional gene expression programmes. How these programmes are coordinated, however, is largely unknown. We found that the transcription of miR379–410, a large cluster of brain-specific microRNAs (miRNAs), is induced by increasing neuronal activity in primary rat neurons. Results from chromatin immunoprecipitation and luciferase reporter assays suggest that binding of the transcription factor myocyte enhancing factor 2 (Mef2) upstream of miR379–410 is necessary and sufficient for activity-dependent transcription of the cluster. Mef2-induced expression of at least three individual miRNAs of the miR379–410 cluster is required for activity-dependent dendritic outgrowth of hippocampal neurons. One of these miRNAs, the dendritic miR-134, promotes outgrowth by inhibiting translation of the mRNA encoding for the translational repressor Pumilio2. In summary, we have described a novel regulatory pathway that couples activity-dependent transcription to miRNA-dependent translational control of gene expression during neuronal development.

The EMBO Journal advance online publication, 5 February 2009; doi:10.1038/emboj.2009.10

Subject Categories: chromatin & transcription; neuroscience
Keywords: dendritogenesis; Mef2; microRNA; neuronal activity; Pumilio

*Corresponding author. Interdisziplinäres Zentrum für Neurowissenschaften, SFB488 Junior Group, University of Heidelberg, Im Neuenheimer Feld 345, 69210 Heidelberg, Germany.
Tel.: +49 6221 566210; Fax: +49 6221 567897;
E-mail: schratt@ana.uni-heidelberg.de

⁴These authors contributed equally to this work

Received: 11 September 2008; accepted: 23 December 2008

Introduction

The development and refinement of neuronal circuitry are regulated by both intrinsic and activity-dependent programmes of gene expression (Flavell and Greenberg, 2008). The latter is particularly important at later stages of neuronal development, such as dendritogenesis (Chen and Ghosh, 2005) and synapse formation (Waites *et al.*, 2005). An important layer of regulation is new transcription induced by activity-regulated transcription factors (Hong *et al.*, 2005). For example, CREB has a key function in activity-dependent dendritic outgrowth of central neurons (Lonze and Ginty, 2002; Redmond *et al.*, 2002). On the other hand, the activity-dependent transcription factor, myocyte enhancing factor 2 (Mef2), functions as a negative regulator of excitatory synapse number (Flavell *et al.*, 2006; Shalizi *et al.*, 2006). Morphological abnormalities in dendritic arbourization and postsynaptic structure are common hallmarks of a number of cognitive diseases, for example, mental retardation (Bagni and Greenough, 2005). Activity-dependent regulation of gene expression involves, in addition to the activation of new transcriptional programmes within the nucleus, also post-transcriptional control of pre-existing mRNAs (Steward, 2002). The expression of pre-existing mRNAs is often regulated locally in dendrites close to synaptic contacts (Sutton and Schuman, 2006). Important post-transcriptional regulatory molecules are RNA-binding proteins (i.e. CPEB, Pumilio (Pum), etc.) that regulate transport, stability or translation of the mRNAs in response to activity (Kiebler and Bassell, 2006; Richter, 2007). MicroRNAs (miRNAs) are another class of key post-transcriptional regulators that can bind to the 3'UTR of target mRNAs to downregulate their expression by inducing either mRNA degradation or translational suppression (Kosik, 2006; Fiore *et al.*, 2008). Little is known, however, on how these two mechanisms of activity-dependent gene expression, global transcriptional control and local post-transcriptional control, are coordinated within a neuron.

We have previously shown that miR-134 controls spine morphogenesis in rat hippocampal neuron by repressing local translation of the LimK1 mRNA within dendrites (Schratt *et al.*, 2006). BDNF, which is secreted in response to neuronal activity, relieves the translational block of the LimK1 mRNA thereby allowing spine growth. It is still an open question whether miR-134 function is also controlled globally within a neuron at the transcriptional level. Intriguingly, the miR-134 gene is clustered together with more than 50 other miRNAs within the *Gtl2/Dlk1* locus (referred hereafter as the miR379–410 cluster) (Seitz *et al.*, 2004). Clustered miRNA genes are often co-expressed, a prerequisite for the coordinated control

of related biological processes (He *et al*, 2005). In this study, we provide evidence that the entire miR379–410 cluster is co-regulated at the transcriptional level by neuronal activity in a Mef2-dependent manner. Importantly, activity-dependent regulation of multiple miRNAs from the cluster, including miR-134, is necessary for the correct elaboration of the dendritic tree. Furthermore, we show that the RNA-binding protein Pum2 is a direct miR-134 target and a key mediator of the miR-134 growth-promoting effect on dendritogenesis. Our results point to the miR379–410 cluster, in particular miR-134, as a key component of a mechanism that couples transcriptional and local control of gene expression in response to neuronal activity during the development of neural circuitry.

Results

The miR379–410 cluster is co-regulated by neuronal activity

Recently, we provided evidence that miR-134 regulates activity-dependent control of dendritic mRNA translation in response to BDNF. We decided to investigate whether neuronal activity also regulates miR-134 and possibly the entire miR379–410 cluster globally within the cell at the transcriptional level.

We first tested whether expression of candidate miRNAs of the miR379–410 cluster was coordinately induced by neuronal activity. We used either membrane-depolarizing concentrations of KCl, which leads to Ca²⁺ influx, or the application of BDNF, a growth factor released by synaptic stimulation, as paradigms to mimic neuronal activity in a culture of dissociated neurons (Redmond *et al*, 2002; Wayman *et al*, 2006). Primary cortical neurons cultured for 5 days *in vitro* (5DIV) were treated with either BDNF or KCl for up to 6 h. After isolation of total RNA, the expression of pre-miRNAs that are encoded at different positions within the *GTL2/DLK1* locus was analysed by quantitative RT-PCR (Figure 1A). Consistent with our earlier findings, miRNAs from the miR379–410 cluster (including miR-134) are expressed at very low levels in unstimulated neurons at this early developmental stage. Strikingly, all of the tested pre-miRNAs located within miR379–410 were robustly induced by both BDNF and KCl

stimulation. Similar to the known activity-regulated *cFos* gene, miR379–410 pre-miRNA induction was both rapid and transient, peaking at 2 h and lasting for at least 6 h. The level of the neighbouring *Gtl2* transcript was not affected by KCl and BDNF (Figure 1A–C), demonstrating that our treatment led to a specific induction of the miR379–410 domain.

We next investigated the effect of membrane depolarization on the levels and subcellular localization of one of the miR379–410 miRNAs, miR-134, by *in situ* hybridization (ISH) of primary hippocampal neurons (DIV7). We used a probe that was able to recognize both mature and pre-miR-134. (Figure 1D). Low levels of miR-134 were detectable in unstimulated neurons and KCl led to a robust and specific increase in miR-134 ISH signal, confirming our results obtained with quantitative RT-PCR (Figure 1B). The KCl-mediated increase was completely abolished by pretreatment of neurons with actinomycin D, demonstrating that the increase was due to *de novo* miR-134 transcription (data not shown). The increase of miR-134 upon depolarization was not restricted to the soma but the miR-134 signal was also evident in dendrites (Figure 1D, higher magnification panels). Quantification of the *in situ* signal confirmed the depolarization-induced increase of miR-134 in both the somatic and dendritic compartments (Figure 1E). The robust increase of miR-134 in dendrites suggests a local function in this compartment. So far, our expression analysis did not directly address whether our activity paradigm induces functional miR379–410 miRNAs. To verify that neuronal activation induces the expression of mature and functional miRNAs from the cluster, we used a previously described single cell sensor assay (Mansfield *et al*, 2004). We used bicistronic GFP/dsRED expression vectors ('sensor'), the expression of which is controlled by miR379–410 miRNAs due to two perfectly complementary miRNA-binding sites in the 3'UTR of the dsRED gene. Neurons that express functional miRNA (miRNA positive) are identified by the lack of dsRED due to RISC-mediated cleavage of the dsRED mRNA (Figure 1F). The number of miRNA-positive neurons increased upon depolarization for all tested miR379–410 miRNAs (Figure 1F), validating that neuronal activity induces functional miRNAs. Co-transfection of the sensors with specific 2'-O-methyl antisense oligonucleotides (anti-miRs) confirmed

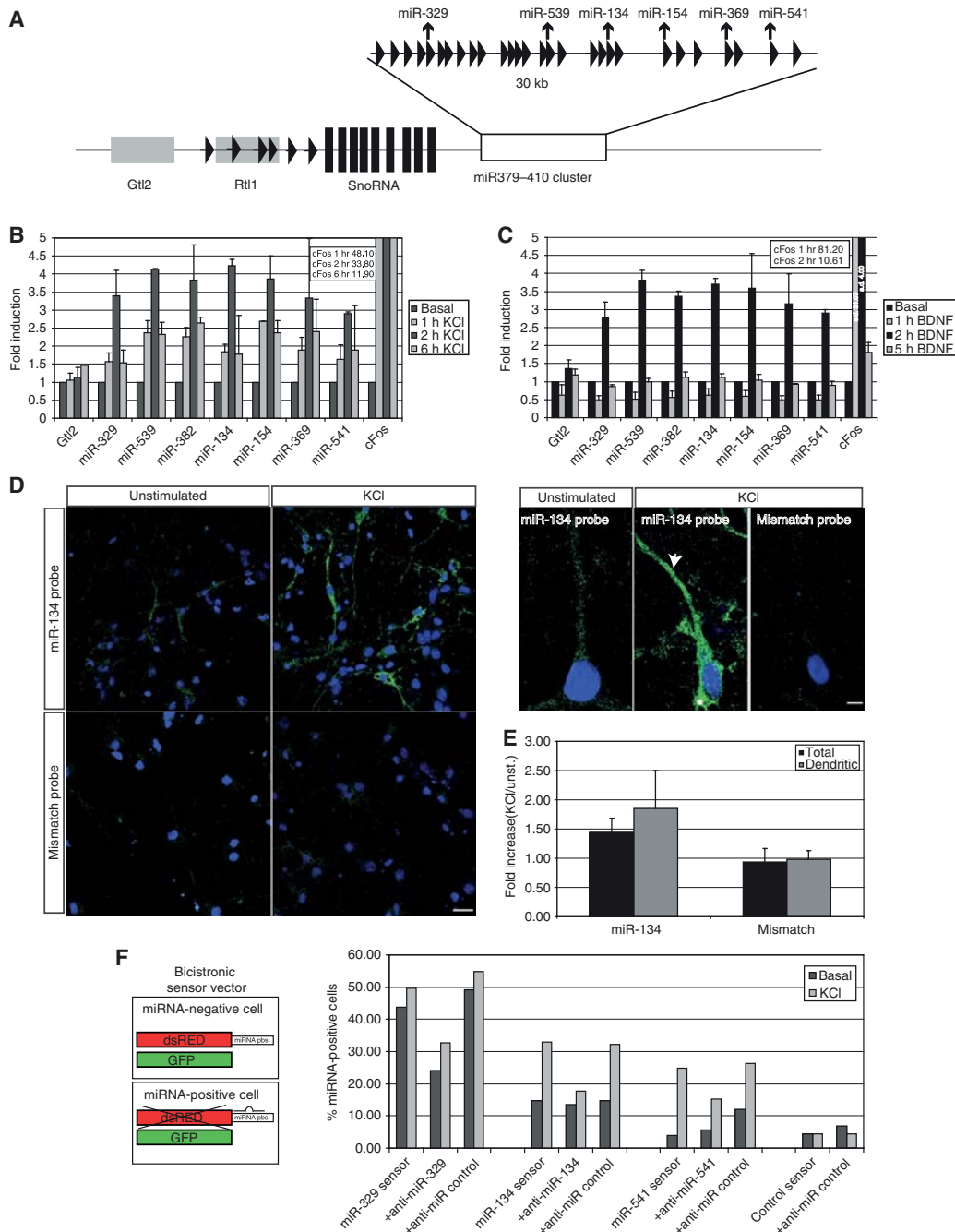
Figure 1 The miR379–410 cluster is co-regulated by neuronal activity. (A) Schematic representation of the mouse *GTL2/RTL1* locus on distal chromosome 12. miRNA genes are indicated by triangles, small nucleolar RNAs (SnoRNA) by filled bars, the non-coding *RTL1* and *GTL2* genes by grey rectangles and the miR379–410 cluster by an open rectangle. Arrows point to miRNAs analysed by RT-PCR and sensor assays. Diagram is not drawn to scale. (B) Membrane depolarization increases miR379–410 precursor expression. Quantitative RT-PCR analysis of total RNA extracted from KCl-stimulated primary cortical neurons. DIV5 cortical neurons were treated for 6 h with 16 mM KCl, and total RNA was isolated at different time points during the stimulation period and analysed by real-time PCR with primers for different miRNA precursors located within the *GTL2/RTL1* locus, *cFos* (positive control) and *GTL2* (negative control). The data are normalized to β 3-tubulin and presented as relative to the basal. Data represent the average of three independent experiments + s.d. *cFos* induction values are out of scale and indicated in the insert. (C) BDNF treatment increases miR379–410 precursor expression. Real-time PCR analysis of total RNA extracted from BDNF-stimulated primary cortical neurons. DIV5 cortical neurons were treated for 6 h with 40 ng/ml BDNF; total RNA was isolated at different time points during the stimulation and analysed as in (B). Data represent the average of three independent experiments + s.d. *cFos* induction values are out of scale and indicated in the insert. (D) Effect of membrane depolarization on the subcellular localization of miR-134 in hippocampal neurons. DIV7 rat hippocampal neurons were stimulated for 6 h with 16 mM KCl, fixed and analysed by fluorescent *in situ* hybridization. A DIG-labelled LNA probe directed against miR-134 (miR-134 probe) and a DIG-labelled control probe of unrelated sequence (mismatch probe) were used (5 pmol each). Representative images for unstimulated cells (left panels) and KCl-treated neurons (right panels) are shown. Higher panels show the robust increase in miR-134 signal in both the neuronal soma (asterisks) and dendrites (arrowheads) upon KCl stimulation. Scale bars: 20 and 5 μ m. (E) Quantification of miR-134 levels obtained by ISH analysis. Ten pictures for each experimental condition were measured to calculate the average intensity of the fluorescent signal obtained with the indicated probes. Data are presented as the fold increase in average intensity in KCl-treated versus unstimulated whole cells (total) and dendrite only (dendritic). Error bars represent the average of two independent experiments + s.d. (F) Membrane depolarization increases functional miR379–410 miRNAs. An miRNA sensor assay was performed in KCl-stimulated hippocampal neurons. The principle of an miRNA sensor assay is described on the left. Right: hippocampal neurons (DIV4) were transfected with the indicated sensors (50 ng) alone or in combination with the indicated anti-miRs (50 nM). After KCl incubation (DIV7), cells were fixed and miRNA-positive cells were scored based on the fluorescent sensor signal. Results from one representative out of three independent experiments are shown.

that the increase in miRNA-positive cells was due to a specific elevation of miRNA activity. These results also demonstrate that anti-miRs can be used to specifically interfere with the function of the KCl-induced miRNAs miR-329, -134 and -541.

Mef2 is necessary for activity-dependent regulation of the miRNA-379–410 cluster

We devised a comparative genomic approach based on sequence conservation to identify regulatory elements

that could mediate activity-dependent transcription of the miR379–410 cluster. Highly conserved regions within 20 kb upstream of the cluster were screened for potential binding sites for activity-regulated transcription factors (Figure 2A). Thereby, we identified 10 potential binding sites for Mef2, a known activity-regulated transcription factor that negatively regulates synapse number in mature hippocampal neurons (Shalizi and Bonni, 2005). The occupancy of the putative Mef2-binding sites (MBSs) *in vivo* was assessed by chromatin



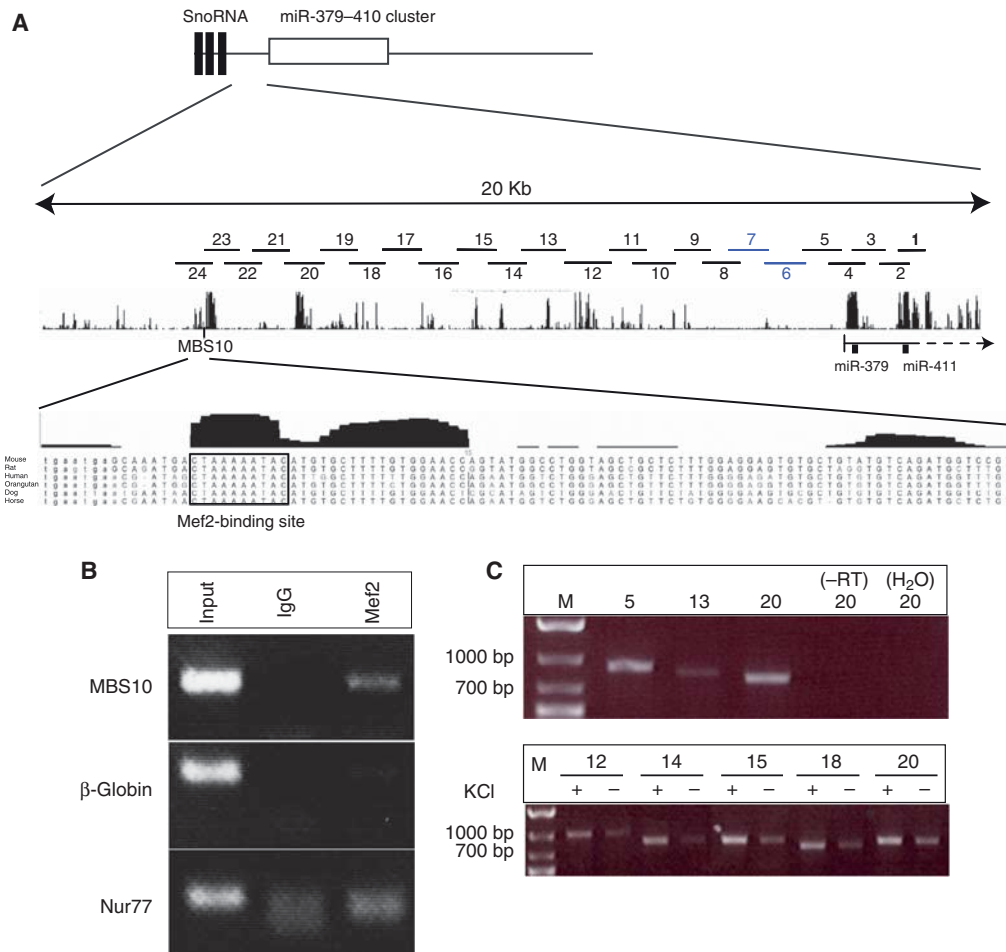


Figure 2 A Mef2-binding site (MBS10) is located upstream of the miR379–410 cluster. (A) Alignment of the 20 kb directly upstream of the miR379–410 cluster. Peaks represent conserved regions, the position of MBS10 and the sequence conservation of the consensus are shown. The different PCR fragments that were amplified are indicated by black numbers, fragments that failed to be amplified due to the repetitive nature of the sequence are indicated by blue numbers. (B) MBS10 is bound by Mef2 in native chromatin *in vivo*. ChIP was performed in primary cortical neurons (5DIV) using an anti-Mef2 antibody or IgG as a control. Primers that specifically amplify the genomic region of MBS10, β -globin or Nur77 promoter were used for PCR amplification. Input corresponds to genomic DNA isolated before immunoprecipitation. One representative out of three independent experiments is shown. (C) A continuous transcript spans the region between MBS10 and miR-379. Semiquantitative RT–PCR analysis was performed on cortical neurons (5DIV) that were either left untreated or membrane depolarized (16 mM KCl, 6 h). Overlapping primer pairs specific for the genomic location indicated in (A) were used. Only the amplification products of a few selected PCR reactions are shown.

immunoprecipitation (ChIP) using DIV5 primary cortical neurons (Figure 2B and data not shown). A PCR product encompassing one of the potential MBS, MBS10, could be specifically amplified from immunoprecipitates of formaldehyde-fixed chromatin using a Mef2-specific antibody (Figure 2B, upper panel), in a similar manner as the known Mef2 target gene Nur77 (Figure 2B, upper and lower panels). In contrast, Mef2 antibodies were unable to enrich chromatin from the β -globin locus that lacks a MBS, confirming the specificity of our ChIP protocol. Therefore, Mef2 is bound to MBS10 in neurons *in vivo*. To begin to assess the relevance of MBS10 in activity-dependent transcription of miR379–410, we first monitored the presence of a transcript between the miR-379 gene and MBS10. Using RT–PCR with a set of overlapping primers located within the region from MBS10 to miR-379, we were able to detect a continuous transcript except for a small gap (Figure 2A and C,

primer pairs 6 and 7, and data not shown). This gap consists of highly repetitive sequence that is likely resistant to PCR amplification. In further support of the existence of a long, continuous transcript spanning the region from MBS10 all the way to the end of the miR379–410 cluster, we found that the detected PCR fragments, similar to the adjacent miRNA genes, were robustly induced by depolarization (Figure 2C). Taken together, our transcript analysis supports the idea that the miR379–410 cluster is transcribed as a single polycistronic unit starting in the proximity of MBS10.

To test the functionality of MBS10, we cloned either the wild-type or a mutated MBS10 upstream of a minimal promoter driving the firefly luciferase reporter gene (pGL3-MBS10). The expression of a constitutively active mutant of Mef2 (Mef2-VP16) in cortical neurons induced luciferase activity from MBS10 reporter construct (Figure 3A) to a

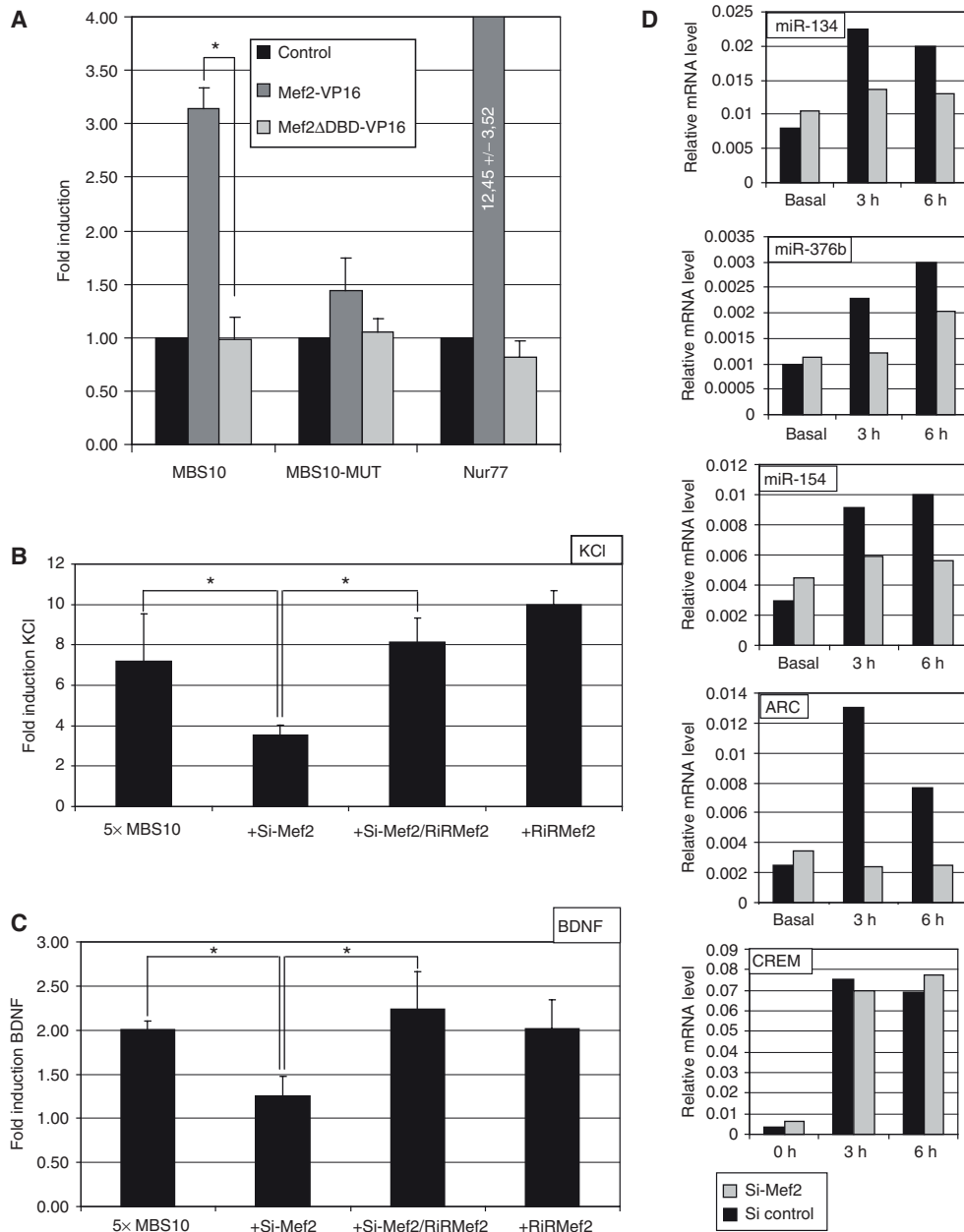


Figure 3 Mef2 is necessary for activity-dependent regulation of the miR379–410 cluster. (A) Binding of Mef2 to MBS10 activates transcription. Reporter genes containing either a wt or mutant MBS10 (MBS10-luc and MBS10-mut-luc, 50 ng) upstream of the luciferase coding region were transfected into cortical neurons (5DIV) along with expression plasmids for constitutively active Mef2 (Mef2-VP16) or a DNA-binding deficient mutant (Mef2- Δ DBD-VP16, 200 ng each). The Mef2 responsive Nur77 reporter was used as a positive control. Luciferase activity was determined and normalized to the internal *Renilla* control. Fold inductions were derived by dividing the normalized luciferase activity of Mef2-expressing neurons to that of control-transfected neurons. Data represent the mean of three independent experiments + s.d. * P < 0.05 (t -test). (B) Mef2 is required for activity-dependent transcription of a MBS10-driven reporter gene. MBS10-luc (100 ng) was transfected into cortical neurons (5DIV) along with a Mef2 shRNA construct (Si-Mef2, 5 ng) and/or an RNAi-resistant Mef2 expression construct (RiRMef2, 100 ng). Neurons were either left untreated or membrane depolarized (57 mM KCl, 6 h). Luciferase activity was determined and normalized to the internal *Renilla* control. Fold inductions were derived by dividing the normalized activity of KCl-treated neurons to that of untreated neurons. Data represents the mean of three independent experiments + s.d. * P < 0.05 (t -test). (C) Mef2 is required for BDNF-dependent transcription of a MBS10-driven reporter gene. Neurons were transfected and treated as in B). Data represents the mean of at least three independent experiments + s.d. * P < 0.05 (t -test). (D) Regulation of activity-dependent transcription of the endogenous miRNAs of the miR379–410 cluster by Mef2. Hippocampal neurons were infected with lentiviruses expressing either an shRNA directed against Mef2 (Si-Mef2) or against an unrelated sequence (Si control). Neurons were stimulated with KCl for up to 6 h, total RNA was isolated at the indicated time points and analysed by quantitative RT-PCR using primers specific for miR379–410 precursors, Arc (positive control) and CREM (negative control). For miR-134, one representative out of three independent experiments is shown.

similar extent as a promoter construct derived from a known Mef2 target gene (pGL3-Nur77). The DNA-binding deficient mutant Mef2 Δ DBD-VP16 failed to increase the activity of both the Nur77 and MBS10 luciferase reporters, suggesting that induction is dependent upon Mef2 binding. This is further supported by the lack of induction of the pGL3-MBS10mut upon co-transfection with Mef2-VP16 (Figure 3A). We next investigated the role of endogenous Mef2 in activity-dependent transcriptional control of the cluster. KCl or BDNF stimulation induced expression of pGL3-MBS10, with a more prominent effect observed in membrane-depolarized neurons (Figure 3B and C). Importantly, both KCl and BDNF (Figure 3B and C)-mediated induction were strongly attenuated upon Mef2 knockdown using a previously published Mef2 shRNA construct (Flavell *et al*, 2006). Simultaneous introduction of an RNAi-resistant Mef2 expression vector (RiRMef2) completely abolished the inhibitory effect of Mef2 knockdown, demonstrating the specificity of the siRNAs. Taken together, results from reporter assays suggest that endogenous Mef2 is required for the depolarization-induced regulation of the miRNA cluster. To confirm that activity-regulated transcription of the endogenous miRNAs is Mef2 dependent, we infected primary neurons using a lentivirus expressing the described Mef2 siRNA. Infected cultures were stimulated with KCl and the levels of selected endogenous miR379–410 pre-miRNAs were assessed by quantitative RT–PCR. For all the miRNAs from the cluster analysed (miR-134 -154, and -376b), Mef2 knockdown significantly reduced the magnitude of KCl-mediated induction (Figure 3D). This effect was specific, as Mef2 knockdown did not affect activity-dependent induction of CREM, a gene that is not regulated by Mef2. Taken together, our data indicate that Mef2 activates miRNA expression in response to neuronal activity by binding to a site located 20 kb upstream of the miRNA cluster.

Activity-dependent expression of miR379–410 cluster miRNAs is necessary for dendritic development

A large number of studies have provided evidence that activity-dependent transcription during early stages of synaptic development has a critical function in dendritic outgrowth (Whitford *et al*, 2002). To address the physiological relevance of activity-dependent transcription of the miR379–410 cluster, we therefore tested whether perturbation of miR379–410 members affected the ability of neurons to elaborate the dendritic tree in response to activity. To mimic activity-dependent dendritogenesis *in vitro*, cultured hippocampal neurons (DIV7) were treated for 6 h with KCl or BDNF and analysed by Sholl analysis (see Materials and methods) at DIV10 (Wayman *et al*, 2006). Both membrane depolarization and BDNF treatment increased the complexity of the dendritic arbour (Figure 4A, left panel) as indicated by a higher number of branches and an increase in the total dendritic length. To obtain a quantitative estimate of activity-dependent changes in complexity, we calculated an induction index by dividing the total number of intersections derived from the Sholl analysis of stimulated neurons to that of unstimulated neurons. Treating neurons with a specific miR-134 anti-miR completely abolished the KCl- and BDNF-mediated increase in dendritic complexity, but had no significant effect on dendrites under basal conditions (Figure 4A–C; Supplementary Figure S1). An antisense oligonucleotide of

unrelated sequence (anti-miR control) had no effect on dendritic complexity under both basal and stimulated conditions, demonstrating the specificity of the anti-miR-134. Furthermore, an miR-134 antisense inhibitor of a different chemistry (LNA-modified nucleotides) had a similar effect on the induction index after both KCl and BDNF stimulation (Supplementary Figure S2). We next extended our analysis to other miRNAs from the cluster. Of the four miRNAs considered, we found that anti-miR inhibition of two of them (miR-381 and -329), also blocked activity-dependent dendritogenesis (Figure 4D). Interestingly, inhibition of two other cluster members (miR-495 and -541) had no effect on dendritic complexity under our experimental conditions (Figure 4D). The lack of a dendritic phenotype is unlikely due to inefficient inhibition of these miRNAs, as anti-miRs effectively interfered with three different miRNAs in our sensors assays including miR-541 (Figure 1F). Thus, activity-dependent expression of multiple, but not all miRNAs from the miR379–410 cluster is required for activity-dependent dendritic growth. The requirement of activity-induced expression of the miR379–410 cluster is further supported by our observation that knock down of its upstream activator Mef2 phenocopies miRNA loss of function (Figure 4E). The negative effect of Mef2 siRNA on KCl-dependent dendritogenesis can be rescued by co-transfection of RiRMef2. These data show a previously unknown function of Mef2 in activity-dependent dendritogenesis and identify miRNAs from the miR379–410 cluster as one of the key mediators of this new role of Mef2.

Pum2 is an miR-134 target

To gain insight into the mechanism by which members of the miR379–410 cluster regulate dendritogenesis, we searched for target mRNAs using the Target Scan prediction algorithm. Initially, we focused on predictions that contained multiple sites for individual members of the miR379–410 cluster. Intriguingly, we found that the RNA-binding protein Pum2, a protein that has been recently implicated in the control of dendrite morphogenesis in *Drosophila melanogaster* (Ye *et al*, 2004), contains in its 3'UTR multiple potential binding sites for functionally important miR379–410 miRNAs (Figures 4D and 5A). Two Pum2 3'UTR of different lengths have been predicted. The shorter one has been experimentally isolated and includes putative binding site for miR-134 and miR-376b. The longer 3'UTR includes, in addition, sites for miR-381 and miR-329. To test whether the predicted miRNA-binding sites are functional, we cloned both Pum2 3'UTRs downstream of the coding region of a firefly luciferase reporter gene, and monitored luciferase activity in the presence of specific anti-miRs in rat cortical neurons. Under conditions of high neuronal activity, inhibition of miR-134 led to a robust increase in relative luciferase activity of the constructs containing the wild-type Pum2 3'UTR (Figure 5B; Supplementary Figure S3). Importantly anti-miR-134 did not affect luciferase activity of the reporter under basal condition (Supplementary Figure S3A), suggesting that after depolarization, newly transcribed miR-134 binds to and downregulates the expression of the Pum2 mRNA. A number of anti-miRs of different sequence, including three directed against members of the miR379–410 cluster (anti-miR-376b, -381 and -329) had no effect demonstrating the specificity of anti-miR-134 (Figure 5B and data not shown). Importantly, miR-134 is

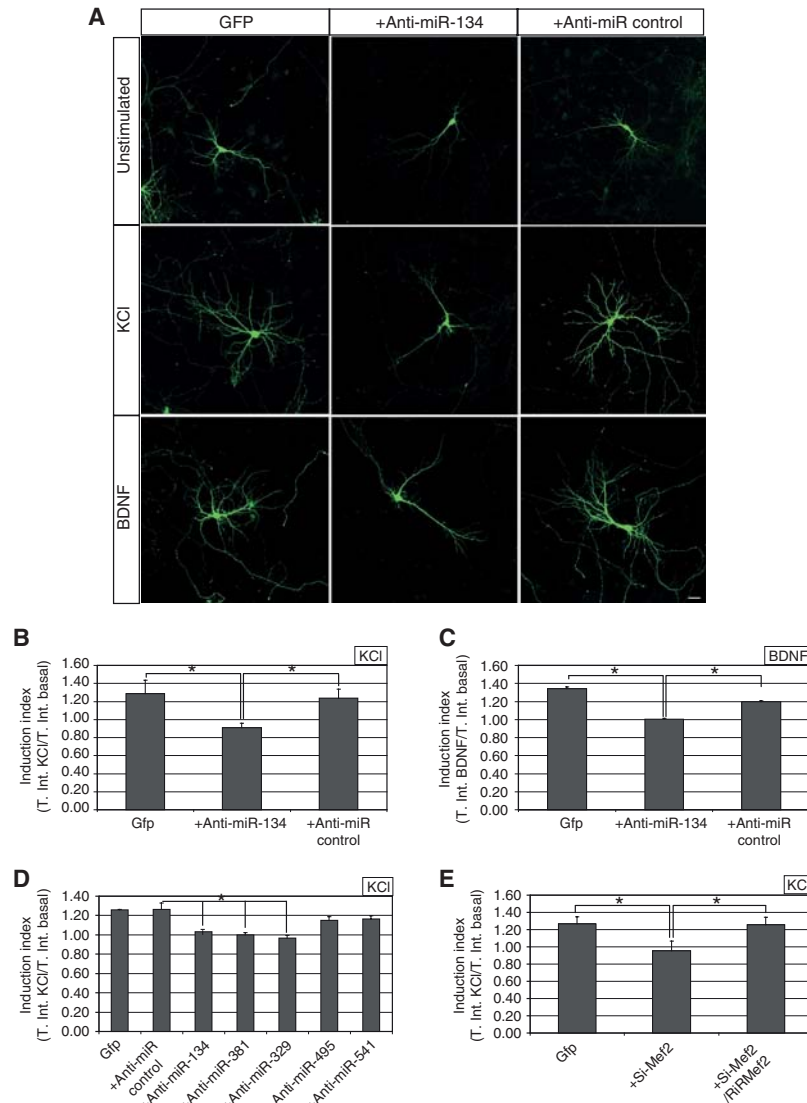


Figure 4 Several miRNAs of the miR371–410 cluster are necessary for activity-dependent dendritogenesis. (A) Hippocampal neurons (4DIV) were transfected with GFP together with the indicated anti-miRs (50 nM). At DIV7, neurons were incubated with 16 mM KCl or 40 ng/ml BDNF for 6 h and dendritic complexity was analysed at DIV10 using Sholl analysis (see Materials and methods for details). Scale bar: 20 μ m. (B) Quantification of the dendritic complexity of KCl-treated neurons after miR-134 inhibition. Dendritic complexity was calculated by Sholl analysis and the effect of the KCl stimulation on the dendritic tree is expressed as induction index (total number of intersection in stimulated neurons divided by the total number of intersection under basal condition). Here, 10–16 cells for condition were analysed in each experiment. Data represent the mean of three independent experiments + s.d. * $P < 0.05$ (*t*-test). (C) Quantification of the dendritic complexity of BDNF-treated neurons after miR-134 inhibition. Conditions and data analysis are the same as in (B). Data represent the mean of at least three independent experiments + s.d. * $P < 0.05$ (*t*-test). (D) Multiple miR379–410 members are necessary for activity-dependent dendritogenesis. Quantification of dendritic complexity of KCl-treated neurons transfected with the indicated anti-miRs (50 nM) was basically as described in (B). Here, 10–16 cells for condition were analysed in each experiment. Data represent the mean of three independent experiments + s.d. * $P < 0.05$ (*t*-test). (E) Mef2 knockdown phenocopies miR-134 loss of function in dendritogenesis. Hippocampal neurons were transfected with GFP together with a Mef2 shRNA (2 ng) and/or a construct expressing an RNAi-resistant form of Mef2 (RiRMef2, 100 ng). Treatment of neurons and data analysis were performed as described in (B). Data represent the mean of three independent experiments + s.d. * $P < 0.05$ (*t*-test).

the most conserved of the five putative binding sites (Figure 5A) we tested, and is present in both predicted isoforms of the Pum2 3'UTR. Both observations suggest a functionally significant role of the miR-134 site in the regulation of Pum2 translation. To verify that inhibition of reporter gene activity was dependent on a functional miR-134-binding

site in the 3'UTR, we cloned a luciferase reporter where the critical seed region in the miR-134 responsive element was mutated. Comparison of the mutated and wild-type Pum2 luciferase reporter activity in cortical neurons after KCl stimulation showed that, first, the mutant reporter is not downregulated after depolarization and, second, co-transfec-

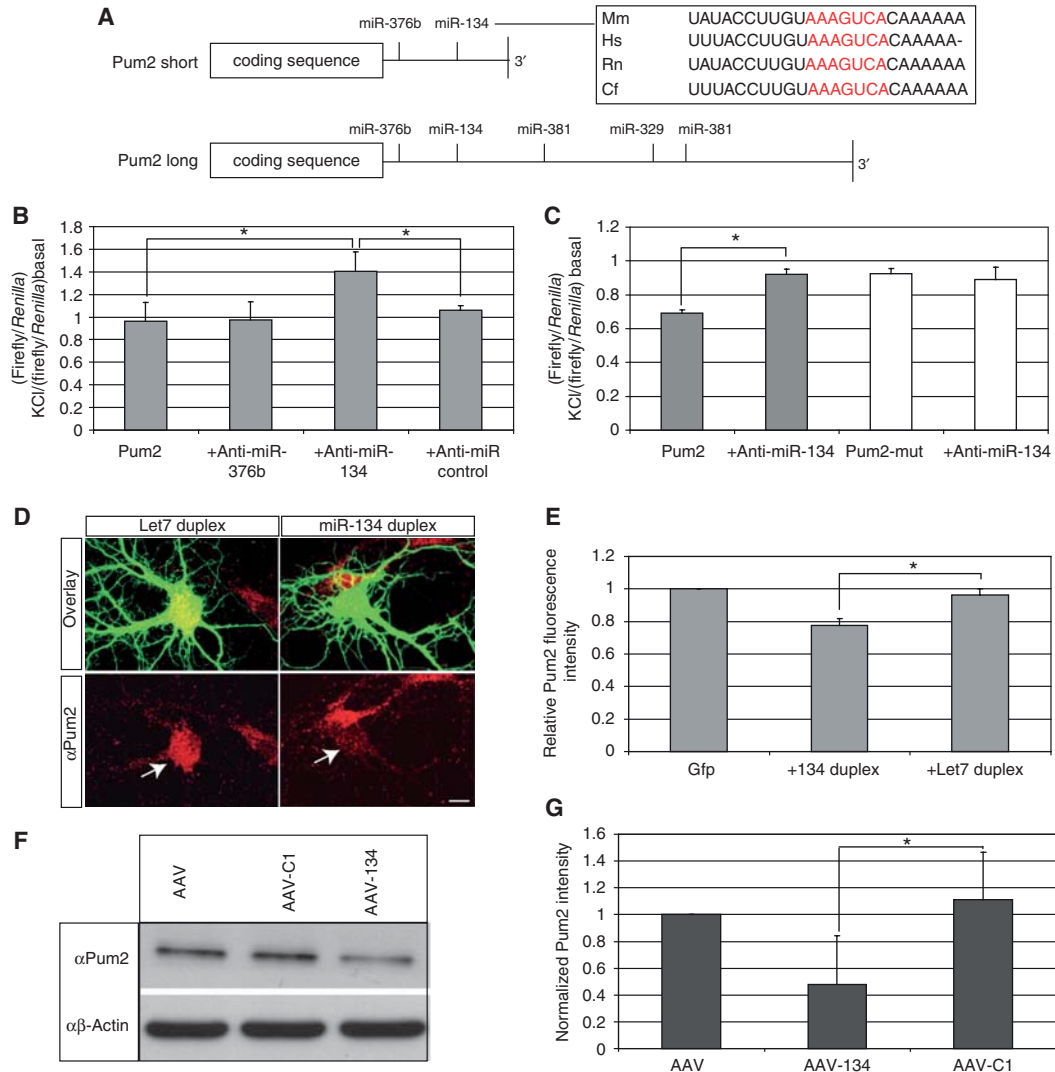


Figure 5 Pum2 is a new miR-134 target gene. (A) Schematic representation of the two predicted 3'UTRs of the Pum2 mRNA. The putative miR379–410 miRNA-binding sites in the two predicted 3'UTRs are indicated. The conservation of the miR-134 site is shown in the box, the seed sequence is in red. (B) Validation of Pum2 as miR-134 target mRNA by dual-luciferase reporter assay in membrane-depolarized cortical neurons. Cortical neurons were transfected with a luciferase reporter gene containing the shorter form of the Pum2 3'UTR downstream of the luciferase coding region (Pum2-luc, 100 ng) together with the indicated anti-miRs (60 nM). At DIV7, neurons were either left untreated or membrane depolarized (16 mM KCl, 6 h). Luciferase activity was determined and normalized to the internal *Renilla* control. Fold inductions were derived by dividing the normalized activity of KCl-treated neurons to that of untreated neurons. Data represent the mean of at least three independent experiments + s.d. * $P < 0.05$ (*t*-test). (C) Downregulation of the Pum2 luciferase reporter by miR-134 requires a functional miRNA-binding site. Cortical neurons were transfected with Pum2-luc or a reporter gene containing mutations in the seed region of the Pum2 miR-134-binding site (Pum2-mut-luc, 100 ng each), together with anti-miR-134 (60 nM) when indicated. Data analysis and presentation were performed as in (B). Data represent the mean of at least three independent experiments + s.d. * $P < 0.05$ (*t*-test). (D) Overexpression of miR-134 in hippocampal neurons downregulates the endogenous Pum2 protein. Hippocampal neurons (4DIV) were transfected with GFP together with either miR-134 or Let7 duplex RNAs (10 nM each). Neurons were fixed at DIV7 and analysed by immunocytochemistry using a rabbit polyclonal anti-Pum2 antibody. Arrows depict cell bodies of representative cells transfected either with Let-7 (left) or miR-134 (right). Note reduced Pum2 staining in miR-134-transfected neurons. Scale bar: 10 μ m. (E) Quantification of the Pum2 fluorescence intensities derived from (D). Signal intensities of Pum2 staining in transfected, GFP-positive neurons were measured for a total of 8–10 cells per experiment. Average intensities for each condition were normalized to control cells transfected with GFP only. Data represent the mean of three independent experiments + s.d. * $P < 0.05$ (*t*-test). (F) AAV-mediated miR-134 overexpression in cortical neurons downregulates Pum2 protein levels. Protein extracts from cortical neurons (DIV10–18) transduced with either AAV, AAV expressing a control shRNA (AAV-C1) or AAV expressing miR-134 (AAV-134) were analysed by western blotting using an anti-Pum2 antibody (upper panel). Probing the same blot with an anti- β -actin antibody served as a loading control (lower panel). (G) Quantification of western blot results shown in (F). The intensity of the Pum2 band was normalized to the respective signal from the β -actin blot, and the normalized Pum2 intensity of the AAV only condition was set to one. Data represent the mean of at least three independent experiments + s.d. * $P < 0.05$ (*t*-test).

tion of pGL3-Pum2mut with anti-miR-134 does not result in an increase in the activity of the reporter (Figure 5C). These results indicate that binding of miR-134 to the 3'UTR of Pum2 is critical for the repression of the reporter after KCl stimulation. Induction of other miRNAs from the cluster appears to be less relevant for the regulation of Pum2 mRNA translation, at least under our experimental conditions.

We next investigated whether miR-134 is able to downregulate the endogenous Pum2 protein. First, overexpression of miR-134 duplex RNA in hippocampal neurons resulted in a significant decrease in endogenous Pum2 protein levels as assessed by immunocytochemistry (Figure 5D and E). As a control, overexpression of an unrelated miRNA (Let-7) did not affect Pum2 levels in transfected neurons (Figure 5D and E).

Second, transduction of rat hippocampal neurons with an adeno-associated virus (AAV) overexpressing miR-134 led to a significant decrease in Pum2 protein levels compared with control conditions as assessed by western blotting. β -Actin levels remained unchanged (Figure 5F and G).

Co-transfection of the Pum2 luciferase reporter together with either Si-Mef2 or Mef2-VP16 confirmed that Mef2 contributes to KCl-mediated inhibition of the reporter (Supplementary Figure S4A) and that activated Mef2 on its own is sufficient to induce a significant decrease in Pum2 reporter gene activity (Supplementary Figure S4B). In summary, our results indicate that miR-134 is a negative regulator of Pum2 protein expression following membrane depolarization. They further suggest that Mef2 is an important component of this pathway, presumably through induction of miR-134.

Downregulation of Pum2 by miR-134 is necessary for activity-dependent dendritogenesis

The *Drosophila* Pum homologue is essential for dendrite morphogenesis in peripheral neurons, suggesting that the Pum2-miR-134 interaction might also be involved in this process in mammals. We used RNA interference to probe the function of Pum2 in miR-134-regulated activity-dependent dendritogenesis. Two siRNAs (Si-Pum2-1 and Si-Pum2-2) directed against the rat Pum2 mRNA were able to efficiently downregulate the expression of recombinant Pum2 in HEK293T cells (Figure 6A). Immunocytochemistry revealed a significant and specific decrease in the endogenous protein in hippocampal neurons upon transfection of one of the active siRNAs, Si-Pum2-2 (Figure 6B). To determine whether Pum2 is a physiologically relevant miR-134 target for activity-dependent dendritogenesis, we asked whether siRNA-mediated reduction of Pum2 levels was able to rescue the reduced dendrite complexity observed upon miR-134 inhibition in membrane-depolarized neurons. To this end, hippocampal neurons were transfected with anti-miR-134 together with either Si-Pum2-2 or a control siRNA (Si control). We found that knock down of Pum2 using two independent siRNAs (Si-Pum2-1 and Si-Pum2-2) specifically rescues the miR-134 loss of function phenotype whereas the Si control had no effect (Figure 6C and D; Supplementary Figure S5). Thus, downregulation of Pum2 protein expression by miR-134 is necessary for activity-dependent dendritogenesis.

We next investigated whether expression of miR-134 or downregulation of Pum2 is sufficient to trigger dendritic outgrowth. Transfection of hippocampal neurons with either miR-134 duplex or Si-Pum2 did not increase basal dendritic

complexity (data not shown). Surprisingly, membrane depolarization also failed to induce dendritic outgrowth in cells overexpressing miR-134 or the Si-Pum2-2 (Figure 6E and F). Thus, both decreasing and increasing Pum2 expression by means of miR-134 perturbation are detrimental to activity-dependent dendritogenesis. Our results are consistent with a role for miR-134 in fine-tuning gene expression during dendritogenesis. Consistent with such a fine-tuning relationship between miR-134 and Pum2, overexpression of Pum2 similarly precludes an activity-dependent increase in dendritic complexity (Figure 6F). Taken together, our results suggest that miR-134 buffers Pum2 levels within a narrow range critical for activity-dependent dendritogenesis (Figure 6G).

Discussion

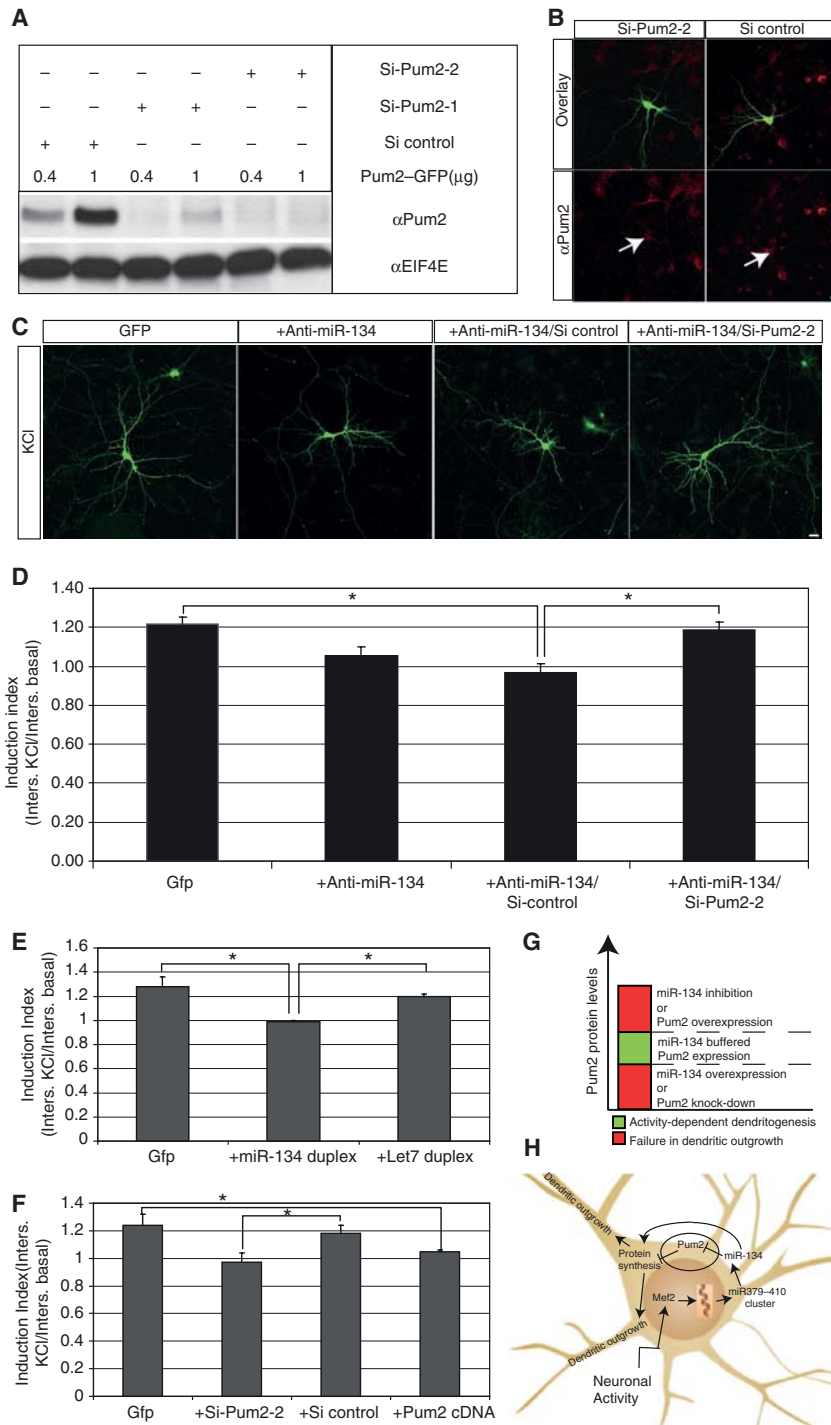
Neurons respond to changes in their activity status by remodelling the dendritic tree and the number and strength of synapses. This morphological and functional plasticity is necessary for correct neuronal development and modulates numerous behavioural adaptations such as memory formation and addiction (Kandel, 2001; Calabresi *et al*, 2007). We have previously shown that several miRNAs enriched in the dendritic compartment control local protein synthesis and are necessary for spine morphogenesis (Schratt *et al*, 2006; Siegel *et al*, 2009). Importantly, the function of one of them, miR-134, is modulated locally by neuronal activity. We now show that activity-dependent regulation of miR-134 is not limited to the dendritic compartment but is controlled globally within the neuron by an activity-dependent transcriptional programme. The miR-134 gene is located within the *Gtl2/Dlk1* locus clustered together with more than 50 other miRNA genes. Membrane depolarization or BDNF treatment enhances the expression of all the miRNAs within the cluster that we tested. We validated these miRNAs as new targets for the activity-regulated transcription factor Mef2, a regulator of synapse number and differentiation, and show that activity-dependent, Mef2-mediated expression of the miRNA cluster is necessary for the development of the dendritic tree in primary neurons. MiR-134 specifically regulates activity-dependent dendritogenesis by a novel pathway, namely the downregulation of the RNA-binding protein and translational repressor Pum2 (Figure 6H). Our results, together with existing data, show that miRNA function is regulated at multiple levels by neuronal activity, and suggest that miRNAs are critical components of the relay that coordinates nuclear programmes of gene expression with local changes in dendritic and synaptic morphology in response to neuronal activity.

Activity-dependent regulation of the miR379-410 cluster

Several lines of evidence suggest that the miR379-410 cluster is co-regulated by neuronal activity and might be transcribed as a single polycistronic unit. First, all the miRNAs located in the distal part of the *GTL2/DLK1* locus show a very similar brain-specific expression pattern (Seitz *et al*, 2004). Second, BDNF and KCl treatment lead to a very similar induction profile of pre-miRNAs from the miR379-410 cluster (Figure 1B and C). Third, knock down of Mef2 greatly reduces the stimulation-induced expression of all the miR379-410 miRNAs we tested (Figure 3D). Finally, we could detect an overlapping transcript by RT-PCR spanning about 20 kb upstream of the

first miRNA within the cluster. Northern blot analysis will be necessary to confirm the existence of a large continuous transcript spanning the entire miR379–410 cluster. We identified a Mef2-binding element (MBS10) about 20 kb upstream of the miR379–410 cluster. Our results show that MBS10 is

occupied by Mef2 *in vivo* and is sufficient to induce upregulation of the expression of a luciferase gene reporter upon Mef2 binding following KCl and BDNF stimulation. Despite its functional importance, it is unclear whether MBS10 is located within a promoter or a long-range enhancer sequence. Fine



mapping of the transcriptional start site should allow discrimination between these two possibilities.

miRNAs of the miR379–410 cluster are necessary for activity-dependent neuronal development

Anti-miR-mediated inhibition of several members of the miR379–410 showed that at least three of them (miR-134, -329 and -381) are necessary for dendritic outgrowth triggered by KCl in hippocampal neurons. The functional consequences of activity-dependent expression of the other members of miR379–410 remain to be determined. A variety of programmes are triggered by neuronal activity, such as cell survival or synapse remodelling. Thus, it is conceivable that multiple aspects of activity-dependent development are controlled by the miR379–410 cluster. Consistently, the sequence of the mature miRNAs is significantly divergent and a recent bioinformatic study revealed a limited degree of overlap in the GO annotations of the different miR379–410 miRNAs (Glazov *et al*, 2008). Recently, altered biogenesis of miR-134 and other members of the miR379–410 cluster has been described in a mouse model of the human microdeletion of the 22q11.2 chromosomal locus (Stark *et al*, 2008). Mice hemizygous for the deletion showed several behavioural and cognitive deficits accompanied by abnormal dendritic arborization in the hippocampus. This animal model further indicates that the miR379–410 cluster has a crucial function in dendritic morphogenesis.

Mef2 negatively regulates synapse number in mature hippocampal neurons and miR-134, the best characterized member of the miR379–410 cluster, negatively regulates dendritic spine size. This suggests that the miR379–410 cluster could also be involved in the Mef2-dependent control of synapse number at later stages of neuronal development. The role of Mef2 in dendritogenesis was previously unknown, presumably as Mef2 is required only for dendrite outgrowth upon neuronal activation. The dual function of Mef2 as a positive regulator of dendritogenesis and negative regulator of synapse number appears at first glance paradoxical. One possible explanation is that at different stages of neuronal development Mef2 might regulate different sets of

target genes. Indeed, known Mef2 targets include both dendrite growth-promoting factors, such as BDNF, and negative regulators of synapse formation and strength, such as Arc and SynGAP (Flavell and Greenberg, 2008). A recent *in vivo* study suggests that Mef2 is a key component of a compensatory mechanism that couples structural plasticity with sensitized response to cocaine in striatal neurons (Pulipparacharuvil *et al*, 2008). It is thus tempting to speculate that the apparently opposing effects of Mef2 on hippocampal neurons are in fact components of the same homeostatic circuit that controls the overall neuronal excitability, by both decreasing synapse number and promoting dendritic outgrowth (Turrigiano, 2007). This is consistent with the observation that Mef2 targets such as miR-134 display a similar dichotomy. MiR-134 is necessary for activity-dependent dendritogenesis and negatively regulates spine growth by regulating Pum2 and LimK1, respectively. Strikingly, BDNF upregulates miR-134 transcription, whereas, within the dendrite, BDNF relieves the inhibition of the known miR-134 target LimK1 to promote spine development. Therefore, synaptic stimulation might elevate miR-134 expression throughout the cell while inactivating miR-134 locally within stimulated spines. This could be a mechanism to permit spine growth specifically at active synapses without changing the overall excitability of the neuron.

In recent studies, the CREB-regulated miR-132 was shown to control activity-dependent dendritic growth by regulating the Rho family GTPase-activating protein p250GAP (Vo *et al*, 2005; Cheng *et al*, 2007; Wayman *et al*, 2008). Thus, at least two independent miRNA pathways coordinately regulate dendritic plasticity. Further studies are necessary to analyse the extent of cross-talk between CREB- and Mef2-regulated miRNA pathways in dendrite development.

Pum2 is a new miR-134 target necessary for activity-dependent dendritogenesis

We have shown that the RNA-binding protein Pum2 is a new *bona fide* miR-134 target. The presence of predicted binding sites for other members of the miR379–410 cluster in the Pum2 3'UTR suggested that multiple miRNAs are necessary

Figure 6 Pum2 is a physiological target of miR-134 during activity-dependent dendritogenesis. (A) Two independent Pum2 shRNAs efficiently downregulate the expression of recombinant Pum2. Western blot analysis of HEK293T cell lysates transfected with the indicated amounts of GFP–Pum2 expression vectors, two Pum2 shRNAs as well as a control shRNA (4 ng each) were analysed by western blot using an anti-Pum2 antibody and an anti-eIF4E antibody as a loading control. (B) Si-Pum2-2 efficiently downregulates the expression of the endogenous Pum2 protein. Hippocampal neurons were transfected at DIV4 with GFP together with either Si-Pum2-2 (left) or a control siRNA (right, 2 ng each). The cells were fixed at DIV7 and analysed by immunocytochemistry using an anti-Pum2 antibody. Arrows point to cell bodies of representative transfected neurons. Note the reduced Pum2 signal in the cell transfected with Si-Pum2-2 (left) compared with the control neuron (right). Scale bar: 10 µm. (C) Pum2 knockdown by siRNA rescues the miR-134 loss-of-function phenotype in membrane-depolarized hippocampal neurons. Hippocampal neurons were transfected with GFP in conjunction with the indicated anti-miRs (50 nM) and shRNA constructs (2 ng). At 7DIV, neurons were incubated with 16 mM KCl for 6 h and dendritic complexity was evaluated 3 days later. Scale bar: 20 µm. (D) Quantitative analysis of the dendritogenesis assay shown in (C). The calculation of dendritic complexity and the data presentation are as in Figure 4B. Here, 10–16 cells for condition were analysed in each experiment. Data represent the mean of three independent experiments + s.d. **P* < 0.05 (*t*-test). (E) Overexpression of miR-134 duplex RNA perturbs membrane depolarization-induced dendritic outgrowth. Hippocampal neurons (4DIV) were transfected with GFP together with the indicated duplex RNAs (10 nM), and depolarization was performed at 7DIV followed by the assessment of dendritic complexity at 10DIV, as described in (C). Here, 10–16 cells for condition were analysed in each experiment. Data represent the mean of three independent experiments + s.d. **P* < 0.05 (*t*-test). (F) Both knockdown and overexpression of Pum2 perturb membrane depolarization-induced dendritic outgrowth. Hippocampal neurons (4DIV) were transfected with GFP together with the indicated shRNA (2 ng) or Pum2 expression (100 ng) constructs, and depolarization was performed at 7DIV followed by the assessment of dendritic complexity, as described in (C). Here, 10–16 cells for condition were analysed in each experiment. Data represent the mean of three independent experiments + s.d. **P* < 0.05 (*t*-test). (G) Schematic diagram of the fine-tuning of Pum2 levels by miR-134 in membrane-depolarized neurons, see main text for details. (H) Model for the miR379–410 activity-dependent dendritogenesis pathway. Neuronal activity activates Mef2 which in turn induces the expression of the miR379–410 cluster. Several members of the cluster are necessary for activity-dependent dendritogenesis. Among them is miR-134, which binds to the Pum2 mRNA and downregulates its translation. Lower levels of the translational repressor Pum2 allow for the translation of a set of so far unknown mRNAs that are likely positive regulators of dendrite outgrowth.

to robustly downregulate Pum2 after membrane depolarization. However, miR-134 alone appears to be sufficient to fine-tune Pum2 levels within a functionally critical window. Therefore, we favour the idea that other miR379–410 miRNAs might be involved in the regulation of different aspects of activity-dependent dendritogenesis (e.g. membrane trafficking, cytoskeletal dynamics, etc.) by fine-tuning critical regulators of these pathways. Interestingly, a number of predicted miR379–410 target mRNAs have been associated with dendrite morphogenesis. For example, members of the SMAD and kinesin families (Guo *et al*, 2001; Satoh *et al*, 2008) are predicted targets of miR-329 and -381, respectively (TargetsScan 3.0). Future studies will reveal whether fine-tuning of these genes is a common regulatory function of the miR379–410 cluster.

The epistasis experiments in hippocampal neurons validate the functional relevance of the Pum2–miR-134 interaction. Both inhibition and overexpression of miR-134 and Pum2 compromise activity-dependent dendritogenesis. Similarly, in *Drosophila* peripheral neurons, both depletion and ectopic expression of Pum have a detrimental effect on dendrite morphogenesis. Taken together, these findings support the idea that although Pum2 expression is necessary for activity-dependent dendritogenesis, a careful control of its levels by miR-134 is equally critical for the correct elaboration of the dendritic tree (Ye *et al*, 2004). Thus, the miR-134–Pum2 relationship in membrane-depolarized neurons might be best described by the recently proposed tuning model (Hobert, 2007; Karres *et al*, 2007). In this model, an miRNA buffers the target protein levels within a critical window that is optimal for the cell (Figure 6G). An important implication of the tuning model is that it takes into account the spatial regulation of miRNA targets, for example, during local protein synthesis in dendrites (Tsang *et al*, 2007). As both the Pum2 mRNA and protein are localized in dendrites (Vessey *et al*, 2006; Zhong *et al*, 2006), it is possible that Pum2 and miR-134 functionally interact within this compartment. Pum2 is a translational repressor and a component of somatic and dendritic RNA granules, in particular stress granules (Vessey *et al*, 2006). Therefore, miR-134, by downregulating the Pum2 protein, might induce the redistribution of Pum2 target mRNAs to the local protein synthesis machinery. Interesting candidates are known *Drosophila* Pum targets, such as eukaryotic initiation factor 4E (eIF4E), PSD-95 homologues and a voltage-gated sodium channel (Mee *et al*, 2004; Menon *et al*, 2004; Chen *et al*, 2008).

In summary, we have identified the miR379–410 cluster as a new activity-regulated Mef2 target gene, the expression of which is necessary for dendritic plasticity in hippocampal neurons.

These results represent a road map to investigate the function of these miRNAs in activity-dependent processes *in vivo* and to understand how a neuron coordinates local regulation of protein synthesis with global control of gene expression to properly adapt to its environment.

Materials and methods

DNA constructs

Single cell fluorescent sensor constructs were generated by subcloning of an *EcoRI*–*NotI* flanked dsRED cassette (Clontech) together with a *NotI*–*XbaI* flanked oligonucleotide containing two

perfectly complementary sites to the miRNA of interest, into *EcoRI*–*XbaI* linearized pTracer-CMV (Invitrogen).

The Pum2 3'UTR was amplified from a rat brain cDNA library and cloned into the *XbaI* site of pGL3promoter vector (Promega). To generate pGL3-Pum2mut, the miR-134 seed sequence was replaced with an *XhoI* site by overlapping PCR, resulting in three point mutations in the miR-134-binding site.

Luciferase sensor constructs, pGL3basic-MBS10, MBS10-mut and NUR77, were generated by ligation of annealed oligonucleotides to *XhoI*–*NheI* linearized pGL3basic (Promega). poFluc-3 × MRE, pcDNA3-Mef2-VP16 (constitutively active Mef2), pcDNA3-Mef2ΔDBD-VP16 (mutant Mef2), pcDNA3-Mef2D-RiR (RNAi-resistant Mef2D) and pSuper-Mef2D were kindly provided by ME Greenberg (Harvard Medical School, Boston, USA; Flavell *et al*, 2006). poFluc-5 × MBS10 was generated by substituting *HindIII*–*BglII* flanked 3 × MRE from poFluc-3 × MRE with 5 × MBS10, whereas poFluc control was obtained from self-blunt-end ligation after 3' end filling with Klenow enzyme (Roche Diagnostics). GFP-Pum2 expression vector is a kind gift of Michael Kiebler (Medical University of Vienna, Austria; Vessey *et al*, 2006).

Cell culture, transfection and virus infection of primary neurons

The culture and transfection of dissociated primary cortical and hippocampal neurons from embryonic day 18 (E18) Sprague–Dawley rats (Charles River Laboratories, Sulzfeld, Germany) was as described (Schratt *et al*, 2004). For AAV-mediated overexpression of miR-134, the miR-134 or a control sequence embedded in the miR-30 hairpin was inserted into the 3'UTR of GFP within AAV-6P-SEWB (kind gift of Martin Schwarz, MPIMF Heidelberg; Shevtsova *et al*, 2005). A detailed description and characterization of AAV-134 will be published elsewhere (MC and GS, manuscript in preparation). Lentiviruses expressing Mef2A/D shRNA or a control shRNA have been described previously (Flavell *et al*, 2006).

For stimulation experiments, neurons were either treated with depolarization solution (NaCl 140 mM, KC 155–165 mM, CaCl₂ 2.5 mM, MgCl₂ 1.6 mM, Hepes 10 mM, glucose 24 mM, pH = 7.4) at a final concentration of 16–55 mM KCl or with hBDNF (Peprotech) at 40–60 ng/ml as indicated for up to 6 h.

Single cell fluorescent sensor assay

Hippocampal neurons (DIV4) were transfected with bicistronic reporter constructs (pTracer-CMV-dsRED, 50 ng) and 2'-O-Methyloligonucleotides (50 nM) as indicated. pTracer-CMV-dsRED contains a perfect binding site for miR-134, -329 or -541 at the 3'UTR of dsRED, which leads to degradation of dsRED RNA in the presence of the respective miRNAs. Cells in which the dsRED signal did not exceed background levels were scored as 'miRNA positive'.

ISH

ISH of dissociated hippocampal neurons using DIG-labelled LNA probes (5 pmol; Exiqon) was basically as described with slight modifications (Schratt *et al*, 2006). Signal detection was performed with FITC-conjugated anti-digoxigenin FAB fragments (Roche) and an Alexa Fluor 488 signal amplification kit (Molecular Probes).

ChIP assay

A detailed ChIP protocol can be found in Supplementary data.

Quantitative real-time PCR

Total RNA was isolated by using Qiazol (Qiagen) and genomic DNA contamination was eliminated with TURBO DNase (Ambion). Reverse transcription of RNA was carried out with iScript™ cDNA synthesis kit (Bio-Rad), according to the manufacturer's protocol. Relative quantification of gene expression was conducted with the Applied Biosystems 7300 Real Time PCR System (Applied Biosystems) using the iTaq SybrGreen Supermix with ROX (Bio-Rad). PCR results were normalized to the expression of β-3-tubulin.

Semiquantitative RT-PCR ('transcript walking')

Reverse transcription of 1 μg RNA with 50 ng random hexamers per reaction was carried out with SuperScript III™ first strand synthesis system (Invitrogen), according to the manufacturer's protocol. Advantage[®] 2 PCR Enzyme System (Clontech) was used for RT-PCR (PCR parameters 95 °C for 2 min and 30 cycles of 95 °C for 30 s, 59 °C for 30 s, 68 °C for 1 min 20 s and final extension at 68 °C for 5 min). Oligonucleotide sequences are listed in Supplementary data.

Luciferase assay

Cortical or hippocampal neurons were transfected with pGL3 reporter constructs (100 ng per 48 well) together with anti-miRs (60 nM) at 4–5 DIV and luciferase assays were performed 1 or 2 days later with the Dual-Luciferase Reporter Assay System (Promega).

Dendritogenesis assay, immunocytochemistry and image analysis

Hippocampal neurons (4DIV) were transfected with eGFP (100 ng) alone or in combination with anti-miRs (50 nM), pSuper shRNA constructs (4 ng), pcDNA3 expression constructs (100 ng) or miRNA duplexes (10 nM) as indicated. After stimulation (7DIV), neurons were fixed at 10DIV in 4% paraformaldehyde/sucrose and subjected to fluorescence microscopy analysis.

For immunostaining of the endogenous Pum2 protein, hippocampal neurons were fixed in paraformaldehyde/sucrose, rinsed in PBS and incubated with rabbit polyclonal anti-Pum2 antibody (dilution 1:2000; Acris, Hiddenhausen, Germany, gift of Michael Kiebler) and cyanine-3-conjugated anti-rabbit IgG secondary antibodies (dilution 1:1000), both diluted in 0.02% gelatine–0.5% Triton X-100–PBS.

For image analysis, XY scans ($\times 20$, 1024×1024 pixels) taken with a confocal laser-scanning microscope (LSM 5 Pascal; Zeiss, Germany) were used. A grid of concentric circles spaced by $20 \mu\text{m}$ was placed on the cell bodies of GFP-positive neurons, and the numbers of dendrites crossing each circle was counted. A total of 12–16 random cells chosen in a blinded manner were analysed per experimental condition.

To quantify Pum2 protein levels by immunofluorescence, a total of 8–10 random GFP-positive cells per condition were imaged ($\times 40$

objective, 1024×1024 pixels) and the signal intensity in the red channel (anti-Pum2) was measured using ImageJ software.

Western blotting

Western blotting was performed as described previously (Schratt *et al*, 2004). The following primary antibodies were used: rabbit anti-Pum2-antibody (dilution 1:5000; Acris), mouse anti- β -actin (1:15000; MMS-435P; Covance), rabbit anti-eIF4E (1:10000; no. 9742; Cell Signaling). Primary antibodies were recognized either by an HRP-conjugated goat anti-rabbit antibody (1:20000; 401315; Calbiochem) or an HRP-conjugated rabbit anti-mouse antibody (1:20000; 402335; Calbiochem).

Bioinformatics

The prediction of MBSs was carried out with MAPPER (Marinescu *et al*, 2005), JASPAR (Sandelin *et al*, 2004) and rVISTA 2.0 (Loots and Ovcharenko, 2004) web servers. The sequence conservation between mouse and human was determined using BlastN.

Supplementary data

Supplementary data are available at *The EMBO Journal* Online (<http://www.embojournal.org>).

Acknowledgements

We thank M Kiebler for generously providing reagents and M Schwarz for initial help with AAV production. The excellent technical assistance of T Wüst is greatly acknowledged. This study was supported by grants from the DFG (SFB488) and HFSP (CDA) to GS and from the NIH (NS028829) to MEG.

References

- Bagni C, Greenough WT (2005) From mRNP trafficking to spine dysmorphogenesis: the roots of fragile X syndrome. *Nat Rev Neurosci* **6**: 376–387
- Calabresi P, Picconi B, Tozzi A, Di Filippo M (2007) Dopamine-mediated regulation of corticostriatal synaptic plasticity. *Trends Neurosci* **30**: 211–219
- Chen G, Li W, Zhang QS, Regulski M, Sinha N, Barditch J, Tully T, Krainer AR, Zhang MQ, Dubnau J (2008) Identification of synaptic targets of *Drosophila* pumilio. *PLoS Comput Biol* **4**: e1000026
- Chen Y, Ghosh A (2005) Regulation of dendritic development by neuronal activity. *J Neurobiol* **64**: 4–10
- Cheng HY, Papp JW, Varlamova O, Dziema H, Russell B, Curfman JP, Nakazawa T, Shimizu K, Okamura H, Impey S, Obrietan K (2007) MicroRNA modulation of circadian-clock period and entrainment. *Neuron* **54**: 813–829
- Fiore R, Siegel G, Schratt G (2008) MicroRNA function in neuronal development, plasticity and disease. *Biochim Biophys Acta* **1779**: 471–478
- Flavell SW, Cowan CW, Kim TK, Greer PL, Lin Y, Paradis S, Griffith EC, Hu LS, Chen C, Greenberg ME (2006) Activity-dependent regulation of MEF2 transcription factors suppresses excitatory synapse number. *Science* **311**: 1008–1012
- Flavell SW, Greenberg ME (2008) Signaling mechanisms linking neuronal activity to gene expression and plasticity of the nervous system. *Annu Rev Neurosci* **31**: 563–590
- Glazov EA, McWilliam S, Barris WC, Dalrymple BP (2008) Origin, evolution, and biological role of miRNA cluster in DLK-DIO3 genomic region in placental mammals. *Mol Biol Evol* **25**: 939–948
- Guo X, Lin Y, Horbinski C, Drahusuk KM, Kim IJ, Kaplan PL, Lein P, Wang T, Higgins D (2001) Dendritic growth induced by BMP-7 requires Smad1 and proteasome activity. *J Neurobiol* **48**: 120–130
- He L, Thomson JM, Hemann MT, Hernando-Monge E, Mu D, Goodson S, Powers S, Cordon-Cardo C, Lowe SW, Hannon GJ, Hammond SM (2005) A microRNA polycistron as a potential human oncogene. *Nature* **435**: 828–833
- Hoertig O (2007) miRNAs play a tune. *Cell* **131**: 22–24
- Hong EJ, West AE, Greenberg ME (2005) Transcriptional control of cognitive development. *Curr Opin Neurobiol* **15**: 21–28
- Kandel ER (2001) The molecular biology of memory storage: a dialogue between genes and synapses. *Science* **294**: 1030–1038
- Karres JS, Hilgers V, Carrera I, Treisman J, Cohen SM (2007) The conserved microRNA miR-8 tunes atrophin levels to prevent neurodegeneration in *Drosophila*. *Cell* **131**: 136–145
- Kiebler MA, Bassell GJ (2006) Neuronal RNA granules: movers and makers. *Neuron* **51**: 685–690
- Kosik KS (2006) The neuronal microRNA system. *Nat Rev Neurosci* **7**: 911–920
- Lonze BE, Ginty DD (2002) Function and regulation of CREB family transcription factors in the nervous system. *Neuron* **35**: 605–623
- Loots GG, Ovcharenko I (2004) rVISTA 2.0: evolutionary analysis of transcription factor binding sites. *Nucleic Acids Res* **32**: W217–W221
- Mansfield JH, Harfe BD, Nissen R, Obenaus J, Srineel J, Chaudhuri A, Farzan-Kashani R, Zuker M, Pasquinelli AE, Ruvkun G, Sharp PA, Tabin CJ, McManus MT (2004) MicroRNA-responsive ‘sensor’ transgenes uncover Hox-like and other developmentally regulated patterns of vertebrate microRNA expression. *Nat Genet* **36**: 1079–1083
- Marinescu VD, Kohane IS, Riva A (2005) The MAPPER database: a multi-genome catalog of putative transcription factor binding sites. *Nucleic Acids Res* **33**: D91–D97
- Mee CJ, Pym EC, Moffat KG, Baines RA (2004) Regulation of neuronal excitability through pumilio-dependent control of a sodium channel gene. *J Neurosci* **24**: 8695–8703
- Menon KP, Sanyal S, Habara Y, Sanchez R, Wharton RP, Ramaswami M, Zinn K (2004) The translational repressor Pumilio regulates presynaptic morphology and controls postsynaptic accumulation of translation factor eIF-4E. *Neuron* **44**: 663–676
- Pulipparacharuvil S, Renthal W, Hale CF, Taniguchi M, Xiao G, Kumar A, Russo SJ, Sikder D, Dewey CM, Davis MM, Greengard P, Nairn AC, Nestler EJ, Cowan CW (2008) Cocaine regulates MEF2 to control synaptic and behavioral plasticity. *Neuron* **59**: 621–633
- Redmond L, Kashani AH, Ghosh A (2002) Calcium regulation of dendritic growth via CaM kinase IV and CREB-mediated transcription. *Neuron* **34**: 999–1010
- Richter JD (2007) CPEB: a life in translation. *Trends Biochem Sci* **32**: 279–285
- Sandelin A, Alkema W, Engstrom P, Wasserman WW, Lenhard B (2004) JASPAR: an open-access database for eukaryotic transcription factor binding profiles. *Nucleic Acids Res* **32**: D91–D94
- Satoh D, Sato D, Tsuyama T, Saito M, Ohkura H, Rolls MM, Ishikawa F, Uemura T (2008) Spatial control of branching within dendritic arbors by dynein-dependent transport of Rab5-endosomes. *Nat Cell Biol* **10**: 1164–1171

- Schratt GM, Nigh EA, Chen WG, Hu L, Greenberg ME (2004) BDNF regulates the translation of a select group of mRNAs by a mammalian target of rapamycin-phosphatidylinositol 3-kinase-dependent pathway during neuronal development. *J Neurosci* **24**: 9366–9377
- Schratt GM, Tuebing F, Nigh EA, Kane CG, Sabatini ME, Kiebler M, Greenberg ME (2006) A brain-specific microRNA regulates dendritic spine development. *Nature* **439**: 283–289
- Seitz H, Royo H, Bortolin ML, Lin SP, Ferguson-Smith AC, Cavaillie J (2004) A large imprinted microRNA gene cluster at the mouse Dlk1-Gtl2 domain. *Genome Res* **14**: 1741–1748
- Shalizi A, Gaudilliere B, Yuan Z, Stegmuller J, Shirogane T, Ge Q, Tan Y, Schulman B, Harper JW, Bonni A (2006) A calcium-regulated MEF2 sumoylation switch controls postsynaptic differentiation. *Science* **311**: 1012–1017
- Shalizi AK, Bonni A (2005) Brawn for brains: the role of MEF2 proteins in the developing nervous system. *Curr Top Dev Biol* **69**: 239–266
- Shevtsova Z, Malik JM, Michel U, Bahr M, Kugler S (2005) Promoters and serotypes: targeting of adeno-associated virus vectors for gene transfer in the rat central nervous system *in vitro* and *in vivo*. *Exp Physiol* **90**: 53–59
- Siegel G, Obernosterer G, Fiore R, Oehmen M, Bicker S, Khudayberdiev S, Leuschner PF, Busch CJL, Kane C, Hübel K, Rengarajan B, Drepper C, Waldmann H, Kauppinen S, Greenberg ME, Draguhn A, Rehmsmeier M, Martinez J, Schratt G (2009) A functional screen implicates microRNA-138-dependent regulation of the depalmitoylation enzyme APT1 in dendritic spine morphogenesis. *Nat Cell Biol* (in press)
- Stark KL, Xu B, Bagchi A, Lai WS, Liu H, Hsu R, Wan X, Pavlidis P, Mills AA, Karayiorgou M, Gogos JA (2008) Altered brain microRNA biogenesis contributes to phenotypic deficits in a 22q11-deletion mouse model. *Nat Genet* **40**: 751–760
- Steward O (2002) mRNA at synapses, synaptic plasticity, and memory consolidation. *Neuron* **36**: 338–340
- Sutton MA, Schuman EM (2006) Dendritic protein synthesis, synaptic plasticity, and memory. *Cell* **127**: 49–58
- Tsang J, Zhu J, van Oudenaarden A (2007) MicroRNA-mediated feedback and feedforward loops are recurrent network motifs in mammals. *Mol Cell* **26**: 753–767
- Turrigiano G (2007) Homeostatic signaling: the positive side of negative feedback. *Curr Opin Neurobiol* **17**: 318–324
- Vessey JP, Vaccani A, Xie Y, Dahm R, Karra D, Kiebler MA, Macchi P (2006) Dendritic localization of the translational repressor Pumilio 2 and its contribution to dendritic stress granules. *J Neurosci* **26**: 6496–6508
- Vo N, Klein ME, Varlamova O, Keller DM, Yamamoto T, Goodman RH, Impey S (2005) A cAMP-response element binding protein-induced microRNA regulates neuronal morphogenesis. *Proc Natl Acad Sci U S A* **102**: 16426–16431
- Waites CL, Craig AM, Garner CC (2005) Mechanisms of vertebrate synaptogenesis. *Annu Rev Neurosci* **28**: 251–274
- Wayman GA, Davare M, Ando H, Fortin D, Varlamova O, Cheng HY, Marks D, Obrietan K, Soderling TR, Goodman RH, Impey S (2008) An activity-regulated microRNA controls dendritic plasticity by down-regulating p250GAP. *Proc Natl Acad Sci USA* **105**: 9093–9098
- Wayman GA, Impey S, Marks D, Saneyoshi T, Grant WF, Derkach V, Soderling TR (2006) Activity-dependent dendritic arborization mediated by CaM-kinase I activation and enhanced CREB-dependent transcription of Wnt-2. *Neuron* **50**: 897–909
- Whitford KL, Dijkhuizen P, Polleux F, Ghosh A (2002) Molecular control of cortical dendrite development. *Annu Rev Neurosci* **25**: 127–149
- Ye B, Petritsch C, Clark IE, Gavis ER, Jan LY, Jan YN (2004) Nanos and Pumilio are essential for dendrite morphogenesis in *Drosophila* peripheral neurons. *Curr Biol* **14**: 314–321
- Zhong J, Zhang T, Bloch LM (2006) Dendritic mRNAs encode diversified functionalities in hippocampal pyramidal neurons. *BMC Neurosci* **7**: 17



The EMBO Journal is published by Nature Publishing Group on behalf of European Molecular Biology Organization. This article is licensed under a Creative Commons Attribution-NonCommercial-Share Alike 3.0 Licence. [<http://creativecommons.org/licenses/by-nc-sa/3.0/>]

Supplementary Figures

Supplementary figure S1

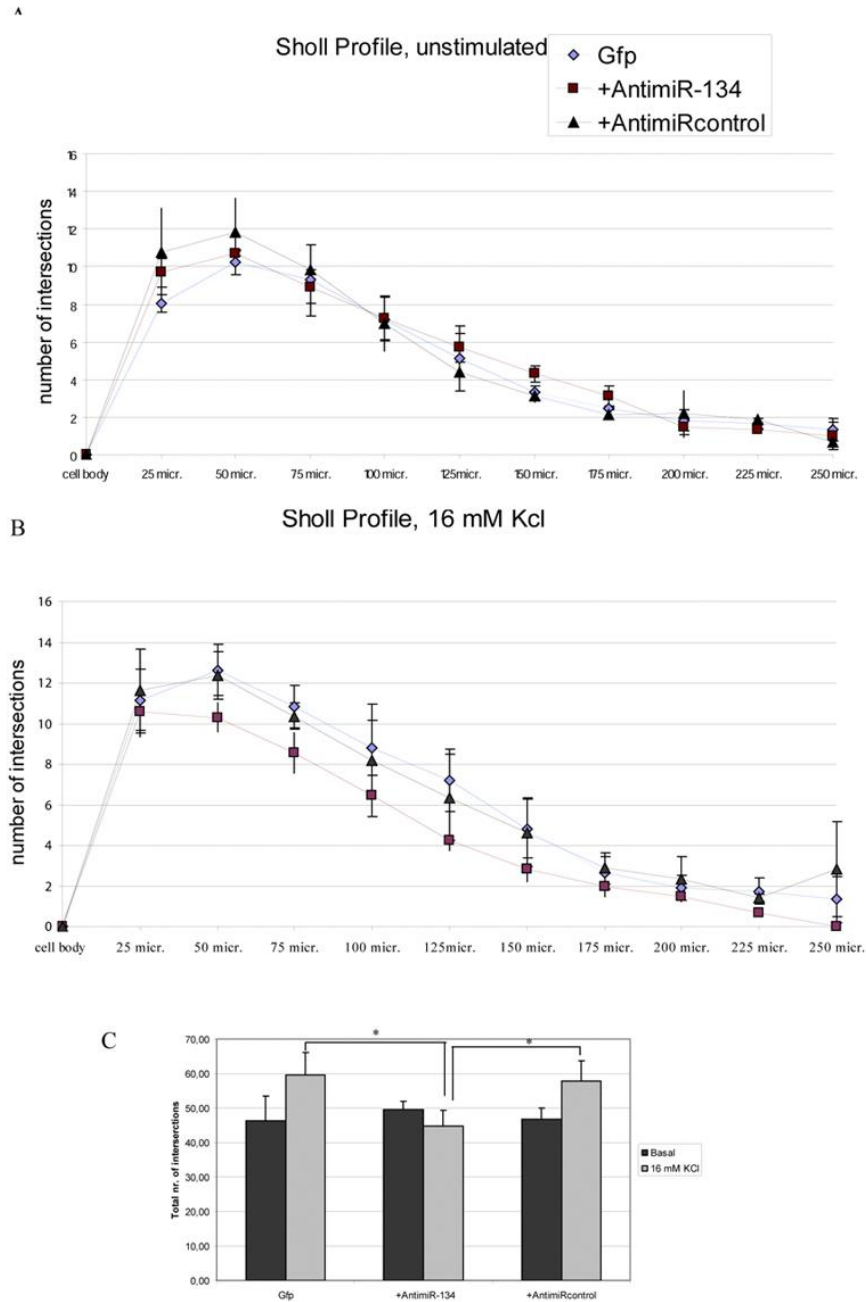


Figure S1: Detailed analysis of dendritic complexity upon miR-134 inhibition. Neurons were treated as described in the figure legend of Fig. 4A. A) Complete Sholl profile of neurons treated with the indicated antimiRs. AntimiR treatment does not affect dendritic complexity under basal growth conditions. Data represent the mean of at least three experiments + STDV. B) Complete Sholl profile of neurons treated with the indicated antimiRs in the presence of depolarizing concentrations of KCl (6h, 16 mM). AntimiR-134 treated neurons (dark rectangles) display a shift of the profile towards lower numbers of intersections. Data represent the mean of at least three experiments + STDV. C) Cumulative data plot showing the total number of intersections for the neurons analyzed in S1A, B. Data represent the mean of at least three experiments + STDV. * $p < 0.05$ (t-test).

Supplementary figure S2

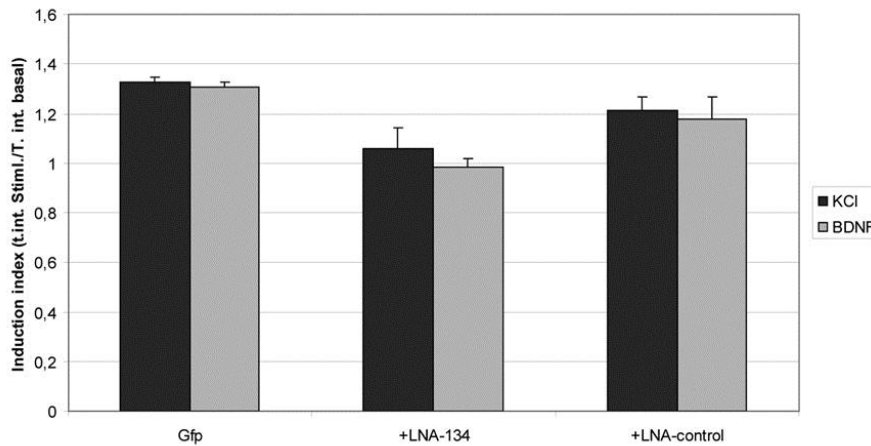


Figure S2: LNA mediated inhibition of miR-134 blocks the activity- and BDNF-induced increase in dendritic complexity. Data analysis and presentation was performed as in Fig. 4B, C. Data represents the mean of 2 experiments + STDV.

Supplementary figure S3

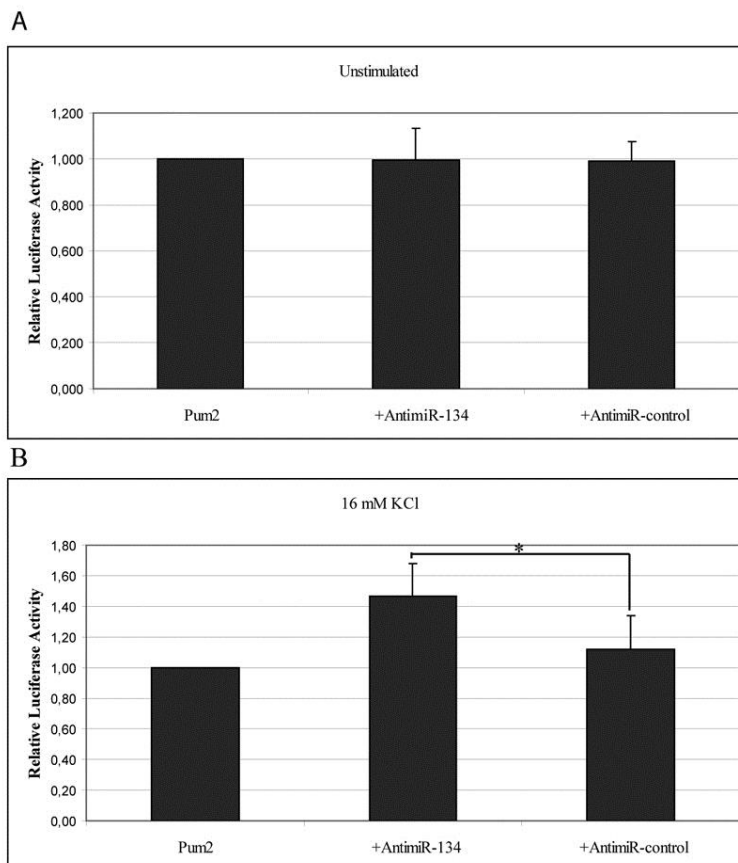


Figure S3: miR-134 inhibition does not change relative luciferase activity of the Pum2 wild-type reporter gene in unstimulated cortical neurons. Neurons were transfected and analyzed as described in the figure legend of Fig. 5B. Data represent the mean of at least three experiments + STDV. *p < 0.05 (t-test).

Supplementary figure 4

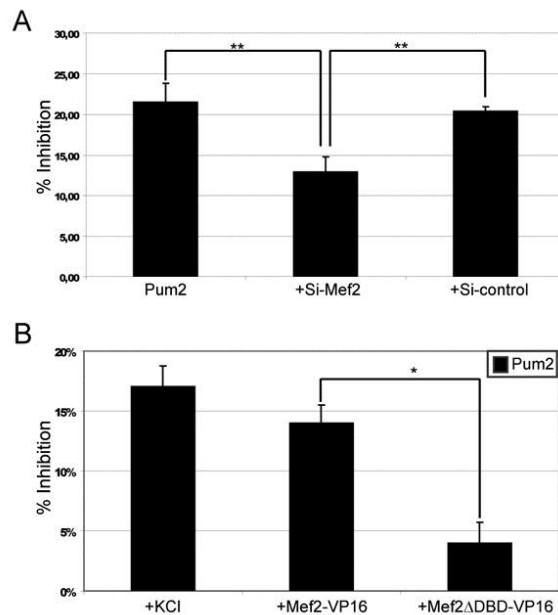


Figure S4: A) Mef2 is necessary for downregulation of the Pum2 luciferase reporter. Pum2-luc was transfected into cortical neurons (5DIV) along with the Mef2 shRNA (Si-Mef2) or a control shRNA (Si-control). Neurons were treated as in Fig. 5B. The percent inhibition of the relative luciferase activity of the Pum2 reporter after membrane depolarization is plotted. Data represents the mean of three independent experiments + STDV. $**p < 0,01$ (t-test). B) Mef2 is sufficient for downregulation of the Pum2 luciferase reporter. Pum2-luc was transfected into cortical neurons (5DIV) alone or along with Mef2-VP16 or Mef2 Δ DBD-VP16. At DIV7 luciferase activity was determined and normalized to the internal Renilla control. The percent inhibition of the relative luciferase activity of the Pum2 reporter after either membrane depolarization or cotransfection with the indicated expression vectors is plotted. Data represents the mean of three independent experiments + STDV. $*p < 0,05$ (t-test).

Supplementary figure S5

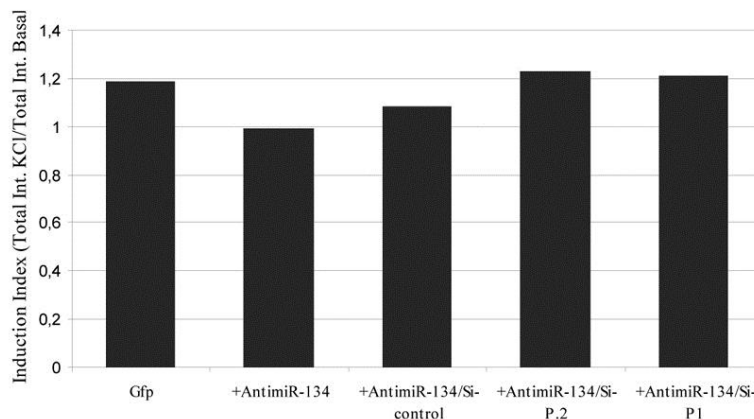


Figure S5: Two independent Pum2 shRNA constructs (Si-Pum2-1, Si-Pum2-2) rescue the reduced dendritic complexity caused by miR-134 inhibition. Neurons were transfected and analyzed as described in the figure legend of Fig. 6D. One representative is shown.

Supplementary figure S6

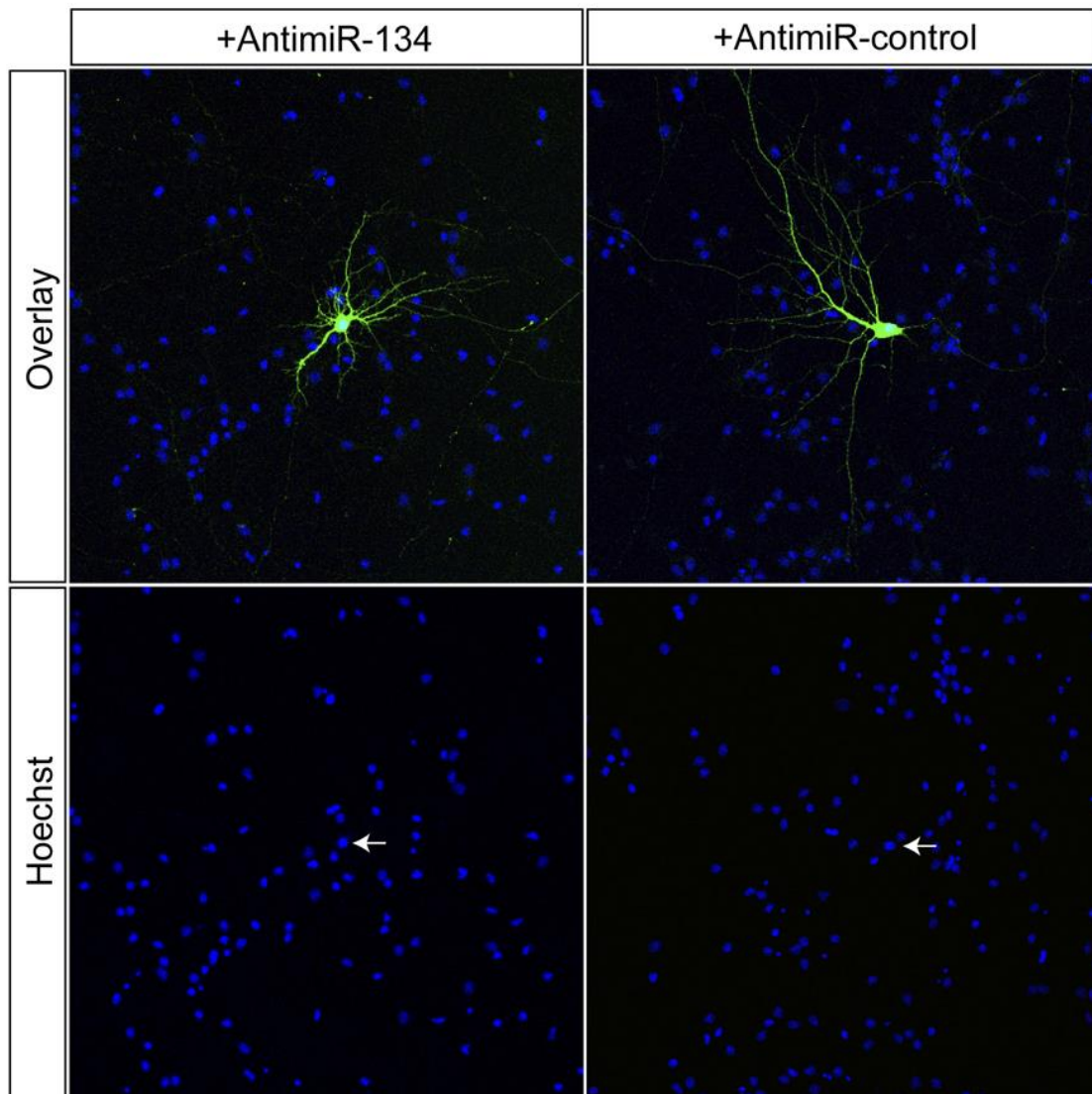


Fig S6: KCl stimulation and AntimiRs transfection do not induce nuclear fragmentation in rat hippocampal neurons. Representative images of membrane depolarized DIV10 hippocampal neurons transfected with GFP along with either AntimiR-134 or antimiR-control as described in the legend of fig 4. Nuclei were counterstained using Hoechst.

Supplementary Material

Chromatin immunoprecipitation (ChIP) assay

Cortical neurons (DIV5) at a density of 10^7 cells were treated with 1 % formaldehyde for 10 min at 37°C and then 0.125 M of glycine was added for 5 min at RT. Cells were pelleted and lysed with SDS lysis buffer (1% SDS, 10 mM EDTA, 50 mM Tris, protease inhibitors, pH 8.1), then incubated for 10 min on ice. The lysate was sonicated 40 times with 20 pulses and 25 sec pause between cycles, using a “cooled bath sonicator”- Sonifier 450 (Branson, duty cycle 90%, power 6.0). Sonicated lysates were centrifuged (13000 rpm, 4°C, 10 min), and the supernatant was diluted 10 fold in ChIP dilution buffer (0.01 % SDS, 1.1 % Triton X-100, 1.2 mM EDTA, 16.7 mM Tris-HCl, pH 8.1, 167 mM NaCl, protease inhibitors). 1-2% of diluted sonicated lysate was saved as input, while 2 ml of diluted cell supernatant was pre-cleared with 30 μ l of Salmon Sperm DNA (Invitrogen)/Protein A Agarose (Sigma)-50% slurry for 1 hour at 4°C with constant rotation. Chromatin was immunoprecipitated with 2 μ g of antibody (Normal rabbit IgG (sc-2027) and anti-mef2 (sc-313), both from Santa Cruz) overnight at 4°C. The histone/antibody complex was collected with addition of 20 μ l Salmon Sperm DNA/Protein A Agarose and incubation for 2 hours at 4°C. Protein A Agarose/antibody/histone complexes were washed with the following buffers at 4°C and centrifuged (2000 rpm, 4°C, 2 min): 2x with Low salt buffer (0.1 % SDS, 1% Triton X-100, 2 mM EDTA, 20 mM Tris-HCl, pH 8.1, 150 mM NaCl), 2x with High salt buffer (0.1 % SDS, 1% Triton X-100, 2 mM EDTA, 20 mM Tris-HCl, pH 8.1, 500 mM NaCl), 1x with LiCl buffer (0.25 M LiCl, 1 % IGEPAL-CA630, 1 % deoxycholic acid, 1 mM EDTA, 10 mM Tris, pH 8.1) and 3x with TE buffer at RT. The histone/antibody complex was eluted with 2x 250 μ l Elution buffer (1 % SDS, 0.1 M NaHCO₃) and crosslinking was reversed by the addition of 20 μ l 5 M NaCl and subsequent incubation for 4 hours at 65°C. 10 μ l of 0.5 M EDTA, 20 μ l 1 M Tris-HCl, pH 6.5 and 2 μ l of 10 mg/ml Proteinase K were added to the eluate and incubated for 1 hour at 45°C. The DNA was recovered by Phenol/Chloroform/Isopropanol extraction. The Expand High Fidelity PCR System (Roche) was used to amplify DNA from chromatin immunoprecipitated template DNA. The PCR parameters were: 95°C for 2 min and 41 cycles of 95°C 30 sec, 55-63°C 30 sec, 72°C 30 sec.

Cell culture and transfection

We decreased the efficiency of transfection of hippocampal neurons to simplify the analysis of the dendritic tree after membrane depolarization. Neither our stimulation protocols nor antimiRs transfection induced apoptosis as measured by Hoechst staining (Fig. S6). Since Mef2 proteins are known to promote calcium-dependent neuronal survival, we co-expressed BclX_L (a pro survival Bcl-2 family member) in the Mef2 knock down experiments, to further exclude that the reduced dendritic complexity of membrane depolarized neurons was not a

consequence of altered neuronal survival.

DNA and RNA oligonucleotides

Cloning and mutagenesis

pum2-3'UTR-fw: AGGCTCTAGAGTGAATTACCAAAACACCAACCCAA

pum2-3'UTR-rev: AATTGCTAGCGGAGCTGCTTTAACCATGTTCAAA

pum2-3'UTR-mut-fw: AACTCGAGAAAAAATAGTTTTTAAAGGGAAAAGTACAA

pum2-3'UTR-mut-rev: AAAAATAATTTTTTCTCGAGTTACAAGGTATAAATTTA

pum2-3'UTR-rev2: AGGCCTCAGACTGTGGTAATCAATCTCAGTCCAA

MBS10-fw: CTAGCAGATGACTAAAATACATGTGCTTTTGTGGAACCGGTATGC

MBS10-rev: TCGAGCATAACCGGTTCCACAAAAGCACATGTATTTTTAGTCATCTG

MBS10-mut-fw: CTAGCAGATGACGACACATCCATGTGCTTTTGTGGAACCGGTATGC

MBS10-mut-rev: TCGAGCATAACCGGTTCCACAAAAGCACATGGATGTGTCGTCATCTG

nur77-lucfw:

CTAGCTGGAAGCTACTATATTTAGCCGGCGCAGCGGGCGAGAGGAAAATAATTTATAGA

TCAAACAATC

nur77-lucrev:

TCGAGATTGTTTGATCTATAAATAGTTTTCTCTCGCCCGCTGCGCCGGCTAAATATAGT

AGCTTCCAG

3xMBS10-fw (sequencing carried out after cloning revealed a construct with 5xMBS10, which was used in subsequent experiments):

AGCTTGCTAAAATAACCCCTCGAGGCCCTAAAATAACCCCTCGAGGCCCTAAAATAAC

CCCTCGA

3xMBS10-rev (5xMBS10):

GATCTCGAGGGGGTATTTTTAGGGCCTCGAGGGGTATTTTTAGGGCCTCGAGGGGTAT

TTTTAGCA

miR-134sensor-fw:

GGCCGCTCCCTCTGGTCAACCAGTCACACTCCCTCTGGTCAACCAGTCACT

miR-134sensor-rev:

CTAGAGTGTCTGGTTGTCCTGTGGGTGTGTGTCTGGTTGTCCTGTGGGTGC

miR-329sensor-fw:

GGCCGCAAAAAGGTTAGCTGGGTGTGTTACAAAAGGTTAGCTGGGTGTGTTT

miR-329sensor-rev:

CTAGAAACACACCCAGCTAACCTTTTGTAAACACACCCAGCTAACCTTTTGC

miR-541sensor-fw:

GGCCGCAGTGTGACCAACATCAGAATCCCTTACAGTGTGACCAACATCAGAATCCCTTT

miR-541sensor-rev:

CTAGAAAGGGATTCTGATGTTGGTCACACTGTAAGGGATTCTGATGTTGGTCACACTGC

miR-controlsensor-fw:

GGCCGCAAGGGATTCTGATGTTGGTCACACTACAAGGGATTCTGATGTTGGTCACACTT

miR-controlsensor-rev:

CTAGAAGTGTGACCAACATCAGAATCCCTTGTAGTGTGACCAACATCAGAATCCCTTGC

Chromatin immunoprecipitation

nur77-chipfw: CCTGGTTCGGTATTTCGG

nur77-chiprev: AGCGCGGATTGTTTGATC

betaglobin-fw: TCTAGAAGGTACCCTCATGGCTGAA

betaglobin-rev: GGATATGCCCTGTGGAGTGTGAC

MBS10-fw: CCCTATCATGGGCGTTTGTTTACA

MBS10-rev: GCAGGGAGGATGTCACAAAGCAT

qPCR

Gtl2-fw: TGG AATAGGCCAACATCGTCA

Gtl2-rev: AGGCTCTGTGTCCATGTGTCC

premiR-329-fw: CGCTTCTGGTACCGGAAGAG

premiR-329-rev: GGTTAGCTGGGTGTGTTTCATTC

premiR-539-fw: TGAGGAGAAATTATCCTTGGTGTG

premiR-539-rev: CTCGAAAAGAAATTACCCTTGTATGA

premiR-382-fw: TTGAAGAGAAGTTGTTTCGTGGTG

premiR-382-rev: GTGTTGTCCGTGAATGATTCGT

premiR-134-fw: GGGTGTGTGACTGGTTGACCA

premiR-134-rev: GGGTTGGTGA CTAGGTGGCC

premiR-154-fw: TGCTTGAAGATAGGTTATCCGTGTT

premiR-154-rev: GG TACTGAAAAATAGGTCAACCGTG

premiR-369-fw: G TACTTGAAGGGAGATCGACCG

premiR-369-rev: AGATCAACCATGTATTATT CGAAGTCAG

premiR-541-fw: GCCAAAATCAGAGAAGGGATTC

premiR-541-rev: GTATGGATTCTGTGTTCCGCCAC

c-fos-fw: CATCATCTAGGCC CAGTGGC

c-fos-rev: AGGAACCAGACAGGTCCACATCT

beta3tubulin-fw: CCCCAGGGCTCAAGATGTC

beta3tubulin-rev: CGCTTGAACAGCTCCTGGAT

In situ hybridization

mmu-miR-134 (LNA): cccctctggtcaaccagtcaca

mmu-miR-134 MISMATCH (LNA): tccctctggtcaaggattccga

Synthetic RNA oligos (duplexes):

MiR-134 sense: 5'Phospho-ugugacugguugaccagagga

MiR-134 as: 5'Phospho-ccucuggucaaccaguauacu

Let-7c sense: 5'Phospho-ugagguaguagguuguauugguu

Let-7c as: 5'-Phospho-ccaauacaaccuacuacuuuaa

2'O-methyl-oligoribonucleotides (AntimiRs):

AntimiR-381: AGCTACAGAGAGCTTGCCCTTGTATAGTCA

AntimiR-329: GTCAAAAAGGTTTGCTGGGTGTGTTGTCA

AntimiR-495: TCGAAAGAAGTGCACCATGTTTGTTTAGCT

AntimiR-541: TGAGAGTGTGACCAACATCAGAATCCCTTTCAC

Antimircontrol: CATCACGTACGCGGAATACTTCGAAATGACC

AntimiR-134: TCTCTCCCTCTGGTCAACCAGTCACAAGGCT

Primers for „transcript walking“

1-fw: CTTTGCCTCGGCGTCTCTG

1-rev: CAGGATGGTACGGACTGGATG

2-fw: AAGGAGCTGGTACAGGGTTTCAA

2-rev: GAGCTTATGTCATTTCCCATCATG

3-fw: GGTGTTACCAACAGCGAGGAA

3-rev: ACTACTCCACAAATGCTGCTTACGT

4-fw: GCAGTACATGGCAAGAATGACC

4-rev: ATTTCCCTCAATGCTCAGAACAGG

5-fw: AGGCATAGCATGGTGACTIONGTT

5-rev: AGCTTTTCTGAGGCCTGATTTG

6-fw: CTATGCCAAACATATCTCCCTTTCC

6-rev: AGCTCACCTTACTCCCATACACCT

7-fw: GACTGAGCTGGGGAGATGAGAC

7-rev: TGGCAGGCAGTAATTAAGTGTTCA

8-fw: GCACTCAGCCAACTTCCAGC
8-rev: GATCTGCAACCCTATGCTAAGCA
9-fw: GCCTAATAACTAAAAGCGACGGAGT
9-rev: CACATGGGTGAAGAAAGGAAAGT
10-fw: GTTTCACGGGCCGTTAAAGTG
10-rev: AACAGGGTAGATTTAACTCCGTCTG
11-fw: AACTCAGCATTTTTGTGTGTGCAC
11-rev: AACAGATCCCGCATCTAAAGTCA
12-fw: CACTGTCAGGCGCAACTACAG
12-rev: CAGGTAACAGTGAACGTGCACAC
13-fw: CTGTGAACCACCATGTGGTAACC
13-rev: TAGTTGCGCCTGACAGTGAGAA
14-fw: CTTTCCTCCCCTCAGCATCTC
14-rev: CTTAGAGCACTAGCTGGTCTTGCA
15-fw: GCTGCTGCCATCCTGATCTTC
15-rev: ATCCATTTCCCTGGCACCATA
16-fw: TTTCCATCCCCACTGCTTTTAC
16-rev: GAGACCAAAGGAACCTATCCTCAG
17-fw: CAGGAGAATTGGGAGTCGCTAG
17-rev: CAAGGAGTGTGAGCTGGCAA
18-fw: TTCCCACTTGGTGCTCCTGT
18-rev: TCTAGTCCGGAAAAATGCAACAG
19-fw: CAAGTCTCTGGTGTATACGGTGCT
19-rev: CAGTGACAGTTCCCAAACCT
20-fw: GAGTATGTGTCTGGCTCAGGTA CTG
20-rev: AGTCTCCCAGACAGAGCGTGTC
21-fw: GCAGAGCATCCAATCTTACAGCA
21-rev: CACATCTCGTAAAGAGGCACAGG
22-fw: CCCTCCTATCAGACAACAGACAGTT
22-rev: GGTGGCTGTATTAATGACTGTAGTGAC
23-fw: GTGAAATGGAAGCCCTGGATC
23-rev: GACGAATCCTCACGGCTGAA
24-fw: GGTTAGGGAGCAAATCTGTCAGC
24-rev: CTGGAAGGCAGCATTGTCCT

5.2 The DEAH-box helicase DHX36 mediates dendritic localization of the neuronal precursor-microRNA-134

Bicker S, **Khudayberdiev S**, Weiss K, Zocher K, Baumeister S, Schrott G
(2013) Genes Dev 27: 991-996

The DEAH-box helicase DHX36 mediates dendritic localization of the neuronal precursor-microRNA-134

Silvia Bicker,¹ Sharof Khudayberdiev,¹
Kerstin Weiß,¹ Kathleen Zocher,¹
Stefan Baumeister,² and Gerhard Schratt^{1,3}

¹Institut für Physiologische Chemie, Biochemisch-Pharmakologisches Centrum Marburg, Philipps-Universität Marburg, 35032 Marburg, Germany; ²Fachbereich Biologie-Protein Analytik, Philipps-Universität Marburg, 35032 Marburg, Germany

Specific microRNAs (miRNAs), including miR-134, localize to neuronal dendrites, where they control synaptic protein synthesis and plasticity. However, the mechanism of miRNA transport is unknown. We found that the neuronal precursor-miRNA-134 (pre-miR-134) accumulates in dendrites of hippocampal neurons and at synapses in vivo. Dendritic localization of pre-miR-134 is mediated by the DEAH-box helicase DHX36, which directly associates with the pre-miR-134 terminal loop. DHX36 function is required for miR-134-dependent inhibition of target gene expression and the control of dendritic spine size. Dendritically localized pre-miR-134 could provide a local source of miR-134 that can be mobilized in an activity-dependent manner during plasticity.

Supplemental material is available for this article.

Received November 30, 2012; revised version accepted April 5, 2013.

MicroRNAs (miRNAs) are important regulators of morphological and functional plasticity in the developing and mature nervous system (Ashraf et al. 2006; Schratt et al. 2006; Rajasethupathy et al. 2009; Gao et al. 2010). Specific miRNAs control plasticity by binding to dendritic mRNAs (Schuman et al. 2006; Bramham and Wells 2007; Martin and Ephrussi 2009), thereby modulating the local synthesis of the respective proteins at synapses in an activity-dependent manner (Schratt et al. 2006; Banerjee et al. 2009; Fiore et al. 2009; Muddashetty et al. 2011). The biogenesis of miRNAs involves two subsequent RNase-dependent cleavage steps: Drosha-mediated processing of primary miRNA transcripts (pri-miRNAs) in the nucleus followed by Dicer-mediated processing of 70- to 100-nucleotide (nt) stem-loop precursors (precursor-miRNAs [pre-miRNAs]) in the cytoplasm (Kim 2005; Krol et al. 2010). miRNA biogenesis can be regulated by sequence-specific RNA-binding proteins (RBPs) that preferentially interact with

[*Keywords:* dendritic transport; DHX36; precursor-microRNA; protein synthesis; synaptic plasticity]

³Corresponding author

E-mail gerhard.schratt@staff.uni-marburg.de

Article is online at <http://www.genesdev.org/cgi/doi/10.1101/gad.211243.112>.

the terminal loop structure of pri- and pre-miRNAs (Krol et al. 2010; Newman and Hammond 2010). Interestingly, miR-29b contains a sequence element at the 3' end of the mature miRNA that directs its nuclear localization (Hwang et al. 2007), but nothing is known about miRNA sequence determinants responsible for localization to specific cytoplasmic compartments, such as the synaptodendritic compartment of neurons.

We speculated that dendritic localization of specific miRNAs could occur at the pre-miRNA stage, possibly by the presence of sequence elements within pre-miRNA terminal loops that serve as binding sites for RBPs, which are in turn part of transport complexes. Dendritic localization of specific pre-miRNAs would offer the advantage of a local source of miRNAs that could be mobilized, for example, in response to synaptic activity.

Results and Discussion

To interrogate synaptodendritic localization of pre-miRNAs, we selected 16 previously identified dendritic miRNAs (Schratt et al. 2006; Siegel et al. 2009) and determined corresponding pre-miRNA levels in synaptosomes by quantitative RT-PCR (qRT-PCR). We found that for two of these candidates (pre-miR-7a-2 and pre-miR-134), the degree of synaptic enrichment was significantly higher compared with the nuclear U6 snRNA and at least equal to the known dendritic noncoding RNA BC1 (Brosius and Tiedge 2001), suggesting that these pre-miRNAs are actively transported into the synaptodendritic compartment (Fig. 1A). Due to the well-documented synaptic functions of miR-134 (Schratt et al. 2006; Fiore et al. 2009; Gao et al. 2010), we decided to focus on pre-miR-134. Synaptic enrichment of pre-miR-134 was validated by Northern blot of synaptosomal and whole-brain RNA preparations (Supplemental Fig. S1; Siegel et al. 2009). Since synaptosomes contain both pre- and postsynaptic compartments, we performed locked nucleic acid (LNA)-based fluorescent in situ hybridization (FISH) in rat hippocampal neurons (7 d in vitro [DIV]) (Fig. 1B) to determine the subcellular localization of pre-miR-134. BDNF (brain-derived neurotrophic factor) treatment of neurons was used to increase pre-miR-134 expression (Fiore et al. 2009). Using a FISH probe specifically recognizing the loop sequence of pre-miR-134 (Supplemental Fig. S2), we detected a specific signal in the neuronal cell body as well as discrete punctate staining in proximal and distal parts of MAP2-positive dendrites (Fig. 1B, top panel, insert at higher magnification). In contrast, expression of pre-miR-137, which was not enriched in synaptosomes, was restricted to the cell body compartment (Fig. 1B, bottom panel). Quantification of FISH signals along the entire length of multiple dendrites confirms the specific dendritic localization of pre-miR-134 (Fig. 1C). The specificity of our FISH protocol was validated with negative (scrambled LNA oligonucleotide) and positive (LNA oligonucleotide recognizing mature miR-134) (Schratt et al. 2006) control probes (Supplemental Fig. S3). The presence of pre-miR-134 and pre-miR-7a-2, but not pre-miR-137, in processes of rat hippocampal neurons was further confirmed using a compartmentalized culture system (Fig. 1D; Supplemental Fig. S4a,b). This system also faithfully recapitulated process enrichment of mature miR-134 but not of the nondendritic miR-133b (Supplemental

miR-134 (pre-miR-150C134) largely regained the capacity to localize to dendrites (Fig. 2E; Supplemental Fig. S7b). Together, these experiments suggest that the pre-miR-134 loop sequence is an important determinant of pre-miR-134 dendritic localization.

We speculated that specific RBPs that interact with the pre-miR-134 loop might be responsible for directed transport to the synpto-dendritic compartment. To identify proteins that selectively interact with the pre-miR-134 loop, we performed pull-down experiments by incubating rat forebrain protein extract with biotin-tagged pre-miR-134 or respective mutants coupled to streptavidin beads (Fig. 3A, Heo et al. 2008, 2009). Thereby, we identified one band above 100 kDa that was specifically present in eluates from pull-downs with wild-type pre-miR-134 but not with pre-miR-150 or pre-miR-134C150 (Fig. 3B, arrow). We identified this protein as DHX36 by mass spectrometry

(Supplemental Table T1). In addition, we identified DHX9 (Fig. 3B, arrow) as a protein that interacts with all tested pre-miRNAs, in accordance with a described function of DHX9 within RNA-induced silencing complex (RISC) (Robb and Rana 2007). The specific interaction of pre-miR-134 with DHX36 could be confirmed by Western blot using an anti-DHX36 antibody (Fig. 3C, top panel). Importantly, Dicer interacted with all three pre-miRNAs (Fig. 3C, middle panel), demonstrating that all of them were per se competent in protein binding. An unrelated protein, eIF3 η , did not specifically interact with any of the tested pre-miRNAs (Fig. 3C, bottom panel). In the case of other dendritically localized pre-miRNAs, the interaction with DHX36 was strongly reduced (Fig. 3D,E), suggesting that DHX36 preferentially interacts with pre-miR-134. Affinity-purified full-length DHX36 and the isolated DHX36 N-terminal domain, which contains an RNA-binding motif (Chalupnikova et al. 2008), both associated with radio-labeled pre-miR-134 in electrophoretic mobility shift assay (EMSA) *in vitro* (Supplemental Fig. S8), demonstrating a direct interaction between DHX36 and pre-miR-134. Using *in vitro* pre-miRNA cleavage assays (Leuschner and Martinez 2007), we found that DHX36 interfered with cleavage of synthetic pre-miR-134 by recombinant Dicer but not with Dicer-mediated pre-miR-150 cleavage (Fig. 3F,G). Together, our experiments demonstrate that DHX36 directly interacts with pre-miR-134 and reduces Dicer-mediated pre-miR-134 cleavage *in vitro*.

We next addressed whether DHX36 functions in dendritic localization of pre-miR-134. DHX36 was shown to resolve secondary nucleic acid structures in the nucleus (Vaughn et al. 2005) and regulate RNA metabolism in the cytoplasm in nonneuronal cells (Tran et al. 2004; Chalupnikova et al. 2008; Zhang et al. 2011). However, DHX36 has not yet been studied in neurons. Using compartmentalized primary rat hippocampal neuron cultures, we detected DHX36 expression in both the cell body and, to a lesser extent, the process compartment (Fig. 4A). In further support of a function of DHX36 in neuronal processes, ectopically expressed GFP-DHX36 fusion protein localized to dendrites and axons (Supplemental Fig. S9). To test whether pre-miR-134 interacts with DHX36 in neurons, we transfected cortical neurons at 6 DIV with either pre-miR-134 or pre-miR-150 and performed an RNA immunoprecipitation (RNA-IP) assay. We found that transfected pre-miR-134, in contrast to pre-miR-150, was specifically enriched in anti-DHX36 compared with IgG immunoprecipitates, as judged by qRT-PCR (Fig. 4B). This finding suggests that endogenous DHX36 and synthetic pre-miR-134 interact in neurons. To investigate the function of DHX36, we designed shRNA expression constructs targeting different regions of the rat DHX36 mRNA and assessed their efficiency by nucleofection (Fig. 4C). To assess the role of DHX36 in dendritic transport of pre-miR-134, we combined plasmid-based knockdown of DHX36 (3 d of expression) with short-term transfection of Cy3-labeled pre-miRNAs. To rule out potential effects of DHX36 knockdown on miR-134 processing, we decided to study subcellular distribution of synthetic Cy3-pre-miR-134 shortly after transfection. At 2.5 h after transfection, Cy3-pre-miR-134 was found to be excluded from the nucleus, and the vast majority of Cy3-pre-miR-134 was still not processed (Supplemental Fig. S6). Neurons transfected with the two most effective DHX36 shRNAs displayed a significant reduction in the percentage of

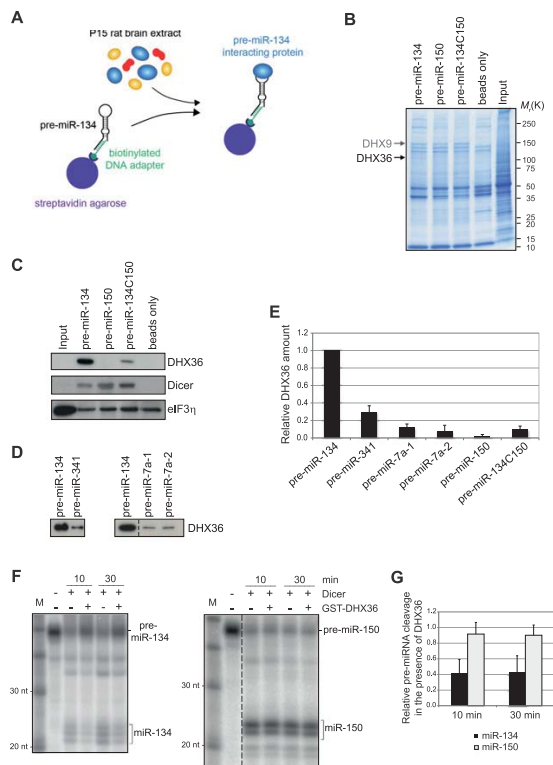


Figure 3. DHX36 interacts with the pre-miR-134 terminal loop. (A) Scheme of the purification strategy used to isolate pre-miR-134-interacting proteins from P15 rat brain extract. (B) Coomassie gel of pull-downs using rat P15 brain extract and the indicated pre-miRNAs. Arrows point to bands that were identified by mass spectrometry as DHX9 (~140 kDa) and DHX36 (~110 kDa). (C) Western blot against the indicated proteins with extracts from pull-downs shown in B. (D) Western blot against DHX36 with extracts from the indicated pre-miRNA pull-downs. (E) Quantification of DHX36 binding in pre-miRNA pull-down experiments (pre-miR-134 = 1; mean \pm SD, n = 3). (F) *In vitro* pre-miRNA cleavage assay. pre-miRNAs were incubated with recombinant Dicer for the indicated time in either the presence or absence of GST-DHX36. The position of pre-miRNAs and mature miRNAs is indicated. (G) Ratio of mature miRNA to pre-miRNA as an index for Dicer cleavage activity (mean \pm SD, n = 4–5; conditions without DHX36 were set to 1 for both time points).

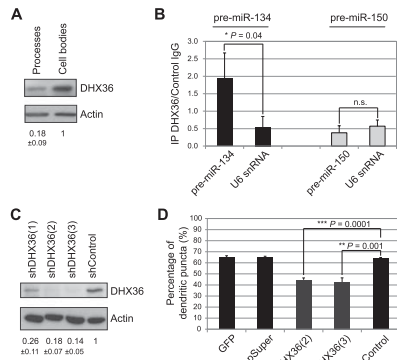


Figure 4. DHX36 is required for dendritic localization of pre-miR-134 in hippocampal neurons. (A) Western blot against the indicated proteins with extracts from process or cell body fractions of hippocampal neurons. Quantification of band intensities is indicated below (mean ± SD, $n = 3$). (B) RNA-IP of cortical neurons transfected with the indicated pre-miRNAs using a DHX36 or control IgG antibody. Ratio of RNA amounts from DHX36 immunoprecipitates to control IgG immunoprecipitates as determined by qRT-PCR is shown (mean ± SD, $n = 3$). (C) Western blot against the indicated proteins with extracts from hippocampal neurons nucleofected with the indicated shRNA-expressing constructs. Quantification of band intensities is indicated below (mean ± SD, $n = 2$). (D) Percentage of dendritic Cy3-pre-miR-134 puncta observed in hippocampal neurons transfected with the indicated constructs (mean ± SD, $n = 3$, ANOVA: $F(4;10) = 84$, $P < 0.001$; 30 neurons per condition).

dendritic Cy3-pre-miR-134 puncta (Fig. 4D; Supplemental Fig. S10a). DHX36 knockdown did not affect global levels of pre-miR-134 and mature miR-134 (Supplemental Fig. S10b,c). These results suggest that DHX36 is specifically required for the accumulation of pre-miR-134 in neuronal dendrites.

Finally, we addressed whether DHX36-dependent localization of pre-miR-134 might contribute to the activity of miR-134 in dendrites. For these experiments, we first used a luciferase reporter gene that contains a perfect miR-134-binding site in the context of the *Limk1* 3' untranslated region (UTR; *Limk1* 134pbds) (Christensen et al. 2010). The *Limk1* 3' UTR confers dendritic localization of the reporter (Schratt et al. 2006), allowing us to study the role of DHX36 in local translation. Upon DHX36 knockdown, expression of the *Limk1* 134pbds reporter gene was significantly increased compared with control conditions, whereas expression of a reporter gene containing a mutated miR-134-binding site was unaffected (Fig. 5A). In addition, both a *Pum2* luciferase reporter gene containing a single miR-134-binding site (Fiore et al. 2009) and endogenous *Limk1* protein expression were similarly induced by DHX36 knockdown in neurons (Fig. 5B; Supplemental Fig. S10d). Together, these results demonstrate that DHX36 knockdown results in an increased expression of known dendritic miR-134 target genes, possibly due to reduced dendritic pre-miR-134 accumulation. Nevertheless, based on our data, we cannot rule out that derepression of miR-134 targets in the cell body might also contribute to the observed effects of DHX36 knockdown. Finally, we interrogated whether DHX36 knockdown had an impact on neuronal function, possibly via regulation of miR-134 activity. Toward this end, we analyzed dendritic spine morphology, since we previously found that treatment of hippocampal neurons with miR-134 function-blocking antisense oligonucleotides

led to elevated spine size (Schratt et al. 2006). Consistent with reduced dendritic miR-134 activity upon DHX36 knockdown, we found that neurons transfected with a DHX36 shRNA construct contained a higher fraction of large mushroom-shaped spines compared with neurons transfected with a control shRNA (Fig. 5C; Supplemental Fig. S11). Accordingly, the average spine volume of neurons transfected with two independent DHX36 shRNA constructs was significantly higher compared with control conditions (Fig. 5D). This result demonstrates that DHX36 negatively regulates dendritic spine morphogenesis in hippocampal neurons. It is further consistent with the idea that DHX36-dependent pre-miR-134 accumulation in dendrites could be important for neuronal function.

Taken together, our results show that DHX36 plays a role in dendritic localization of pre-miR-134 and spine

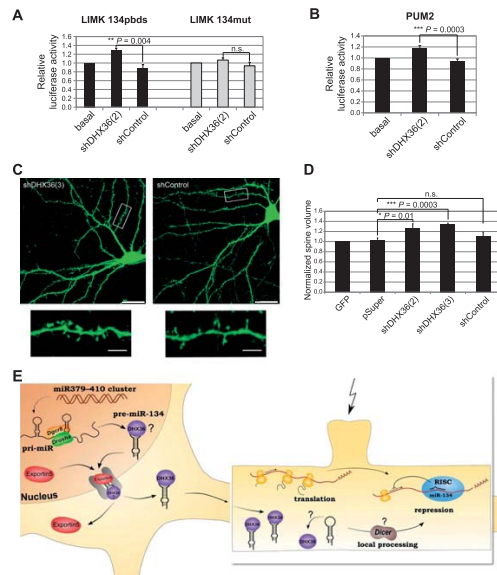


Figure 5. DHX36 is required for miR-134-regulated neuronal functions. (A,B) Reporter gene activity in primary neurons transfected with the indicated shRNA constructs and firefly luciferase reporters containing *Limk1* (A, 15 DIV hippocampal neurons) and *Pum2* (B, 15 DIV cortical neurons) 3' UTRs. Cotransfection of empty *Renilla* reporter served as transfection control. Relative luciferase activity represents the ratio of firefly to *Renilla* activity; basal condition was set to 1 (mean ± SD, $n = 3$, each experimental condition measured in duplicates within one experiment). (C) Representative images of hippocampal neurons transfected with either shDHX36(3) (left) or shControl (right) shRNAs. Inserts at higher magnification illustrate increased proportion of large, mushroom-shaped spines in the shDHX36 condition compared with shControl. Bars: main panels, 20 μm; inserts, 5 μm. (D) Quantification of average normalized spine volume as determined by the ratio of GFP signal in dendritic spines to total cell intensity. GFP-only condition was set to 1 (mean ± SD, $n = 3$; ANOVA: $F(3;8) = 15,921$, $P = 0.001$; 18 neurons per condition; 150–200 spines per neuron). (E) Working model for the role of DHX36 in pre-miR-134 dendritic transport and processing. The pre-miR-134 loop contains a *cis*-acting dendritic targeting element that is recognized by DHX36, resulting in pre-miR-134 transport to the dendrite. In the postsynaptic compartment, stimulation of specific dendritic spines (flash) may trigger Dicer-dependent pre-miRNA processing (possibly involving release of DHX36), thereby enabling an enhanced production of mature miR-134 and repression of miR-134 target mRNAs.

morphogenesis, a process regulated by miR-134 (Fig. 5E). This adds subcellular localization to the growing list of functions for proteins that associate with the terminal loop of specific pre-miRNAs (Krol et al. 2010). The presumptive DHX36-binding site within the pre-miR-134 central loop is not present in the loop of other dendritic pre-miRNAs, which, together with our *in vitro* binding assays, suggests that distinct localization mechanisms are used by specific dendritic pre-miRNAs. Previously, we found that mature miR-134 is delivered to dendrites when transfected into neurons (Schratt et al. 2006). The underlying mechanism is unknown but could involve cotransport of miR-134 with its dendritic target mRNAs, such as *Limk1*. We speculate that dendritically localized pre-miR-134 might, in parallel, provide a pool of miR-134 that can be rapidly mobilized in response to activity. This local pool could be important to reinforce miR-134-mediated repression of gene expression, for example, in conditions of chronically elevated activity that are known to induce homeostatic synaptic scaling (Turrigiano 2008). The molecular mechanisms involved in a possible local control of miR-134 production in dendrites are currently unknown. Dicer has been detected in synaptosomes (Lugli et al. 2005), suggesting that pre-miR-134 could undergo local Dicer-dependent processing at synapses. Since DHX36 competes with Dicer *in vitro* (Fig. 3F) and Argonaute complexes that contain DHX36 are devoid of Dicer activity (Hock et al. 2007), we speculate that pre-miR-134 has to be released from DHX36 upon activity to allow efficient pre-miR-134 processing at the synapse (Fig. 5E). Future work will address the mechanism of activity-dependent local processing of pre-miR-134 and its significance for dendritic protein synthesis and synaptic plasticity.

Materials and methods

Cell culture

Primary hippocampal and cortical embryonic (embryonic day 18) neuron cultures were prepared and cultured as described (Schratt et al. 2006). For compartmentalized neuron cultures, dissociated hippocampal neurons were plated onto 1- μ m pore and 30-mm diameter polyethylene terephthalate (PET) membrane filter inserts (Millipore) that were matrix-coated with poly-L-lysine (Sigma-Aldrich) and Laminin (BD Biosciences) on the top and bottom (Poon et al. 2006).

Transfections

Transfections of primary neurons using Lipofectamine 2000 (Invitrogen) were performed as described (Siegel et al. 2009). For validation of shRNA efficacy, primary cortical neurons of rat embryos (E18) were nucleofected using the P3 Primary Cell 4D-Nucleofector kit (Lonza), program DC-104, according to the manufacturer's instructions. Transfections of primary hippocampal or cortical neurons with *in vitro* transcribed pre-miRNAs (25–75 nM) were performed using siPORT NeoFX transfection agent (Ambion).

Preparation of synaptosomes

Synaptosomes were prepared from postnatal day 15 (P15) Sprague-Dawley rat pups as previously described (Schratt et al. 2004).

In vitro transcription of pre-miRNAs

Pre-miRNAs were *in vitro* transcribed from dsDNA templates (Supplemental Material) using the MEGAshortscript T7 kit (Ambion) according to the manufacturer's instructions, with a template concentration of 150 nM and an incubation time of 4 h at 37°C. pre-miRNAs were purified using illustra MicroSpin G-25 columns (GE Healthcare).

RNA labeling

Labeling of pre-miRNAs by Cy3 was performed using the Label IT nucleic acid labeling kit (Mirus) according to the manufacturer's instructions. For Dicer assays, pre-miRNAs were 5' end-labeled using [γ -³²P] ATP (PerkinElmer) as previously described (Leuschner and Martinez 2007).

Subcellular localization of *in vitro* transcribed pre-miRNAs

Rat hippocampal neurons were transfected at 6 DIV with 30 nM Cy3-labeled precursors using siPORT NeoFX transfection agent (Ambion) for 2 h. Fifteen minutes post-transfection, cells were treated with Cell Scrub buffer (Genlantis) for 5 min to remove extracellular Cy3 complexes, fixed, and stained for MAP2 to visualize dendrites. Nuclei were counterstained with Hoechst (Invitrogen). Data sets were blinded to the experimental conditions, and Z-stack images (seven consecutive optical sections per stack) were taken with an LSM 5 Pascal confocal microscope (Zeiss). ImageJ software ("analyze particles" option) was used for subsequent analysis of intracellular Cy3 puncta distribution. For quantification, the average percentage of dendritic puncta compared with the total number of intracellular puncta was determined for each pre-miRNA.

RNA pull-down

The RNA pull-down approach used in this study was based on a previously described protocol for isolation of pre-let-7-binding proteins concerning the general procedure (Heo et al. 2008) and on a protocol for FMRP immunoprecipitation concerning brain lysate preparation (Edbauer et al. 2010). See the Supplemental Material for further details.

RNA-IP

For RNA-IP, cortical neurons were transfected with *in vitro* transcribed pre-miRNAs and immunoprecipitated using rabbit anti-DHX36 antibody (Novus Biologicals). RNA-IP was performed using the same buffer system as described for the RNA pull-down approach. A detailed protocol can be found in the Supplemental Material.

FISH

Dissociated hippocampal neurons were treated with BDNF (PeproTech, 50 ng/mL) for 2 h before fixation. FISH was performed as previously described (Fiore et al. 2009) using FITC-labeled LNA probes (5 pmol per well in the 24-well format; Exiqon) directed against the pre-miR-134 loop, the pre-miR-137 loop, the mature miR-134 sequence, and a control probe of unrelated sequence (scramble). Signals were further amplified by a two-step antibody procedure. Neurons were costained for the dendritic protein MAP2.

Luciferase assay

Primary neurons were transfected in duplicates with 50 ng of pGL3 firefly reporter constructs and equal amounts of empty *Renilla* reporter as transfection control. For DHX36 knockdown, neurons were cotransfected with 20 ng of the respective pSuper construct. Luciferase assays were performed after 3 d of expression using the Dual-Luciferase reporter assay system (Promega) on the GloMax R96 Microplate Luminometer (Promega).

Spine analysis

For spine analysis, images were taken on an LSM5 Zeiss Pascal confocal microscope and analyzed with ImageJ software as previously described (Siegel et al. 2009). For each condition, spines from 18 representative hippocampal neurons (150–200 spines per neuron) derived from three independent experiments were measured.

Antibodies

Primary antibodies used in this study were as follows: mouse anti- β -actin antibody (Sigma), rabbit anti-DHX36 antibody (Novus Biologicals); immunoprecipitation, Western, goat anti-DHX36 antibody (Santa Cruz Biotechnology); Western, rabbit anti-Dicer antibody (D-349; provided by Witold Filipowicz, FMI Basel), goat anti-eIF3 η antibody (Santa Cruz Biotechnology), Alexa488 rabbit anti-FITC antibody (Molecular Probes), rabbit

anti-GFAP antibody (DAKO), mouse anti-MAP2 antibody (Sigma), and rabbit anti-NUP153 antibody (Abcam).

Plasmids

shRNA sequences (summarized in the Supplemental Material) were designed using the online available Dharmacon siRNA design center and cloned into pSuper (Oligoengine). Reporter plasmids pGL3 Limk1 134pbds (Christensen et al. 2010), pGL3 Limk1 134mut (Schratt et al. 2006), and pGL3 Pum2(long) (Fiore et al. 2009) have been described. pAcG3XE-RHAU-His6, pGEX-2T-GST-Nter, and pEGFP-C1-DHX36 were provided by Yoshikuni Nagamine (Friedrich Miescher Institute, Basel, Switzerland).

Dicer assay

[³²P] 5' end-labeled pre-miRNAs (20,000 counts per minute [cpm]) were incubated in a processing reaction with 1 U of recombinant Dicer (Recombinant Dicer Enzyme kit, Genlantis) for 10–30 min at 37°C in either the absence or presence (preincubation for 1 h at room temperature) of 30 nM GST-DHX36 (full-length). Reaction products were resolved on a 15% denaturing PAGE and visualized by autoradiography.

Mass spectrometry analysis

MALDI was performed using an Autoflex Bruker Daltonics mass spectrometer. Data analysis was done with the MASCOT program (Matrix Science). A detailed protocol can be found in the Supplemental Material.

Statistics

For each data set, three independent biological experiments were performed if not stated otherwise. Error bars represent standard deviation. *P*-values were calculated with Student's *t*-test (two-tailed, type 2) for one-way comparisons and with ANOVA followed by post-hoc test (Student's *t*-test with Bonferroni correction) for multi-way comparisons.

Acknowledgments

We thank W. Filipowicz and Y. Nagamine for providing reagents; U. Beck, E. Becker, N. Braun, K. Burk, R. Condrum, G. Jarosch, H. Kaiser, B. Kowalski, and T. Wüst for excellent technical assistance; and R. Fiore for critically reading the manuscript. This work was funded by the DFG (SFB593) and the EMBO Young Investigator Program. S.B. is a recipient of a DOC-FORTE fellowship of the Austrian Academy of Sciences.

References

Ashraf SI, McLoon AL, Scarsic SM, Kunes S. 2006. Synaptic protein synthesis associated with memory is regulated by the RISC pathway in *Drosophila*. *Cell* **124**: 191–205.

Banerjee S, Neveu P, Kosik KS. 2009. A coordinated local translational control point at the synapse involving relief from silencing and MOV10 degradation. *Neuron* **64**: 871–884.

Bramham CR, Wells DG. 2007. Dendritic mRNA: Transport, translation and function. *Nat Rev Neurosci* **8**: 776–789.

Brosius J, Tiedge H. 2001. Neuronal BC1 RNA: Intracellular transport and activity-dependent modulation. *Results Probl Cell Differ* **34**: 129–138.

Chalupnikova K, Lattmann S, Selak N, Iwamoto F, Fujiki Y, Nagamine Y. 2008. Recruitment of the RNA helicase RHAU to stress granules via a unique RNA-binding domain. *J Biol Chem* **283**: 35186–35198.

Christensen M, Larsen LA, Kauppinen S, Schratt G. 2010. Recombinant adeno-associated virus-mediated microRNA delivery into the post-natal mouse brain reveals a role for miR-134 in dendritogenesis in vivo. *Front Neural Circuits* **3**: 16.

Edbauer D, Neilson JR, Foster KA, Wang CF, Seeburg DP, Batterton MN, Tada T, Dolan BM, Sharp PA, Sheng M. 2010. Regulation of synaptic structure and function by FMRP-associated microRNAs miR-125b and miR-132. *Neuron* **65**: 373–384.

Fiore R, Khudayberdiev S, Christensen M, Siegel G, Flavell SW, Kim TK, Greenberg ME, Schratt G. 2009. Mef2-mediated transcription of the miR379-410 cluster regulates activity-dependent dendritogenesis by fine-tuning Pumilio2 protein levels. *EMBO J* **28**: 697–710.

Gao J, Wang WY, Mao YW, Graff J, Guan JS, Pan L, Mak G, Kim D, Su SC, Tsai LH. 2010. A novel pathway regulates memory and plasticity via SIRT1 and miR-134. *Nature* **466**: 1105–1109.

Heo I, Joo C, Cho J, Ha M, Han J, Kim VN. 2008. Lin28 mediates the terminal uridylation of let-7 precursor microRNA. *Mol Cell* **32**: 276–284.

Heo I, Joo C, Kim YK, Ha M, Yoon MJ, Cho J, Yeom KH, Han J, Kim VN. 2009. TUT4 in concert with Lin28 suppresses microRNA biogenesis through pre-microRNA uridylation. *Cell* **138**: 696–708.

Hock J, Weinmann L, Ender C, Rudel S, Kremmer E, Raabe M, Urlaub H, Meister G. 2007. Proteomic and functional analysis of Argonaute-containing mRNA-protein complexes in human cells. *EMBO Rep* **8**: 1052–1060.

Hwang HW, Wentzel EA, Mendell JT. 2007. A hexanucleotide element directs microRNA nuclear import. *Science* **315**: 97–100.

Kim VN. 2005. MicroRNA biogenesis: Coordinated cropping and dicing. *Nat Rev Mol Cell Biol* **6**: 376–385.

Krol J, Loedige I, Filipowicz W. 2010. The widespread regulation of microRNA biogenesis, function and decay. *Nat Rev Genet* **11**: 597–610.

Leuschner PJ, Martinez J. 2007. In vitro analysis of microRNA processing using recombinant Dicer and cytoplasmic extracts of HeLa cells. *Methods* **43**: 105–109.

Lugli G, Larson J, Martone ME, Jones Y, Smalheiser NR. 2005. Dicer and eIF2c are enriched at postsynaptic densities in adult mouse brain and are modified by neuronal activity in a calpain-dependent manner. *J Neurochem* **94**: 896–905.

Martin KC, Ephrussi A. 2009. mRNA localization: Gene expression in the spatial dimension. *Cell* **136**: 719–730.

Muddashetty RS, Nalavadi VC, Gross C, Yao X, Xing L, Laur O, Warren ST, Bassell GJ. 2011. Reversible inhibition of PSD-95 mRNA translation by miR-125a, FMRP phosphorylation, and mGluR signaling. *Mol Cell* **42**: 673–688.

Newman MA, Hammond SM. 2010. Emerging paradigms of regulated microRNA processing. *Genes Dev* **24**: 1086–1092.

Poon MM, Choi SH, Jamieson CA, Geschwind DH, Martin KC. 2006. Identification of process-localized mRNAs from cultured rodent hippocampal neurons. *J Neurosci* **26**: 13390–13399.

Rajasekharan P, Fiumara F, Sheridan R, Betel D, Puthanveetil SV, Russo JJ, Sander C, Tuschl T, Kandel E. 2009. Characterization of small RNAs in aplysia reveals a role for miR-124 in constraining synaptic plasticity through CREB. *Neuron* **63**: 803–817.

Robb GB, Rana TM. 2007. RNA helicase A interacts with RISC in human cells and functions in RISC loading. *Mol Cell* **26**: 523–537.

Schratt GM, Nigh EA, Chen WG, Hu L, Greenberg ME. 2004. BDNF regulates the translation of a select group of mRNAs by a mammalian target of rapamycin-phosphatidylinositol 3-kinase-dependent pathway during neuronal development. *J Neurosci* **24**: 9366–9377.

Schratt GM, Tuebing F, Nigh EA, Kane CG, Sabatini ME, Kiebler M, Greenberg ME. 2006. A brain-specific microRNA regulates dendritic spine development. *Nature* **439**: 283–289.

Schuman EM, Dynes JL, Steward O. 2006. Synaptic regulation of translation of dendritic mRNAs. *J Neurosci* **26**: 7143–7146.

Siegel G, Obernosterer G, Fiore R, Oehmen M, Bicker S, Christensen M, Khudayberdiev S, Leuschner PF, Busch CJ, Kane C, et al. 2009. A functional screen implicates microRNA-138-dependent regulation of the depalmitoylation enzyme APT1 in dendritic spine morphogenesis. *Nat Cell Biol* **11**: 705–716.

Tran H, Schilling M, Wirbelauer C, Hess D, Nagamine Y. 2004. Facilitation of mRNA deadenylation and decay by the exosome-bound, DEXH protein RHAU. *Mol Cell* **13**: 101–111.

Turrigiano GG. 2008. The self-tuning neuron: Synaptic scaling of excitatory synapses. *Cell* **135**: 422–435.

Vaughn JP, Creacy SD, Routh ED, Joyner-Butt C, Jenkins GS, Pauli S, Nagamine Y, Akman SA. 2005. The DEXH protein product of the DHX36 gene is the major source of tetramolecular quadruplex G4-DNA resolving activity in HeLa cell lysates. *J Biol Chem* **280**: 38117–38120.

Zhang Z, Kim T, Bao M, Facchinetti V, Jung SY, Chaffari AA, Qin J, Cheng G, Liu YJ. 2011. DDX1, DDX21, and DHX36 helicases form a complex with the adaptor molecule TRIF to sense dsRNA in dendritic cells. *Immunity* **34**: 866–878.

Supplementary Information

Supplementary Materials and Methods

RNA extraction

Total RNA from cultured hippocampal and cortical neurons was isolated using mirVana miRNA Isolation Kit (Ambion). Total RNA from forebrain or synaptosome preparations was isolated using Qiazol reagent (Qiagen) according to manufacturer's instructions. Aliquots of these RNA preparations were further enriched for small RNA molecules using the mirVana miRNA Isolation Kit (Ambion), with a stated cut-off of ~200 nt.

RNA pulldown

Preparation of pre-miRNAs

In vitro transcribed pre-miRNAs were synthesized with a 5' extension complementary to a 3'-end-biotinylated adapter DNA oligonucleotide, which allowed pulldown of pre-miRNA associated proteins with streptavidin-coated beads (based on (Heo et al. 2009)). Sequences for the respective DNA templates and the DNA adapter are summarized below.

Preparation of beads

The 3'-biotinylated DNA adapter was incubated with streptavidin-conjugated agarose beads (Sigma) in buffer A1 (10 mM HEPES (pH 7.4), 100 mM NaCl, 2 mM EDTA), at 4°C for 1 h at constant rotation. Beads were washed twice with buffer B (10 mM HEPES (pH 7.4), 300 mM NaCl, 0.2 mM EDTA) and coupled with the *in vitro* transcribed pre-miRNAs in buffer B supplemented with 1 U μl^{-1} SUPERase inhibitor (Ambion) for 3 h at room temperature at constant rotation. The beads were washed twice with buffer A1 and incubated with precleared cell extract.

Preparation of brain extracts

P15 rat pup brains were homogenized in lysis buffer (10 mM HEPES (pH 7.4), 200 mM NaCl, 30 mM EDTA, 0.5 % Triton X-100; supplemented with 1 U μl^{-1} SUPERase inhibitor (Ambion) and protease inhibitor cocktail (Roche)) with a teflon-coated Dounce-Potter homogenizer by eight up and down strokes. After removing the nuclear fraction by centrifugation at 3,000 x g for 10 min at 4°C, the NaCl

concentration was raised to 400 mM before centrifugation at 15,000 x g for 30 min at 4°C. After adding 100 µg ml⁻¹ yeast tRNA (Sigma) to block unspecific binding, the cell extracts were precleared twice.

Incubation, washing and protein elution

The pre-miRNA loaded beads were incubated with the precleared protein extract over night at 4°C at constant rotation. The beads were washed five times with buffer A4 (10 mM HEPES (pH 7.4), 400 mM NaCl, 2 mM EDTA; supplemented with 0.1 U ml⁻¹ SUPERase inhibitor). Buffers for the first four washes contained 10 µg ml⁻¹ yeast tRNA. Bound proteins were eluted with Western blot sample buffer and separated by SDS-PAGE using a 4 – 15 % gradient gel (Mini-Protean TGX gels, Bio-Rad). Proteins were stained using Colloidal Blue Staining Kit (Invitrogen), and analyzed by MALDI-TOF mass spectrometry on an Autoflex Bruker Daltonics mass spectrometer.

RNA-immunoprecipitation (RNA-IP)

Primary cortical neurons grown for 6 days on 3.5 cm dishes were collected 2 h after transfection of *in vitro* transcribed pre-miRNAs. The cells were incubated in lysis buffer (10 mM HEPES (pH 7.4), 200 mM NaCl, 30 mM EDTA; 0.5 % Triton X-100; supplemented with 0.1 U µl⁻¹ SUPERase inhibitor (Ambion) and protease inhibitor cocktail (Roche)) for 15 min at 4°C at constant rotation followed by homogenization using a 23-gauge needle. After centrifugation at 16,000 x g for 15 min at 4°C to remove cell debris, 100 µg ml⁻¹ yeast tRNA (Sigma) was added to block unspecific binding. The cell extract was precleared twice with Protein A agarose (Sigma) before incubation with 10 µg of rabbit anti-DHX36 antibody (Novus Biologicals) or rabbit control IgG (Santa Cruz) over night at constant rotation at 4°C. Beads (pre-blocked with 0.5 % BSA) were added and extracts incubated for 4 h at constant rotation at 4°C. The beads were washed five times with buffer A2 (10 mM HEPES (pH 7.4), 200 mM NaCl, 2 mM EDTA, supplemented with 0.1 U ml⁻¹ SUPERase inhibitor) and the salt concentration was gradually increased up to 400 mM NaCl. Buffers for the first four washes contained 10 µg ml⁻¹ yeast tRNA. Bound RNA was extracted with the mirVana miRNA Isolation Kit (Ambion) and analyzed by real-time qRT-PCR.

Real-time qRT-PCR

RNA samples were treated with TURBO DNase (Ambion) and reverse transcribed with the iScript cDNA synthesis kit (Bio-Rad) according to manufacturer's instructions. Quantitative real-time PCR was performed with the StepOnePlus Real-Time PCR System (Applied Biosystems), using iTaq SYBR Green Supermix with ROX (Bio-Rad) for detection of pre- miRNAs and mRNA and TaqMan MicroRNA Assay kits (Applied Biosystems) for detection of mature miRNAs. Primer sequences are summarized below.

Northern blot analysis

Northern blots for detection of small RNAs were performed as previously described, using radiolabelled DNA oligonucleotides as probes (Schratt et al. 2006).

Western blot analysis

Protein lysates were resolved by SDS-PAGE, transferred onto poly-vinylidene difluoride (PVDF) membrane (GE Healthcare) and probed as previously described (Siegel et al. 2009).

Immunocytochemistry

Immunostaining of endogenous MAP2, TAU-1 or overexpressed DHX36-GFP in dissociated hippocampal neurons was performed as described (Fiore et al. 2009).

Quantification of Cy3-pre-miRNA localization

For analysis of Cy3-pre-miRNA subcellular distribution, maximum projections from Z-stacks were thresholded in ImageJ. The MAP2 channel was used to create separate masks for the dendrites and the cell body. The function “analyze particles” was used to count the number of Cy3 puncta (size $\geq 0.10 \mu\text{m}^{-2}$) within the MAP2 mask. Each particle count was visually inspected to avoid false-positive signals from extracellular particles. Finally, the number of dendritic particles was determined and compared to the total number of intracellular particles per cell to obtain a value for dendritic localization.

Protein expression and purification

GST-DHX36(200) was expressed in *E. coli* BL21 (DE3) and full-length GST-DHX36 was produced in Sf9 cells and purified using glutathione sepharose 4B beads (GE Healthcare) as described before (Tran et al. 2004). The purity of

recombinant proteins was analyzed by 10 % SDS-PAGE and Coomassie staining.

Electrophoretic mobility shift assay (EMSA)

[³²P] internally labeled *in vitro* transcribed pre-miRNAs (20,000 cpm) were incubated with increasing amounts of purified recombinant GST-DHX36 (full-length) (80 nM – 160 nM) or of the truncated protein GST-DHX36(200) (1 μM – 3.4 μM) in EMSA buffer (50 mM Tris- Acetate (pH 7.8), 100 mM KCl, 10 mM NaCl, 3 mM MgCl₂, 70 mM glycine, 5 % glycerol (v/v), 10 mM EDTA; supplemented with 0.5 U μl⁻¹ SUPERase inhibitor (Ambion)) for 1 h at room temperature. Given the previously reported interaction of GST-DHX36 with guanine quadruplex (G4) structures, Z33-G4 DNA served as positive control (Giri et al. 2011). The samples were subsequently analyzed by electrophoresis on an 8 % native polyacrylamide gel and visualized by autoradiography using the Cyclone Plus Phosphor Imager (PerkinElmer).

Mass spectrometry analysis

Processing of proteins for mass spectrometry

The protein spots were subjected to in-gel trypsin digestion before MS analysis as described (Hellman et al. 1995). The peptide mixtures from the tryptic digests were desalted, concentrated and washed using C18 tips (Sigma) following the manufacturer's protocol. Concentrated peptides were eluted directly onto a ground stainless steel MALDI target plate. Subsequently the peptide solution was overlaid with α-cyano-4-hydroxycinnamic acid (Bruker Daltonics) and air dried before analysis in the mass spectrometer.

Mass spectrometry

All MS was performed using an Autoflex Bruker Daltonics mass spectrometer equipped with a nitrogen laser (laser 337 nm, 3 ns pulse width, and 50 Hz repetition rate). Peptide mass fingerprint spectra were acquired in the reflectron positive mode with a pulsed extraction using approximately 150 laser shots. The spectra were acquired after an external calibration using reference peptides (Peptide mixture II; Bruker Daltonics). The spectra were further calibrated using trypsin autolysis peaks as internal standards (842.5100, 2211.1046 Da). Monoisotopic masses were assigned and processed using Biotoools™ and FlexAnalysis™ software (Bruker Daltonics) before submitting them for database

searches.

Database searching

Peptide mass fingerprint data were processed using the Biotoools FlexAnalysis software before submission to the MASCOT program (Matrix Science) for searches against the nonredundant NCBI database. The parameters used for all the MASCOT peptide mass fingerprint searches were as follows: (i) taxonomy *Mus musculus*, (ii) search all molecular masses and all *pI*, (iii) allow up to one missed proteolytic cleavage and (iv) a peptide mass tolerance of 100 ppm. (v) Methionine oxidation was considered as an optional modification and (vi) cysteine carbamidomethylation as a fixed modification in all the searches. Matches to proteins were considered unambiguous when the probability score was significant using the Mascot score with a *P*-value < 0.05.

Lipofectamine RNAiMAX transfection

Lipofectamine RNAiMAX was mixed with culture medium (w/o antibiotics) and incubated for 10 min at room temperature. siRNA duplexes (Thermo Scientific) were pre-diluted in culture medium (w/o antibiotics) at a final transfection concentration of 50 nM. RNAiMAX and siRNA predilutions were combined, incubated for 20 min at room temperature, further diluted 1:5 in culture medium (w/o antibiotics) and applied to the cells. After 5 h, cells were treated with 20 μ M AP5 for 30 min before changing to culture medium.

Antibodies

Additional primary antibodies used for supplemental experiments: rabbit anti-MAP2 antibody (Cell Signaling Technology) and mouse anti-TAU-1 antibody (Millipore).

DNA, LNA and RNA oligonucleotides

Real-time qRT-PCR

pre-miR-134 fw: TGTGACTGGTTGACCAGAGGG

pre-miR-134 rev: GGTGACTAGGTGGCCACAG

pre-miR-7a-1 fw: TGTGTGGAAGACTAGTGATTTTGTGT

pre-miR-7a-1 rev: GCAGACTGTGATTTGTTGTCGTCT

pre-miR-7a-2 fw: CTGTCTGGAAGACTAGTGATTTTGTG

pre-miR-7a-2 rev: GACTTGTTGTTGGACACAGACACA

pre-miR-7b fw: TGGAAGACTTGTGATTTTGTGTTG

pre-miR-7b rev: TGGCTGTGACTTGTTGTCATATCA
pre-miR-218a-1 fw: TCTGTTGTGCTTGATCTAACCATGT
pre-miR-218a-1 rev: TGACGGAACCATGTTTTACTCATAC
pre-miR-218a-2 fw: TTGTGCTTGATCTAACCATGTGG
pre-miR-218a-2 rev: GGTGCTTGACAGAACCATGTTC
pre-miR-341 fw: GATCGCTCGGTCTGTCAGTC
pre-miR-341 rev: CGACTGACCGACCGACC
pre-miR-138-1/2 fw: AGCTGGTGTGGAATCAGGC
pre-miR-138-1 rev: TGTTGTGAAGTAGCCGTTCTCTGA
pre-miR-138-2 rev: GTGAAATAGCCGGTAAGAGGAT
pre-miR-376b fw: AAAGGTGGATATTCCTTCTATGGTTAC
pre-miR-376b rev: TCCTCTATGATTATCCAGGAAGCA
pre-miR-9a-1 fw: CTTTGGTTATCTAGCTGTATGAGTGGTG
pre-miR-9a-1 rev: CGGTTATCTAGCTTTATGAAGACTCCA
pre-miR-9a-2 fw: ATCTTTGGTTATCTAGCTGTATGAGTGTATT
pre-miR-9a-2 rev: TTTCGGTTATCTAGCTTTATGAAGACC
pre-miR-9a-3 fw: TGGTTATCTAGCTGTATGAGTGCCA
pre-miR-9a-3 rev: GGTTATCTAGCTTTATGACGGCTCTG
pre-miR-98 fw: GGGTGAGGTAGTAAGTTGTATTGTTGTG
pre-miR-98 rev: GTTATCTTCTTATTGGGGCCTAAAATC
pre-miR-137 fw: GGTGACGGGTATTCTTGGGT
pre-miR-137 rev: CGACTACGCGTATTCTTAAGCAAT
pre-miR-29a fw: GGATGACTGATTTCTTTTGGTGTTTC
pre-miR-29a rev: AACCGATTTTCAGATGGTGCTAGA
pre-miR-150 fw: TCTCCCAACCCTTGTACCAGTG
pre-miR-150 rev: CCAGGCCTGTACCAGGGTCT
DHX36 fw: GCATCCGGCCCACCTTAA
DHX36 rev: CTCTTCTCGCCGTTTCATCCA
BC1 fw: GTTGGGGATTTAGCTCAGTGGTAG
BC1 rev: AAGGTTGTGTGTGCCAGTTACCT
U6 snRNA fw: CTCGCTTCGGCAGCACA
U6 snRNA rev: AACGCTTCACGAATTTGCGT
GAPDH fw: GCCTTCTCTTGTGACAAAGTGGA
GAPDH rev: CCGTGGGTAGAGTCATACTGGAA

LNA FISH probes (Exiqon)

pre-miR-134 miRCURY LNA detection probe:

5'- FITC – GGGTGAACAAAGTGCACG – 3'

pre-miR-137 miRCURY LNA detection probe:

5'- FITC – AACACGTAATCCGTATT – 3'

miR-134 miRCURY LNA detection probe:

5'- FITC – CCCCTCTGGTCAACCAGTCACA – 3'

scramble miRCURY LNA detection probe:

5'- FITC – GTGTAACACGTCTATACGCCCA – 3'

In vitro transcription

pre-miRNAs

pre-miR-134 fw1:

AATTTAATACGACTCACTATAGGTGACTGGTTGACCAGAG

pre-miR-134 rev1:

GGTCAACCAGTCACCTATAGTGAGTCGTATTAATT

pre-miR-134 fw2:

GGGCGTGCACTTTGTTACCCTGTGGGCCACCTAGTCACCAA

pre-miR-134 rev2:

TGGTGACTAGGTGGCCACAGGGTGAACAAAGTGCACGCCCTCT

pre-miR-150 fw1:

AATTTAATACGACTCACTATAGTCTCCCAACCCTTGTACCAG

pre-miR-150 rev1:

TACAAGGGTTGGGAGACTATAGTGAGTCGTATTAATT

pre-miR-150 fw2:

TGCTGTGCCTCAGACCCTGGTACAGGCCTGGGGGACAG

pre-miR-150 rev2:

CTGTCCCCAGGCCTGTACCAGGGTCTGAGGCACAGCACTGG

pre-miR-134L150 fw2:

GGGCTGTGCCTCAGACCCTGTGGGCCACCTAGTCACCAA

pre-miR-134L150rev2:

TTGGTGACTAGGTGGCCACAGGGTCTGAGGCACAGCCCCTCT

pre-miR-150L134

fw2:TGCGTGCACTTTGTTACCCTGGTACAGGCCTGGGGGACAG

pre-miR-150L134 rev2:

CTGTCCCCAGGCCTGTACCAGGGTGAACAAAGTGCACGCACTGG

pre-miR-134C150 fw2:

GGGCGTGCTGCCTGTTACCCTGTGGGCCACCTAGTCACCAA

pre-miR-134C150 rev2:

TTGGTGACTAGGTGGCCACAGGGTGAACAGGCAGCACGCCCTCT

pre-miR-150C134 fw2:

TGCTGACTTTCAGACCCTGGTACAGGCCTGGGGGACAG

pre-miR-150C134 rev2:

CTGTCCCCCAGGCCTGTACCAGGGTCTGAAAGTCAGCACTGG

TAG pre-miRNAs for RNA pulldown

TAG-pre-fw:AATTTAATACGACTCACTATAG

TAG-pre-rev:AGTGAGTCGTATTAATT

TAG-pre-miR-134fw1:GGAGAATAGATAGTTGTGACTGGTTGACCAGAGGGGCG

TAG-pre-miR-134rev1:CCTCTGGTCAACCAGTCACAACTATCTATTCTCCCTAT

TAG-pre-miR-134fw2:TGCACTTTGTTACCCTGTGGGCCACCTAGTCACCAA

TAG-pre-miR-134rev2:

TTGGTGACTAGGTGGCCACAGGGTGAACAAAGTGCACGCC

TAG-pre-miR-150fw1:GGAGAATAGATAGTTCTCCAACCCTTGTACCAGTGTCT

TAG-pre-miR-150rev1:CTGGTACAAGGGTGGGAGAACTATCTATTCTCCCTAT

TAG-pre-miR-150fw2:GTGCCTCAGACCCTGGTACAGGCCTGGGGGACA

TAG-pre-miR-150rev2:TGTCCCCCAGGCCTGTACCAGGGTCTGAGGCACAGCA

TAG-pre- miR-134C150fw: TGCTGCCTGTTACCCTGTGGGCCACCTAGTCACCAA

TAG-pre- miR-134C150rev:

TTGGTGACTAGGTGGCCACAGGGTGAACAGGCAGCACGCC

TAG-pre-miR-341fw1:GGAGAATAGATAGTCGGTCCGCGATCGCTCGGTCTGT

TAG-pre-miR-341rev1:ACCGAGCGATCGGCCGACCGACTATCTATTCTCCCTAT

TAG-pre-miR-341fw2:CAGTCAGTCGGTCCGTCGATCGGTCCGTCGGT

TAG-pre-miR-341rev2:ACCGACCGACCGATCGACCGACCGACTGACTGACAG

TAG-pre-miR-7a-fw1:GGAGAATAGATAGTTGGAAGACTAGTGATTTTGTGTT

TAG-pre-miR-7a-rev1:ACAAAATCACTAGTCTTCCAACCTATCTATTCTCCCTAT

TAG-pre-miR-7a-1fw2:TTTAGATAACTAAGACGACAACAATCACAGTCTGCCAT

TAG-pre-miR-7a-1rev2: TGGCAGACTGTGATTTGTTGTCGTCTTAGTTATCTAAAAACA

TAG-pre-miR-7a-2fw2:GTGTCTGTGTCCAACAACAAGTCCCAGTCTGCCACA

TAG-pre-miR-7a-2rev2: TGTGGCAGACTGGGACTTGTGTTGGACACAGACACAACA

DNA adapter

5' – ACTATCTATTCTCCC – 3' biotin

pSuper constructs

shDHX36(1)_fw1: GATCCCCCCTTAAGGGTCGCGAGATATTCAAGAGA

shDHX36(1)_fw2: TATCTCGCGACCCTTAAGGTTTTTA

shDHX36(1)_rev1: AGCTTAAAAACCTTAAGGGTCGCGAGATATCTCTTGAA

shDHX36(1)_rev2: TATCTCGCGACCCTTAAGGGGG

shDHX36(2)_fw1: GATCCCCGCACATGGATGAACGGCGATTCAAGAGA

shDHX36(2)_fw2: TCGCCGTTTCATCCATGTGCTTTTTTA

shDHX36(2)_rev1: AGCTTAAAAAGCACATGGATGAACGGCGATCTCTTGAA

shDHX36(2)_rev2: TCGCCGTTTCATCCATGTGCGGG

shDHX36(3)_fw1: GATCCCCGGAAGAAGCTAAACGGCGTTTCAAGAGA

shDHX36(3)_fw2: ACGCCGTTTAGCTTCTTCCTTTTTA

shDHX36(3)_rev1: AGCTTAAAAAGGAAGAAGCTAAACGGCGTTCTCTTGAA

shDHX36(3)_rev2: ACGCCGTTTAGCTTCTTCCGGG

shControl_fw1: GATCCCCAACCTTGTGGTCCTTAGGTTCAAGAGA

shControl_fw2: CCTAAGGACCACAAGGTTTTTTTTTA

shControl_rev1: AGCTTAAAAAAAACCTTGTGGTCCTTAGGTCTCTTGAA

shControl_rev2: CCTAAGGACCACAAGGTTTGGG

siRNA duplexes (Thermo Scientific)

siDHX36(2)_sense: 5' – GCACAUGGAUGAACGGCGAdTdT – 3'

siDHX36(2)_antisense: 5'P – UGCGCGUUCAUCCAUGUGCdTdT – 3'

siDHX36(2)_sense: 5' – GGAAGAAGCUAAACGGCGUdTdT – 3'

siDHX36(2)_antisense: 5'P – ACGCCGUUUAGCUUCUUCdTdT – 3'

siControl_sense: 5' – AAACCUUGUGGUCCUUAGGdTdT – 3'

siControl_antisense: 5'P – CCUAAGGACCACAAGGUUUdTdT – 3'

Tab T1.: Identification of DHX36 by MALDI-MS. 9 out of 14 masses detected are matching peptides of DHX36.

aa start - end	observed mass	Mr (expt)	Mr (calc)	ppm	peptide sequence
2 - 11	1370.57	1369.57	1369.57	-2	M.SYDYHQSWSR.D Acetyl (Protein N-term)
230 - 244	1840.96	1839.95	1839.94	7	K.TTQVTQFILDNYIER.G
296 - 317	2567.28	2566.28	2566.32	-17	R.KQGSILYCTTGIIQLWLQSDSR.L
318 - 332	1733.91	1732.91	1732.91	-3	R.LSSVSHIVLDEIHER.N
613 - 626	1645.89	1644.88	1644.87	6	R.ASLDDYQLPEILR.T
641 - 650	1096.62	1095.62	1095.61	7	R.LGGIAYFLSR.L
792 - 807	1675.87	1674.86	1674.85	8	K.GQFAEHLLGAGFVSSR.S
814 - 835	2431.25	2430.24	2430.29	-23	K.ANINSDNEKIIKAVICAGLYPK.V
915 - 934	2417.17	2416.17	2416.19	-10	K.DKDQEIIAVDEWIVFQSPER.I
unmatched	1062.69				
unmatched	2284.15				
unmatched	2298.17				
unmatched	3338.65				
unmatched	3494.76				

Supplementary Figures

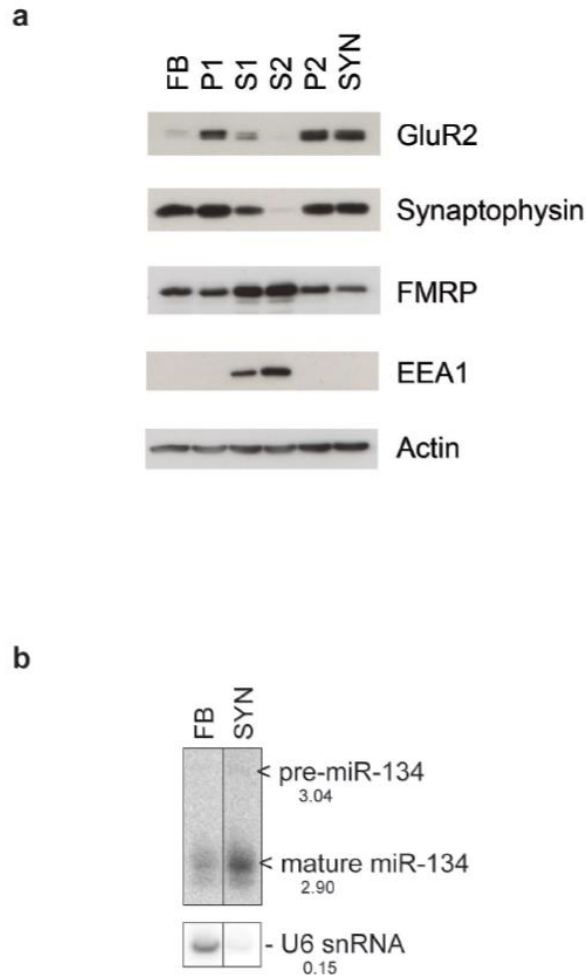


Figure S1: Characterization of synaptosomal fractionation. (a) Representative Western blot of fractions obtained during synaptosome preparation for indicated marker proteins. FB: forebrain; P1: pellet 1 (nuclei); S1: low-speed centrifugation supernatant 1; S2: high-speed centrifugation supernatant 2 (cytosol); P2: pellet 2 (membrane); SYN: synaptosomes. GluR2: AMPA-type glutamate receptor subunit 2 (postsynapse); FMRP: Fragile-X syndrome mental retardation protein; EEA1: early endosomal antigen-1 (cytosol). (b) Levels of (pre-)miR-134 and U6 snRNA in P15 rat forebrain (FB) and synaptosomes (SYN) measured by Northern blot. Ratio of SYN to FB signal is indicated.

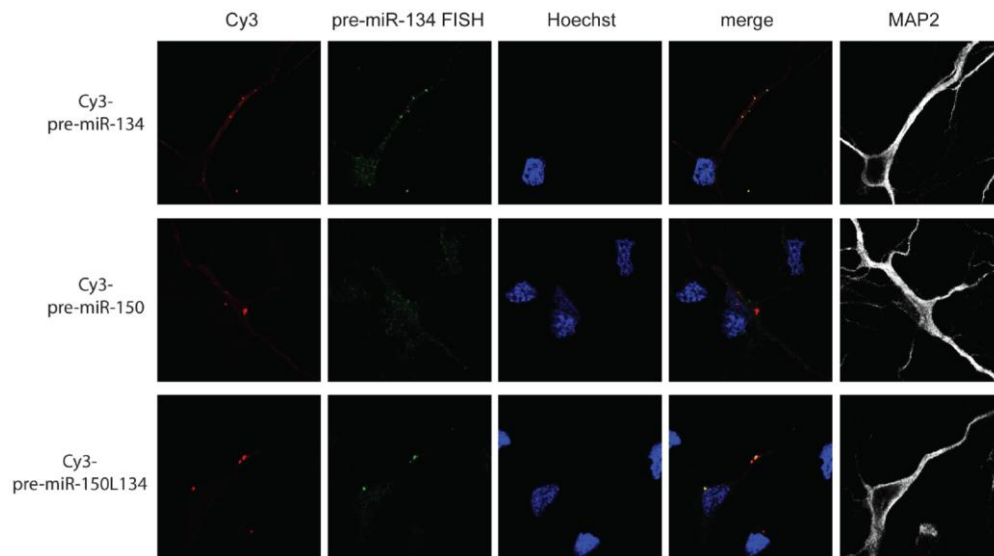


Figure S2: Characterization of pre-miR-134 fluorescent *in situ* hybridization (FISH) probe specificity. FISH analysis of neurons transfected with the indicated Cy3-labeled pre- miRNAs (red) using a pre-miR-134 specific probe (green) directed against the pre-miR-134 terminal loop. Neurons were counterstained with Hoechst (blue) and MAP2 (white).

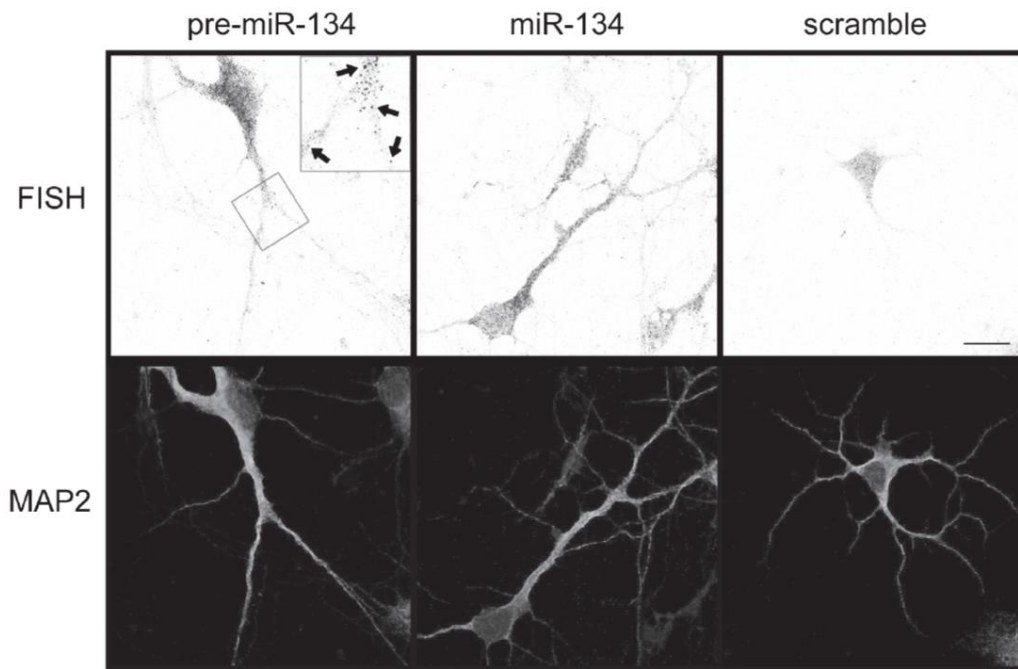


Figure S3: FISH for pre-miR-134 and mature miR-134. Representative images from FISH on BDNF-treated hippocampal neurons (7 DIV) using LNA probes directed against the pre- miR-134 terminal loop (left), mature miR-134 (middle) or an unrelated scramble sequence (right). Arrows within an insert at higher magnification point to pre-miR-134 puncta in distal dendrites. Scale bar = 10 μ m.

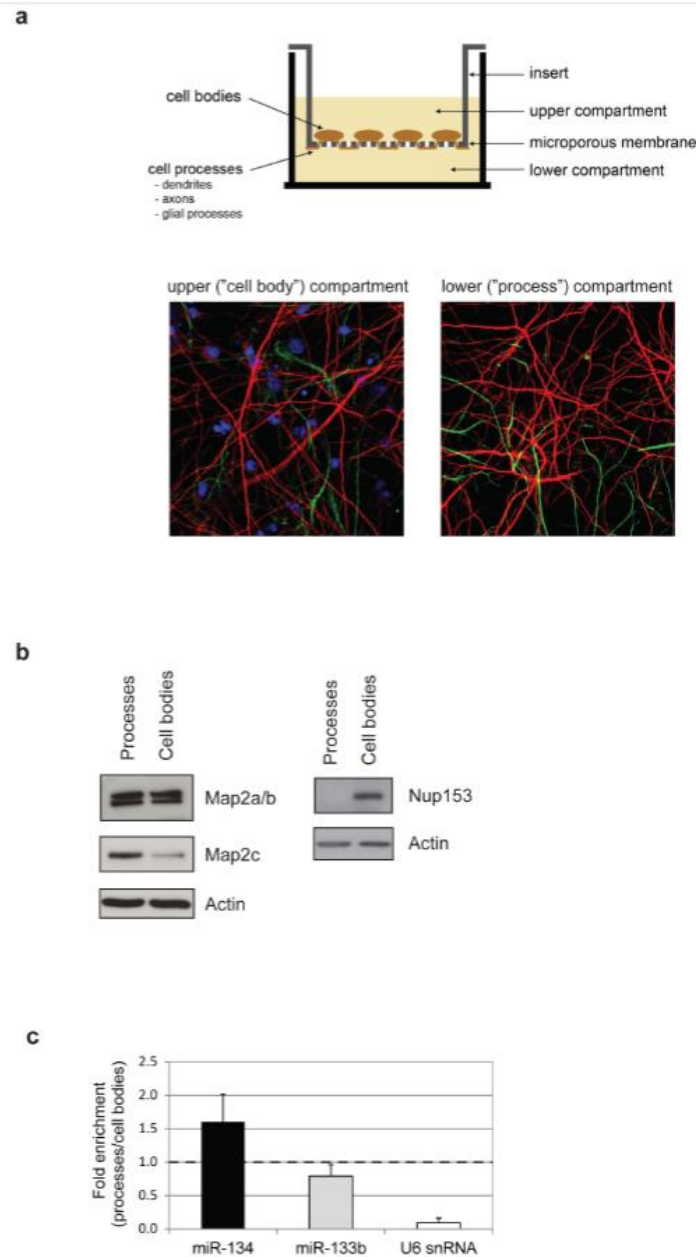


Figure S4: Characterization of primary neuron compartmentalized culture system. (a) Upper panel: schematic of the membrane insert system used for compartmentalization. Lower panels: staining for nuclei (Hoechst, blue), dendrites (MAP2, red) and glial processes (GFAP, green) in cell body and process compartment. Note the absence of nuclei and the enrichment of dendrites in the lower ("process") compartment (right panel). (b) Western blot analysis of indicated marker proteins in extracts obtained from the process or cell body compartment. (c) qRT-PCR measurement of indicated miRNAs and U6 snRNA in RNA samples obtained from process or cell body compartment. Ratio of RNA in process compartment to cell body compartment is shown (mean +/- s.d., n = 3).

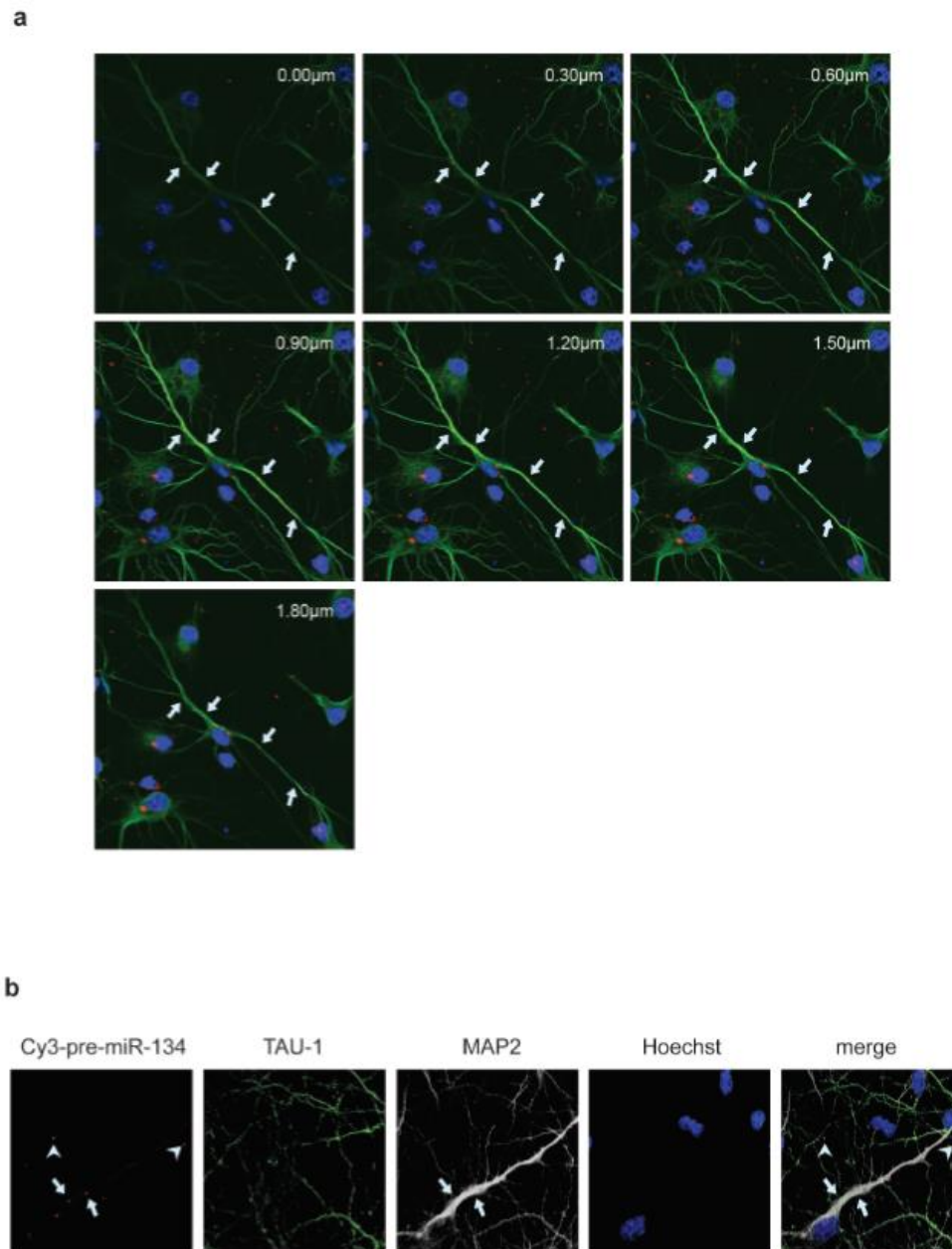


Figure S5: Intracellular localization of transfected Cy3-pre-miRNAs. (a) Consecutive images from a representative confocal Z-stack (0.3 μm interval) of a hippocampal neuron transfected with Cy3-pre-miR-134. Arrows point to the location of individual Cy3-pre-miR-134 puncta throughout the stack. Green: MAP2 immunostaining; blue: Hoechst nuclear staining. (b) Representative images of neurons transfected with Cy3-pre-miR-134 (red) and counterstained for the axonal marker TAU-1 (green), the dendritic marker MAP2 (white) and the nuclear marker Hoechst (blue). Arrows point to Cy3-pre-miR-134 puncta localizing to dendrites, arrowheads to Cy3-pre-miR-134 puncta co-localizing neither with axons nor dendrites.

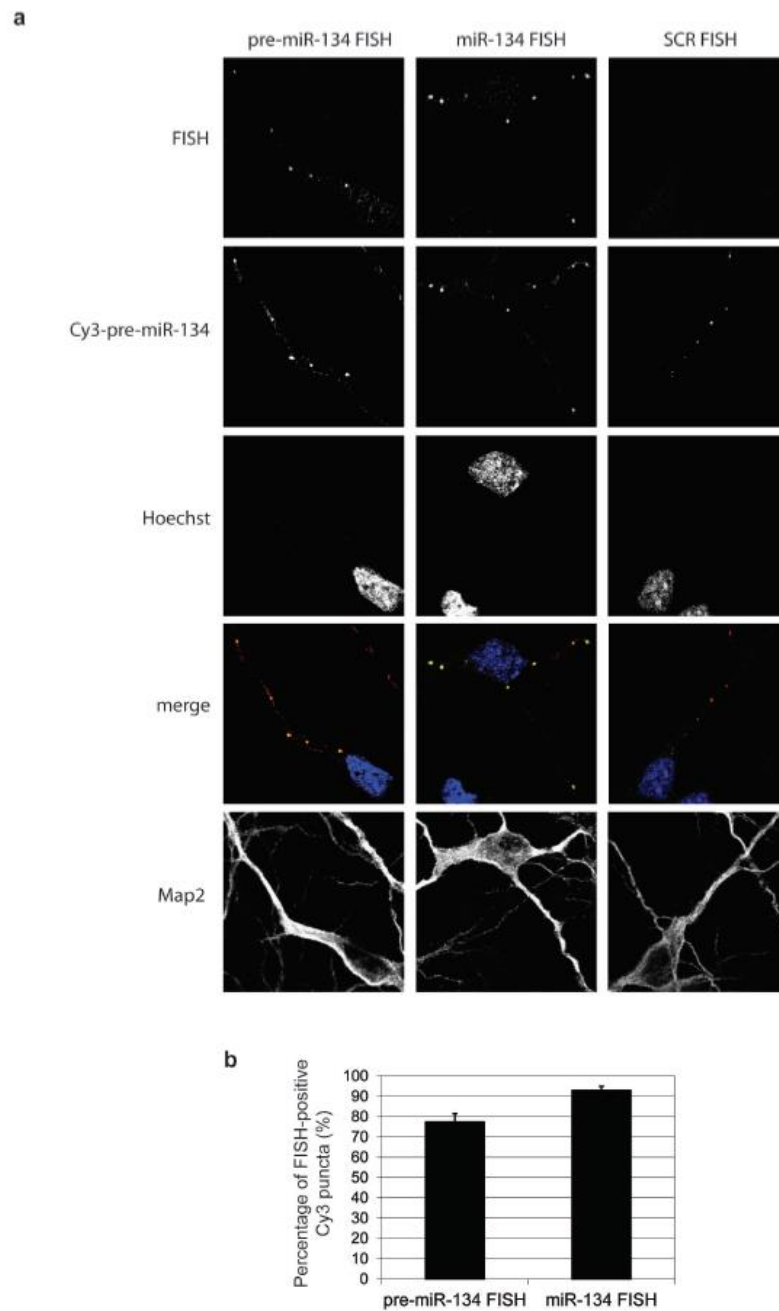


Figure S6: The majority of transfected pre-miR-134 is not processed within the first 2.5 hours. (a) FISH analysis of neurons transfected with Cy3-pre-miR-134 using the indicated probes (top). (b) Quantification of FISH signals obtained for pre-miR-134 and mature miR-. Percentage of FISH-positive Cy3 puncta is shown (mean \pm s.d., n = 2).

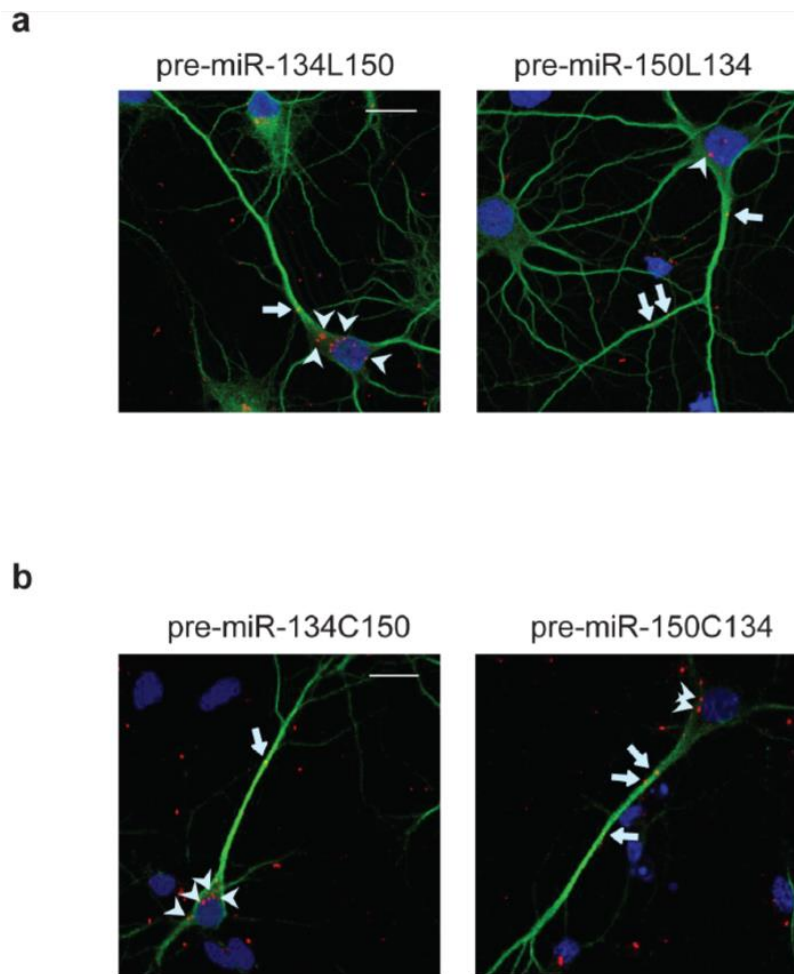


Figure S7: Subcellular localization of pre-miR-134 and pre-miR-150 mutants. (a) Representative images of neurons transfected with Cy3-pre-miR-134L150 (miR-134 mutant containing the miR-150 terminal loop) or Cy3-pre-miR-150L134 (miR-150 mutant containing the miR-134 terminal loop) and counterstained for the dendritic marker MAP2 (green) and the nuclear marker Hoechst (blue). Arrows point to Cy3-positive puncta localizing to dendrites, arrowheads to Cy3-positive puncta localizing to the cell body. Scale bar = 10 μ m. (b) as in (a), except that Cy3-pre-miR-134C150 (miR-134 mutant containing only the central five nucleotides of the miR-150 terminal loop) or Cy3-pre-miR-150C134 (miR-150 mutant containing only the central five nucleotides of the miR-134 terminal loop) were transfected.

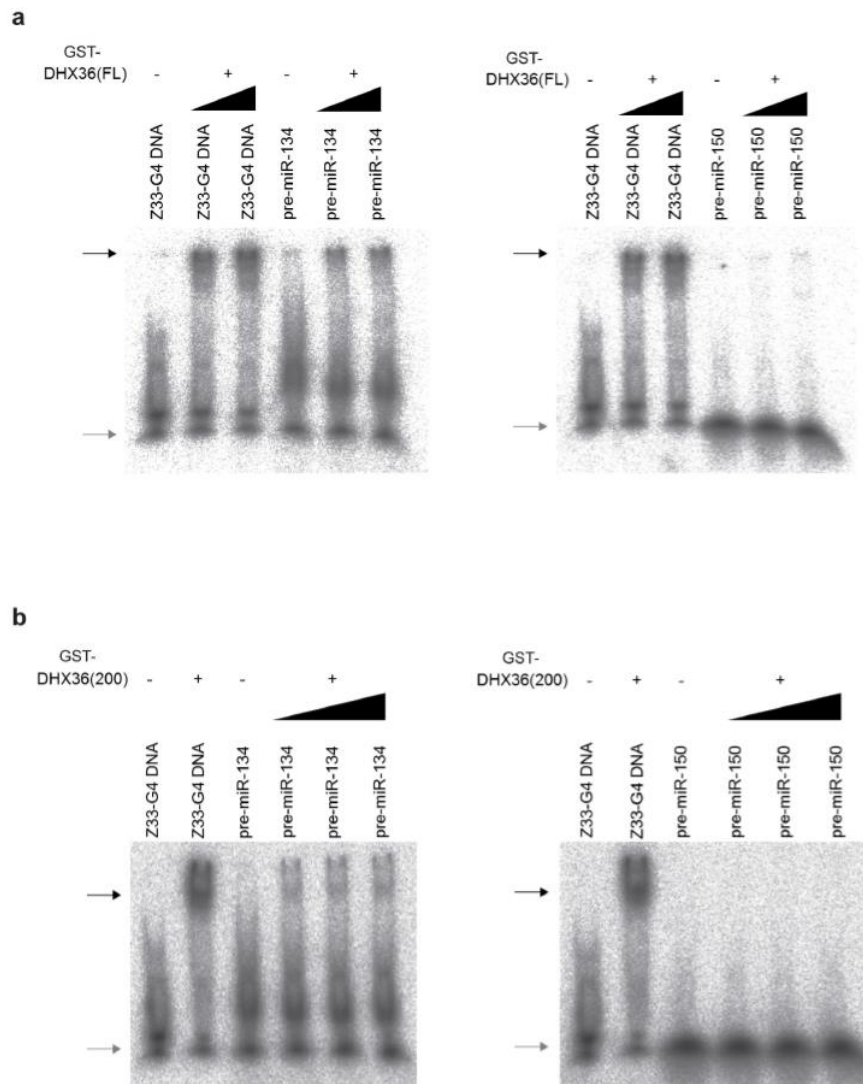


Figure S8: DHX36 binds directly to pre-miR-134. (a) Increasing amounts of GST-DHX36 (full-length, FL) purified from insect cells were incubated with Z33-G4 DNA or indicated pre-miRNAs and subjected to EMSA. Lower arrow points to the uncomplexed probe, upper arrow to a lower mobility band representing a nucleic acid/protein complex. (b) Same as in (a), except that a bacterially expressed, N-terminal DHX36 fragment (GST-DHX36(200)) was used in the assay.

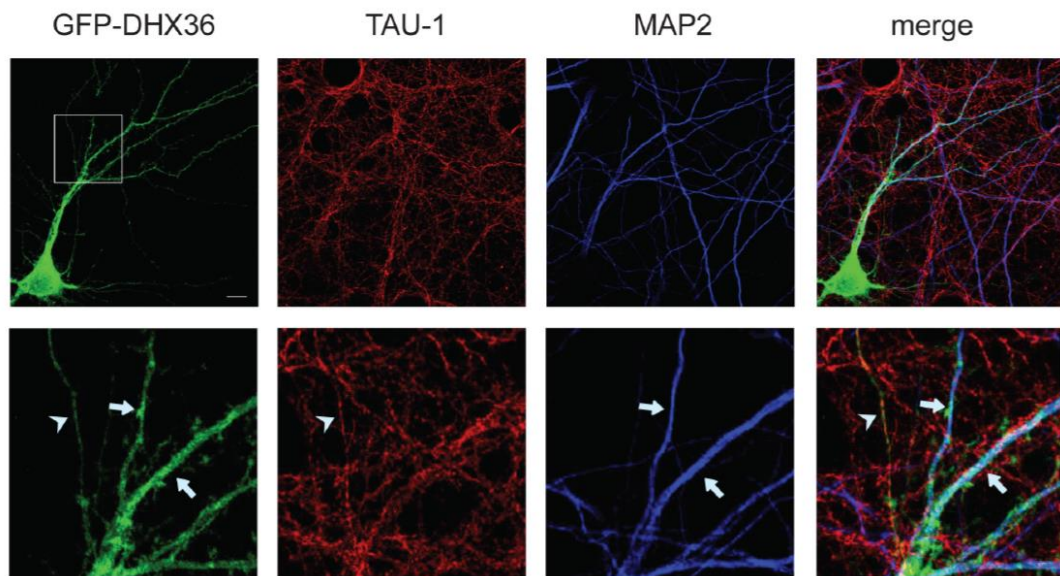


Figure S9: Subcellular localization of recombinant DHX36 in neurons. Representative confocal microscopy images of hippocampal neurons transfected with DHX36-EGFP and counterstained with the axonal marker TAU-1 (red) and the dendritic marker MAP2 (blue). Arrows point to DHX36-EGFP localization in dendrites, arrowhead to DHX36-EGFP localization in the axon. Scale bar = 10 μ m.

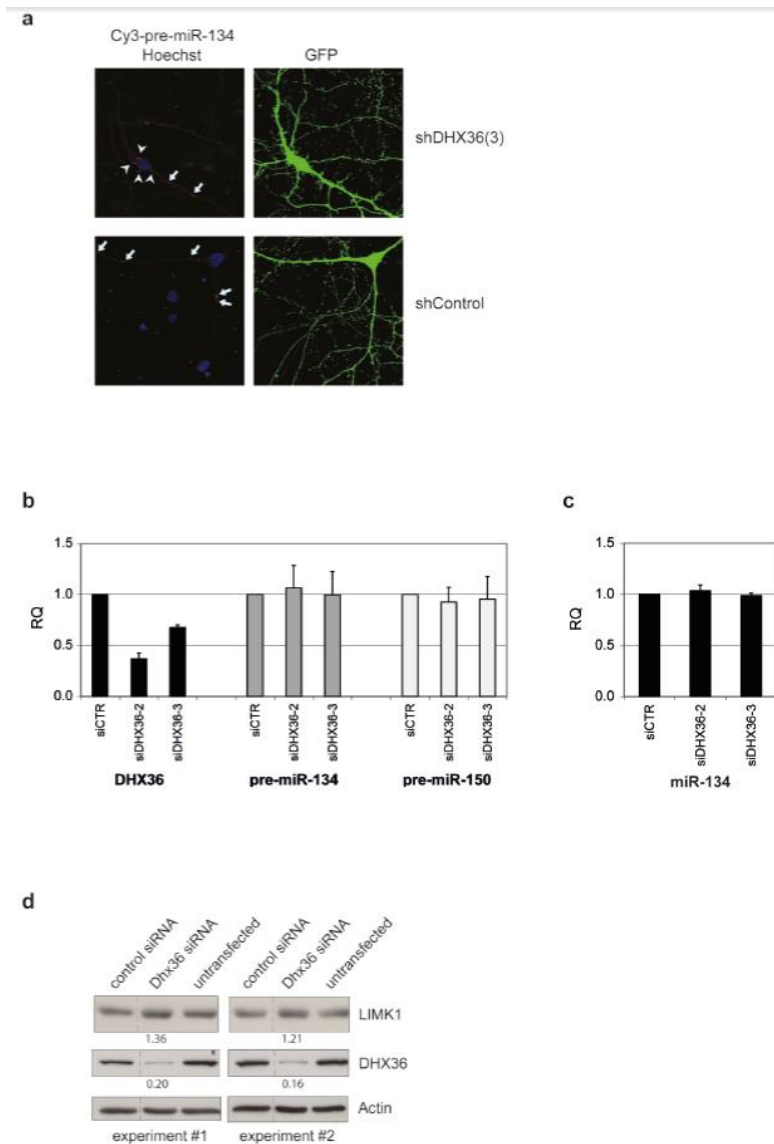


Figure S10: Pre-miR-134 localization, expression and Limk1 protein expression upon DHX36 knockdown in neurons. (a) Representative confocal microscopy images of hippocampal neurons transfected with Cy3-pre-miR-134, GFP and indicated shRNA constructs. Arrows point to Cy3-positive puncta localizing to dendrites, arrowheads to Cy3-positive puncta localizing to the cell body. Scale bar = 10 μ m. (b, c) Quantitative RT-PCR analysis of total RNA derived from neurons transfected with the indicated siRNA duplexes. Primers specifically recognizing DHX36 mRNA, pre-miR-134, pre-miR-150 and mature miR-134 were used. Values represent the average of three independent experiments \pm s.d., siCTR (control) condition was set to one for each transcript. (d) Western blots employing neuronal lysates obtained from two independent Lipofectamine RNAiMAX transfections with the indicated synthetic siRNAs. Band intensities for DHX36 siRNA relative to the control siRNA condition are shown below the blots.

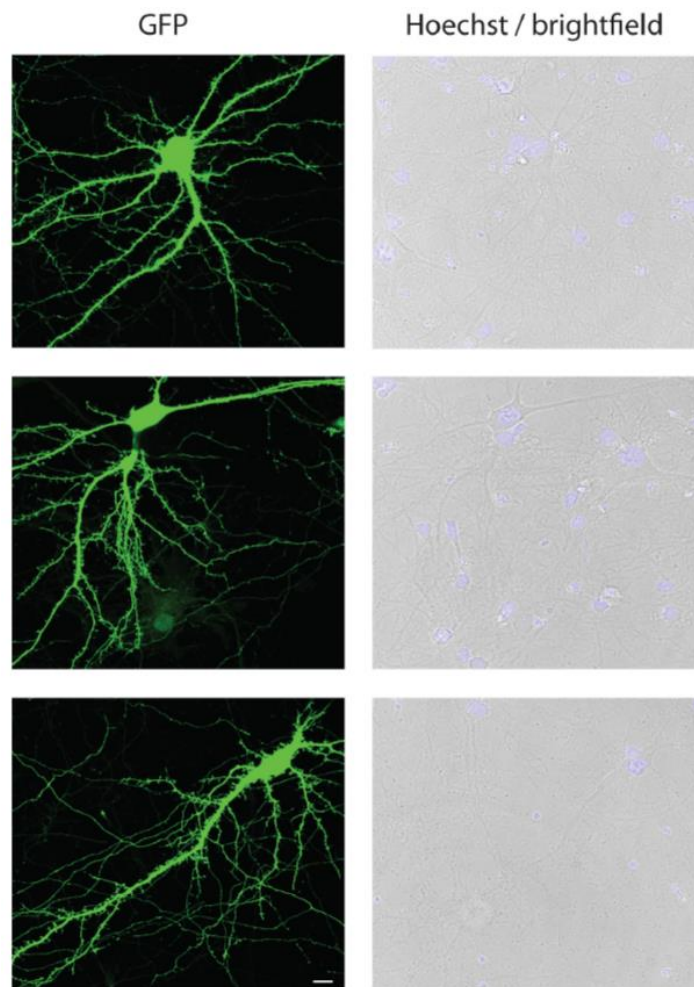


Figure S11: Morphology of DHX36 knockdown hippocampal neurons. Representative fluorescent (left panel) and brightfield (right panel) images of three hippocampal neurons transfected with eGFP and shDHX36. Hoechst counterstain was performed to visualize nuclear integrity.

Supplementary References

Fiore R, Khudayberdiev S, Christensen M, Siegel G, Flavell SW, Kim TK, Greenberg ME, Schratt G. 2009. Mef2-mediated transcription of the miR379-410 cluster regulates activity-dependent dendritogenesis by fine-tuning Pumilio2 protein levels. *Embo J* **28**: 697-710.

Giri B, Smaldino PJ, Thys RG, Creacy SD, Routh ED, Hantgan RR, Lattmann S, Nagamine Y, Akman SA, Vaughn JP. 2011. G4 resolvase 1 tightly binds and unwinds unimolecular G4-DNA. *Nucleic Acids Res* **39**: 7161-7178.

Hellman U, Wernstedt C, Gonez J, Heldin CH. 1995. Improvement of an "In-Gel" digestion procedure for the micropreparation of internal protein fragments for amino acid sequencing. *Anal Biochem* **224**: 451-455.

Heo I, Joo C, Kim YK, Ha M, Yoon MJ, Cho J, Yeom KH, Han J, Kim VN. 2009. TUT4 in concert with Lin28 suppresses microRNA biogenesis through pre-microRNA uridylation. *Cell* **138**: 696-708.

Schratt GM, Tuebing F, Nigh EA, Kane CG, Sabatini ME, Kiebler M, Greenberg ME. 2006. A brain-specific microRNA regulates dendritic spine development. *Nature* **439**: 283- 289.

Tran H, Schilling M, Wirbelauer C, Hess D, Nagamine Y. 2004. Facilitation of mRNA deadenylation and decay by the exosome-bound, DExH protein RHAU. *Mol Cell* **13**: 101-111.

5.3 A comprehensive characterization of the nuclear microRNA repertoire of post-mitotic neurons

Running title: Nuclear miRNAs in neurons

Sharof Abdumalikovich Khudayberdiev, Federico Zampa, Marek Rajman and Gerhard Schratt*.

Institut für Physiologische Chemie, Biochemisch-Pharmakologisches Centrum ,
Philipps-Universität Marburg, Marburg, Germany

* Correspondence and requests for materials should be addressed to G. S.

Prof. Dr. Gerhard Schratt
Institut für Physiologische Chemie
Biochemisch-Pharmakologisches Centrum
Philipps-Universität Marburg
Karl-von-Frisch-Str. 1
35032 Marburg, Germany
gerhard.schratt@staff.uni-marburg.de

Word count: 9974

Figures: 8 + 7 (supplementary)

Tables: 2 + 8 (supplementary)

5.3.1 Abstract

MicroRNAs (miRNAs) are small non-coding RNAs with important functions in the development and plasticity of post-mitotic neurons. In addition to the well-described cytoplasmic function of miRNAs in post-transcriptional gene regulation, recent studies suggested that miRNAs could also be involved in transcriptional and post-transcriptional regulatory processes in the nuclei of proliferating cells. However, whether miRNAs localize to and function within the nucleus of post-mitotic neurons is unknown. Using a combination of microarray hybridization and small RNA deep sequencing, we identified a specific subset of miRNAs which are enriched in the nuclei of neurons. Nuclear enrichment of specific candidate miRNAs (miR-25 and miR-92a) could be independently validated by Northern blot, quantitative real-time PCR (qRT-PCR) and fluorescence *in situ* hybridization (FISH). By cross-comparison to published reports, we found that nuclear accumulation of miRNAs might be linked to a down-regulation of miRNA expression during *in vitro* development of cortical neurons. Importantly, by generating a comprehensive isomiR profile of the nuclear and cytoplasmic compartment, we found a significant overrepresentation of guanine nucleotides at the 3' terminus of nuclear-enriched isomiRs, suggesting the presence of neuron-specific mechanisms involved in miRNA nuclear localization. In conclusion, our results provide a starting point for future studies addressing the nuclear function of specific miRNAs and the detailed mechanisms underlying subcellular localization of miRNAs in neurons and possibly other polarized cell types.

Key words: miRNA, isomiR, neuronal development, plasticity, deep sequencing, microarray

5.3.2 Introduction

MicroRNAs (miRNAs) are an important class of small regulatory non-coding RNAs with a size of 18-25 nucleotides (nt). The canonical miRNA biogenesis pathway starts with the generation of the primary miRNA (pri-miRNA) transcript by RNA polymerase II mediated transcription. The pri-miRNA transcript is cleaved by the microprocessor complex, containing among other proteins Drosha and Di George Syndrome critical region gene 8 (DGCR8) proteins, which results in ~ 70 nt hairpin-like precursor miRNAs (pre-miRNA). Pre-miRNAs are subsequently exported to the cytoplasm by the nuclear export receptor Exportin-5 (Zeng and Cullen, 2004), where they are further cleaved by Dicer to produce an intermediate RNA duplex. One strand of this duplex (known as guide miRNA) binds to an Argonaute family protein (Ago) 1-4, the core component of the miRNA-associated RNA-induced silencing complex (miRISC). MiRISC mainly functions in the cytoplasmic compartment by translational inhibition and/or degradation of target mRNAs. MiRNAs are implicated in many steps of neuronal development and the function of mature neurons, including synaptic plasticity, learning and memory (Fiore et al., 2011). Interestingly, several recent studies suggest that miRNAs, in addition to their well-defined role in the cytoplasm, may also be involved in the regulation of gene expression in the nucleus of mammalian cells.

First, it was shown that miRNAs are present in the nuclear compartment. Some of them are even enriched in the nuclei or nucleoli of cancer cell lines (Hwang et al., 2007; Liao et al., 2010; Park et al., 2010; Li et al., 2013), myoblasts (Politz et al., 2009) and neural stem cells (Jeffries et al., 2011). Second, the key components of the miRNA pathway, such as Ago (Tan et al., 2009), Dicer (Sinkkonen et al., 2010) and multiple glycine/tryptophan repeat containing protein - GW182 (Till et al., 2007; Nishi et al., 2013), are detected in the nucleus. Third, Ago proteins associate with splicing factors (Ameyar-Zazoua et al., 2012) and regulate siRNA-mediated alternative splicing (Allo et al., 2009). Fourth, some miRNAs were shown to post-transcriptionally regulate gene expression in the nucleus (Hansen et al., 2011; Tang et al., 2012). Finally, several miRNAs (and siRNAs) were identified to control gene expression by binding to the promoter of target genes, thereby triggering epigenetic changes, such as DNA methylation (Morris et al., 2004) and histone modification (Kim et al., 2008; Place et al., 2008; Benhamed et al., 2012).

Epigenetic modifications and alternative mRNA splicing, apart from being important in neuronal differentiation, are also implicated in activity-dependent gene expression in mature neurons (Norris and Calarco, 2012; Zovkic et al., 2013), an essential mechanism for synaptic plasticity, learning and memory. Furthermore, genes undergoing alternative mRNA splicing are overrepresented in the brain (Yeo et al., 2004), suggesting that specific molecular mechanisms that lead to transcript diversity must be present in the brain. However, whether miRNAs can regulate gene expression by any of the

aforementioned mechanisms in the neuronal nucleus is not known. A prerequisite for the study of miRNA function in the nucleus of post-mitotic neurons is the a priori knowledge of the nuclear miRNA repository. However, to date nuclear miRNAs have only been identified from proliferating cells, and it can be expected that terminally differentiated cells like neurons have a completely different miRNA expression profile.

In the present study, using microarray and deep sequencing technologies, we identified miRNAs which are enriched in the nuclei of rat primary cortical neurons. Our results suggest that employing a combination of microarray and deep sequencing technologies to determine nuclear-enriched miRNAs can yield more accurate results than using each method separately. Accordingly, we could validate differential expression of specific nuclear-enriched miRNAs by Northern blot, quantitative real-time PCR (qRT-PCR) and fluorescence *in situ* hybridization (FISH). By cross-comparison to published reports we observed that expression levels of nuclear-enriched miRNAs in general decline during development of neurons, suggesting that these miRNAs could play a role in early developmental stages of neurons. Importantly, by generating a comprehensive isomiR profile of the nuclear and cytoplasmic compartment, we found that the most 3' terminal nucleotide of miRNA species is a robust predictor of nuclear enrichment. In conclusion, our results provide a roadmap for future studies addressing the detailed mechanisms underlying subcellular localization of miRNAs in neurons and possibly other polarized cell types.

5.3.3 Materials and Methods

5.3.3.1 Primary neuronal culture

Primary cortical and hippocampal neuron cultures were prepared from embryonic day 18 (E18) Sprague-Dawley rats (Charles River Laboratories) as previously described (Schratt et al., 2006). Cortical and hippocampal cultures were maintained in Neurobasal (NB) medium containing 2% B27 supplement, penicillin-streptomycin (100 U/ml penicillin, 100 µg/ml streptomycin), and GlutaMax (1 mM). All reagents were purchased from Life Technologies. Glia-depleted cultures were obtained by supplementing FUDR solution (10 µM) starting from day *in vitro* 0 (DIV0). FUDR solution was prepared by mixing equimolar amount of fluorodeoxyuridine (Sigma) and uridine (Sigma). Glia-enriched cultures were maintained in the standard medium, except B27 supplement was exchanged to 10 % FBS (Life Technologies). When indicated, cells were treated for 2 hours with 40 ng/mL of BDNF (PeproTech) or 55 mM of KCl solution.

5.3.3.2 Nuclear fractionation protocol

For nuclear fractionation, 40 million cells from cortical cultures at DIV7 were used. Cells were washed once with 10 mL of ice-cold 1 x Phosphate buffered saline (PBS; Life Technologies) and were scraped into ice-cold 1xPBS using cell lifters (Corning). Then cells were pelleted by centrifugation at 100 g speed for 5 min at 4 °C. Subsequently, cell pellet was resuspended in 600 µl of ice-cold hypotonic homogenization buffer (HHB; 10 mM KCl, 1.5 mM MgCl₂, 1 mM Na-EDTA, 1 mM Na-EGTA, 10 mM Tris-HCl pH = 7.4, 1 mM DTT, 2 µl RNasin Plus RNase inhibitor (Promega)) and was incubated on ice for 30 min. After supplying cell suspension with 600 µl of 0.2 % Igepal CA630 containing HHB, it was homogenized with 40 stokes in a Dounce potter. From the obtained cell lysate, nuclear and cytoplasmic fractions were separated by centrifugation at 720 g speed for 5 min at 4°C. The nuclear fraction (pellet) was washed three times with 1.5 mL of isotonic homogenization buffer (IHB; HHB, supplemented with 250 mM sucrose). The total RNA from nuclear (pellet) and cytoplasmic (supernatant) fractions was extracted using peqGOLD TriFast reagent (Pepqlab) per manufacturer's instructions. On average, 15-20% of the total RNA derived from the fractionation originated from the nucleus. For determination of nuclear and cytoplasmic protein markers, the nuclear pellet obtained after washes with IHB was resuspended in RIPA buffer (10 mM NaCl, 1% Triton X-100, 0.5 % Sodiumdeoxycholate, 1 mM EGTA, 0.05 % SDS, 50 mM Tris-HCl pH=8.0, add fresh 5x protease inhibitor cocktail (Roche)).

5.3.3.3 Western blotting

Western blotting was performed as previously described (Siegel et al., 2009). The following primary antibodies were used: anti-HDAC2-rabbit monoclonal (Abcam) and anti-beta Actin-mouse monoclonal (Sigma).

5.3.3.4 RNA extraction, size selection of small RNAs and microarray procedure

12 µg of total RNA from nuclear and cytoplasmic fractions was supplemented with spike-in oligoribonucleotides (18 nt, 5-Phos-AGCGUGUAGGGAUCCAAA-3; 24 nt, 5-Phos-GGCCAACGUUCUCAACAAUAGUGA-3; 30 nt, 5-Phos-GGCAUUAACGCGGCCGCUCUACAAUAGUGA-3; 50 femtomoles of each; <http://bartellab.wi.mit.edu/protocols.html>) and mixed with the same volume of Gel loading buffer II (Life Technologies). RNA was separated using denaturing urea 15 % PAGE gel (SequaGel System, National Diagnostics), which was run in 1 x TBE (89 mM Tris/ 89 mM Borate/ 2 mM EDTA) buffer at 30 Watts. Gel was stained with 2 x SYBR GOLD dye (Life Technologies; in 1 x TBE) for 10 min and gel pieces corresponding to small RNAs of 15-35 nt size were cut out. Small RNAs were eluted by incubation of gel pieces in 300 mM NaCl solution overnight at 4°C with constant rotation. Precipitation of RNA was carried out by addition of 2.5-3 volume of 100 % EtOH to a supernatant and incubation at -20 °C for at least 2h. Pellet was resuspended in 20 µl of DEPC-treated H₂O. For miRNA profiling analysis, 14 µl of small RNA, obtained from each sample, were sent to microRNA Microarray Service provided by LC Sciences (Texas, USA). In brief, three biological replicates of nuclear fractionated samples (three nuclear and three cytoplasmic samples) were labeled with Cy3 (nuclear) and Cy5 (cytoplasmic), and then were hybridized on a single microarray chip (dual-sample hybridization). The signal values were derived by background subtraction and global normalization. A transcript to be listed as detectable should have met at least two conditions: signal intensity higher than 3×(background standard deviation) and spot CV < 0.5. CV was calculated by (standard deviation)/(signal intensity). When repeating probes are present on an array, a transcript was listed as detectable only if the signals from at least 50% of the repeating probes were above detection level. The data obtained from LC Sciences was further normalized to a signal intensity value of 24 nt spike-in oligoribonucleotides. The probes on the array were based on miRBase version 16 that contained 679 rat miRNAs. For expression analysis, only miRNAs that possessed average signal intensity values of at least 35 (higher than $\log_2[\text{average signal intensity}] = 5$) after background subtraction (where signal intensity values of miRNAs that were same as the background signal were considered as zero), in either of the cellular fractions, were considered. Nuclear enrichment score (NEnS) was calculated by taking logarithm base 2 of the ratio of (average nuclear signal intensity value)/(average cytoplasmic signal intensity value). Statistical analysis was performed on signal intensity values with Student's t-test (two-tail, paired). The calculation of Pearson's coefficient between different microarray datasets was performed in Excel (Analysis ToolPak add-in) and was based on log₂ transformed signal intensity values of miRNAs.

5.3.3.5 Deep sequencing

Small RNA libraries were constructed and sequenced by EMBL genomic core facility (Heidelberg, Germany). In brief, 4 small RNA libraries (2 nuclear and 2 cytoplasmic)

representing 2 biological replicates were prepared using small RNA sample prep assay (Illumina) as per manufacturer's instructions. Each of the small RNA libraries was sequenced for 36 cycles in a single lane of one Illumina HiSeq flow cell. Raw sequencing reads were trimmed from 3' adapter (TCGTATGCCGTCTTCTGCTTG) and filtered according to quality using default parameters of Fastx-Toolkit for fastq data on a Galaxy, a web-based genome analysis tool ((Goecks et al., 2010); <https://main.g2.bx.psu.edu/>). Sequencing reads that contained only adapter sequence or those that initially (before trimming) did not contain adapter sequence, as well as reads shorter than 15 nucleotides were discarded. Furthermore, only reads that have at least 2 identical sequence counts in each of the libraries were considered for analysis ("clean reads"). Clean reads were mapped to the rat mature miRNAs (miRBase v19) using default parameters (one mismatch, 3 nt in the 3' or 5'-trimming variants, 3 nt in the 3'-addition variants) of Miraligner software (Pantano et al., 2010). The rest of the unmapped reads were first mapped to rat premiRNAs (miRBase v19) and then to other classes of non-coding RNAs (snoRNAs, snRNAs, rRNAs, tRNAs, mitochondrial tRNAs, mitochondrial rRNAs, miscRNAs; sequences were retrieved from Ensembl genome database (rn4) using BioMart portal, <http://central.biomart.org/>), piRNAs (<http://www.ncrna.org/frnadb/>, <http://www.noncode.org/>), mRNAs (mRNA_coding sequence, 3'UTR, -1000_transcription_start_site+5UTR; sequences were retrieved from Ensembl genome database (rn4) using BioMart portal, <http://central.biomart.org/>) and finally to rat genome (ftp://ftp.ccb.jhu.edu/pub/data/bowtie_indexes/; USCS rn4) in a sequential order using bowtie-0.12.8 software (Langmead, 2010) allowing up to 2 mismatches. All read counts that were mapped to the sequences from aforementioned RNA/DNA databases were used to normalize between nuclear and cytoplasmic small RNA libraries. After normalization, miRNAs represented by at least 100 reads in one of the cellular compartments were considered for further analysis. Nuclear enrichment score (NENs) was calculated by taking logarithm base 2 of the ratio of (average nuclear read count)/(average cytoplasmic read count). The rank based comparison of microarray and deep sequencing was performed by Rank Sum function of RankProdIt (<http://strep-microarray.sbs.surrey.ac.uk/RankProducts/>; (Laing and Smith, 2010).

5.3.3.6 Quantitative real-time PCR

The total RNA extraction from neuronal cultures was performed using PeqGOLD TriFast reagent per manufacturer's instructions. RNA samples were treated with TURBO DNase (Ambion). For detection of small nuclear RNAs (U1, U4, U6), pre-miRNAs and mRNAs (GAPDH), 200 ng of total RNA sample was reverse transcribed with iScript cDNA synthesis kit (Bio-Rad) and quantitative real-time PCR (qRT-PCR) was performed on the StepOnePlus Real-Time PCR System (Applied Biosystems), using iTaq SYBR Green Supermix with ROX (Bio-Rad). For detection of mature miRNAs, 50 ng of total RNA sample was reverse transcribed using the TaqMan MicroRNA Reverse Transcription Kit and qRT-PCR was performed on the StepOnePlus Real-Time PCR System (Applied Biosystems), using TaqMan MicroRNA Assay (Applied Biosystems). Each sample was

measured in duplicate – or triplicates. qRT-PCR data from nuclear fractionated samples were analyzed by $2^{-\Delta Ct}$ ($2^{-(NUC Ct - CYT Ct)}$) method (ΔCt method). Data obtained from whole-cell RNA (developmental, neuron, glia-specific expression) were analyzed by $\Delta\Delta Ct$ method, where Ct values were first normalized to an internal control (eg. U6) and then to the reference sample, which was arbitrarily set to 1. For statistical analysis (Student's and Welch's t-tests) the data, which was normalized only to U6 was used. Primers used for the qRT-PCR are provided as supplementary data (Table S8).

5.3.3.7 Northern blot

10 – 20 μ g of total RNA were separated using denaturing urea 15 % PAGE gel (Mini-PROTEAN system; Bio-Rad) in 1x TBE and blotted onto a GeneScreen Plus nylon membrane (PerkinElmer) in pre-cooled 0.5x TBE. Radioactively labeled Decade marker (Ambion) was used as molecular marker. RNAs were crosslinked to the membrane by UV irradiation (1,200 mJ), followed by baking of the membrane for 30 min at 80 °C. The membrane was pre-incubated in hybridization buffer (5xSSC, 20 mM Na₂HPO₄ (pH=7.2), 7 % SDS, 2 x Denhardt's solution, 40 μ g/mL salmon sperm DNA) for at least 2 h at 50 °C at constant rotation, followed by incubation overnight at 50 °C in hybridization buffer containing the denatured [³²P] labeled DNA probe. The membrane was washed twice for 10 min and twice for 30 min at 50 °C with non-stringent wash solution (3 x SSC, 25 mM NaH₂PO₄ (pH=7.5), 5 % SDS, 10 x Denhardt's solution) and once for 5 min at 50 °C with stringent wash solution (1 x SSC, 1 % SDS). Signals were detected by autoradiography using the Cyclone Plus Phosphor Imager (PerkinElmer). The membrane was stripped (0.1 % SDS, 5 mM Na-EDTA, preheated to 95 °C) for 1 h and re-used several times to detect additional miRNAs and U6 snRNA. DNA probes are provided as supplementary data (Table S8).

5.3.3.8 Fluorescence in-situ hybridization (FISH)

FISH was performed on dissociated hippocampal neurons at 5 DIV. Cells were fixed with 4 % PFA/4 % sucrose/DEPC-PBS for 15 min at room temperature and washed three times with DEPC-PBS. After permeabilization using 0.2 % Tween/DEPC-PBS for 2 min, cells were washed twice with DEPC-PBS and treated for 5 min with 0.1 M TEA (Triethanolamine-acetic acid in DEPC-H₂O, pH 8.0) and for 10 min with freshly prepared 0.25 % Acetic Anhydride in 0.1 M TEA. Cells were washed three times with DEPC-PBS and pre-incubated in hybridization buffer at 55 °C for 1 h. Subsequently, hybridization was carried out overnight at 55 °C, using hybridization buffer supplemented with denatured (5 min 85 °C, 5 min on ice) DIG (or FITC)-labeled LNA probes (Exiqon; 5 pmol per well in the 24-well format) directed against relevant miRNA. Cells were washed twice in 2x SSC and twice in 0.2x SSC, 30 minutes each. After two washes with PBS, cells were permeabilized with 0.2 % Tween/PBS for 2 min and washed again twice with PBS. Depending on the condition, for signal amplification and co-immunostaining, cells were incubated with first set of antibody dilutions (anti-MAP2–mouse (Sigma) + anti-DIG–FITC (Roche) for U6, miR-25 and miR-92a; anti-MAP2–mouse + anti-FITC–Alexa488–rabbit

(Life Technologies) for miR-9) in blocking solution (0.5 % Blocking Reagent in PBS (Roche)) for 1.5 h at room temperature. After four washes with PBS, second set of antibodies (anti-Mouse–Alexa546 (Life Technologies) + anti-FITC–Alexa488–rabbit; anti-Mouse–Alexa546, respectively) was applied for 30 min at room temperature. Then cells were washed four more times with PBS and incubated in the last antibody (anti-Rabbit–Alexa488 (Life Technologies)) solution for 30 min. Cells were washed three times with PBS (second wash with Hoechst dye - 1:20,000) and mounted on microscope slides using Aqua- Poly/Mount (Polysciences). FISH experiments were analyzed using the 63x objective of the LSM 5 Pascal laser scanning confocal microscope (Zeiss), with identical settings for specific probes. For z-stacks, 3 consecutive optical sections were taken at a 0.4 μm interval with a resolution of 1024 x 1024 pixels. Maximum projections of the z-stack images were used for subsequent analysis of the signal intensities in nucleus and cytoplasm with the ImageJ software. LNA probes are provided as supplementary data (Table S8).

5.3.3.9 Immunocytochemistry

Immunostaining of endogenous MAP2 (anti-MAP2–mouse (Sigma) and GFAP (anti-GFAP–rabbit (DakoCytomation)) in dissociated hippocampal neurons (18 DIV) was performed as described (Siegel et al. 2009).

5.3.3.10 Developmental expression score

DES was calculated by log₂ transforming the ration of miRNA expression values obtained from prefrontal cortex of post-natal day 3 (P3) and embryonic day 10 (E10) rats in the published report by Yao and colleagues (Yao et al., 2012).

5.3.3.11 IsomiR analysis

IsomiRs with at least 10 reads in one of the cellular fractions were considered for analysis presented in Figures 7B,C. The relative nuclear enrichment score (rNE_nS) was calculated as a ratio of nuclear versus cytoplasmic percentage proportion of a certain miRNA variants (isomiRs) and therefore should be distinguished from NES (which is an absolute value). For example, miRNA isoforms of miR-1 are isomiR-1.1 (constitutes 20% of miR-1 with 20 read counts in the nucleus; 30 % with 60 reads in the cytoplasm), isomiR-1.2 (30% and 30 reads, nucleus; 50 % and 100 reads, cytoplasm) and isomiR-1.3 (50% and 50 reads, nucleus; 20% and 40 reads, cytoplasm). The rNE_nSs for these isomiRs are $20/30=0.66$, $30/50=0.6$ and $50/20=2.5$, respectively, although NES for the same isomiRs constitute $20/60=0.33$, $30/100=0.3$ and $50/40=1.25$, respectively. The usage of rNE_nS allows to determine the impact of 3'terminal nucleotide modification of isomiRs on preferential nuclear localization, since it calculates overall proportion of isomiR read counts in the specific cellular compartment independent of whether it is underrepresented in the other cellular compartment. The frequency of nucleotides at 3' last 5 nt was calculated using WebLogo ((Crooks et al., 2004); <http://weblogo.berkeley.edu/>).

5.3.3.12 Statistical analysis

Experiments are reported as mean \pm standard deviation (SD) and based on three (if not otherwise stated) independent replications. Statistical significance was calculated using Student's (for samples with equal variance) and Welch's t-tests (for samples with unequal variance), and for multiple comparisons Bonferroni correction was applied (Benjamini et al., 2001).

5.3.4 Results

5.3.4.1 Microarray profiling of nuclear and cytoplasmic miRNAs

To characterize miRNAs preferentially localizing to neuronal nuclei, we decided to undertake a biochemical fractionation approach that separates the nuclear and cytoplasmic compartment of rat primary cortical neurons cultured for 7 days *in vitro* (DIV). After isolation of total RNA from both compartments, the efficacy of nuclear fractionation was determined by the quantification of expression levels of small nuclear RNAs (snRNA U1, U4, U6; all strictly localized in the nucleus) and Glyceraldehyde 3-phosphate dehydrogenase (GAPDH) mRNA by qRT-PCR (Figures 1A and S1A). As expected, snRNAs were highly enriched in the nuclear compartment, whereas GAPDH mRNA was strongly depleted. Similar to the results obtained from qRT-PCR, we observed a 6-fold enrichment in the nuclear compartment for U6 snRNA with Northern blot assay (Figure 1B). Furthermore, the results from Western blotting showed exclusive expression of the protein markers HDAC2 and beta-Actin in the nuclear and cytoplasmic fraction, respectively (Figure 1C). Together, these results demonstrate that the used fractionation protocol can effectively separate nuclear and cytoplasmic compartments.

As a common practice, the raw data obtained from high throughput methods such as microarray are first normalized before the differential expression between two samples is calculated. Since we wanted to calculate the absolute enrichment of miRNAs in the nuclear compartment compared to the cytoplasmic compartment, we supplemented total RNA samples with spike-in oligoribonucleotides (18nt, 24nt, 30 nt) for normalization. Furthermore, in order to detect hybridization signals originating primarily from mature miRNAs, we size-selected total small RNAs (from 15 to 35 nucleotides) from equal amounts (12 µg) of nuclear and cytoplasmic total RNA by 15% denaturing urea polyacrylamide gel electrophoresis (PAGE).

To determine expression levels of nuclear and cytoplasmic mature miRNAs, size-selected small RNA samples (3 nuclear and 3 cytoplasmic samples) were analyzed by miRNA microarrays (LCSciences), containing probes for 679 rat mature miRNAs (miRBase version 16). In total, we were able to detect 267 mature miRNAs which were common to both nucleus and cytoplasm (Table S1). To check the reproducibility of microarray profiling, we compared data obtained from three different biological replicates of fractionations. All three biological replicates performed with cytoplasmic fractions exhibited similar expression patterns (Pearson's correlation coefficient, $r = 0.93-0.95$; Figure 1D). Likewise, all nuclear fractions showed comparable expression, albeit with a slightly lower correlation coefficient ($r = 0.89-0.94$; Figure 1D). Together, these data suggest that fractionations were reproducible and the microarray profiling procedure and normalization was appropriate. Interestingly, samples from nuclear and cytoplasmic compartments had a lower correlation coefficient ($r = 0.74-0.85$) between datasets (Figure 1D), implying that the miRNA expression profiles of nuclear and cytoplasmic

compartments are distinct. The average expression of the majority of miRNAs was lower in the nucleus compared to the cytoplasm (Figure 1E), indicating that most of the miRNAs, as expected, are preferentially located in the cytoplasm.

To identify a set of nuclear-enriched miRNAs, we first calculated a nuclear enrichment score (NEnS; $\log_2(\text{NUC}/\text{CYT})$) for all miRNAs, by \log_2 transforming the average ratio of nuclear/cytoplasmic signal intensity values (Table S1). The NEnS for individual miRNAs ranged from 10.14 to -3.50 with a median of -1.12, suggesting that on average miRNA expression in the cytoplasm is ~2 fold higher than in the nucleus. From a total of 267 miRNAs, 91 miRNAs (34.1%) displayed a statistically significant differential distribution between nuclear and cytoplasmic compartments (student's t-test, $p < 0.05$; Table S2). Among them, 86 (32.6%) miRNAs were preferentially found in the cytoplasm, and only 4 (1.5%; miR-133b*, miR-365*, miR-328a*, miR-92a) in the nucleus. Three of these miRNAs (miR-133b*, miR-365* and miR-328*) were not previously reported to be expressed in neuronal cells. Therefore, to validate our results and to obtain a more comprehensive coverage of nuclear miRNAs, we decided to perform in addition deep sequencing of small RNAs from our fractionation experiment.

5.3.4.2 Deep sequencing of small RNAs from nuclear and cytoplasmic fractions

In comparison to microarrays, deep sequencing-based profiling of small RNAs is more sensitive and allows to study the expression of miRNAs at nucleotide resolution. Furthermore, it allows to discriminate mature and precursor forms of miRNAs. Importantly, it also provides information about variable isoforms of miRNAs, so called isomiRs, and the nature of the associated nucleotide modifications. We used the Illumina-platform for deep-sequencing of small RNA libraries obtained from different compartments of rat primary cortical neurons (DIV7). To ascertain reproducibility of the results, we used two biological replicates for each cellular fraction. Moreover, to obtain a deep coverage of all possible isomiRs and to eliminate the effect of multiplexing artifacts which can result from different barcodes used in small RNA libraries, each of the small RNA libraries (2 nuclear and 2 cytoplasmic) were sequenced in individual lanes of one Illumina HiSeq flow cell.

In total, we obtained ~62 and ~66 million sequence read counts for nuclear and cytoplasmic fractions, respectively. After filtering reads according to the length (>15 nt), contamination (adapter sequences), quality and abundance (at least 2 identical reads per unique sequence), ~19 and ~41 million "clean" reads, respectively, remained for further analysis. These reads were mapped to the publicly available rat RNA and genomic databases (rn4; Table 1; see Methods). To compare the abundance of read counts between two cellular fractions, a normalization according to the total number of mapped clean reads (nuclear - 17,883,861; cytoplasmic - 37,917,208) was performed. Interestingly, the number of normalized read counts from the nucleus matching to mature

miRNA was 3-4 fold lower (depending on biological replicate) than in the cytoplasm (Figure 2A and Table S3). As expected, the nucleolar/nuclear small RNAs (snoRNA and snRNA) were highly enriched (63-89 fold and 16-17 fold, respectively) in the nuclear fraction; in contrast, cytoplasmic tRNAs were depleted (3 fold) in this fraction, again showing the purity of the cellular fractions used for sequencing. Furthermore, the expression of mature miRNAs in two biological replicates for each cellular fraction showed very high Pearson's correlation coefficient (nuclear, $r = 0.99$; cytoplasmic, $r = 0.98$), demonstrating a high reproducibility of the experiments (Figures 2B,C).

In total, we identified 335 miRNAs represented by at least 100 reads in one of the cellular compartments (Table S4). The size distribution of reads mapping to mature miRNAs peaks at 23 nt (Figure 2D), but not at 22 nt as was previously observed (Lee et al., 2010), probably owing to the high expression of miR-9 (49 % and 44 % of total reads in nuclear and cytoplasmic fractions, respectively). The overall distribution of read length in the nucleus was similar to the cytoplasm, but as mentioned above, with less total reads. The NEnS for individual miRNA ranged from 1.88 to -5.58 and the median was -2.08, when all detected miRNAs are considered (Table S4). Only two miRNAs, miR-143 and miR-126* possessed a positive NEnS, indicating that these miRNAs are enriched in the nucleus according to deep sequencing. Since only 2 biological replicates were generated, the statistical parametric analysis was not applicable.

5.3.4.3 Comparison of microarray and deep sequencing

220 miRNAs were commonly detected by both microarray and deep sequencing methods, whereas 47 and 115 were specific for microarray or deep sequencing, respectively (Figure 3A). The comparison of miRNA expression ($\log_2(\text{signal intensity or read count})$) data obtained with these two methods showed a Pearson's correlation coefficient of 0.63 and 0.71 for nuclear and cytoplasmic miRNAs, respectively (Figures 3B,C), suggesting that overall there is a correlation in the expression patterns between the datasets obtained from different methods. However the correlation coefficient is much lower compared to biological replicates (Figures 1D and 2B,C). The major effect contributing to the difference between the data is probably that deep sequencing is more sensitive than microarray as illustrated in Figures 3B and C. The points corresponding to the low expressed miRNAs (data points $\log_2 = \sim 5$ on y-axis) according to microarray are shifted toward the right side of the x-axis, indicating that deep sequencing, in contrast to microarray, can effectively detect and discriminate between low expressed miRNAs. This is even more apparent in the nuclear fraction (Figure 3C). Since the NEnS of miRNAs is calculated from the \log_2 transformed ratio of nuclear and cytoplasmic expression levels (signal intensity or read counts), a cross-platform difference in detection efficacy of miRNA expression might result in rather different NEnS for the same miRNA depending on the method. Indeed, NEnS scores for miRNAs obtained from microarray and deep-sequencing experiments showed no correlation (Pearson's correlation coefficient, $r < 0.1$, data not shown), and therefore statistical parametric analysis was not applicable. Hence

we sought to employ alternative statistical methods to compare datasets from microarray and deep sequencing.

Rank-based non-parametric statistics employs the ranks instead of actual expression levels to identify differentially expressed genes (Hong et al., 2006). Therefore this type of analysis is less sensitive to “noise” between the data obtained using different high-throughput platforms, such as microarray (Hong and Breitling, 2008) and deep sequencing (Llorens et al., 2013), and allows determining the genes, in our case miRNAs, which are consistently high-ranked in data obtained using different methods. We used the Rank Sum method to identify miRNAs, which possess consistently high (higher than other miRNAs) NEnS ranking in both microarray and deep sequencing, and therefore potentially might be enriched in the nucleus (Hong et al., 2006; Laing and Smith, 2010). For this analysis miRNAs that were detected by both platforms (220) were considered. As illustrated in the rank-based heatmap, miRNAs are color-coded from red to white in descending rank order for each biological replicate separately (Figure 4, columns 1-5 and Table S5) and together (Figure 4, column 6 and Table S5). Despite some differences in the ranking, the overall ranking of miRNAs is highly similar not only between different biological replicates, but also between different technological platforms. After applying Benjamini-Hochberg false discovery rate (FDR) of 0.05 for multiple testing (Benjamini et al., 2001), we identified 8 miRNAs, which were significantly higher ranked among the biological replicate experiments of microarray and deep sequencing (Table 2), suggesting that these miRNA might be preferentially localized to the neuronal nuclei compared to the vast majority of miRNAs. Importantly, the synaptic miR-7a and miR-138 (Siegel et al., 2009) were among the 10 most low ranked miRNAs (i.e. cytoplasmic; Table 2), suggesting that the rank-based analysis method is able to faithfully detect differences in the intracellular distribution of miRNAs.

5.3.4.4 Validation of nuclear-enriched miRNA candidates identified by profiling approaches

To validate results obtained using microarray and deep sequencing with a Rank Sum analysis, we decided to perform Northern blot, which allows size-separation and visualization of miRNAs with different sizes, including mature miRNA. As shown in Figure 5A (and Figures S1B,C), the mature form of 4 highly ranked miRNAs (miR-92a, miR-25, miR-27a and miR-92b) was higher or equally expressed in the nuclear fraction compared to the cytoplasm. In contrast, a low-ranked miRNA, miR-138 (rank = 214), showed the opposite expression pattern. Interestingly, if only one method, for instance deep sequencing, is taken into account to calculate nuclear-enrichment, then the ranks for miR-92a, miR-25, miR-27a and miR-92b are 7, 31, 28 and 34, respectively (Table S5). According to the same method miR-132 is ranked 3, implying that this miRNA should be more nuclear enriched than the other four. However, miR-132 possessed slightly less signal in the nucleus compared to the cytoplasm by Northern, which is more in line with the ranking (rank=19) when both methods (Rank Sum) are taken into account (Table

S5). A similar rank correction is observed for miR-19b (deep seq rank=49; Rank Sum rank=184), for which Northern showed a similar depletion of signal in the nucleus compared to the cytoplasm as miR-138 (Figure 5A). Likewise, the miRNAs highly ranked using only microarray data are either not detected by deep sequencing (miR-133b*, miR-365* and miR-328*) or their ranking (Rank Sum) is decreased considerably (miR-1224; Figure 5A and Table S5). This is in line with the Northern blot data which suggests that the nuclear signal for these miRNAs is possibly originating from by-products of pre-mRNA splicing or noncoding RNA transcription, but not from the mature miRNA (Figure 5A). Taken together, these results confirm that some of the highly ranked miRNAs (miR-92a, miR-25, miR-27a and miR-92b) are indeed enriched in the nucleus and also indicates the robustness of the rank-based statistical analysis to identify nuclear-enriched or -depleted miRNAs.

In addition to Northern blot assay, we further validated nuclear enrichment of the two top candidate miRNAs, miR-25 and miR-92a using TaqMan qRT-PCR. In agreement with results from Northern blot, miR-25 and miR-92a showed a significant nuclear enrichment compared to GAPDH, with a NUC/CYT fold change of 1.81 and 1.41, respectively (Figure 5B). As expected, the nuclear marker gene U6 was enriched (11.48) in the nucleus, whereas the cytoplasmic marker gene GAPDH was depleted (0.36), once more demonstrating that the cellular fractionation protocol was efficient in separating nuclei and cytoplasm.

For all experiments so far, we used total RNA from nuclear and cytoplasmic compartments. This RNA was obtained from a biochemical fractionation method that relies on differential centrifugation. With this method, it is difficult to achieve complete separation of compartments, and therefore the obtained results might not entirely reflect the natural distribution of miRNAs in intact neurons. Moreover, biochemical preparations likely contain a mixture of RNA from different cell types, e.g. neurons and glia. Thus, we performed in addition fluorescent *in situ* hybridization (FISH) with LNA probes to precisely determine localization of nuclear-enriched miRNAs (miR-25 and miR-92a) in intact primary rat hippocampal neurons (DIV5) at the single cell level (Figure 5C). After application of a FISH probe against miR-25 and miR-92a a stronger fluorescent signal in the neuronal nucleus compared to the cytoplasm was observed, indicating that these miRNAs are preferentially localized in the nucleus of intact neurons. Conversely, the cells hybridized with a probe against miR-9 (Rank Sum rank=120) displayed a stronger fluorescent signal in the cytoplasm compared to the nucleus. Accordingly, quantification of FISH signal from many cells revealed that the ratio between nuclear and cytoplasmic signals for miR-25 and miR-92a was significantly higher ($p = 0.002$ and 0.0006 , respectively, Student's t-test) than miR-9 (Figure 5D). Taken together, our results from Northern, qRT-PCR and FISH strongly suggest that miR-25 and miR-92a are enriched in the nucleus of post-mitotic primary rat neurons.

5.3.4.5 Developmental expression levels of miRNAs and their nuclear enrichment

In order to obtain a first indication at which developmental stage miR-25 and miR-92a might function in neurons, we performed a developmental time-course experiment, quantifying the relative expression levels of mature miRNAs at 4, 11, 18, 25 DIV in cortical neurons using qRT-PCR (Figure 6A). The expression levels of both miR-25 and miR-92a were significantly declining with the progress of neuronal development, whereby the decrease in expression of miR-25 was more pronounced compared to miR-92a. At the end of the developmental time-course (DIV25), expression levels of miR-25 and miR-92a were reduced by 80 % and 60 %, respectively, compared to DIV4. Taken together, our results indicate that expression of miR-25 and miR-92a is down-regulated during post-mitotic neuronal development. However, since measurements were started at DIV4, we cannot rule out that the peak of expression for these miRNAs is actually even earlier in development.

Based on our observations, we tested the hypothesis that developmental down-regulation might be a common feature of nuclear-enriched miRNAs. We therefore calculated a developmental expression score (DES; see Methods) for each miRNA present in our ranking list based on a recent study which reported genome-wide miRNA expression profiles during development of the rat cortex *in vivo* (Yao et al., 2012). A negative DES would hereby indicate that the expression level of the respective miRNA is down-regulated during rat cortex development. Indeed, we observed a trend toward an increase of the average DES from high (nuclear-enriched) to low (cytoplasmic-enriched) ranking miRNAs, suggesting that down-regulation during rat cerebral cortex development is a common feature of nuclear-enriched miRNAs (Figure S1D and Table S6). Accordingly, the DES of two extreme groups consisting of the 10 highest and lowest ranked miRNAs (hence, the most reliable in terms of nucleo-cytoplasmic localization), differ significantly ($p= 0.028$; Student's t-test) with an average DES of -2.35 and -0.39, respectively (Figure 6B).

Taken together these findings suggest that nuclear-enriched miRNAs in general might be expressed at early stages of neuronal development and that their decline in expression levels during development correlates with nuclear enrichment.

5.3.4.6 MiR-25 and miR-92a are specifically enriched in neuronal nuclei, but not in glia

Results from recent publications suggest that miR-25 and miR-92a might be preferentially expressed in glia compared to neurons (Jovicic et al., 2013). In order to investigate the contribution of glial cells to the expression of miR-25 and miR-92a in our primary cortical neuronal cultures, we further decided to test expression levels of these miRNAs in glia-depleted and glia-enriched neuronal cultures. Primary cortical neurons prepared with our standard protocol contain a substantial amount of proliferating glial

cells (10-20 % of total cells at DIV7, data not shown). We therefore considered the possibility that glia-derived miRNAs could significantly contribute to the results concerning nuclear-enrichment of miRNAs in neurons. To obtain glia-depleted culture, we cultured cells in the presence of a potent inhibitor of cell proliferation, 2'-Deoxy-5-fluorouridine (FUDR), and relative expression levels of miRNAs were assessed by qRT-PCR. Depletion of glial cells in our cultures was verified by the quantification of the astrocytic marker gene glial fibrillary acidic protein (GFAP), which was almost completely absent in FUDR-treated cultures (Figures 6C and S2A). The expression of neuronal marker genes, miR-134 and MAP2 were not significantly affected by FUDR-treatment, suggesting that the overall contribution of RNA from glial cells to the total RNA in our mixed cultures is small. Importantly, the nuclear-enriched miRNAs, miR-25 and miR-92a, in contrast to GFAP, were only slightly reduced in FUDR-treated cultures, showing that the expression of these miRNAs in our mixed cultures is predominantly derived from neurons, with a small contribution from glia.

Experiments carried out on glia-depleted cultures indicate that the overall contribution of glial cells to the expression of nuclear-enriched miRNAs in our mixed cultures is small. However, they do not rule out that the expression of these miRNAs in an individual glial cell is in fact higher compared to that in an individual neuron. We therefore established a culture protocol that strongly favors the growth of glial cells (approximately 50-60 % are glial cells; data not shown). In glia-enriched cultures, we could detect higher expression of GFAP, and lower expression of miR-134 and MAP2 compared to mixed culture, suggesting that these culture conditions indeed favored the growth of glial cells (Figure S2B). Interestingly, miR-25 and miR-92a displayed a 2.2 and 1.5 fold, respectively, higher expression in glia-enriched cultures compared to mixed culture, suggesting that expression of these miRNAs is in fact higher in individual glial cells compared to neurons.

Finally, we wanted to compare nuclear enrichment in glial cells and neurons. For this we fractionated mixed and FUDR-treated cultures in nuclei and cytoplasm, and then measured RNA expression by TaqMan qRT-PCR (Figure 6D). Interestingly, the nuclear enrichment of both miR-25 and miR-92a was on average 3-fold higher in FUDR-treated cultures compared to mixed cultures. In contrast there was no significant change in the nuclear enrichment of miR-134, miR-138 and U6 snRNA, demonstrating the specificity of the assay. These results suggest that miR-25 and miR-92a are specifically enriched in the nucleus of neurons, but not glial cells, where they might instead preferentially localize to the cytoplasm.

In summary, although miR-25 and miR-92a are clearly expressed in glial cells, the major contributors to their expression in mixed cultures are neurons. Furthermore, nuclear-enrichment of these miRNAs is a specific feature of neurons. These results are

consistent with FISH and suggest a specific function of miR-25 and miR-92a in the nucleus of post-mitotic neurons.

5.3.4.7 Inspection of nuclear miRNAs for common sequence characteristics

Since localization of RNAs to distinct cellular compartments is known to be dependent on specific cis-acting sequences (Jambhekar and Derisi, 2007), we decided to search for common cis-acting elements that might target miRNAs to the neuronal nucleus. In this regard, it was shown that a 3' hexanucleotide motif (AGUGUU) is sufficient to direct miR-29b into the nucleus of HeLa cells (Hwang et al., 2007; Jeffries et al., 2010). Furthermore, it was reported that in human neural progenitor cells, 7 out of 21 miRNAs with preferential nuclear localization possess an ASUS (S = G or C; this motif is also included in the aforementioned miR-29b) motif within the last 3' 9 nucleotides (Jeffries et al., 2011). However, the ASUS motif was neither enriched nor depleted in the last 3' 10 nt of two extreme groups consisting of the top 20 high-ranked and top 20 low-ranked miRNAs (Table S5), suggesting that in contrast to the results from non-neuronal systems (Jeffries et al., 2011) the ASUS motif does not function as a nuclear localization signal in neurons.

Furthermore, it was reported that miRNAs which have the same seed sequence and a similar composition of the nine 3'-terminal nucleotides, are likely to be enriched in the same cellular compartment (nuclear or cytoplasmic; (Jeffries et al., 2011)). In agreement, we found that three members of a miRNA family (miR-92a (rank=1), miR-25 (rank=2) and miR-92b (rank=4)) which in addition to the seed share a common 3' terminus are high ranked, whereas another member of the same family with a different 3' terminus (miR-363 (rank=85); Figure S3) is low ranked. However, some other miRNA pairs with similar nucleotide composition, such as miR-27a (rank=3)/miR-27b (rank=153) or miR-130b (rank=7)/miR-130a (rank=130) were not ranked together (Figure S3), suggesting that having the same seed together with a similar 3' terminus alone is not sufficient to confer nuclear enrichment in neurons. Therefore, in addition to the similarity of seed and 3'-terminus, other sequence elements might also be important for nuclear localization of miRNAs.

A closer inspection of the nuclear rank list revealed that highly ranked miRNAs have a tendency to contain a guanine (G) at the 3' terminus, whereas low ranking miRNAs often end with a uridine (U; Figure S4). However, a statistical analysis of the two extreme groups (top 10 high-ranked and 10 low-ranked miRNAs) did not show a significant difference (data not shown). We further investigated if the high-ranked miRNAs share any other sequence motifs. However, none of the online available multiple alignment and motif finding tools (ClustalW, MEME, LocARNA, Gibbs motif sampler) found any over-represented motifs among nuclear-enriched miRNAs (data not shown).

Taken together, bioinformatic inspection of miRNAs for putative cis-acting sequence elements revealed that in contrast to previously published results, the ASUS motif at the 3' region of miRNAs is evenly distributed through-out our ranking list, suggesting that in neurons this motif is unlikely to participate in nuclear localization. Moreover, a similar nucleotide composition alone is not a faithful predictor of nuclear enrichment, implying that nuclear localization of miRNAs probably involves multiple, sequence- and structure dependent mechanisms.

5.3.4.8 IsomiRs with a 3'-terminal guanine preferentially localize to a nucleus

Analysis of mature miRNA localization did not reveal the presence of a common sequence element responsible for nuclear accumulation. However, a slight trend for the presence of a 3' terminal guanine was observed (Figure S4). We therefore took advantage of the high sequence coverage of our deep sequencing datasets, which allows the analysis of individual isomiRs, even those expressed at low levels. IsomiRs are variants of canonical miRNAs containing 5' and 3'-end variations, which either result from a variability in the cleavage of Drosha and Dicer (templated nucleotide addition (TA) or trimming) or from non-templated nucleotide addition (NTA; Figure 7A) catalyzed by nucleotidyltransferases.

As previously reported by several groups (Lee et al., 2010; Zhou et al., 2012), we also found that the abundance of isomiR types was miRNA specific. For instance, the sequence reads for the canonical form (miRBase v19) and for 3' terminal single nucleotide templated addition (TA_1) forms of miR-138 were equally abundant and together comprised more than 50 % (cytoplasm) -70% (nucleus) of the total reads for this miRNA (Figure S5). In contrast, for miR-25 and miR-92a the canonical and TA_1 forms, respectively, were overrepresented by 70% in both cellular compartments (Figure S5). In order to determine the overall abundance of specific isomiRs in the nuclear and the cytoplasmic fractions we calculated the percentage of the isomiRs, considering the entire nuclear or cytoplasmic sample. MiR-9 was excluded from the analysis, since the read counts for this miRNA comprise 49 % and 44 % of the total reads in nuclear and cytoplasmic fractions, respectively, and therefore might change the overall isomiR profile considerably. Our analysis showed that canonical miRNAs added to 42.93% and 43.76% of the total nuclear and cytoplasmic sequence reads, respectively (Figure 7B). As previously reported (Wyman et al., 2011; Zhou et al., 2012), the most abundant form of isomiRs were non-templated additions of single adenine (7.16% -nucleus; 8.40% - cytoplasm) and uracil (6.37%-nucleus; 6.58%-cytoplasm) nucleotides, both of which were slightly overrepresented in the cytoplasm. Interestingly, an overall relatively rare non-templated addition of a single guanine (NTA_G) was four-fold higher in the nucleus (1.30%) compared to the cytoplasm (0.31%). Furthermore, isomiRs with templated addition of a single guanine (TA_G) were also more prominent in the nuclear (2.59%) than in the cytoplasmic (1.56%) fraction (Figure 7C). This calculation is based on the

abundance of the sequence reads, and distributions might be skewed by a few isomiRs of very abundant miRNAs. We note that the top 15 highly expressed miRNAs together account for 77.5% (cytoplasm) of all sequencing reads. In order to avoid the influence of the read counts, we first calculated a relative nuclear enrichment score (rNEnS; % of the nuclear fraction/ % of the cytoplasmic fraction for a respective miRNA; see Methods) of isomiRs and then quantified the type (A, U, G, C) and occurrence of nucleotides at the 3'-terminus of each unique sequence. Although we will be not able to differentiate the source of the last nucleotide variation (trimming, templated or non-templated additions) with this analysis, we can obtain an estimate how the 3'-terminal nucleotide influences nuclear localization. Strikingly, guanine at the 3'-terminus of isomiRs with a high rNEnS was strongly overrepresented compared other nucleotides (Figures 8A,B). However, as the rNEnS declined guanine at the 3' terminus became less frequent, whereas other nucleotides (A, U and C) were now more prominent. A closer inspection of specific miRNA isomiRs (Figure S6) confirmed our observation that isomiRs with a high rNEnS tend to possess a guanine nucleotide at their 3'-terminus. This data implies that 3' guanine could promote nuclear accumulation of isomiRs.

In order to determine whether the source of the 3'-terminal G (canonical, trimmed, NTA or TA) independent of the remaining sequence has an impact on nuclear localization, we calculated rNEnS for different isomiRs (Figures 8C,D,E,F). Strikingly, the average rNEnS for non-templated (NTA_G; 4.08) and templated guanine added (TA_G; 2.99) isomiRs were significantly higher ($p=4.2E-13$ and $6.8E-07$, respectively; Welch t-test) than the average rNEnS of all canonical isomiRs (1.17), irrespective of the 3'-terminal nucleotide (Figure 8C). In contrast, the average rNEnS for NTA_C (0.95; $p=4.9E-06$) and NTA_A (0.99; $p=2.6E-06$) was lower than for all canonical isomiRs. These results suggest either the possibility of targeted guanylation in the nucleus or enhanced localization to the nucleus of isomiRs already possessing a 3' guanine due to NTA_G or TA_G. We next calculated the impact of the 3' terminal nucleotide in canonical isomiRs. Surprisingly, the average rNEnS for canonical isomiR_Gs (1.63) was also significantly higher than canonical isomiR_C (1.1; $p=1.8E-09$), _A (1.0; $p=4.3E-12$) and _U (1.1; $p=1.6E-10$) (Figure 8D). Furthermore, one nucleotide trimming of canonical isomiR_C, _A and _U and thereby exposing a guanine, but not other nucleotides at the 3' terminus, increased significantly the rNEnS for these isomiRs (Trim_N>G; N= A, C or U; Figures 8E and S7). Conversely, one nucleotide trimming of canonical isomiR_G and thereby exposing nucleotides other than guanine at the 3' terminus significantly decreased the rNEnS (Figure 8F). Together, these results strongly argue that the guanine nucleotide at the 3'-terminus *per se* might lead to a preferential nuclear localization of isomiRs.

Taken together, we found that isomiRs possessing a 3' terminal guanine nucleotide show preferential localization to the nucleus. The "origin" of this 3' terminal guanine (NTA, TA, trimmed or canonical) further influences the extent of nuclear localization.

5.3.5 Discussion

It is increasingly recognized that miRNAs, in addition to their well described role as post-transcriptional regulators of mRNA translation/stability in the cytoplasm, are also involved in transcriptional (Kim et al., 2008;Place et al., 2008;Benhamed et al., 2012) and post-transcriptional (Hansen et al., 2011;Tang et al., 2012) regulatory processes in the nuclei of proliferating cells. However, a function of miRNAs in the nucleus of post-mitotic cells has not been described. As a first step in the determination of a putative nuclear role of miRNAs, we assessed the complete miRNA nuclear-enrichment profile and sequence-specific requirements that might aid (or be responsible for) the nuclear localization of miRNAs (and their isomiRs) in rat post-mitotic primary neurons.

In this study, we applied the two most common high-throughput profiling technologies, microarray and deep sequencing, to identify the nucleo-cytoplasmic distribution of miRNAs. In line with previous reports (Liao et al., 2010;Jeffries et al., 2011) we also detected the expression of almost all cytoplasmic miRNA counterparts in the nucleus. However, unlike these previous publications, our results from both profiling methods suggested that the majority of miRNAs are enriched in the cytoplasm and only a small subset in the nucleus. The discrepancy between these earlier findings and our current observations might be due to different cell types (cancer cell line (Liao et al., 2010), neural progenitor cells (Jeffries et al., 2011), post-mitotic neurons (this study)) used in these studies. It is also possible that the data normalization (Jeffries et al., 2011) and the power (Liao et al., 2010) of statistical analysis might have contributed. The normalization method performed by Jeffries and colleagues (2011) assumes that only a minority of genes are differentially expressed between conditions (i.e. normalized to the mean/median expression value of all miRNAs detected within the single replicate experiment). Without a priori knowledge of nucleo-cytoplasmic distribution of miRNAs, this type of data normalization might not be appropriate to measure the absolute differences in the expression levels of miRNAs (although this does not affect the nuclear-enrichment ranking between miRNAs) in nuclear and cytoplasmic compartment, since it equalizes otherwise initially different expression profiles in these compartments. To overcome this limitation and to measure absolute miRNA expression levels we therefore used exogenous controls, spike-in oligoribonucleotides (microarray) and total RNA/genomic mapped reads (deep sequencing) for cross-compartmental normalization of miRNA expression. Liao and colleagues used only one biological replicate for deep sequencing, thereby lacking any statistical power. In contrast, we used 5 biological replicates (3 for microarray and 2 for deep sequencing) and identified nuclear-enriched miRNAs in neurons based on the non-parametric Rank Sum method. Interestingly, the application of both microarray and deep sequencing gives more reliable results than each method separately with regard to the identity of nuclear-enriched miRNAs. Based on further validation results (Northern blot) of nuclear- and cytoplasmic-enriched miRNAs we presume that at most 5% of the 220 miRNAs analyzed by both profiling methods are

truly nuclear-enriched miRNAs, although additional experiments are required to validate the expression of more high ranked miRNA candidates.

In addition to the overall distribution of miRNAs between the nuclear and cytoplasmic compartments, there is also little overlap regarding the identity of nuclear-enriched miRNAs among our and earlier reports, which might be accounted for by cell-type and differentiation stage (proliferating vs. non-proliferating) specific differences in miRNA expression. For example, members of the miR-25 family (miR-25 and miR-92a) are found to be preferentially localized in the cytoplasm of human neural stem cells (Jeffries et al., 2011), whereas we found that these miRNAs are enriched in the nuclei of post-mitotic neurons. Furthermore, the miR-25 family members are overexpressed in different cancer types (Kim et al., 2009; Li et al., 2009), and are implicated in the inhibition of pro-apoptotic and anti-proliferative genes such as tumor protein 53 (Kumar et al., 2011) and BCL-2 family protein (Bim; (Tsuchida et al., 2011; Zhang et al., 2012), a regulation which presumably occurs in the cytoplasm. Therefore it is likely that in the early stages of neural development (e.g. in neural progenitors), miR-25 family members localize to the cytoplasm and are involved in the post-transcriptional regulation of proteins involved in the control of cell cycle and proliferation. Indeed, overexpression of miR-25 increased the proliferation of mouse neural stem/progenitor cells (NSPC; (Brett et al., 2011)) and also induced re-entry into mitosis of post-mitotic neurons from zebrafish spinal cord by directly inhibiting the expression of p57 cell-cycle inhibitor (cdkn1c) (Rodriguez-Aznar et al., 2013). Likewise, miR-25 family members might suppress the expression of neuronal phenotype promoting genes in the cytoplasm of glial cells, since the gene ontology (GO) terms, such as neuron development and differentiation, are enriched in the predicted mRNA targets for these miRNAs. In contrast, we found that miR-25 and miR-92a preferentially localize to the nucleus of post-mitotic neurons, where they might be involved in the regulation of gene expression in the nuclei of post-mitotic neurons. Recently, miR-25 was reported to inhibit the expression of the sarco(endo)plasmic reticulum Ca²⁺ ATPase (SERCA2) by binding to the 3'-UTR of SERCA2 mRNA in the cytoplasm of post-mitotic neurons (Earls et al., 2012). It is therefore likely that miR-25, and possibly other nuclear-enriched miRNAs, are also involved in post-transcriptional gene regulation in mature neurons. A future challenge will be to specifically manipulate the nuclear and cytoplasmic pools of miRNAs to elucidate compartment-specific functions.

Since we observed a positive correlation between developmentally down-regulated and nuclear-enriched miRNAs, it is tempting to speculate that developmental stage-specific changes in biogenesis and/or degradation of these miRNAs might contribute to an enrichment of specific miRNAs in the nucleus. In addition to miRNA degradation in the cytoplasm, it is conceivable that targeting (or confinement) of miRNAs to the nucleus may be a mechanism to "remove" miRNAs from the cytoplasm to avoid regulation of cytoplasmic mRNA targets. Since the subcellular compartment of miRNA degradation

remains unknown (Ruegger and Grosshans, 2012), it is possible that nuclear localization could be used to target miRNAs for degradation. Accordingly, some of the exoribonucleases such as ribosomal RNA-processing protein 41 (RRP41), exoribonuclease 1 (ERI-1) and 5' to 3' exoribonuclease XRN2, which are involved in miRNA degradation in metazoans (Ruegger and Grosshans, 2012), were shown to shuttle between the nucleus and cytoplasm (Ansel et al., 2008; Schmid and Jensen, 2008; Nagarajan et al., 2013) and participate in nuclear functions, e.g. ribosomal RNA biogenesis. A possible nuclear degradation of miRNAs is further supported by the observation that transfected siRNAs and endogenous miRNAs are enriched in the nucleolus (Ohrt et al., 2006; Politz et al., 2009). In this respect, studying the stability and localization of mature miRNAs upon their specific delivery into the nucleus or cytoplasm might help to identify the cellular compartment(s) important for degradation of mature miRNAs. Interestingly, it was shown that the turn-over of miRNAs in neurons can be regulated in an activity-dependent manner (Krol et al., 2010). It would be therefore important to determine the role of the nucleus in the rapid turnover of miRNAs in response to activity.

Irrespective of miRNA turnover, specific miRNAs (such as miR-25 and miR-92a) might perform distinct functions depending on the cell type and/or the developmental (metabolic) stage of a cell. For example, in neural stem cells and glial cells, some miRNAs repress neuron-promoting (and anti-proliferation) genes, e.g. by targeting the respective mRNAs and preventing their "leaky" expression in the cytoplasm. In post-mitotic neurons, the same miRNAs might be imported to the nucleus, where they could be involved in transcriptional or posttranscriptional regulation of gene expression as has been shown for some miRNAs and siRNAs in cancer cell lines (Kim et al., 2008; Place et al., 2008; Allo et al., 2009; Tang et al., 2012). In the future, the analysis of miRNA nucleocytoplasmic expression during differentiation of neural stem cells to fully differentiated neurons will be required to determine the exact time-point when the cytoplasmic function of specific neuronal miRNAs is switched to a function in the nucleus.

One of the mechanisms that miRNAs could employ to regulate transcriptional gene expression in the nucleus is by introducing epigenetic modification marks to DNA (methylation) and histone (acetylation and methylation) proteins. To clarify whether nuclear-enriched miRNAs are directly involved in epigenetic control of gene expression, specific manipulation of nuclear miRNAs followed by transcriptional and/or epigenetic profiling will be needed.

We also investigated whether cis-acting elements in mature miRNAs might direct them into the nucleus. Surprisingly, we identified that isomiRs, and to a smaller extent canonical miRNAs, containing 3'-terminal guanine nucleotides are preferentially localized within the nucleus. In addition, we found that the source of the 3' terminal G strongly influences nuclear fate. For example, isomiRs with NTA_G are the most nuclear

enriched, followed by isomiR_Gs obtained from one 3' nucleotide trimming, and then canonical isomiR_G for which the 3'-terminal is generated by Dicer/Drosha. IsomiR_Gs, independent of the source of the 3'-terminal guanine, could favor nuclear localization in at least two ways. First, the 3' terminal guanine could confer higher stability in the nucleus. Second, binding of specific proteins to isomiR_Gs could mediate active transport from the cytoplasm to the nucleus. The active import of isomiR_Gs (as well as other isomiRs) to the nucleus might be performed by Argonaute proteins, which were shown to shuttle between the nuclear and cytoplasmic compartments (Weinmann et al., 2009; Nishi et al., 2013). Since Argonaute proteins (AGO 1-3) show different global small RNA binding pattern (Dueck et al., 2012), one could speculate that one of the AGO isoforms might specifically associate with isomiR_Gs and import them to the nucleus. In addition, RNA-binding proteins other than AGO might also be involved in nucleo-cytoplasmic shuttling of isomiRs. Non-templated addition of guanine to the 3' terminus appears to further enhance nuclear accumulation. NTA_G could either happen in the nucleus after import, or in the cytoplasm followed by nuclear import. The identity of the guanylyltransferase(s) responsible for the production of NTA_Gs is unknown. Known metazoan RNA guanylyltransferases which are part of the mRNA cap-synthesis complex are unlikely to be involved in isomiR_G production, since these guanylyltransferases transfer a guanine monophosphate nucleoside to the nascent 5' diphosphate mRNA end (Ghosh and Lima, 2010), but not the 3' end. Apart from guanylation at the 3' of miRNAs, the only example where terminal guanylyltransferase activity was observed is specific guanylation of European yellow lupine (*Lupinus luteus*) 5s rRNA at the 3' end in Hela cell extract (Wyszko et al., 1996). However, the responsible enzyme as well as physiological significance of this modification is not known. Interestingly, isomiRs with non-templated guanine addition are more abundant in mouse hippocampus (Zhou et al., 2012) and cerebellum (Wyman et al., 2011) compared to other tissues, suggesting that 3' non-templated addition of guanine could be a brain-specific phenomenon. In this regard, determination of the identity and subcellular localization of guanylyltransferase responsible for NTA_G in neurons will be highly informative.

Taken together, our results indicate that mammalian neurons have a distinct subset of nuclear-enriched miRNAs, and that their localization to the nucleus might be linked to the developmental stage-specific down-regulation of miRNA expression. Furthermore, we uncovered that the type of nucleotide at the 3'-terminus of miRNA/isomiR can significantly influence subcellular localization of miRNAs in neurons. In the future, it will be important to characterize the physiological role of nuclear-enriched miRNAs in neurons, as well as the molecular mechanisms underlying nucleo-cytoplasmic localization, with a focus on the role of 3' terminal guanylation. This will not only increase our understanding of neuronal development, but also provide important new insights into general aspects of miRNA metabolism.

5.3.6 Conflict of interest statement:

The authors declare that they have no conflict of interests.

5.3.7 Author contributions:

SAK, FZ and MR performed experiments; SAK performed data analysis (if not otherwise stated); SAK and GS wrote the manuscript; GS supervised the project.

5.3.8 Acknowledgements:

We thank G. Jarosch, E.Becker, R. Gondrum and T. Wüst for excellent technical assistance, and R. Fiore for critically reading the manuscript. This work was funded by the Deutsche Forschungsgemeinschaft (DFG-SFB593) and the European Research Council (ERC Starting Grant „Neuromir“).

5.3.9 References

Allo, M., Buggiano, V., Fededa, J.P., Petrillo, E., Schor, I., De La Mata, M., Agirre, E., Plass, M., Eyra, E., Elela, S.A., Klinck, R., Chabot, B., and Kornblihtt, A.R. (2009). Control of alternative splicing through siRNA-mediated transcriptional gene silencing. *Nat Struct Mol Biol* 16, 717-724.

Ameyar-Zazoua, M., Rachez, C., Souidi, M., Robin, P., Fritsch, L., Young, R., Morozova, N., Fenouil, R., Descostes, N., Andrau, J.C., Mathieu, J., Hamiche, A., Ait-Si-Ali, S., Muchardt, C., Batsche, E., and Harel-Bellan, A. (2012). Argonaute proteins couple chromatin silencing to alternative splicing. *Nat Struct Mol Biol* 19, 998-1004.

Ansel, K.M., Pastor, W.A., Rath, N., Lapan, A.D., Glasmacher, E., Wolf, C., Smith, L.C., Papadopoulou, N., Lamperti, E.D., Tahiliani, M., Ellwart, J.W., Shi, Y., Kremmer, E., Rao, A., and Heissmeyer, V. (2008). Mouse Eri1 interacts with the ribosome and catalyzes 5.8S rRNA processing. *Nat Struct Mol Biol* 15, 523-530.

Benhamed, M., Herbig, U., Ye, T., Dejean, A., and Bischof, O. (2012). Senescence is an endogenous trigger for microRNA-directed transcriptional gene silencing in human cells. *Nature Cell Biology* 14, 266-+.

Benjamini, Y., Drai, D., Elmer, G., Kafkafi, N., and Golani, I. (2001). Controlling the false discovery rate in behavior genetics research. *Behav Brain Res* 125, 279-284.

Brett, J.O., Renault, V.M., Rafalski, V.A., Webb, A.E., and Brunet, A. (2011). The microRNA cluster miR-106b~25 regulates adult neural stem/progenitor cell proliferation and neuronal differentiation. *Aging (Albany NY)* 3, 108-124.

Crooks, G.E., Hon, G., Chandonia, J.M., and Brenner, S.E. (2004). WebLogo: a sequence logo generator. *Genome Res* 14, 1188-1190.

Dueck, A., Ziegler, C., Eichner, A., Berezikov, E., and Meister, G. (2012). microRNAs associated with the different human Argonaute proteins. *Nucleic Acids Res* 40, 9850-9862.

Earls, L.R., Fricke, R.G., Yu, J., Berry, R.B., Baldwin, L.T., and Zakharenko, S.S. (2012). Age-dependent microRNA control of synaptic plasticity in 22q11 deletion syndrome and schizophrenia. *J Neurosci* 32, 14132-14144.

Fiore, R., Khudayberdiev, S., Saba, R., and Schratt, G. (2011). MicroRNA function in the nervous system. *Prog Mol Biol Transl Sci* 102, 47-100.

Ghosh, A., and Lima, C.D. (2010). Enzymology of RNA cap synthesis. *Wiley Interdiscip Rev RNA* 1, 152-172.

Goecks, J., Nekrutenko, A., and Taylor, J. (2010). Galaxy: a comprehensive approach for supporting accessible, reproducible, and transparent computational research in the life sciences. *Genome Biol* 11, R86.

Hansen, T.B., Wiklund, E.D., Bramsen, J.B., Villadsen, S.B., Statham, A.L., Clark, S.J., and Kjems, J. (2011). miRNA-dependent gene silencing involving Ago2-mediated cleavage of a circular antisense RNA. *EMBO J* 30, 4414-4422.

Hong, F., and Breitling, R. (2008). A comparison of meta-analysis methods for detecting differentially expressed genes in microarray experiments. *Bioinformatics* 24, 374-382.

Hong, F., Breitling, R., Mcentee, C.W., Wittner, B.S., Nemhauser, J.L., and Chory, J. (2006). RankProd: a bioconductor package for detecting differentially expressed genes in meta-analysis. *Bioinformatics* 22, 2825-2827.

Hwang, H.W., Wentzel, E.A., and Mendell, J.T. (2007). A hexanucleotide element directs microRNA nuclear import. *Science* 315, 97-100.

Jambhekar, A., and Derisi, J.L. (2007). Cis-acting determinants of asymmetric, cytoplasmic RNA transport. *RNA* 13, 625-642.

Jeffries, C.D., Fried, H.M., and Perkins, D.O. (2010). Additional layers of gene regulatory complexity from recently discovered microRNA mechanisms. *Int J Biochem Cell Biol* 42, 1236-1242.

Jeffries, C.D., Fried, H.M., and Perkins, D.O. (2011). Nuclear and cytoplasmic localization of neural stem cell microRNAs. *RNA* 17, 675-686.

Jovicic, A., Roshan, R., Moiso, N., Pradervand, S., Moser, R., Pillai, B., and Luthi-Carter, R. (2013). Comprehensive expression analyses of neural cell-type-specific miRNAs identify new determinants of the specification and maintenance of neuronal phenotypes. *J Neurosci* 33, 5127-5137.

Kim, D.H., Saetrom, P., Snove, O., Jr., and Rossi, J.J. (2008). MicroRNA-directed transcriptional gene silencing in mammalian cells. *Proc Natl Acad Sci U S A* 105, 16230-16235.

Kim, Y.K., Yu, J., Han, T.S., Park, S.Y., Namkoong, B., Kim, D.H., Hur, K., Yoo, M.W., Lee, H.J., Yang, H.K., and Kim, V.N. (2009). Functional links between clustered microRNAs: suppression of cell-cycle inhibitors by microRNA clusters in gastric cancer. *Nucleic Acids Res* 37, 1672-1681.

Krol, J., Loedige, I., and Filipowicz, W. (2010). The widespread regulation of microRNA biogenesis, function and decay. *Nat Rev Genet* 11, 597-610.

Kumar, M., Lu, Z., Takwi, A.A., Chen, W., Callander, N.S., Ramos, K.S., Young, K.H., and Li, Y. (2011). Negative regulation of the tumor suppressor p53 gene by microRNAs. *Oncogene* 30, 843-853.

Laing, E., and Smith, C.P. (2010). RankProdIt: A web-interactive Rank Products analysis tool. *BMC Res Notes* 3, 221.

Langmead, B. (2010). Aligning short sequencing reads with Bowtie. *Curr Protoc Bioinformatics* Chapter 11, Unit 11 17.

Lee, L.W., Zhang, S., Etheridge, A., Ma, L., Martin, D., Galas, D., and Wang, K. (2010). Complexity of the microRNA repertoire revealed by next-generation sequencing. *RNA* 16, 2170-2180.

Li, Y., Tan, W., Neo, T.W., Aung, M.O., Wasser, S., Lim, S.G., and Tan, T.M. (2009). Role of the miR-106b-25 microRNA cluster in hepatocellular carcinoma. *Cancer Sci* 100, 1234-1242.

Li, Z.F., Liang, Y.M., Lau, P.N., Shen, W., Wang, D.K., Cheung, W.T., Xue, C.J., Poon, L.M., and Lam, Y.W. (2013). Dynamic Localisation of Mature MicroRNAs in Human Nucleoli is Influenced by Exogenous Genetic Materials. *PLoS One* 8, e70869.

Liao, J.Y., Ma, L.M., Guo, Y.H., Zhang, Y.C., Zhou, H., Shao, P., Chen, Y.Q., and Qu, L.H. (2010). Deep sequencing of human nuclear and cytoplasmic small RNAs reveals an unexpectedly complex subcellular distribution of miRNAs and tRNA 3' trailers. *PLoS One* 5, e10563.

Llorens, F., Hummel, M., Pantano, L., Pastor, X., Vivancos, A., Castillo, E., Mattlin, H., Ferrer, A., Ingham, M., Noguera, M., Kofler, R., Dohm, J.C., Pluvinet, R., Bayes, M., Himmelbauer, H., Del Rio, J.A., Marti, E., and Sumoy, L. (2013). Microarray and deep sequencing cross-platform analysis of the mirNome and isomiR variation in response to epidermal growth factor. *BMC Genomics* 14, 371.

Morris, K.V., Chan, S.W., Jacobsen, S.E., and Looney, D.J. (2004). Small interfering RNA-induced transcriptional gene silencing in human cells. *Science* 305, 1289-1292.

Nagarajan, V.K., Jones, C.I., Newbury, S.F., and Green, P.J. (2013). XRN 5'→3' exoribonucleases: structure, mechanisms and functions. *Biochim Biophys Acta* 1829, 590-603.

Nishi, K., Nishi, A., Nagasawa, T., and Ui-Tei, K. (2013). Human TNRC6A is an Argonaute-navigator protein for microRNA-mediated gene silencing in the nucleus. *RNA* 19, 17-35.

Norris, A.D., and Calarco, J.A. (2012). Emerging Roles of Alternative Pre-mRNA Splicing Regulation in Neuronal Development and Function. *Front Neurosci* 6, 122.

Ohr, T., Merkle, D., Birkenfeld, K., Echeverri, C.J., and Schwill, P. (2006). In situ fluorescence analysis demonstrates active siRNA exclusion from the nucleus by Exportin 5. *Nucleic Acids Res* 34, 1369-1380.

Pantano, L., Estivill, X., and Marti, E. (2010). SeqBuster, a bioinformatic tool for the processing and analysis of small RNAs datasets, reveals ubiquitous miRNA modifications in human embryonic cells. *Nucleic Acids Res* 38, e34.

Park, C.W., Zeng, Y., Zhang, X., Subramanian, S., and Steer, C.J. (2010). Mature microRNAs identified in highly purified nuclei from HCT116 colon cancer cells. *RNA Biol* 7, 606-614.

Place, R.F., Li, L.C., Pookot, D., Noonan, E.J., and Dahiya, R. (2008). MicroRNA-373 induces expression of genes with complementary promoter sequences. *Proc Natl Acad Sci U S A* 105, 1608-1613.

Politz, J.C., Hogan, E.M., and Pederson, T. (2009). MicroRNAs with a nucleolar location. *RNA* 15, 1705-1715.

Rodriguez-Aznar, E., Barrallo-Gimeno, A., and Nieto, M.A. (2013). Scratch2 prevents cell cycle re-entry by repressing miR-25 in postmitotic primary neurons. *J Neurosci* 33, 5095-5105.

Ruegger, S., and Grosshans, H. (2012). MicroRNA turnover: when, how, and why. *Trends Biochem Sci* 37, 436-446.

Schmid, M., and Jensen, T.H. (2008). The exosome: a multipurpose RNA-decay machine. *Trends Biochem Sci* 33, 501-510.

Siegel, G., Obernosterer, G., Fiore, R., Oehmen, M., Bicker, S., Christensen, M., Khudayberdiev, S., Leuschner, P.F., Busch, C.J., Kane, C., Hubel, K., Dekker, F., Hedberg, C., Rengarajan, B., Drepper, C., Waldmann, H., Kauppinen, S., Greenberg, M.E., Draguhn, A., Rehmsmeier, M., Martinez, J., and Schratt, G.M. (2009). A functional screen implicates microRNA-138-dependent regulation of the depalmitoylation enzyme APT1 in dendritic spine morphogenesis. *Nature Cell Biology* 11, 705-716.

Sinkkonen, L., Hugenschmidt, T., Filipowicz, W., and Svoboda, P. (2010). Dicer is associated with ribosomal DNA chromatin in mammalian cells. *PLoS One* 5, e12175.

Tan, G.S., Garchow, B.G., Liu, X., Yeung, J., Morris, J.P.T., Cuellar, T.L., Mcmanus, M.T., and Kiriakidou, M. (2009). Expanded RNA-binding activities of mammalian Argonaute 2. *Nucleic Acids Res* 37, 7533-7545.

Tang, R., Li, L., Zhu, D., Hou, D., Cao, T., Gu, H., Zhang, J., Chen, J., Zhang, C.Y., and Zen, K. (2012). Mouse miRNA-709 directly regulates miRNA-15a/16-1 biogenesis at the posttranscriptional level in the nucleus: evidence for a microRNA hierarchy system. *Cell Res* 22, 504-515.

Till, S., Lejeune, E., Thermann, R., Bortfeld, M., Hothorn, M., Enderle, D., Heinrich, C., Hentze, M.W., and Ladurner, A.G. (2007). A conserved motif in Argonaute-interacting proteins mediates functional interactions through the Argonaute PIWI domain. *Nat Struct Mol Biol* 14, 897-903.

Tsuchida, A., Ohno, S., Wu, W., Borjigin, N., Fujita, K., Aoki, T., Ueda, S., Takanashi, M., and Kuroda, M. (2011). miR-92 is a key oncogenic component of the miR-17-92 cluster in colon cancer. *Cancer Sci* 102, 2264-2271.

Weinmann, L., Hock, J., Ivacevic, T., Ohrt, T., Mutze, J., Schwille, P., Kremmer, E., Benes, V., Urlaub, H., and Meister, G. (2009). Importin 8 is a gene silencing factor that targets argonaute proteins to distinct mRNAs. *Cell* 136, 496-507.

Wyman, S.K., Knouf, E.C., Parkin, R.K., Fritz, B.R., Lin, D.W., Dennis, L.M., Krouse, M.A., Webster, P.J., and Tewari, M. (2011). Post-transcriptional generation of miRNA variants by multiple nucleotidyl transferases contributes to miRNA transcriptome complexity. *Genome Res* 21, 1450-1461.

Wyszko, E., Szweykowska-Kulinska, Z., and Barciszewska, M.Z. (1996). Specific guanylation of *Lupinus luteus* 5S rRNA at its 3' end in HeLa cell extract. *Biochem Mol Biol Int* 39, 1221-1227.

Yao, M.J., Chen, G., Zhao, P.P., Lu, M.H., Jian, J., Liu, M.F., and Yuan, X.B. (2012). Transcriptome analysis of microRNAs in developing cerebral cortex of rat. *BMC Genomics* 13, 232.

Yeo, G., Holste, D., Kreiman, G., and Burge, C.B. (2004). Variation in alternative splicing across human tissues. *Genome Biol* 5, R74.

Zeng, Y., and Cullen, B.R. (2004). Structural requirements for pre-microRNA binding and nuclear export by Exportin 5. *Nucleic Acids Res* 32, 4776-4785.

Zhang, H., Zuo, Z., Lu, X., Wang, L., Wang, H., and Zhu, Z. (2012). MiR-25 regulates apoptosis by targeting Bim in human ovarian cancer. *Oncol Rep* 27, 594-598.

Zhou, H., Arcila, M.L., Li, Z., Lee, E.J., Henzler, C., Liu, J., Rana, T.M., and Kosik, K.S. (2012). Deep annotation of mouse iso-miR and iso-moR variation. *Nucleic Acids Res* 40, 5864-5875.

Zovkic, I.B., Guzman-Karlsson, M.C., and Sweatt, J.D. (2013). Epigenetic regulation of memory formation and maintenance. *Learn Mem* 20, 61-74.

5.3.10 Tables

Table 1. The summary of small RNA deep sequencing. Numbers represent raw (non-normalized) read counts. * disc_discarded

	Total NUC read counts	Total CYT read counts	Total read counts
Total	62,931,202	65,995,793	128,926,995
disc*_ <15 nt	7,163,839	7,572,786	14,736,625
disc_adapter only	870,091	1,389,233	2,259,324
disc_non-clipped	29,780,435	10,399,717	40,180,152
disc_qual_low	1,156,960	2,065,820	3,222,780
disc_one read per condition	4,968,122	3,930,256	8,898,378
mature miRNA (miRBase v19)	3,171,512	23,941,026	27,112,538
precursor miRNA (miRBase v19)	72,675	576,251	648,926
snoRNA	5,880,089	166,704	6,046,793
snRNA	2,352,776	300,101	2,652,877
rRNA	181,268	436,816	618,084
tRNA	247,157	1,688,530	1,935,687
Mt_tRNA	66,111	463,741	529,852
Mt_rRNA	87,352	147,452	234,804
miscRNA	218,657	466,009	684,666
piRNA	387,290	672,414	1,059,704
mRNA_coding sequence	104,619	330,211	434,830
mRNA_3UTR	96,117	92,012	188,129
mRNA_1000 TSS + 5UTR	138,915	289,055	427,970
rat genome (rn4)	4,879,323	8,346,886	13,226,209
mappable_all	17,883,861	37,917,208	55,801,069
not mapped	913,165	2,663,540	3,576,705

Table 2. Top 10 high-ranked and top 10 low-ranked miRNAs according to Rank Sum method.

miRNA_name	Rank	Sum rank
rno-miR-92a	1	
rno-miR-25	2	
rno-miR-27a	3	
rno-miR-92b	4	
rno-let-7bs	5	
rno-miR-93	6	
rno-miR-130b	7	
rno-miR-320	8	
rno-miR-874	9	
rno-miR-24	10	
rno-miR-127s	211	
rno-miR-22	212	
rno-miR-101a	213	
rno-miR-138	214	
rno-miR-98	215	
rno-miR-532-3p	216	
rno-miR-331	217	
rno-miR-434s	218	
rno-miR-329s	219	
rno-miR-7a	220	

5.3.11 Figures

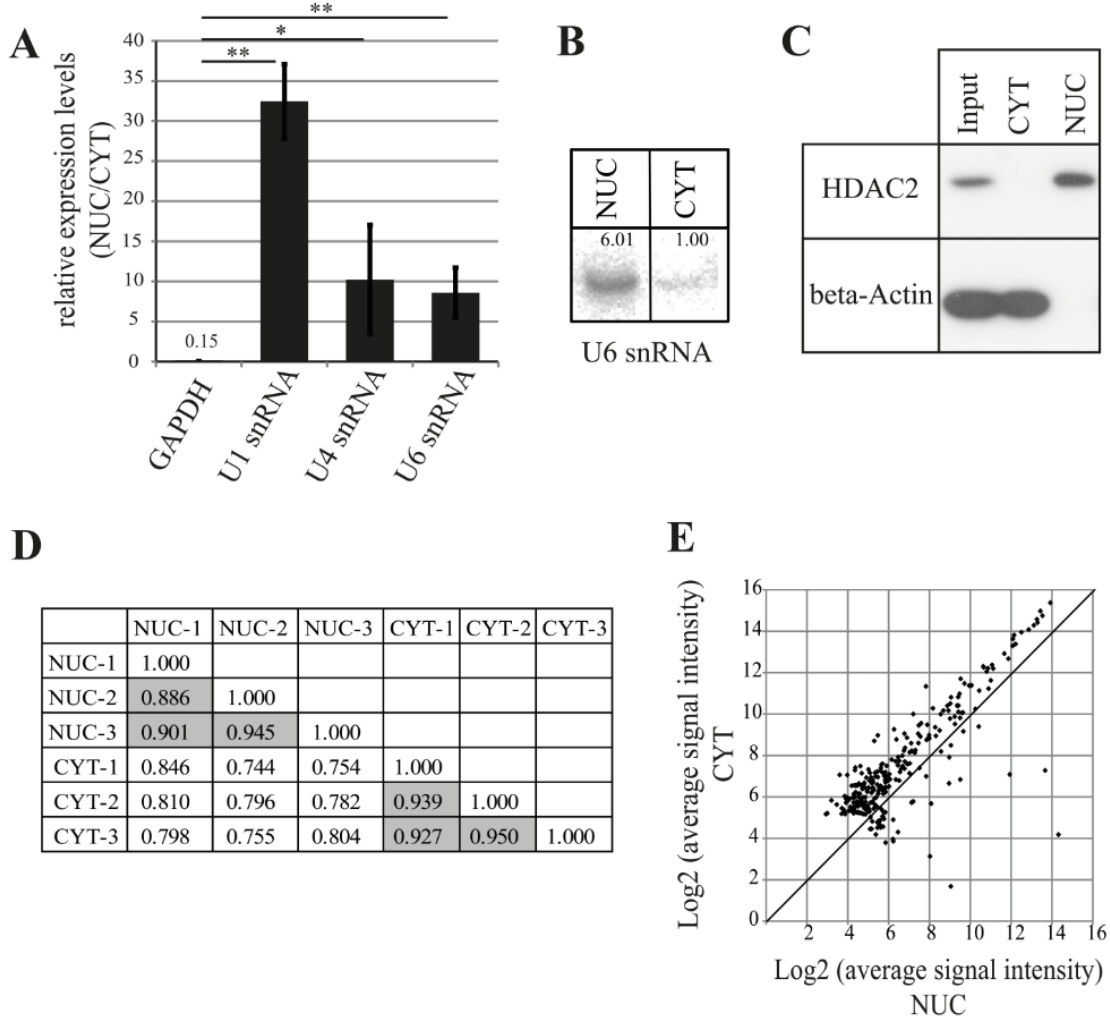


Figure 1. MiRNA profiling by microarray after nucleo-cytoplasmic fractionation of neurons. (A) qRT-PCR analysis of marker genes to validate the fractionation protocol. The fold enrichment (y-axis) of marker genes in the nucleus was calculated by the 2-dCT (2-(NUC Ct – CYT Ct)) method. Bar plots show mean \pm standard deviation (SD; n=3). Statistical significance was determined using Student's t-test with Bonferroni correction (*, $p < 0.05$; **, $p < 0.01$). (B) Northern blot analysis of the nuclear marker U6 snRNA in nuclear and cytoplasmic fractions. Intensity of the signal was quantified using ImageJ. (C) Detection of nuclear (HDAC2, histone deacetylase 2) and cytoplasmic (beta-Actin) marker proteins in the subcellular fractions using Western blotting assay. Whole cell lysate was used as an input sample. This experiment was performed by a PhD student in our lab, Federico Zampa. (D) Comparison of different biological replicates from microarray experiments. Pearson's correlation coefficients between indicated samples

are shown. Data on grey background represents correlation coefficients for biological replicates from the same cellular fraction. (E) Distribution of miRNA expression in the nucleus and the cytoplasm. Scatterplot of log₂ transformed signal intensity values for miRNAs from nuclear (x-axis) and cytoplasmic (y-axis) fractions (267). Dots above the diagonal indicate cytoplasmic enrichment, below, nuclear enrichment of the respective miRNAs.

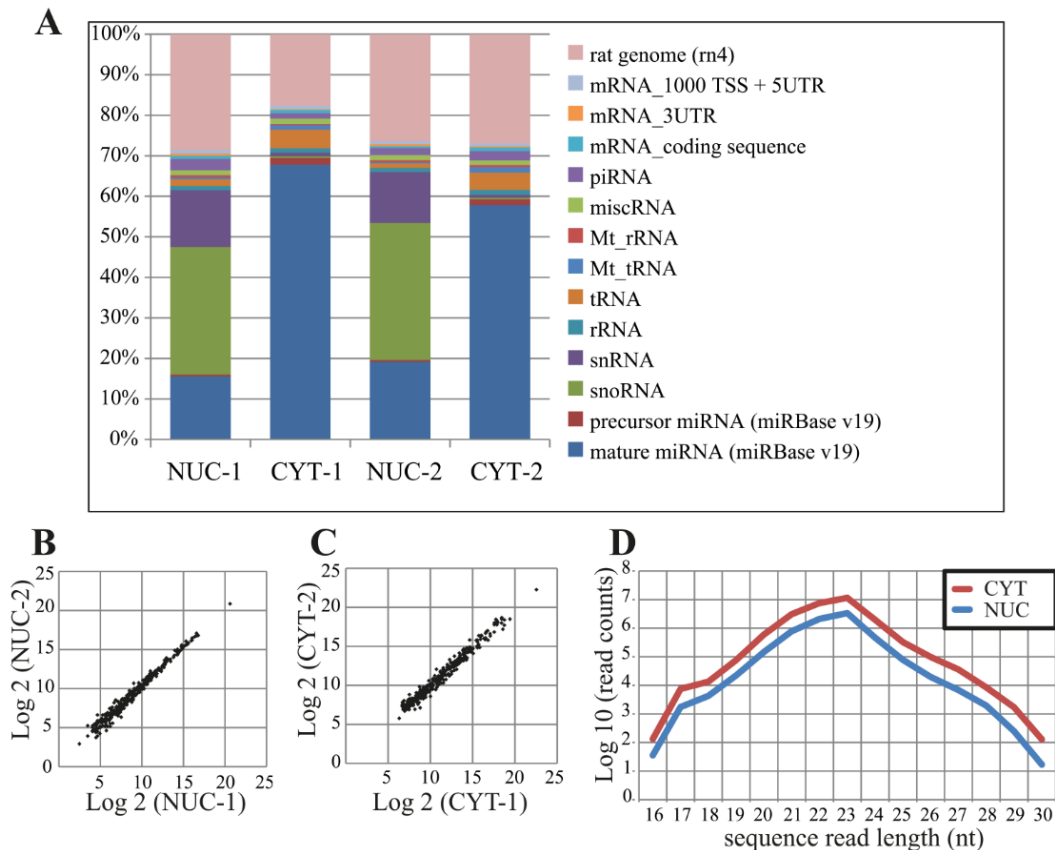


Figure 2. Small RNA deep sequencing after nucleo-cytoplasmic fractionation of neurons. (A) Proportional distribution of mapped sequencing read counts in the small RNA libraries. The total read counts were set to 100% for each small RNA library. (B, C) Scatterplots of log₂ transformed read counts mapping to mature miRNAs from the nuclear (B) and cytoplasmic (C) fractions (two biological replicates each). (D) The sequence length distribution (x-axis) of reads mapping to mature miRNAs. The read counts (y-axis) were log₁₀ transformed.

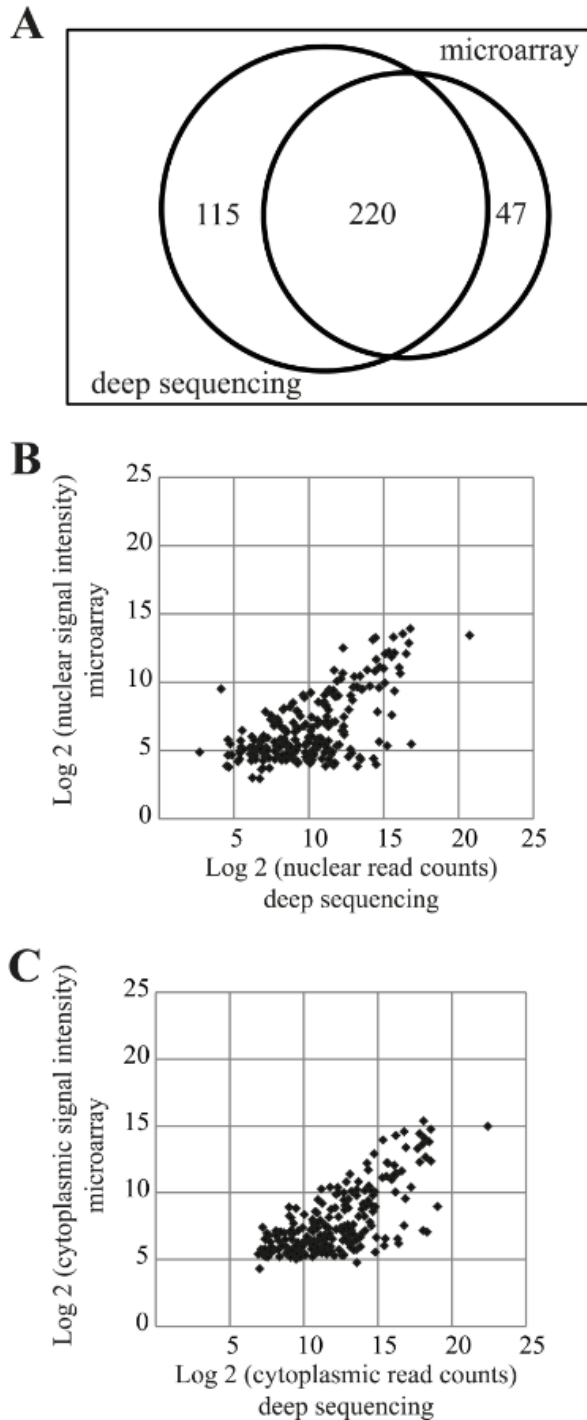


Figure 3. Comparison of miRNA expression profiles obtained from miRNA microarrays and small RNA deep sequencing. (A) Venn diagram illustrating miRNAs detected by the two different methods. 220 miRNAs were detected by both methods. (B, C) Scatterplot of \log_2 transformed signal intensity values (microarray, y-axis) and read counts (deep sequencing, x-axis) for miRNAs detected in the nuclear (B) or cytoplasmic (C) fractions.

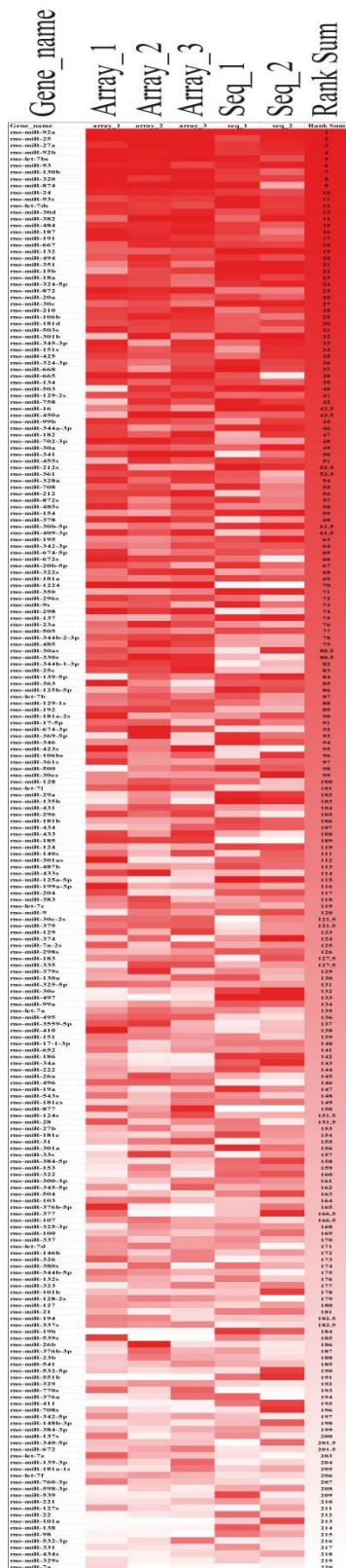


Figure 4. Alignment of miRNAs according to their miRNA nuclear enrichment scores (NENs) obtained with microarrays and deep sequencing. MiRNAs were ranked from high (red) to low (white) NENs for each experiment separately (array_1, _2, _3, seq_1, _2), and then the average ranking was calculated and arranged in descending order based on the Rank Sum method (Laing & Smith, 2010).

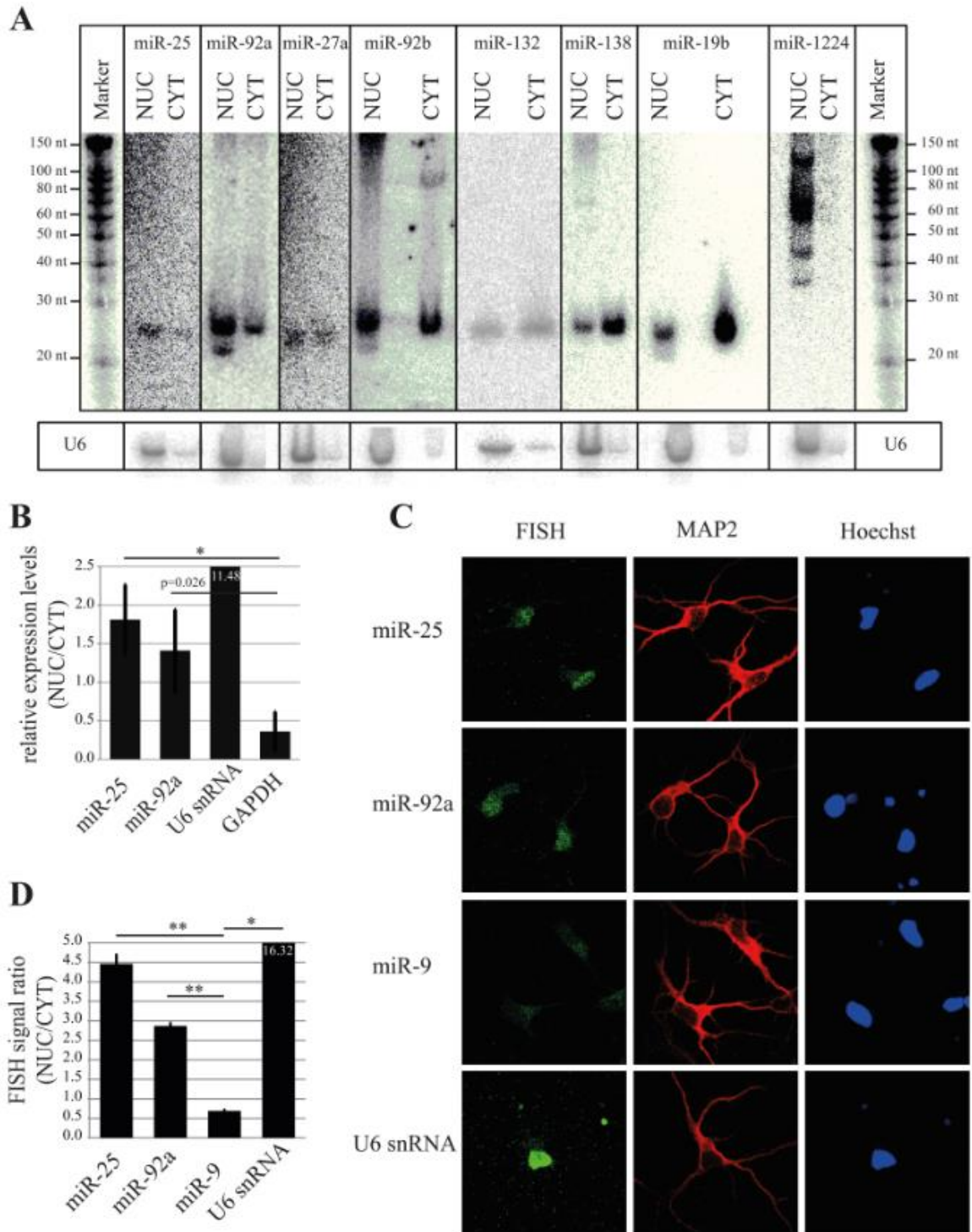


Figure 5. Validation of nuclear expression for selected miRNA candidates. A) Northern blot analysis of nuclear-enriched (miR-25, miR-92a, miR-27a, miR-92b) and -depleted miRNAs (miR-138, miR-19b). As a control for the fractionation efficacy, U6 snRNA was probed. (B) qRT-PCR analysis of nuclear-enriched miRNAs (miR-25 and

miR-92a). The fold enrichment (y-axis) of miRNAs and marker genes (U6 snRNA and GAPDH) in the nucleus was calculated by the $2^{-\Delta C_T}$ ($2^{-(\text{NUC Ct} - \text{CYT Ct})}$) method. Bar plots show mean \pm SD (n=3). Statistical significance was determined using Student's t-test with Bonferroni correction (*, p<0.05). (C) Subcellular localization of the indicated miRNAs as assessed by with fluorescent in-situ hybridization assay (FISH) using Digoxigenin (DIG) labeled miRCURY LNA probes (green). FISH for U6 was used as a positive control for nuclear localization. MAP2 protein was used to identify neurons (red). Hoechst counterstain was used to label nuclei (blue). (D) Quantification of nuclear localization from FISH experiment presented in C. Signal intensities within the nucleus and cytoplasm were determined with ImageJ. The ratios of nuclear/cytoplasmic signal intensities are shown as an indicator for nuclear enrichment. Bar plots show mean \pm SD (n=2; 10 cells per condition of a single experiment). Statistical significance was determined using Student's t-test with Bonferroni correction (*, p<0.05; **, p<0.01).

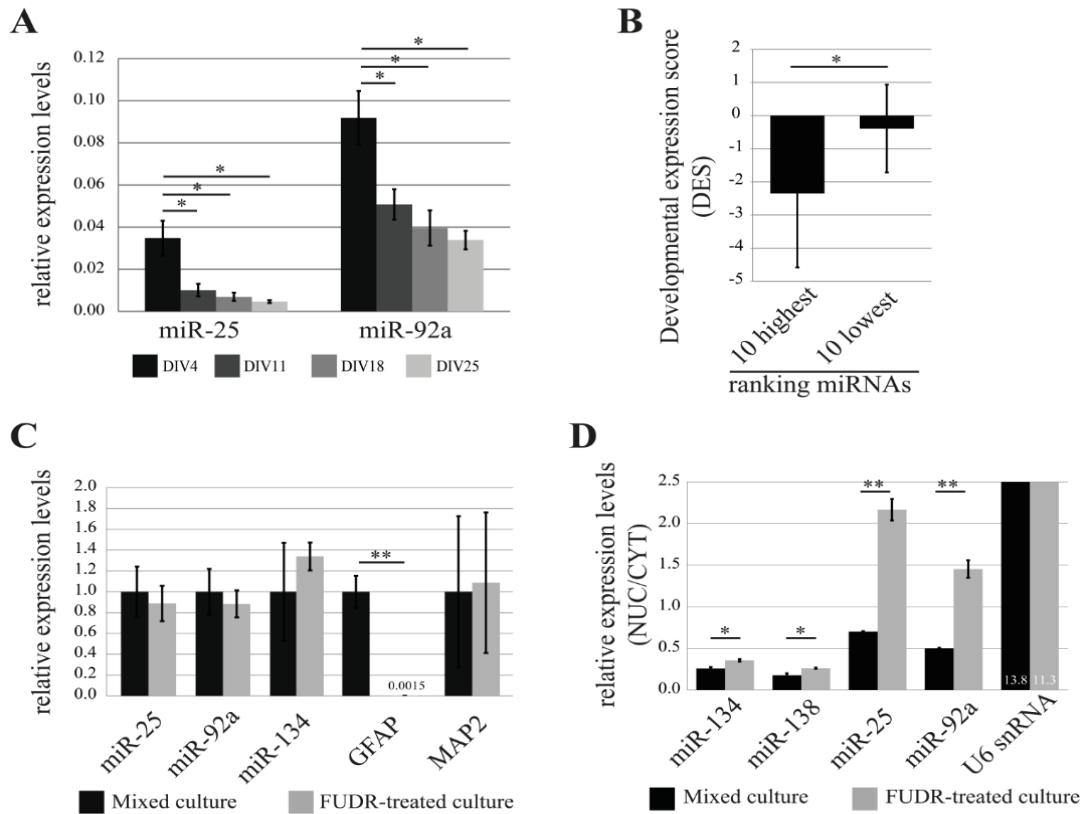


Figure 6. Developmental stage and cell type specific expression of the nuclear-enriched miRNAs, miR-25 and miR-92a. (A) Relative expression (normalized to U6 snRNA) levels of miR-25 and miR-92a during *in vitro* development of primary cortical neurons was determined by qRT-PCR analysis. Bar plots show mean \pm SD (n=2). Statistical significance was determined using Student's t-test with Bonferroni correction (*, $p < 0.05$). (B) Developmental expression score (DES; $\log_2(P3/E10)$ from (Yao et al, 2012); y-axis) comparison of 10 highest and lowest ranked miRNAs. Error bars represent standard deviation from the mean DES within each group. Statistical significance was determined using Student's t-test ($p = 0.028$). (C) Expression of miR-25 and miR-92a in mixed cultures and neuronal-enriched cultures (FUDR-treated). The relative expression levels of indicated RNAs were obtained by the ddCt method. RNA levels in mixed cultures were arbitrarily set to 1. Bar plots show mean \pm SD (n=3). SD for mixed culture condition was determined after normalization to an internal control RNA (U6 snRNA). Statistical significance was determined based on U6 snRNA normalized values using Student's t-test with Bonferroni correction (**, $p < 0.01$). (D) Nuclear-enrichment of miRNA expression in mixed and neuron-enriched (FUDR-treated) cultures. The expression level of miRNAs was determined using qRT-PCR analysis with TaqMan microRNA assay. Bar plots show mean \pm SD (n=2). Statistical significance was determined using Student's t-test with Bonferroni correction (*, $p < 0.05$; **, $p < 0.01$).

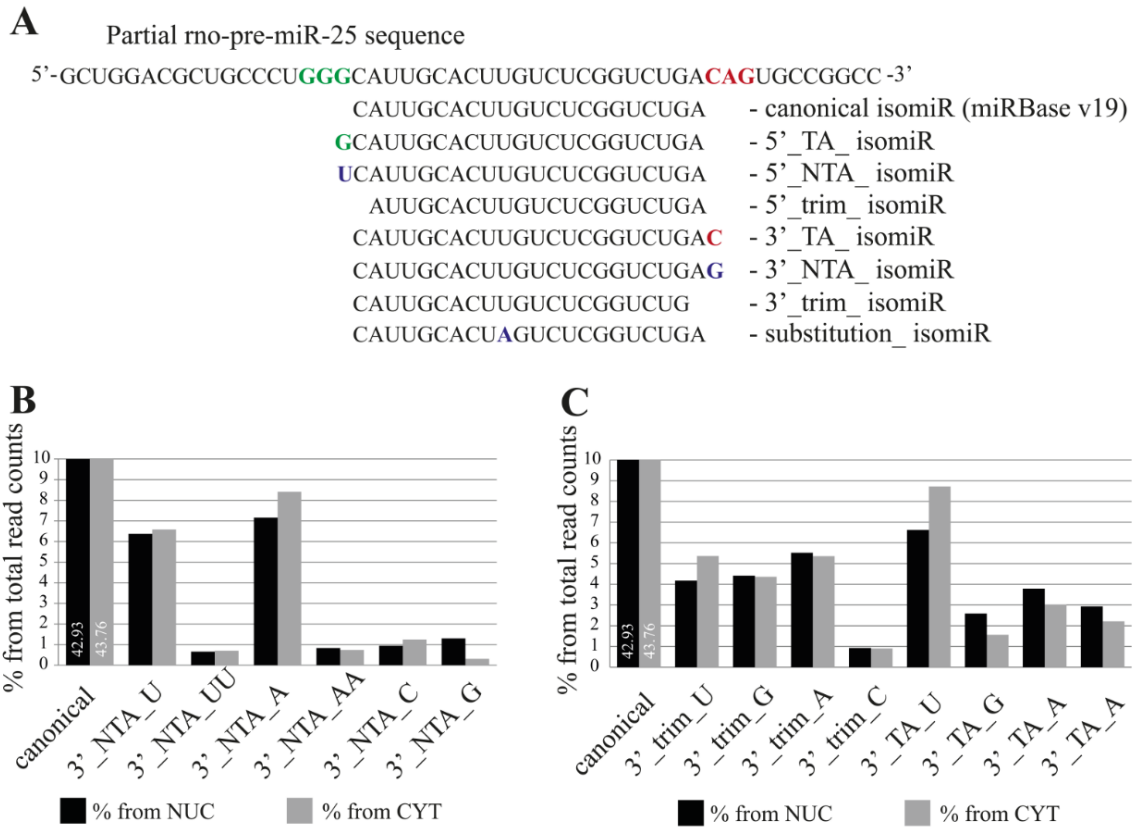


Figure 7. The distribution of isomiRs between nuclear and cytoplasmic fractions of neurons. (A) Definition of different isomiR species. For illustration, miR-25 isomiRs aligned to the pre-mir-25 sequence are shown (TA, templated addition; NTA, non-templated addition; trim, trimmed). (B, C) Proportion of specific isomiRs from the total sequence reads which mapped to miRNAs in the nuclear (black) and the cytoplasmic (grey) fractions. (B) Proportion of isomiRs with specific 3' non-templated additions. (C) Proportion of isomiRs with 3' trimmed and templated additions. The respective added or trimmed nucleotides are indicated for specific isomiRs.

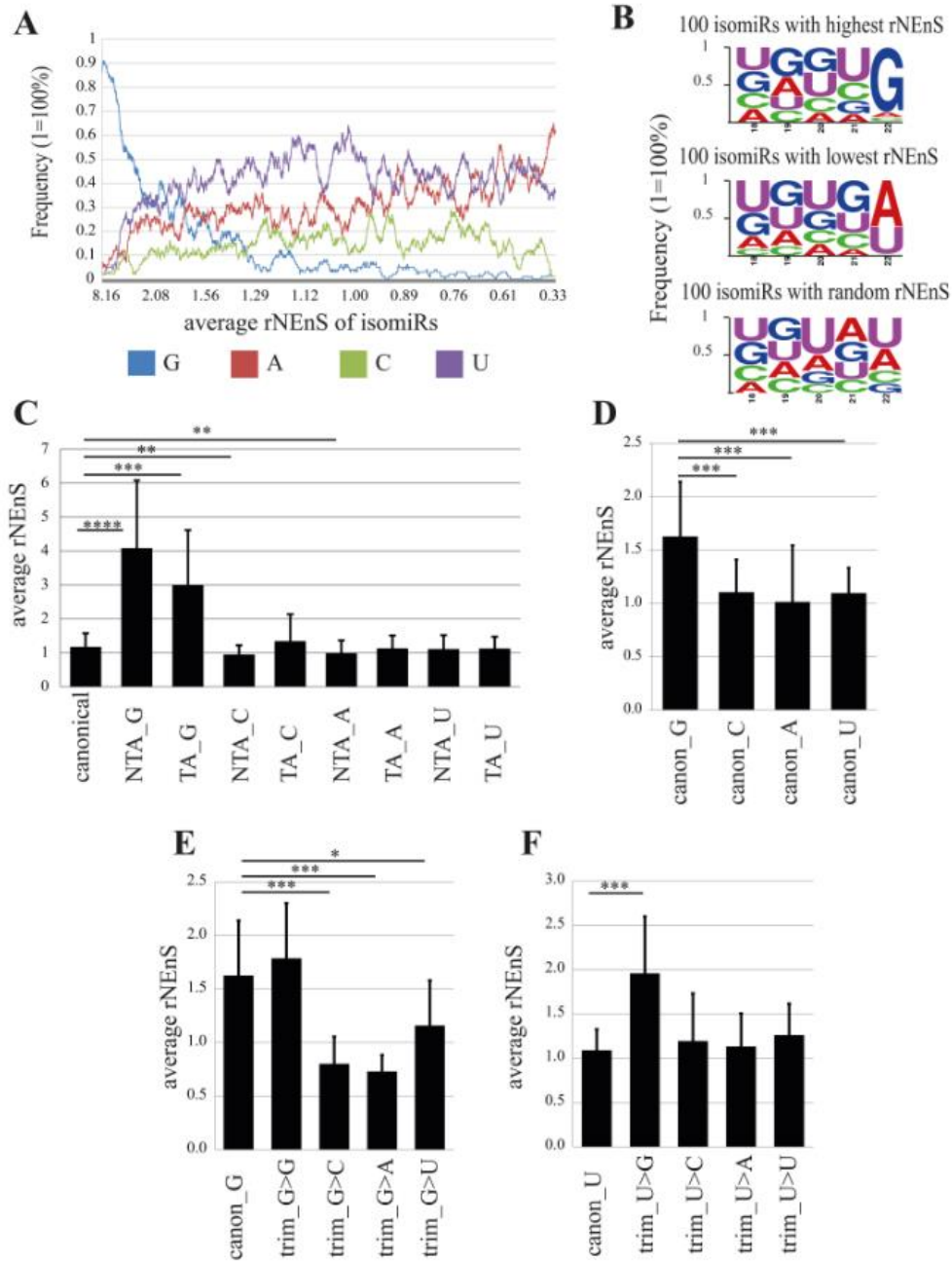


Figure 8. The impact of the 3' terminal nucleotide on nuclear localization. (A) Frequency of different nucleotides at the 3'-terminus of isomiRs depending on the relative nuclear enrichment score (rNEoS). Nucleotide frequency (y-axis) was calculated using moving window technique, where window length was set as 100 and the average frequency values were calculated by moving the window with one step at a time from isomiRs (in total 4661) possessing high to low rNEoS. In the x-axis, the average rNEoS of isomiRs using moving window technique with the same parameters as above is

depicted. (B) Frequency of different nucleotides in the 3' terminal 5 nts of 100 isomiRs with highest (upper panel), lowest (middle panel) and random rNEnS (lower panel). (C) Impact of 3' non-templated (NTA) and templated additions (TA) on the relative nuclear localization. Bar plots show mean \pm SD (n= from 31 (TA_G) to 306 (canonical)). Statistical significance was determined using Welch's t-test (unequal variance) with Bonferroni correction (*, $p < 0.05$; **, $p < 0.001$; ***, $p < 0.00001$; ****, $p < 1.0 \cdot 10^{-10}$). (D) rNEnS for canonical isomiRs containing different 3' terminal nucleotides. Bar plots show mean \pm SD (canon_G, n=57; canon_C, n=62; canon_A, n=75; canon_U, n=112). Statistical significance was determined using Welch's t-test (unequal variance) with Bonferroni correction (*, $p < 0.05$; **, $p < 0.001$; ***, $p < 1.0 \cdot 10^{-7}$). (E, F) Impact of trimming on the nuclear localization of isomiRs. (E) rNEnS for canonical isomiR_G that underwent 3' trimming, thereby exposing the indicated nucleotide. Bar plots show mean \pm SD (canon_G, n=57; trim_G>G, n=12; trim_G>C, n=14; trim_G>A, n=17; trim_G>U, n=9). Statistical significance was determined using Welch's t-test (unequal variance) with Bonferroni correction (*, $p < 0.05$; **, $p < 0.001$; ***, $p < 1.0 \cdot 10^{-5}$). (F) rNEnS for canonical isomiR_C that underwent 3' trimming, thereby exposing the indicated nucleotide. Bar plots show mean \pm SD (canon_U, n=112; trim_U>G, n=32; trim_U>C, n=29; trim_U>A, n=10; trim_U>U, n=20). Statistical significance was determined using Welch's t-test (unequal variance) with Bonferroni correction (*, $p < 0.05$; **, $p < 0.001$; ***, $p < 1.0 \cdot 10^{-5}$).

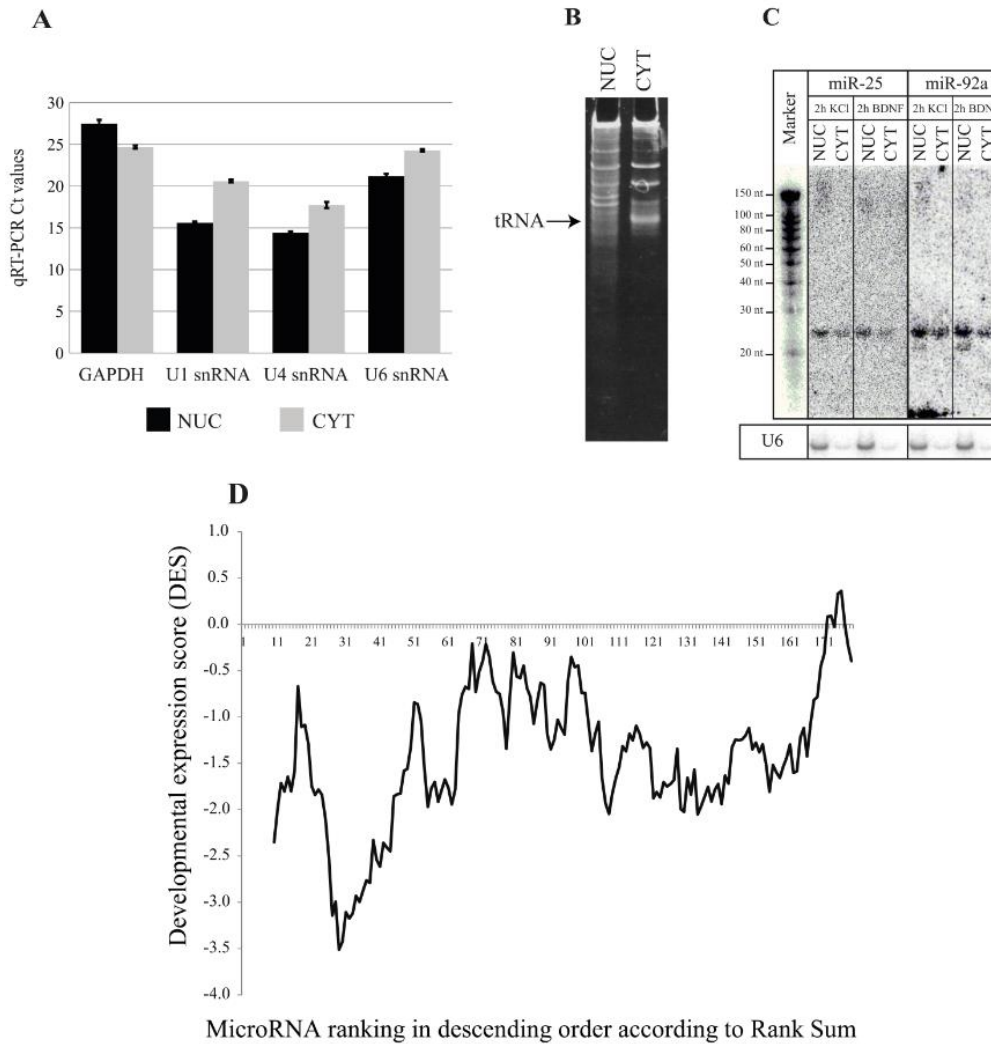


Figure S1. (A) Cycle threshold (Ct) values for markers measured with qRT-PCR in Figure 1a. (B) Denaturing 15 % PAGE gel showing equal loading of RNAs before membrane transfer for Northern blotting. The gel was stained with 2x SYBR Gold dye (Life Technologies) for 5 min and was imaged using E-BOX VX2 gel documentation system (PeqLab). (C) Northern blot analysis of miR-25 and miR-92a using cytoplasmic and nuclear RNA from neurons treated with KCl and BDNF. (D) MicroRNA ranking (Rank Sum) and distribution of an average developmental expression score (DES). DES was calculated by log2 transforming the ration of miRNA read counts from prefrontal cortex of post-natal day 3 (P3) and embryonic day 10 (E10) rats in the published report of Yao and colleagues (2012). DES of 179 (out of 220) miRNAs that were detected both by us and Yao and colleagues (2012) were employed for analysis. The average DES (y-axis) was calculated using moving window technique, where window length was set as 10 and the average values were calculated by moving the window with one step at a time from high to low ranking miRNAs. In the x-axis, the ranking number of miRNAs in descending order is depicted.

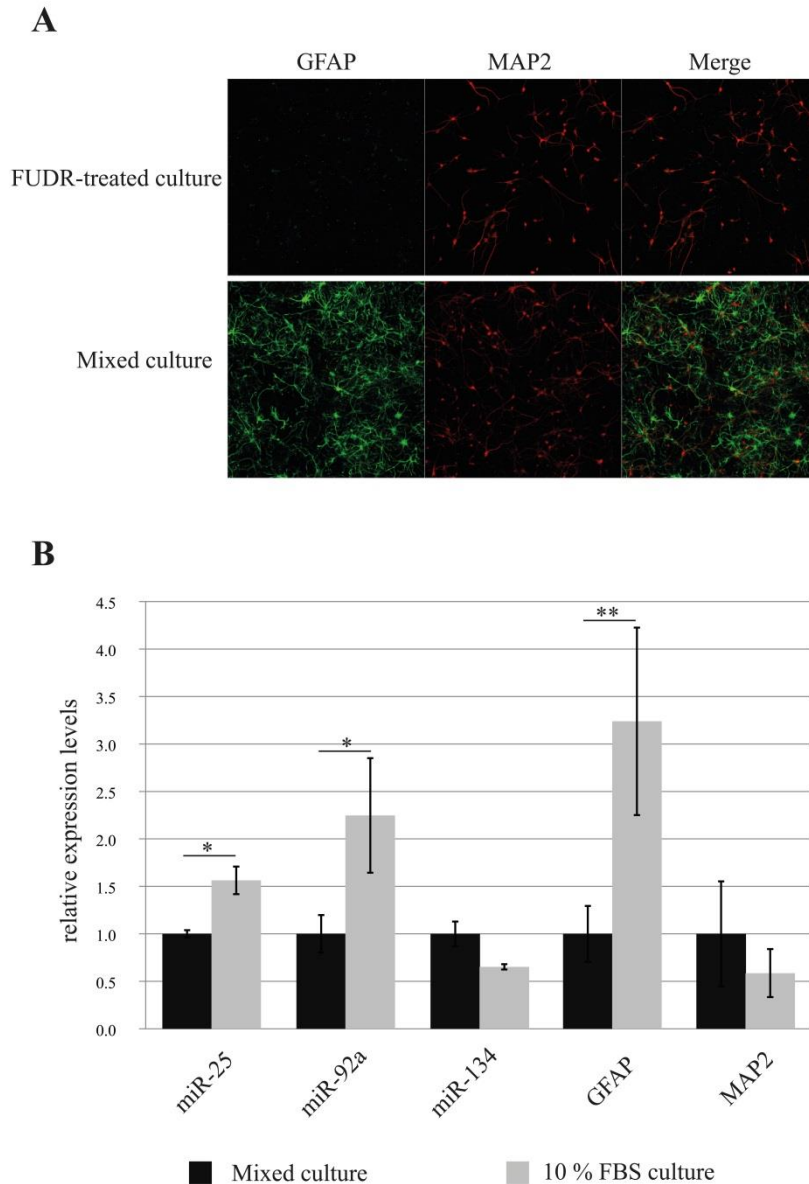


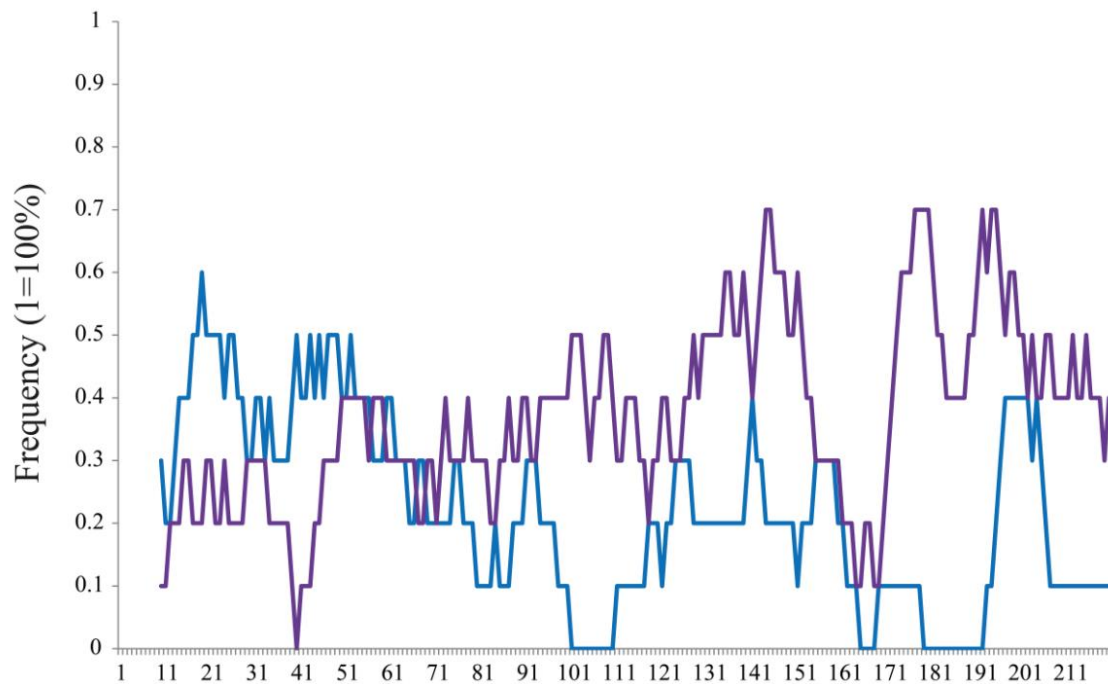
Figure S2. (A) Immunostaining of primary hippocampal cultures for neuronal (MAP2, red) and astrocytic (GFAP, green) marker proteins after treatment with FUDR. Cultures were treated with 10 μ M FUDR at DIV3 and fixed at DIV18. This experiment was performed by a post-doctoral fellow from our lab, Marek Rajman(B) Expression of indicated RNAs in mixed cultures and glia-enriched (10 % FBS-treated). The relative expression levels of indicated RNAs were obtained by the ddCt method. RNA levels in mixed cultures were arbitrarily set to 1. Bar plots show mean \pm SD (n=2). SD for mixed culture condition was determined after normalization to an internal control RNA (U6 snRNA). Statistical significance was determined based on U6 snRNA normalized values using Student's t-test with Bonferroni correction (*, $p < 0.05$; **, $p < 0.01$).

miR-25	CAUUGCACUUGUCUCGGUCUGA
miR-92a	UAUUGCACUUGUCCCGGCCUG
miR-92b	UAUUGCACUCGUC CCGGCCUCC
miR-363	AAUUGCACG -GUAUCCAUCUGU

miR-130a	CAGUGCAAUGUUA AAAGGGCAU
miR-130b	CAGUGCAAUGAUG AAAGGGCAU

miR-27a	UUCACAGUGGCUAAGUUC CGC
miR-27b	UUCACAGUGGCUAAGUUC UGC

Figure S3. Sequence similarity of miRNAs. Members of miRNA families possessing the same seed sequence are depicted in separate rectangular boxes. Red colored letters indicate conserved nucleotides between depicted family members. Blue colored letters indicate partial conservation (miR-25/92a/92b).



MicroRNA ranking in descending order according to Rank Sum

■ G ■ U

Figure S4. Frequency of guanine (G, blue) and uracil (U, violet) nucleotides at the 3'-terminus of mature miRNAs (miRBase v18) depending on the NEnS. Frequency of nucleotide was calculated using moving window technique, where window length was set as 20 and the average occurrence values were calculated by moving the window with one step at a time from high to low ranking miRNAs. In the x-axis, the ranking number of miRNAs in descending order is depicted.

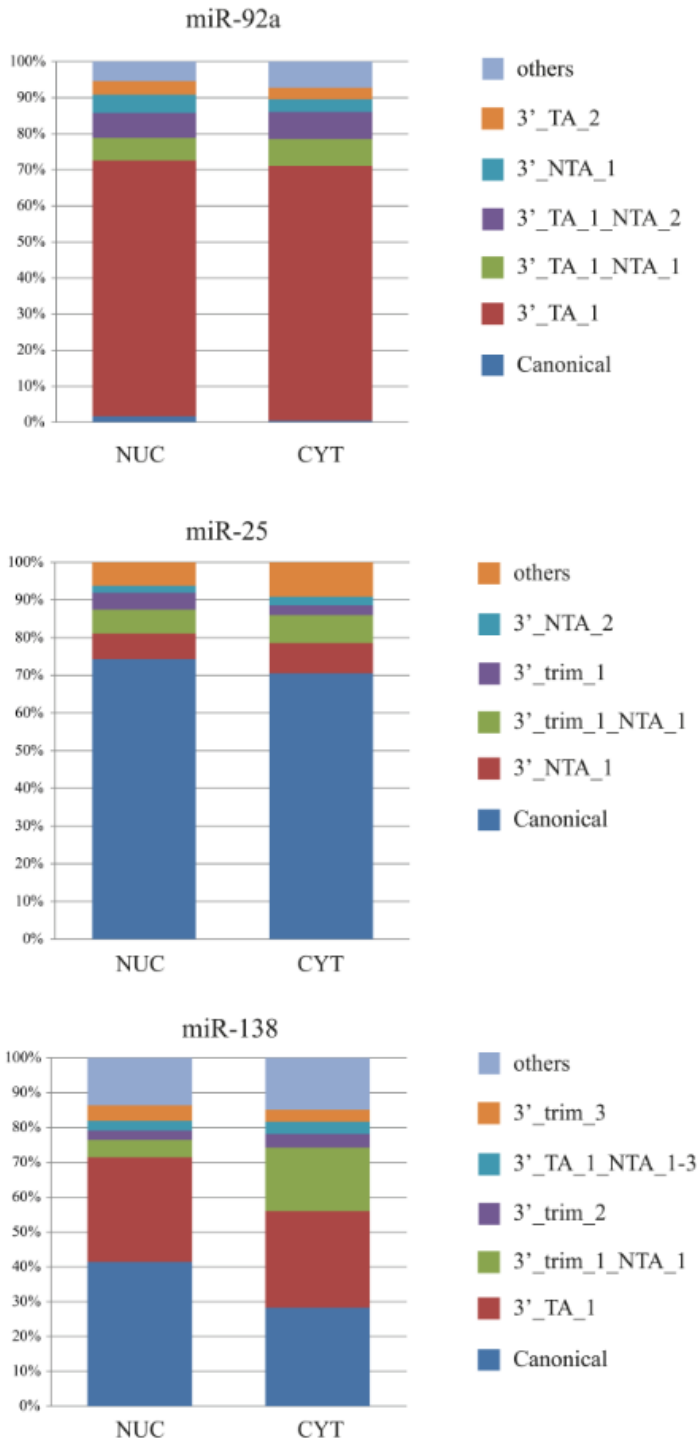


Figure S5. Proportion of specific isomiRs from the total sequence reads mapped to the respective miRNAs in the nuclear and the cytoplasmic fractions.

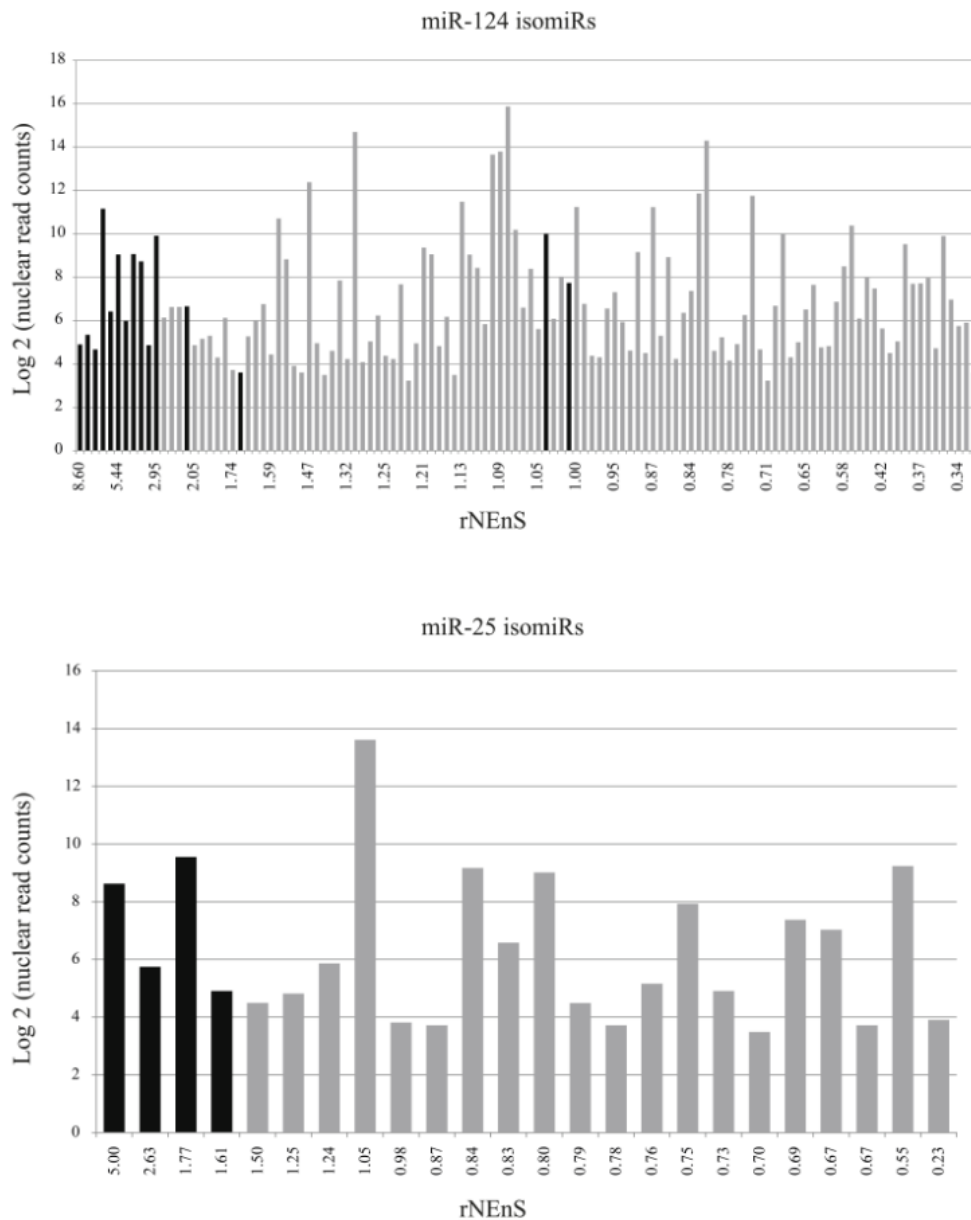


Figure S6. Relative NEnS and 3'terminal guanine nucleotide of specific miRNA (miR-124 and miR-25) isomiRs. On the y-axis, the log₂ transformed read counts from nuclear fraction, and on the x-axis, rNEnS for each isomiR is depicted. Black colored bars indicate isomiRs that possess guanine nucleotide at the 3'-terminus.

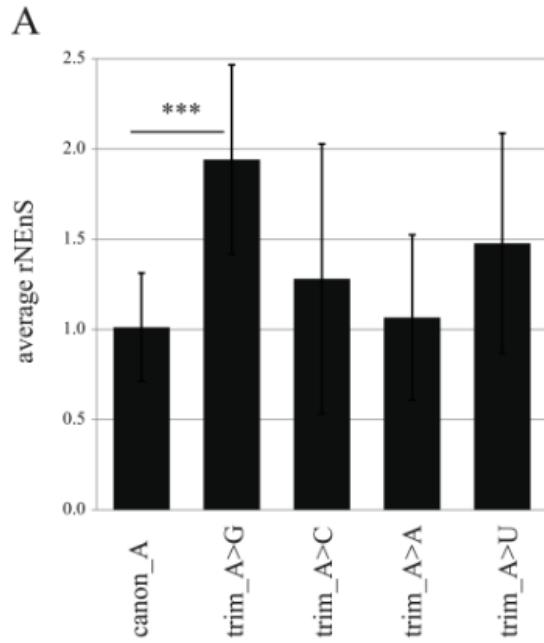
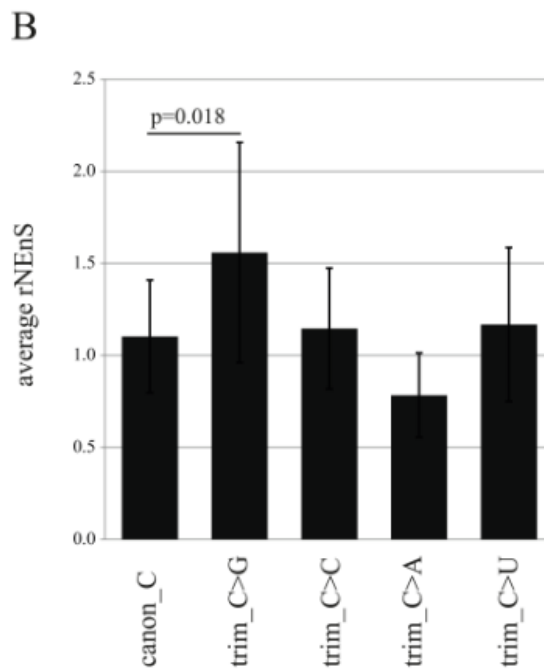


Figure S7. Impact of trimming on nuclear localization of isomiRs. (A) rNEEnS for canonical isomiR_A that underwent 3' trimming, thereby exposing the indicated nucleotide. Bar plots show mean \pm SD (canon_A, n=75; trim_A>G, n=25; trim_A>C, n=18; trim_A>A, n=8; trim_A>U, n=10). Statistical significance was determined using Welch's t-test (unequal variance) with Bonferroni correction (*, $p < 0.05$; **, $p < 0.001$; ***, $p < 1.0 \times 10^{-5}$). (B) rNEEnS for canonical isomiR_C that underwent 3' trimming, thereby exposing the indicated nucleotide. Bar plots show mean \pm SD (canon_C, n=62; trim_C>G, n=13; trim_C>C, n=17; trim_C>A, n=2; trim_C>U, n=9). Statistical significance was determined using Welch's t-test (unequal variance) and none of the comparisons passed the Bonferroni correction (*, $p < 0.05$).



5.3.12 Supplementary table legends

Supplementary tables were submitted to a journal as a datasheets and are available online (http://www.frontiersin.org/molecular_neuroscience/10.3389/fnmol.2013.00043/abstract). For this thesis, I burned the files on a CD and attached it to the back cover of the thesis.

Table S1. miRNAs and their respective signal intensity values (24 nt spike-in normalized) obtained from microarray profiling.

Table S2. miRNAs with significant ($p < 0.05$, Student's t-test) differential expression between nuclear and cytoplasmic fractions.

Table S3. Normalized sequence read counts (deep sequencing) mapped to different non-coding RNAs and genomic databases.

Table S4. miRNAs and their respective read counts obtained from deep sequencing profiling of the nuclear and the cytoplasmic fractions. The nuclear enrichment score (NEoS) for each miRNA was calculated.

Table S5. miRNAs ranked according to Rank Sum method.

Table S6. miRNAs ranked according to Rank Sum method and their respective developmental expression score (DES).

Table S7. IsomiRs from nuclear and cytoplasmic fraction.

Table S8. Primers and probes.

6. APPENDIX

6.1 Publications:

Journal articles

1. Fiore, R.*, **Khudayberdiev, S.***, Christensen, M., Siegel, G., Flavell, S.W., Kim, T.K., Greenberg, M.E., and Schratt, G. (2009). Mef2-mediated transcription of the miR379-410 cluster regulates activity-dependent dendritogenesis by fine-tuning Pumilio2 protein levels. *EMBO J* 28, 697-710
2. Siegel, G., Obernosterer, G., Fiore, R., Oehmen, M., Bicker, S., Christensen, M., **Khudayberdiev, S.**, Leuschner, P.F., Busch, C.J., Kane, C., Hubel, K., Dekker, F., Hedberg, C., Rengarajan, B., Drepper, C., Waldmann, H., Kauppinen, S., Greenberg, M.E., Draguhn, A., Rehmsmeier, M., Martinez, J., and Schratt, G.M. (2009). A functional screen implicates microRNA-138-dependent regulation of the depalmitoylation enzyme APT1 in dendritic spine morphogenesis. *Nature Cell Biology* 11, 705-716.
3. Bicker, S., **Khudayberdiev, S.**, Weiss, K., Zocher, K., Baumeister, S., and Schratt, G. (2013). The DEAH-box helicase DHX36 mediates dendritic localization of the neuronal precursor-microRNA-134. *Genes Dev* 27, 991-996
4. **Khudayberdiev S.A**, Zampa F, Rajman M, Schratt G (2013) A comprehensive characterization of the nuclear microRNA repertoire of post-mitotic neurons. *Front. Mol. Neurosci.* 6:43. doi: 10.3389/fnmol.2013.00043 (accepted for publication).

Addendum article

5. **Khudayberdiev, S.**, Fiore, R., and Schratt, G. (2009). MicroRNA as modulators of neuronal responses. *Commun Integr Biol* 2, 411-413.

Review article

6. Fiore, R*., **Khudayberdiev, S.***, Saba, R.*, and Schratt, G. (2011). MicroRNA function in the nervous system. *Prog Mol Biol Transl Sci* 102, 47-100.

*with equal contribution

6.2 List of academic teachers

The following list represents my academic teachers in Samarkand/Uzbekistan (UZ), Heidelberg (HD) and Marburg.

Allanazarova (UZ)	Mahmudova (UZ)
Bading (HD)	Meyer (HD)
Boutros (HD)	Niehrs (HD)
Brunner (HD)	Normurodov (UZ)
Clayton (HD)	Nosirov (UZ)
Davronov (UZ)	Paro (HD)
Dick (HD)	Pollerberg (HD)
Doberstein (HD)	Pulatova (UZ)
Gruss (HD)	Rajamurodov (UZ)
Halimov (UZ)	Rausch (HD)
Hell (HD)	Robinson (HD)
Hodjayev (UZ)	Schratt
Hurt (HD)	Schuster (HD)
Islomov (UZ)	Schütz (HD)
Ismailov (UZ)	Seedorf (HD)
Jabborov (UZ)	Sinning (HD)
Jurayev (UZ)	Umurzakova (UZ)
Kabulova (UZ)	Uralov (UZ)
Keldiyorov (UZ)	Vogt (HD)
Klingmüller (HD)	Wieland (HD)
Kuner (HD)	Wiemann (HD)
Lahanov (UZ)	Wittbrodt (HD)
Lyko (HD)	

6.3 Acknowledgements

I wish to express my deepest gratitude to my supervisor Prof. Dr. Gerhard Schratt for giving me the opportunity to perform my PhD work as a member of his research group. His scientific guidance, never-ending optimism, encouragement and support have been always as a source of motivation. Once more thank you very much!

My sincere thanks to Roberto Fiore, who is always open for any discussion, shared endless number of cigarettes, and many more other things that he helped me with.

I am very thankful to Silvia Bicker for her optimism and being open to provide any help, including the translation of the summary of this thesis to German language.

I would like to thank Juliane Thümmeler for being a great colleague, a lab-bench neighbor and a babysitter.

Sincere thanks to all members of AG Schratt, specifically, Peter Störchel, Jeremy Valluy, Kerstin Weiss, Ayla Aksoy Aksel, Federico Zampa, Marek Rajman, Bernd Kösters, Christian Wrocklage, Birgit Rost, Cecillia Patrascan, Martin Lackinger for helpful discussions, encouragement and all kind of assistance during whole period of the PhD project. In addition, I am grateful from my colleagues for uncountable number of non-research related support provided from each of them. To name each occasion will be enough to write a book on its own. It is fun working with you all and thanks for offering a helping hand whenever needed.

Special thanks to our dream team of technical assistants, Gertraud Jarosch, Renate Gondrum, Eva Becker, Karlheinz Burk, Heinrich Kaiser, Ute Beck, Bettina Kowalski for their excellent work in providing primary cells, ordering and preparing reagents, simply for making my lab life easier. The administrative paper routine would have been too confusing without a skillful work of Irena Müller.

I would like to thank my colleagues and friends acquired during “Heidelberg time”, Gabrielle Siegel, Tatjana Wüst, Mette Christensen, Güney Akbalik and many others for a great support (scientific and moral) and unforgettable socializing events. Special thanks to Reuben Saba for being an excellent roommate, a running partner and a friend.

I would like to extend my thanks to the staff in BPC Marburg, specifically AG Grosse and AG Culmsee for being helpful on any occasion.

My parents, who believe and always support me, deserve my deepest gratitude and love.

My three angels, Dilbar, Malika and Mehribon, thank you very much for your support and patience. No words are sufficient to express my love to you.

